



**HAL**  
open science

# The impact of climate change and human management on the water cycle of China: dealing with uncertainties

Xudong Zhou

► **To cite this version:**

Xudong Zhou. The impact of climate change and human management on the water cycle of China: dealing with uncertainties. Meteorology. Université Paris Saclay (COMUE), 2018. English. NNT: 2018SACLX097 . tel-02388501

**HAL Id: tel-02388501**

**<https://pastel.hal.science/tel-02388501>**

Submitted on 2 Dec 2019

**HAL** is a multi-disciplinary open access archive for the deposit and dissemination of scientific research documents, whether they are published or not. The documents may come from teaching and research institutions in France or abroad, or from public or private research centers.

L'archive ouverte pluridisciplinaire **HAL**, est destinée au dépôt et à la diffusion de documents scientifiques de niveau recherche, publiés ou non, émanant des établissements d'enseignement et de recherche français ou étrangers, des laboratoires publics ou privés.

# The Impact of Climate Change and Human Management on the Water Cycle of China: Dealing with Uncertainties

Thèse de doctorat de l'Université Paris-Saclay  
préparée à l'École Polytechnique

Ecole doctorale n°579 Sciences mécaniques et énergétiques, matériaux et  
géosciences (SMEMAG)  
Spécialité de doctorat : météorologie, océanographie, physique de l'environnement

Thèse présentée et soutenue à Palaiseau, le 4 Décembre 2018, par

**MONSIEUR XUDONG ZHOU**

Composition du Jury :

M. Laurent LI Directeur de recherche, Laboratoire de Météorologie Dynamique	Président
M. Aaron BOONE Chargé de recherche, Centre National de Recherches Météorologiques	Rapporteur
Mme. Eleanor BLYTH Directeur de recherche, Centre for Ecology & Hydrology	Rapportrice
M. Philippe CIAIS Directeur de recherche, Laboratoire des Sciences du Climat et de l'Environnement	Examineur
M. Jan POLCHER Directeur de recherche, Laboratoire de Météorologie Dynamique	Directeur de thèse
M. Tao YANG Professeur, Hohai University	Co-directeur de thèse



# Résumé en français

## Introduction

Les changements climatiques et les interventions humaines ont modifié le cycle de l'eau terrestre au cours des dernières décennies. La modélisation du débit des rivières, qui mesure avec précision l'état du système hydrologique, est un moyen pratique de quantifier et de comprendre les impacts du climat et des activités humaines. Cependant, de nombreuses sources d'incertitude peuvent affecter l'exactitude de l'estimation du débit. Ces sources incluent les incertitudes dans les variables atmosphériques qui sont utilisées pour forcer les modèles, les incertitudes dans le modèle lui-même (structure et paramètres du modèle) et les incertitudes dans la formulation des activités humaines. Sur la base de la revue des études en cours présentées dans le chapitre 1, cette thèse a pour objectifs de 1) quantifier et comparer les incertitudes de différentes sources, 2) d'attribuer le biais du modèle à différentes sources d'incertitudes et 3) d'évaluer l'impact des activités humaines dans le contexte d'autres sources d'incertitudes. De nouvelles approches sont développées pour ces objectifs et toutes les applications sont centrées sur les régions chinoises.

## Quantification de l'incertitude avec une nouvelle approche

L'incertitude existe dans les variables atmosphériques (p.e., les précipitations) et peut être estimée à partir de plusieurs jeux de données. Le chapitre 2 introduit une nouvelle approche tridimensionnelle de partitionnement de la variance, particulièrement adaptée à la quantification de l'incertitude entre plusieurs jeux de données comportant des variations temporelles et spatiales. Les multiples jeux de données qui nous intéressent sont organisés selon trois dimensions (c'est-à-dire le temps, l'espace et l'ensemble) illustrées dans la Figure 1.

L'incertitude  $U_e$  est estimée sous la forme du rapport de la racine carrée de la variance à la dimension d'ensemble ( $V_e$ ) et de la moyenne du grand ensemble de tous les jeux de données ( $\mu$ ).

$$U_e = \sqrt{V_e}/\mu \quad (1)$$

La variance d'ensemble ( $V_e$ ) est une intégration de la moyenne de quatre types de variances de données d'origine ( $\overline{\sigma_e^2}$ ), la moyenne temporelle ( $\overline{\sigma_{e-t}^2}$ ), la moyenne spatiale ( $\overline{\sigma_{e-s}^2}$ ) et la grande moyenne ( $\sigma_e^2(\mu_{ts})$ ).

$$V_e = \frac{mn(l-1)}{3(mnl-1)} \left[ \frac{\overline{\sigma_{e-t}^2} + \overline{\sigma_{e-s}^2}}{2} + \overline{\sigma_e^2} + \sigma_e^2(\mu_{ts}) \right] \quad (2)$$

$m, n, l$  sont les tailles en trois dimensions, respectivement. Parmi les différentes variances, les  $\overline{\sigma_{e-t}^2}$  et  $\overline{\sigma_{e-s}^2}$  sont des mesures couramment utilisées pour estimer l'incertitude dans diverses études, tandis que les variations temporelles ou spatiales doivent être éliminées en raison de la limite de leur algorithme pour estimer ces deux métriques.

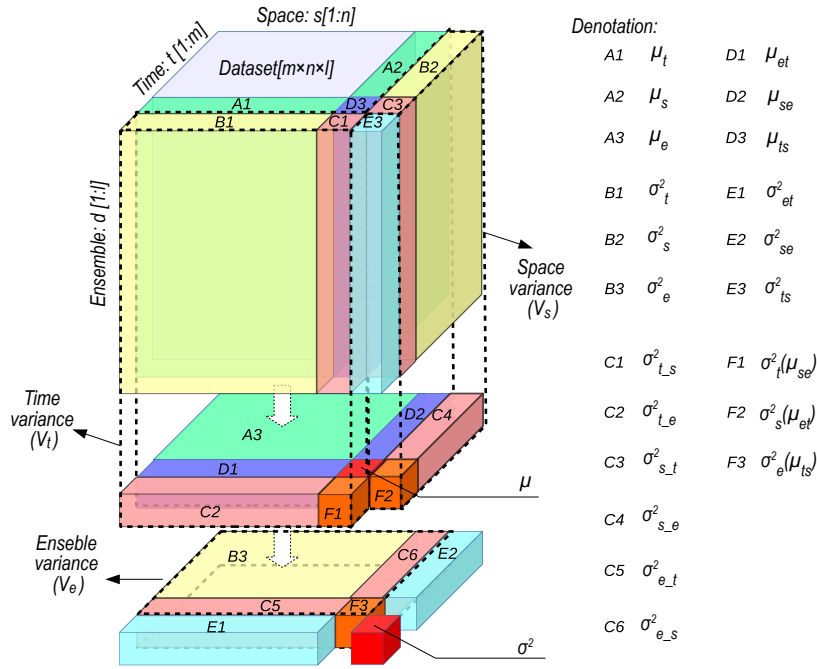


FIGURE 1 – L’illustration de l’approche de partitionnement de variance en trois dimensions. Le jeu de données d’origine est organisé en trois dimensions : temps, espace et ensemble (la zone bleue). Les détails des dénominations et des formulations peuvent être trouvés dans le Chapitre 2, Figure 2.1 et Annexe A.

La mise en œuvre de la nouvelle estimation de l’incertitude ( $U_e$ ) pour différents produits de précipitation (Table 2.1) montre que  $U_e$  est généralement plus grand que les deux mesures classiques  $\sigma_{e_t}^2$  et  $\sigma_{e_s}^2$  (rapport de la racine carrée de leurs valeurs à la moyenne, Figure 2) car temporelle et spatiale les variations sont prises en compte dans l’estimation  $U_e$ . Les différents produits de précipitation basés sur des pluviomètres ont le moins d’incertitude car ils se basent sur des observations similaires et les méthodes d’interpolation n’entraînent pas de grande différence entre les jeux de données. Les ensembles de données de précipitations combinées avec les observations, les satellites, les prévisions et les données de réanalyse ont un  $U_e$  modéré, car ils reposent sur différentes sources de produits, tandis que les observations contraindront les valeurs proches du système réel. Le plus grand  $U_e$  se trouve parmi les modèles de circulation générale (GCMs) car il n’y a pas de contrainte sur la variabilité temporelle dans les modèles de GCMs. Les variations du modèle et les différences dans les conditions initiales entraîneront de grandes différences dans la production finale des précipitations dans le GCMs.  $U_e$  est plus grand pour les grandes régions (région 9,10,11) que pour les petites régions en raison des plus fortes hétérogénéités spatiales.

## Attribuer le biais de décharge à différentes sources d’incertitude

Différentes incertitudes peuvent survenir et interagir les unes avec les autres, ce qui rend difficile la détermination de la source l’incertitude principale et de comparer les sources d’incertitudes. Le chapitre 3 introduit un cadre ORCHIDEE-Budyko, qui permet d’attribuer le biais de la décharge modélisée par un modèle de surface terrestre à différentes sources (p.e., variables atmosphériques, structures de modèle) avec l’hypothèse de Budyko.

Le concept de base peut être expliqué à l’aide de l’illustration de la Figure 3. Nous dispersons les points qui représentent les relations entre l’évapotranspiration potentielle

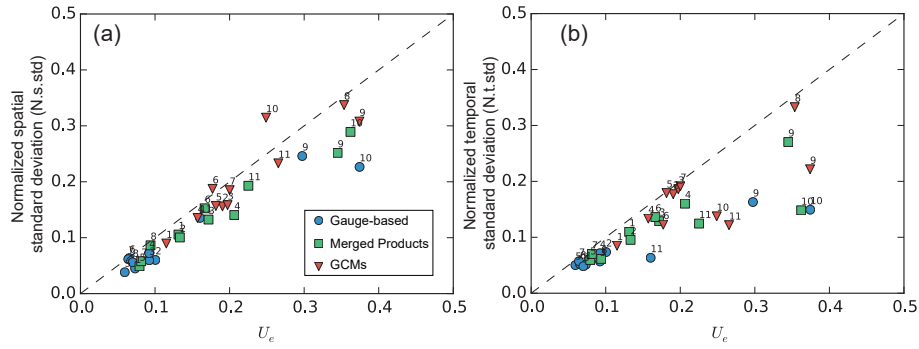


FIGURE 2 – La relation entre  $U_e$  et (a) l'écart type spatial normalisé - N.s.std ( $\sqrt{\sigma_{e_t}^2/\mu}$ ) et (b) le temps normalisé écart type - N.t.std ( $\sqrt{\sigma_{e_s}^2/\mu}$ ). Les valeurs proches des symboles indiquent différentes régions spécifiées dans la Figure 2.2.

annuelle modélisée et l'évapotranspiration réelle modélisée avec la précipitation (points rouges). Le point A représente l'état moyen de la simulation du modèle et la courbe représente la relation de Budyko estimée suivant l'état modélisé. Comme il existe des incertitudes dans de nombreuses sources, le débit estimé de la rivière est différent des observations. Les points B, C, D représentent trois états supposés différents qui pourraient modifier les simulations du modèle pour correspondre aux observations des débits en modifiant uniquement le  $P$  (point B) ou le  $PET$  (point C) ou le  $ET$  (point D). La différence entre leurs nouvelles valeurs de  $P$ ,  $PET$ ,  $ET$  aux nouveaux états (B, C, D) peut être expliquée par les différentes incertitudes. Les variations de  $P$  et de  $PET$  sont attribuées à l'incertitude des variables atmosphériques et les variations de  $ET$  sont attribuées à la structure et aux paramètres du modèle. Cependant, cette approche ne donne qu'un éventail des incertitudes maximal. L'état naturel réel se situe très probablement dans la zone ombrée de la Figure 3. La possibilité de sources d'incertitude différentes peut être évaluée en consultant d'autres études dans des régions présentant des caractéristiques climatiques ou géophysiques similaires, mais pour lesquelles les données sont moins incertaines.

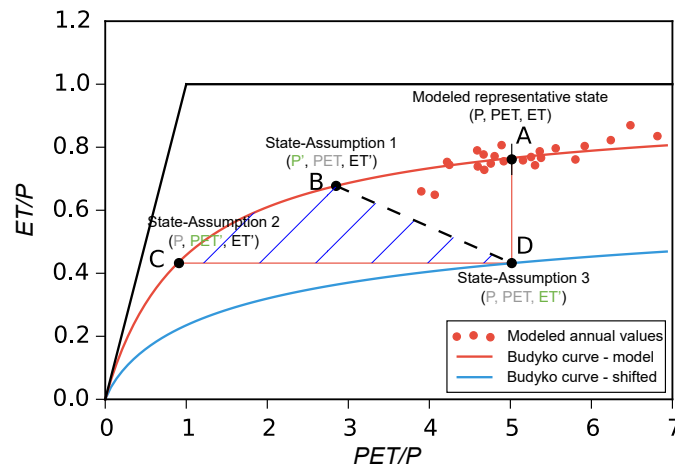


FIGURE 3 – L'illustration du cadre ORCHIDEE-Budyko.

La mise en œuvre dans le bassin versant source de la rivière Tarim (Yarkand par exemple) est présentée dans la table 1. La décharge observée pour le Yarkand est 140,4 mm/an alors qu'ORCHIDEE la sous-estime à 59,0 mm/an. Il existe trois options différentes (B, C et D)

pour faire correspondre le débit lorsque nous augmentons les précipitations de 76,1%, passant de 247,3 mm/an à 435,4 mm/an (point B), ou que nous réduisons le *PET* de 81,9%, de 1240,4 mm/an à 225,0 mm/an (point C) ou nous diminuons le *ET* de 43,2% de 188,3 mm/an à 106,9 mm/an.

TABLE 1 – Les valeurs moyennes annuelles pour différentes composantes eau-énergie (*P*, *ET*, *PET*; unités en mm/an) et leurs relations (*P - ET*, *PET/P* et *ET/P*) pour les trois sous-bassins amont. Yarkand est pris comme exemple et la table complète se trouve dans la Table 3.5. Les scénarios correspondent aux diagnostics du modèle actuel (A) et des trois hypothèses de biais énumérées ci-dessus de B à D. Les valeurs en gras sont les principaux facteurs modifiés au sein des trois composantes du cycle eau-énergie. Le rapport de variation (C.R.) indique le rapport entre la valeur de changement et la valeur d'origine (unité en %). Alors que la plage de biais (B.R.) indique le biais entre valeurs actuelles et ce qu'elles devraient être (unité en %).

	<i>P</i>	<i>PET</i>	<i>ET</i>	<i>P - ET</i>	<i>PET/P</i>	<i>ET/P</i>	Facteur	C.R.	B.R.	
Yarkand	A	247,3	1240,4	188,3	59,0	5,02	0,76	-	-	-
	B	<b>435,4</b>	1240,4	<b>294,9</b>	140,5	2,85	0,68	<i>P</i>	76,1	-43,2
	C	247,3	<b>225,0</b>	<b>106,9</b>	140,4	0,91	0,43	<i>PET</i>	-81,9	451,2
	D	247,3	1240,4	<b>106,9</b>	140,4	5,02	0,43	<i>ET</i>	-43,2	76,1

En faisant référence à d'autres études sur des régions présentant des caractéristiques climatiques ou géophysiques similaires, nous évaluons la possibilité de différentes sources d'incertitude. Les résultats montrent que dans le bassin versant de Yarkand, l'apport d'eau dans le système (*P*) est certainement sous-estimé car il devrait y avoir un ratio plus élevé de fonte des glaciers et une tendance plus élevée du débit compte tenu de sa fraction de surface de glacier élevée. Cependant, le biais en *P* n'est pas le seul facteur en cause, puisque *PET* est excessivement élevé (1240,4 mm/an) pour cette région montagneuse, car les régions proches ne disposent que de 580 à 720 mm/an de *PET*. *PET* n'est également pas le seul facteur d'incertitude, car le chargement de *PET* uniquement réduira le rapport *PET/P* (indice d'aridité) à 0,91, ce qui est peu probable pour une région aux précipitations limitées. La surestimation de *ET* est possible, mais ce n'est pas le seul facteur à prendre en compte, car seule la modification de *ET* augmentera le rapport *PET/P* à 5,02, ce qui n'est pas une valeur réaliste pour le captage en rivière. Les explications complètes se trouvent dans les sections 3.4.3 et la Table 3.6.

## Activités humaines et comparaisons des grandeurs

Les activités humaines sont des facteurs importants qui modifient le cycle naturel de l'eau et le débit des rivières. Le chapitre 4 passe en revue les études associées aux différents types d'activités humaines et à leurs impacts sur le débit des rivières en termes de débit totale et extrêmes. L'impact de l'activité humaine sur le débit des rivières a été généralisé à la Figure 4.

Différentes utilisations des sols et régulations des barrages ont lieu à différents endroits et leurs impacts sur les régimes de débits des rivières peuvent entraîner des variations dans les amplitudes et phases. La modification des forêts (déforestation et reboisement) modifie à la fois la valeur totale de l'apport en eau et les débits extrêmes des rivières (pics de crue et faible débit). L'expansion de la zone urbaine augmente le pic d'inondation et réduit le temps de résidence de l'eau dans la zone. Il augmente également la valeur totale de l'apport en eau en raison de la moindre évaporation. L'eau utilisée à des fins domestiques et industrielles modifie

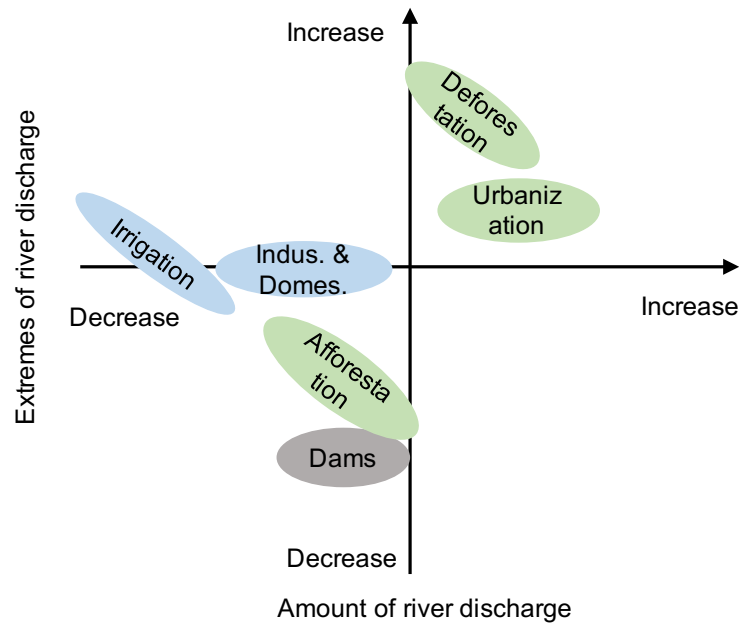


FIGURE 4 – Le résumé illustratif de l’impact de l’utilisation des terres et des eaux ainsi que des barrages sur le débit des rivières.

peu le débit du fleuve (2,0 % en moyenne pour la Chine), tandis que la consommation d’eau agricole diminue le rendement total en eau de 7,4 % (en moyenne pour la Chine) pour les cultures. La consommation d’eau a très peu d’impact sur les débits extrêmes, tandis que la régulation du barrage modifie principalement le cycle inter-annuel en diminuant les fortes crues et en augmentant les débits faibles. La quantité totale d’eau diminue légèrement à cause des barrages en raison de l’augmentation de la surface de l’eau et de l’utilisation de l’eau pour l’agriculture essentiellement.

Le chapitre 4 passe également en revue les approches utilisées pour quantifier les impacts humains sur le débit des rivières. Ils sont classés en deux groupes différents selon que l’impact humain est estimé directement par les modèles. Les concepts de base, les modèles exacts, les études de cas, les avantages et les inconvénients des deux groupes d’approche sont détaillés dans le chapitre 4.

Le chapitre 4 évalue également l’impact de l’utilisation de l’eau par l’homme et de la régulation de l’eau en comparant les débits observés des cours d’eau et des cours d’eau naturalisés à 84 stations sur les fleuves de Chine. Trois mesures différentes sont utilisées pour quantifier les changements sous forme de valeurs moyennes  $\mu$  représentant le débit annuel total du fleuve et deux mesures de mise en phase, la période de concentration  $C_p$  représentant la période au cours de laquelle le débit de la rivière est le plus élevé et le degré de concentration  $C_d$  représentant la magnitude de décharge dans la période du débit maximal (équation 4.13 - 4.18). Les résultats montrent que l’impact humain est faible dans le sud de la Chine, tandis qu’il est important dans les régions du nord où l’agriculture est très développée. Les principales caractéristiques de l’impact humain sont les suivantes : 1) le débit total de la rivière diminue ( $\Delta\mu < 0$ ), 2) la période de concentration est retardée ( $\Delta C_p > 0$ ) car la consommation d’eau est concentrée au printemps et au début de l’été lorsque le débit naturel du fleuve n’a pas atteint son niveau le plus élevé. En période d’inondation, lorsque le débit de la rivière est élevé, les besoins en eau de l’homme (impact humain) deviennent moins importants. 3) Le degré de concentration diminue ( $\Delta C_d < 0$ ), indiquant que le débit de la rivière est distribué de manière

plus uniforme après la réglementation humaine.

Les changements dans les métriques du débit de la rivière dus aux interventions humaines sont comparés à l'incertitude du débit naturel modélisé (Figure 5). La différence entre des simulations forcées par différentes entrées atmosphérique est due à la limitation de nos connaissances sur les variables naturelles, y compris le forçage et les modèles. Les métriques ( $\mu$ ,  $C_p$  ou  $C_d$ ) sont estimées séparément pour des simulations de décharge conduites avec différentes entrées de forçage (WFDEI\_CMA, E2O, ITPCAS, WFDEI\_CRU). L'incertitude de la décharge modélisée est évaluée comme étant la différence des métriques ( $\Delta\mu$ ,  $\Delta C_p$  ou  $\Delta C_d$ ) pour un forçage donné (E2O, ITPCAS, WFDEI\_CRU) par rapport à forçage de référence (WFDEI\_CMA). Les comparaisons pour chaque bassin versant est tracée dans la Figure 5.

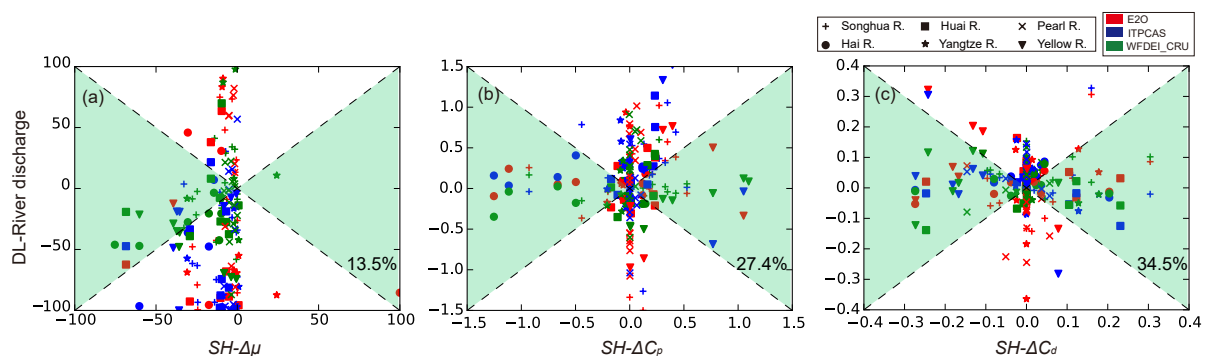


FIGURE 5 – Comparaison des impacts humains et de l'incertitude de la simulation de décharge entraînée par différents intrants de forçage.

Les résultats montrent que la différence entre le débit simulé du fleuve, qui est causé par la limitation des connaissances, est plus grande que le décalage du débit du fleuve dû aux interventions humaines dans la plupart des régions en termes de débit moyen ( $\Delta\mu$ ) (Figure 5). Cela signifie que le choix d'un forçage différent entraînera une différence de simulation de décharge plus grande que ce qui peut être détecté comme étant l'impact humain. L'estimation de l'impact humain n'est donc pas crédible dans ce cas. Cependant, l'écart de différence dû à la limitation des connaissances est moins important pour les métriques de phasage que la période de concentration ( $\Delta C_p$ ) et la degré de concentration ( $\Delta C_d$ ) que pour les valeurs moyennes degré de concentration. La proportion de captages qui remplissaient la condition, à savoir que la différence due à la limitation des connaissances est moins importante que le changement dû à l'impact humain, est plus élevée pour  $\Delta C_p$  et  $\Delta C_d$ . Par conséquent,  $C_p$  et  $C_d$  sont de meilleurs indicateurs que les moyens pour attribuer l'impact humain. Nous appliquons le même processus aux précipitations et à l'évapotranspiration potentielle dans le chapitre 4, et les résultats montrent que nous avons déjà une bonne connaissance de la phase des variables de forçage, mais la capacité du modèle à estimer la phase de débit du fleuve doit encore être améliorée.

## Conclusions et perspectives

En conclusion, cette thèse porte principalement sur les incertitudes inhérentes à l'évaluation de l'impact du changement climatique et à la gestion humaine sur le cycle de l'eau. Les incertitudes des variables atmosphériques sont estimées avec une nouvelle approche de partitionnement de variance en trois dimensions. Le biais de décharge entre les simulations et les observations est attribué aux incertitudes du forçage et à celles dues aux modèles. Les

résultats montrent que les incertitudes dans le forçage sont grandes et plus grandes que celles pouvant être causées par les modèles. L'impact humain évalué par la différence entre le débit observé et le débit naturalisé est inférieur aux incertitudes liées au débit modélisé pour la plupart des régions, en particulier dans le sud de la Chine. Cela indique que l'attribution des changements à l'impact humain n'est pas possible pour ces régions. Alors que, pour la zone d'irrigation intensive (p.e., le nord de la Chine, le centre du Yangtsé), l'impact humain est plus important que les incertitudes, ce qui permet de penser que les changements pourront être attribués aux activités humaines.

La perspective de cette thèse appelle des améliorations dans les modèles pour qu'ils traitent mieux des activités humaines. Les interactions des interventions humaines avec le système d'eau naturel doivent être considérées à une résolution plus élevée de la modélisation de la surface terrestre. L'analyse des incertitudes est également nécessaire pour l'évaluation de l'impact de l'homme, en particulier dans les régions fortement incertaines (p.e., forçage de variables ou de modèles). Ces développements proposés pour les modèles de surface seront discutés plus en détail dans ma thèse chinoise qui sera publiée dans six mois.



# Remerciements

I would like first to thank Jan Polcher, my thesis supervisor at Laboratoire de Météorologie Dynamique, Paris. I still remember you showed me around the lab on the first day I arrived. It seems you opened a door for me to a new world. You not only helped me a lot on the thesis but also taught me how to do scientific works in a right way. I thank you for your supervision during the last three years.

I would also like to thank Tao Yang, my Chinese supervisor at Hohai University, Nanjing. It is now the eighth year since I knew you. I very appreciate it that you guided me in the first steps of doing research and you brought me a lot of new ideas which broaden my knowledge. I also thank you for your support when I am doing the thesis in France.

I would also like to thank Philippe Ciais and Laurent Li to be members of my thesis committee, and for their wise advice during last three years. I thank Eleanor Blyth and Aaron Boone for agreeing to be the reviewers of my manuscript and for their detailed comments and pertinent remarks.

I would also like to thank Thi Kim ngan Ho, Audrey Lemarechal and Xavier Quidelleur for their help in the administration work for my studying in France. I thank Isabelle Ricordel, Philippe Drobinski and other administrative and computer staff at LMD who allowed me to do my research in good conditions.

I would also like to thank all the researchers who have helped to progress my thesis. Particularly, I would also like to Patrice, Matthieu, Zun, Shilong, Xuhui, Shuai, Xiaoming, Feng, Shushi.

I am very grateful to the members of our small working team. Thanks especially to Trung, for your help on the coding and discussion on my questions. And thanks for sharing your stories during our coffee time. Thanks to Fuxing for our discussion on the modelling and after-work entertainment.

Thanks to the people who shared the same office: Adrien, Thibault, Eivind and Marwa. Thanks also to all those who have made my staying colourful: Rodrigo, Bastien, Nicolas, Aurore, Leo, Artemis, Olivier, Marko, Ariel, Sara, Laurent ... Thanks especially to Adrien, Rodrigo, Patrick and those lovely people I could not tell the names for the pleasant time on the basketball court.

My thanks also go to all my friends who lived in the fifth floor of Collège Néerlandais: Akhil, Hassan, Ali, Fouad, Julia, Katia, Martin, Monica, Nana, Selma, Seray ... Thanks especially to Akhil and Hassan for their accompanying and our interesting philosophical discussions. Thanks to Yohanes (John) who is the first foreign friend of mine. Thanks to Shuowen, Yanting, Jia, Xin and other Chinese students for their help when we were together in France.

I would also like to thank the team members in China: Pengfei, Xiaoyan, Zhenya, Tong, Xin, Peng, Xiaoli, Chao... and the classmates Zhenchen, Dongjing, Huating, Wei ... Many

thanks are given to the teachers, classmates and friends during my whole study period.

The most significant thanks are given to my family members. Thanks to my parents and my grandparents for your love and support in my life. Special thanks to my girlfriend Huidi. Thank you for your accompanying in the last six and a half years. Thanks for your understanding and encouragement in my PhD period. Hope we can find our ways and forge ahead together.

Finally, I would like to thank all those I have met and whom I have not had a chance to say thank you. Thank you, et Merci!

# Contents

<b>Résumé en français</b>	<b>iii</b>
<b>Remerciements</b>	<b>xi</b>
<b>1 Introduction</b>	<b>1</b>
1.1 Scientific context	2
1.2 Literature review	3
1.3 Scientific questions and objectives	12
1.4 Plan of the thesis	15
<b>2 Assessment of the uncertainty in precipitation</b>	<b>17</b>
2.1 Introduction	18
2.2 Methodology and datasets	19
2.3 Uncertainty in precipitation products	25
2.4 Variances in precipitation products	34
2.5 Uncertainty and metric comparisons	41
2.6 Discussion and Conclusion	44
<b>3 An ORCHIDEE-Budyko framework to attribute the discharge bias</b>	<b>49</b>
3.1 Introduction	51
3.2 Study area and hydro-meteorological characteristics	53
3.3 Data and Models	54
3.4 Results and discussion	65
3.5 Conclusions	78
<b>4 Human impact on river discharge in China regions - a review</b>	<b>81</b>
4.1 Introduction	82
4.2 How humans change river discharge	83
4.3 Quantification methodologies of the human impacts	96
4.4 Comparisons of human impacts to other uncertainties	106
4.5 Summary	118
<b>5 Conclusions and perspectives</b>	<b>121</b>
5.1 Conclusions	122
5.2 Perspectives	124
<b>A Submitted paper II</b>	<b>127</b>
A.1 Introduction	128
A.2 Methodology	129
A.3 Model application	134
A.4 Discussion and conclusion	138



# 1

## Introduction

### Contents

---

<b>1.1</b>	<b>Scientific context</b> . . . . .	<b>2</b>
<b>1.2</b>	<b>Literature review</b> . . . . .	<b>3</b>
1.2.1	Climate change and hydrological impacts in China . . . . .	3
1.2.2	Uncertainties in modeling discharge . . . . .	6
1.2.3	Uncertainty quantification . . . . .	10
<b>1.3</b>	<b>Scientific questions and objectives</b> . . . . .	<b>12</b>
1.3.1	Scientific questions . . . . .	12
1.3.2	Objectives . . . . .	14
<b>1.4</b>	<b>Plan of the thesis</b> . . . . .	<b>15</b>

---

In this chapter, we present the general background which calls for the further understanding of the topic of uncertainties in climate change and human impacts (section 1.1). Focused on the China regions, we review the associated studies that show the current state of our understanding and the technologies have reached (section 1.2). The scientific questions and the objectives of this thesis are concluded based on the reviewed studies (section 1.3). The thesis structure is introduced in the end (section 1.4).

## 1.1 Scientific context

The global water cycle is undergoing changes in the context of climate change (Gates et al. 2000; Huntington 2006; Gerten et al. 2008). While, the regional signal is more significant as different changes in the trends of river discharge and the occurrence of hydrological extremes (e.g., floods, droughts) are found in different regions (Gates et al. 2000; Wisser et al. 2010; Immerzeel et al. 2010). The spatial variations of hydrological changes are observed in China as well. The river discharge in the Yellow River was sharply decreased in the last century especially in the 1990s as the zero-flow days reached up to 226 days in 1997 (Xu 2004). The occurrence of floods and droughts in the Yangtze River basin are found increasing especially after 2000 (Chen et al. 2014). These regional changes will exert direct influence on local social development and thus require equal attention at a regional scale to that of global scale.

The changes in regional hydrological regimes are a combined result of climate change and human activities (Wang et al. 2010b; Yang et al. 2010; Zhang et al. 2010; Yang et al. 2012a; Zhao et al. 2014; Lu et al. 2015; Jiang and Wang 2016). The changes in climate (e.g., precipitation, temperature) vary across space regarding its trend and its magnitude by the influence of various regional climate systems (IPCC 2013). Moreover, the human activities take place with spatiotemporal variations, and the interactions between human and nature are complex in terms of the physics and the consequences (Piao et al. 2010; Nazemi and Wheeler 2015a; Nazemi and Wheeler 2015b; Wada et al. 2017). It calls for further investigation on how the climate and human are affecting the water cycle as well as the corresponding methodologies for the purpose.

Modeling is a practical way to hindcast the water cycle in the historical period or the future (Döll et al. 2009; Hanasaki et al. 2010; Guimberteau et al. 2012b). Modeling also provides estimates of variables that are difficult to measure but can improve the understanding of water processes (e.g., the soil moisture, the actual evapotranspiration, Potter et al. 2005; Weiß and Menzel 2008). It makes the simulations possible under different scenarios which help to attribute the hydrological changes to different reasons (Chen et al. 2009; Schewe et al. 2014). However, there are many uncertainties which can affect the accuracy of model simulations and result in different conclusions (Beven and Freer 2001; Refsgaard et al. 2006). The uncertainties are either because of the inaccuracy of data measurements or due to the deficiency of the model ability to represent natural physical processes (Moradkhani et al. 2005; Thyer et al. 2009; Montanari et al. 2009). These uncertainties are in many cases interrelated with each other (Renard et al. 2010). Therefore, recognizing the uncertainties and their impact on the water cycle, exploring and disentangling the interactions between uncertainties are essential in the hydrological modeling.

Humans are playing a role in changing the hydrology for the benefit of social development (Haddeland et al. 2006; Wada et al. 2017). However, human interference varies in time and space, and it is especially strong in the area where the agriculture widely distributes and when society is rapidly developing (Haddeland et al. 2006). China is one of the countries that rely highly on agriculture, and it experienced rapid increases in both its population and its economy in the last few decades (Liu et al. 2008; Piao et al. 2010). China also spans a large area with different climate types and topography (Wang et al. 2017a). Thus the water cycle in

China and its responses to the climate and human activities have their different characteristics which need an overall review. The methodologies for estimating the hydrological responses and their peculiarities should be summarized as well for better understanding and utilization of the methodologies.

In this chapter, the current studies on the spatial variations in hydrological changes and the association with climate change and human impacts are reviewed. The descriptions of different uncertainties in hydrological modeling, as well as the current quantification methods of the uncertainties, are also collected and discussed in this chapter. The scientific questions that remain to be investigated are summarized based on the current studies.

## 1.2 Literature review

### 1.2.1 Climate change and hydrological impacts in China

China spans a broad range of longitude and latitude and has complex topographic conditions and climatic features (Wang et al. 2017a). Changes in the climate over China in the meantime have significant spatial variations as the trend in atmospheric variables (e.g., precipitation, temperature) are different at the regional scale (IPCC 2013). In a report by China's National Climate Change Program (CNCCP 2007), it was shown that China observed an average temperature increase of 0.5-0.8 °C during the past 100 years (1900-2000). There was no obvious trend of change in annual precipitation, but there exists considerable variation among regions. The decrease in annual precipitation was significant in the northern China, averaging 2.0-4.0 mm/yr while precipitation was increased in the southern China with a rate of 2.0-6.0 mm/yr. The observed river discharge<sup>1</sup> measures the responses of the land water system to the changing environment, and it has significant spatial variations similar to that of the precipitation. Zhang et al. (2007) analyzed the gauge discharge records in six large river basins in China (i.e., Hai River, Yellow River, Huai River, Yangtze River, Southeast Rivers and Pearl River, Figure 1.1) over period 1950-2004. They concluded that the basins in northern China were experiencing significantly declining in discharge during the study period, especially in the 1990s. Among which the Yellow River, Huai River and Hai River are the basins where the discharge changed significantly. While in southern China, the discharge changes were not apparent (e.g., the Yangtze River, the Southeast and Pearl River). The similar changes are also reported in studies by others and on the tributaries of those large river basins with direct gauge observations (Yang et al. 2005; Yang et al. 2012b; Zhang et al. 2013; Zhao et al. 2013; Wei et al. 2016).

The Yangtze River basin, a representative region of southern China, has the longest river in China with a typical monsoon climate in the middle-low latitudes (Chen et al. 2016). The mean temperature is 14.0 °C and mean precipitation is 1045 mm/yr for the whole Yangtze River basin for 1955-2011 (Chen et al. 2014). The long-term average runoff depth<sup>2</sup> is 515 mm/yr, accounting for 49.2% of the precipitation (Chen et al. 2014). There is a significant

---

<sup>1</sup>Discharge: the volumetric flow rate of water that is transported through a given cross-sectional area.

<sup>2</sup>Runoff depth: the depth to which a watershed (drainage area) would be covered if all of the runoff for a given period of time were uniformly distributed over it.



Figure 1.1 – The map of China and the main rivers.

increase in temperature, but no trend is detected for the precipitation for the Yangtze (Chen et al. 2014). The change in the observed discharge is not significant at the lower Yangtze river (Zhang et al. 2007), while a small but statistically significant increase in discharge and ratio of discharge to precipitation (approximating runoff ratio<sup>3</sup>) is found upstream of the middle Yangtze River (Chen et al. 2014). The increase in the ratio is probably caused by increasing water storage and deforestation, which increases the speed and ratio of surface runoff in the humid Yangtze (Chen et al. 2014). For the source catchment of Yangtze, observed discharge decreased from the 1950s to 1980s and then started increasing in the warming environment (Xiong et al. 2013). Correlation of the discharge change to the cumulative temperature deficit indicates that the glacier melting may induce the discharge increases in the headwater regions of Yangtze River (Xiong et al. 2013). However, the glacier impact is not shown in the middle or lower Yangtze because the proportion of glacier melt becomes small compared to the total runoff in estimations in the lower Yangtze as many river tributaries join the mainstream (Immerzeel et al. 2010). Concerning the seasonal discharge in the middle-low Yangtze, increasing trend (albeit not strong) is detected in the discharge in winter or dry seasons, while the discharge in summer especially in October is decreasing (Chen et al. 2016; Guo et al. 2018). These changes are mainly because of dam constructions and regulations in the Yangtze River basin rather than the climate change as the dams store extra water in flood seasons for reducing the flooding risk and for electricity production, and then it is released in the dry

<sup>3</sup>Runoff ratio: the ratio of the total runoff to the precipitation over a watershed (drainage area).

seasons (Chen et al. 2016). For the other rivers in southern China (e.g., Pearl River, rivers in the southeast), the discharge is mainly influenced by precipitation as for the Yangtze, and the variability of observed discharge is always highly correlated to that of precipitation (Li et al. 2016c). The climate change, especially the precipitation changes, will exert direct impacts on the river discharge.

The Yellow River basin, a representative region of the northern basins, has the second longest river in China with semi-arid climate types (Yang et al. 2015a). The Yellow River originates from the north Qinghai-Tibet Plateau and the changes of water yield<sup>4</sup> in the plateau has significant impacts on the whole Yellow River because the water yield in the upstream accounts for more than 44.8% of that for the whole basin (Wei et al. 2016). The Yellow River has experienced a decreasing trend in discharge ranging from 1.0 mm/10a to 16.1 mm/10a at different gauges (Zhao et al. 2014). The discharge in the 1990s has declined to 34.2% of that in the 1950s (Wei et al. 2016). The zero-flow days occurred in the lower Yellow and increased to the highest (226 days) in 1997 (Xu 2004). Although the changes in forcing variables are also significant as the precipitation was decreased by 11.7 mm/10a (1.9-47 mm/10a, Wei et al. 2016), human activities are generally regarded as the dominant factor of the discharge reduction with their contribution to the discharge ranging between 55-83% by different estimations (Wang et al. 2010b; Yang et al. 2010; Zhao et al. 2014). Various human activities, especially the water consumption for agricultural use, dam storage and the changes in land use are associated with the discharge reduction in different studies (Wei et al. 2016). After 2000, the natural runoff has recovered by 14% in observations, probably because of the combined impacts of precipitation increases (Tang et al. 2013), the reforestation in the middle Yellow (Wang et al. 2011a), and the improved water management among the dams in the whole river basin (Zhang et al. 2009).

With respect to other north river basins such as Songhua River, Liao River, Hai River, Huai River and their tributaries, the observed discharge variations are similar to that of the Yellow River as a significant reduction of discharge is found in the historical period (Zhang et al. 2010; Yang et al. 2012a; Lu et al. 2015; Jiang and Wang 2016). Estimated by different approaches with a set of assumptions, human impacts contribute more to the discharge change than that caused by the climate (Gao et al. 2013; Chang et al. 2016; Jiang and Wang 2016). Increasing water consumption is the main factor controlling discharge change while water projects (e.g., dams and floodgates) also play a role in the discharge change, such as that in the Yellow River (Zhang et al. 2010; Jiang and Wang 2016).

Another hotspot region with significant climate change and hydrological alteration is northwest China, where the climate is dry with very little precipitation (Zhou et al. 2018). The precipitation change varies spatially and shows a remarkable rise in the North Xinjiang (Kong and Pang 2012). Compared to the precipitation, the temperature increase is apparent in northwestern China and over the main rivers of Tarim, Aksu, Heihe River and Urumqi River for instance (Wang et al. 2010b; Kong and Pang 2012). The snowmelt runoff has apparently increased from 1970 to the present in the upstream of the Heihe River (Wang et al. 2010a).

---

<sup>4</sup>Water yield: the total amount of water generated by precipitation, snow and glacier melt and groundwater. It consists of surface runoff, subsurface drainage and groundwater recharge. And it equals to the precipitation over a catchment minus the evapotranspiration back to the atmosphere in area free of glaciers.

The time of snowmelt has shifted ahead and the peak discharge has increased in the snow season (Wang et al. 2010a). Temperature increasing also results in accelerating glacier retreat and increases of glacier melt in the high mountains and river basins where the glacier melting is one of the major sources (e.g., Aksu, Yarkand, Kumalak; Wang et al. 2012a; Kundzewicz et al. 2014; Wang et al. 2017a). Kong and Pang (2012) have pointed out that Kumalak river is more sensitive to climate change than Urumqi River as 57% of the discharge in Kumalak is ice-melt while it is only 9% for the Urumqi River. The relation of the temperature and the glacier melt has been proven with a lag time of the discharge phase (1-3 day time lag between the phases of temperature and the observed discharge, Krysanova et al. 2015).

Although there have been some studies that discussed the climate change impacts on hydrology in northwestern China as presented above, those studies mainly focused on catchments with a very small areas in the river sources regions. Studies for large basins are still lacking. The situation is attributed to two major reasons. First, the collection of high-quality climatic and hydrological data is challenging for large basins because of the coarse gauge network and high heterogeneity of forcing variables in the mountainous area (Zhou et al. 2018). The hydrological processes in the floodplain and oases are more complicated than that in the headwater catchments. Agricultural activities are mainly concentrated over the lower plains and will significantly change the natural discharge, while the effect of human interference in oases is not well understood or quantified in such dry areas (Tao et al. 2011; Zhou et al. 2011).

## Summary

Climate change and the impacts on the hydrology vary in space in mainland China. For the regions in southern China, the precipitation dominates the changes in river discharge, while there are no significant signals in the trends. For the regions in northern China, precipitation has significantly decreased in the last half-century which is in line with the decreasing discharge. However, because humans highly rely on water resources, the contribution of human activities is always regarded as the main contributor to the discharge decline through simulations. Many studies target on eastern China in terms of climate change and hydrological responses because of sufficient data and relatively simple physical interactions in the regions. While for the regions in northwestern China, the estimation of the discharge response is more complicated owing to data scarcity, large spatial heterogeneity, high uncertainty in glacier changes and intensive human activities. The studies over those regions are therefore fewer and need to be strengthened especially in large basins.

### 1.2.2 Uncertainties in modeling discharge

The human impact on river discharge is not easily measurable and needs different models for its estimation. However, the quantitative reconstruction of the changes and impact assessment with models may arrive at different conclusions because the used data are not perfectly describing the natural variables and the models are not perfectly describing the physical processes. There are probably large diversities among the results if different inputs,

different methods or different model settings are used for estimations (Refsgaard et al. 2006). The possible uncertainty sources that may affect the model results are reviewed in this section.

### **Atmospheric variables**

The primary uncertainty comes from the uncertainties in atmospheric variables. For example, as the dominant factor in driving the entire water cycle, the precipitation ( $P$ ) and its measurement are affected by many factors (e.g., the size and location of the orifice of instruments, the recording errors, Dingman 2015; Mcmillan et al. 2012). Wind may significantly reduce the precipitation catch, especially of small drops and snowflakes (Mueller and Kidder 1972; Sevruk 1982). The measurement error tends to be larger for low-intensity precipitation because the amount is not enough to trigger a record and the amount is easy to evaporate (Mcmillan et al. 2012; Neff 1977). The measurement of storm rainfall is also difficult because of the accompanying strong wind. Despite the difficulties of making precipitation measurements, the conversion of precipitation records to what the end users can use introduces other uncertainties. Firstly, because the precipitation records are reported in a fixed short interval (e.g., hourly precipitation, Lenderink and Van Meijgaard 2008), while the data to the public are most in daily, the temporal variations of the records at the sub-daily time scale are therefore not able to be captured with public datasets. Secondly, because the precipitation is measured at point gauges, the precipitation between the gauges are estimated with different interpolation methods which are not necessarily able to describe the spatial heterogeneity (Haddeland 2002). This situation is more serious in the areas with low-gauge density (e.g., mountainous areas, dry areas) and areas with high heterogeneous precipitation events (e.g., orographic rains and storms, Adam et al. 2006; Biemans et al. 2009; D'Orgeval and Polcher 2008). The same problems exist for other forcing variables (e.g., wind speed, temperature, radiation, etc., Xu and Luo 2015). However, because the spatial variations or the impacts of those variables are not as strong as that of the precipitation, the spatial features of other variables have received less attention.

The uncertainty of the temporal and spatial variations in precipitation are partly solved by improving the interpolation algorithms and by using remote sensing (e.g., satellite, radar radiation, Hong et al. 2006; Tapiador et al. 2012). Frequency analysis of hourly precipitation over available gauges reveals the temporal patterns of different precipitation types (e.g., hourly distribution of the precipitation) and can be used to interpolate precipitation in time (Lenderink and Van Meijgaard 2008; Shen et al. 2014). Remote sensing can capture the spatial pattern of the potential precipitation (not the actual precipitation reaching the ground) which helps to describe the spatial heterogeneity (Shen et al. 2014) of the actual precipitation. Statistical approaches have also been developed for the orographic effects of precipitation in mountains (Adam et al. 2006). Precipitation can also be estimated by models (global or regional circulation models). Because these models poorly describe the precipitation spatial patterns, downscaling (e.g., statistically or physical methods) is applied for further usage of the modeled results (Chen et al. 2011; Wilby et al. 2014; Yang et al. 2012b). With the variety of methods, there have been many precipitation datasets that can be used to drive models (Sun et al. 2018). The variations of these precipitation datasets will be quantitatively analyzed in

Chapter 2 in this thesis.

There are many other atmospheric variables (e.g., temperature, radiation, wind) which have similar temporal and spatial variations. Moreover, uncertainties exist for these variables either through measurement or modeling. Although these variables do not directly affect the water flux (e.g., precipitation) entering the system, they change the thermodynamics which can propagate to the estimation of potential evapotranspiration (*PET*). The actual evapotranspiration (*ET*), which denotes the amount of water that leaves land water system and goes back to the atmosphere, will be affected by both the *P* and *PET*. *PET* is not measurable, and there are many kinds of approaches for estimating *PET*. No matter which approach is used, the uncertainty in the aerodynamic variables will propagate to the final *PET* estimations, resulting the uncertainties in *PET*.

## Models

The second source of uncertainty is the model diversity in estimating hydrological responses to climate change. A model is an abstraction, simplification and interpretation of the real world (Refsgaard et al. 2006). Different researchers have developed different algorithms according to their experiments and understanding of the physical processes. The choice of modules is subjective but limited by data sufficiency (Clark et al. 2008). Lumped conceptual models require fewer model inputs than physically based models, and many physical processes in the lumped conceptual models are simplified (e.g., the energy balance, the evaporation estimation, Beven and Freer 2001; Gaume et al. 1998). Moreover, different modules can be selected for the same physical process. For example, both the Green-and-Ampt method and the Horton method estimate the infiltration rates while the Horton equation is empirical (D'Orgeval et al. 2008; Dingman 2015; Yu et al. 1999). The methods for estimating the evaporation are even more varied than that for the infiltration (e.g., the Bowen ratio method, the water-balance method, the Dalton equations, McMahon et al. 2013). The routing processes are simplified using different methods, and two routing module methods can be chosen depending on whether the model is grid-based (e.g., Total Runoff Integrating Pathways-TRIP, Oki and Sud 1998) or basin-based (e.g., Lohmann routing model, Lohmann et al. 1996). All these methods deal with different processes which differ in terms of their basic assumptions, their required data and thus the scope of their application. They are coded to different modules to integrate with the core model. The diversity of modules will result in differences in model outputs, and this can be regarded as the uncertainty in model structures.

These modules have a certain ability to describe the physics. Thus the selection of the module is not very strict. The improvement of the modules is always on the way to integrate the better understanding of physical processes. For example, the land surface model ORCHIDEE (Organizing Carbon and Hydrology In Dynamic EcosystEms) was initially developed in the 1980s by the Laboratoire de Météorologie Dynamique (IPSL-LMD) (Ducoudré et al. 1993). It was directly developed in the GCM but later extracted from the GCM for offline (no coupled) applications (Rosnay and Polcher 1998). The model allowed irrigation interactions with soil moisture after 2003 (Rosnay et al. 2003) and interactions with river discharge after 2005 (Ngo-Duc 2005). Different infiltration methods were tested in 2008 (D'Orgeval and Polcher

2008). The snow and soil freezing scheme was updated in 2012 (Gouttevin et al. 2012). An improved snow scheme was tested in 2013 (Wang et al. 2013a). The routing scheme was also updated recently based on high-resolution (1 km) topography information (Nguyen-Quang et al. 2018). The continuous exploration of the natural physical phenomena with the support of field experiments and numerical models helps drive the development of models and decreases of the uncertainties due to the deficiency of model structures.

The parameters comprise another model uncertainty source. Most of the model parameters have different values over space while they are taken as constants in models for simplification. For example, in the Variable Infiltration Capacity (VIC) model, the maximum soil depth is taken as 1.9 m in the model in all implementations (Rodell et al. 2004). The parameter for the order in variable infiltration equation ranges from 0.2 to 0.6 which is determined by the soil properties, while it is calibrated to be a constant for the entire space (Koch et al. 2016). These parameters are in general “free” and can be calibrated to a particular situation when the model is applied (Refsgaard 1997). However, the shortcoming is that the uncertainty from other sources (e.g., the model inputs and model structures) are probably attributed to the parameters, and in some cases, the parameters will be out of its reliable range to meet the calibration requirements (Zhou et al. 2018). The uncertainty in the parameters is generally reduced by applying field experiments for local studies (El Kateb et al. 2013). However, the parameters obtained from field experiments are still difficult to apply at large scales because of the spatial variations (Haddeland 2002; Xu and Luo 2015). Uncertainty analysis is instead a more popular way to quantify the impacts of parameters to the model results. With the uncertainty analysis, the consequence of the parameter selection can be measured and then controlled within a limit (Beven and Freer 2001). The details of the uncertainty analysis are introduced in section 1.2.3 in this chapter.

### **Human activities**

The third uncertainty is related to human activities (Krzysztofowicz 2001). Human activities (e.g., irrigation, dam regulation, water consumption) have been incorporated into some models as different modules (Hanasaki et al. 2006; Haddeland et al. 2006; Hanasaki et al. 2010; Guimberteau et al. 2012b). Compared to the natural processes, the parameterisation of human activities is more subjective and lacks information. Moreover, there are differences between the real actions and set modules which have been written in models. For example, although the regulation rules for any dams, canal gates and pumps have been set for different occasions, there is a deviation of the real operations from the standard rules because the participation of experts (Ehsani et al. 2016; Nazemi and Wheeler 2015a; Nazemi and Wheeler 2015b). The actual decisions will, to some degree, deviate from what is built in models. These difficulties make the parameterisation hard to correctly represent the human interventions to the natural water cycle.

The uncertainty can also result from unanticipated changes in nature, human goals, interests, activities, demands and impacts especially for future projections (Krzysztofowicz 2001). Concerning human interference with nature, we consider the human impacts to be stable or with a consistent trend in a short future period. However, for example, China’s reform

and opening policy has suddenly stimulated the social-economic development as well as the consumption of water and loss of land area for urbanisation (Liu et al. 2014a; Liu and Tian 2010). On the contrary, from the end of the 20th century, the “Grain for Green” policy has boosted the increasing of forest area, especially in the hydrological-fragile areas. The shift of trends in forest area has caused opposite impacts (increasing river discharge) on the water sphere (Wang et al. 2011a) while negative impacts (decreasing river discharge) are found a few years later which were not considered at the beginning of the afforestation projects (Zhang et al. 2016, discussed in Chapter 4). There are other human activities (e.g., irrigation, dam construction or removal) can start from a specific time in a region but it is difficult to involve them in a model which is designed decades ago without knowing when, where and how the human activities affect the future.

## Summary

In conclusion, there are three major uncertainty sources in hydrological modeling. They are the data uncertainty (also named natural variability or aleatory in the literature), the model uncertainty (also named knowledge uncertainty or epistemic) which includes the uncertainty in model structure and model parameters, and the third uncertainty which results from human interferences. Great efforts (e.g., merged products, improvement in algorithms, experiments) have been done to reduce the uncertainties from the different sources. However, the uncertainties are not and can never be eliminated. Moreover, different uncertainties coexist and also interact in the modeling. There is a necessity to quantify the impact of uncertainty from a single source and separate the impacts from the interaction of multiple sources.

## 1.2.3 Uncertainty quantification

### Uncertainty analysis

The model outputs are subject to imprecision with uncertainty because of the various uncertainty sources introduced above. Uncertainty analysis is a derivation of the probability distribution of the model outputs based on the probabilistic description of model inputs and the models (UNESCO 2005). The uncertainty analysis can be an analytical way that involves all the differentiation of model equations and the exact probability distribution of all model inputs and parameters (Pechlivanidis et al. 2011). It derives the statistics of model output from the knowledge of statistical properties of the system itself and the input data (Langley 2000). However, this approach is strongly limited because of its severe requirements on the data information and model equations (Pechlivanidis et al. 2011). To decrease the difficulty, many assumptions on the data properties and statistical models are required to avoid describing the natural variability and model processes in an overly complex manner (e.g., the standard probability distribution of the parameter, rainfall-runoff equations). Because the method is analyzing the full probability distribution of model input, model structures and model results, it is called probabilistic analysis in Montanari et al. (2009). The philosophy is used by Krzysztofowicz (2002) in a Bayesian Forecasting System and by Montanari and Brath (2004) in a meta-Gaussian rainfall-runoff approach. Other methods based on the Bayesian

basis, can also be used as the probabilistic framework (Montanari 2007), e.g., particle filters (Moradkhani et al. 2005) and Bayesian total error analysis (Thyer et al. 2009).

The alternative solution, which is more commonly used, is to use sampling strategies to derive the statistics of model outputs numerically (Montanari 2007). Uncertainty is quantified by running the model repeatedly with different sets of parameter values sampled from a given probability distribution (Pechlivanidis et al. 2011). Although this approach is computationally expensive, it requires no access to the model equations and avoids simplification of model processes (Pechlivanidis et al. 2011). It thus can be integrated with many existing hydrological models (Zadeh 2005), e.g., TOPMODEL (Beven and Freer 2001), HYMOD (Montanari 2005). The sampling method is the basic philosophy of the Generalized Likelihood Uncertainty Estimation (GLUE) (Beven and Freer 2001; Beven and Prophecy 1993). The Monte Carlo sampling method is always used together with GLUE as it obtains random sampling in the input data space and the system space (Ballio and Guadagnini 2004; Kuczera and Parent 1998). It does not necessarily require the knowledge of the probability of the samples, but the model performance will screen the samples with a given criterion to obtain the collection of samples (Beven and Freer 2001; Beven and Prophecy 1993). With the model results generated by the samples, the statistics (e.g., mean, standard deviation, skewness) and the probability distribution of the model output can be determined. The GLUE-based approaches are limited to the analysis of parameters, and they are not able to deal with the uncertainty in model inputs or model structure (Jacquin and Shamseldin 2007). Because the sampling methods does not provide a probabilistic solution to the parameters, they are regarded as the non-probabilistic way which is different from the probabilistic approach introduced in the previous paragraph (Montanari 2007).

### **Sensitivity tests**

As mentioned above, the analytical approaches desperately require the knowledge of equations on the system input and model itself (Montanari et al. 2009). The sampling approaches are unable to deal with the uncertainties from model inputs and model structures (UNESCO 2005). The sensitivity analysis is instead the most welcoming approach for assessing the impact of different uncertainty sources. The theory of sensitivity analysis is simple since the model simulations are compared in different states with different model settings of interest (e.g., different forcing inputs, different model structure, different model parameters) while keeping all other model settings as the same (UNESCO 2005). The changes in the simulations between different states are regarded as the model sensitivity to the changes in the model settings. Compared to uncertainty analysis, the sensitivity analysis does not need to find and assess all states in the whole feasible spaces, but the users can evaluate any states of interest with very few numbers of model runs compared to the sampling approaches (Tang et al. 2007). The sensitivity test is also a simplification of the sampling approach in assessing the parameter impact by giving only a few parameter settings instead of searching for the whole parameter space. The shortcoming for the sensitivity analysis is that it only evaluates the model sensitivity to the given model settings, it cannot show the real probability distribution of the model outputs (UNESCO 2005). The given model settings are assumed

as equally frequent although they are not in reality and some of the model settings may be probably out of the reliable range because of the low requirement to the understanding of the models (Zhou et al. 2018).

A few implementations of sensitivity tests are listed in Table 1.1. These studies span different regions in China and focus on different hydrological patterns (e.g., total water resources, flood and drought, flood frequency, glacier melt). By applying different numbers and types of the uncertainty sources (e.g., emissions, climate models, downscaling models and hydrological models), the sensitivity of the hydrological change to different uncertainty sources are compared in Table 1.1 in a very simple way as the hydrological sensitivity to different uncertainty sources are placed in an order. The emissions or the downscaling model will not become the primary factor that changes the final model outputs in most of the cases. Because the climate model determines the driving forcing and the hydrological model determine the physical processes of rainfall-runoff change, both are the major factors that result in significant hydrological changes. It is therefore necessary to further investigate how the climate forcing and the hydrological model change the water cycle.

## Summary

In conclusion, knowing the uncertainties from different sources that are further affecting the hydrological model simulations, many studies have focused on different approaches that quantify the hydrological responses to the uncertainties. Uncertainty analysis is frequently used and can be grouped to probabilistic approaches which depend on the full probability distribution, and non-probabilistic approaches which are sampling-based. Sensitivity tests is also an effective way to assess the sensitivity of hydrological responses to different uncertainty sources. Although there have been many implementations related to the uncertainties, research is still needed to deepen the understanding on how the uncertainties, especially from the model inputs and hydrological models, affect the water cycle modeling. The separation of the impact from different sources is not well known. The significance of the human intervention on the water cycle is not clear, especially compared to the uncertainties of the forcing and that of the models.

## 1.3 Scientific questions and objectives

### 1.3.1 Scientific questions

By reviewing the above literature, we can draw a few conclusions as below:

- The model input data uncertainty, especially for the precipitation, has been recognized by the science community. Comparisons between different precipitation datasets have been conducted. However, the precipitation comparison among datasets of different types (e.g., gauge-based datasets, merged productions with satellite or radar, pure model datasets) is lacking, and therefore the uncertainties in different data types are not well assessed.

Table 1.1 – Implementations of sensitivity tests among the emissions, climate models, downscaling models and hydrological models.

No	Region	Target	Emission (RCP)	Climate Model (GCM)	Down-scaling Model	Hydro-logical Model	References
1	Global	water resources		3		8*	Hagemann et al. (2013)
2	China	water availability	2	5*		8*	Li et al. (2016b)
3	Northeastern China	extreme flow	3	6*			Qi et al. (2016)
4	Pearl	flood frequency	3	5	2		Liu et al. (2013a)
5	Xijiang (Pearl)	extreme flow	3	4*	4 *	4	Yuan et al. (2017)
6	Hanjiang (Yangtze)	hydrology	2	20*			Shen et al. (2018)
7	Jinhua (South-east)	High-flow	4	3*	10	3**	Tian et al. (2015)
8	Huai	runoff	3	3			Liu et al. (2012)
9	Benbu (Huai)	drought	3	2		3*	Duan and Mei (2014)
10	Huangfu chuan, xiangxi	discharge		7			Xu and Luo (2015)
11	Tarim	discharge	3	3*			Liu et al. (2013b)
12	Tarim	glacier melt	3	9		6	Duethmann et al. (2016)

Note:

The numbers represent the number of different datasets/methods used in the sensitivity test

\*\* represents that the uncertainty source is the primary

\* represents that the uncertainty source is the primary (or secondary if there is \*\* for any source)

The study case with no stars means the hydrological sensitivity to all sources is equivalent

- The hydrological response to different uncertainty sources are investigated using uncertainty or sensitivity analysis in many implementations. However, the separation of impacts from the interactions of different uncertain sources is not well known, and the reliability of the solutions needs further study and discussion.
- Human activity plays an important role in hydrological changes and is a significant uncertainty source. While, when and how much human activities are affecting the water cycle, particularly in China in the past, present and future, need an overall review. The magnitude of the human impact should also be evaluated and compared with the possible uncertainties from other sources.
- Most of the regions in the eastern Chinese mainland have been well investigated in terms of their climatic characteristics and hydrological changes. However, the regions in northwestern China, e.g., the Tarim basin, have received very little attention owing to the difficulties related to data scarcity, hydrological complexity and human activities. Parallel comparisons to the changes over the whole of China should be conducted as well.

The scientific question are therefore posted as “*what are the magnitudes of various uncertainties, their sources, interactions and spatial variations?*” To address the scientific questions, we need to solve the technical problems as 1) to quantify the uncertainty in the model inputs and the models; 2) to explore the interactions of uncertainty from different sources; 3) to compare the magnitude of human impact with our knowledges of natural variables.

### 1.3.2 Objectives

- Investigate the uncertainties in precipitation, especially for different types of precipitation products; quantify the variances among different precipitation datasets due to the variations between datasets; compare the ensemble variance with the temporal and spatial variances in precipitation patterns; verify the estimated uncertainty with current available technologies.
- Implement a Land Surface Model (ORCHIDEE) in the Tarim basin and estimate the hydrological variables (e.g., discharge, evapotranspiration); analyze the model bias with discharge observations; attributes the bias to uncertainty in model inputs and model structure with a Budyko approach; verify and assess the likelihood of different biases.
- Review the literature of human activities (e.g., land use, water use, dams) in China in the past; review the impact (e.g., magnitudes, spatial and temporal patterns) of different human activities on water cycle; review the methods that are used to quantify the impacts of human activities; categorize the methods and compare the peculiarities of the different methods into different categories;
- Qualify the human impact on river discharge and compare the influence due to the limitation of knowledges of natural variables in the forcing and model simulations;

identify the metrics that can be used to attribute the human impact and identify the catchments where the human impact assessment is easier and with higher confidence.

## 1.4 Plan of the thesis

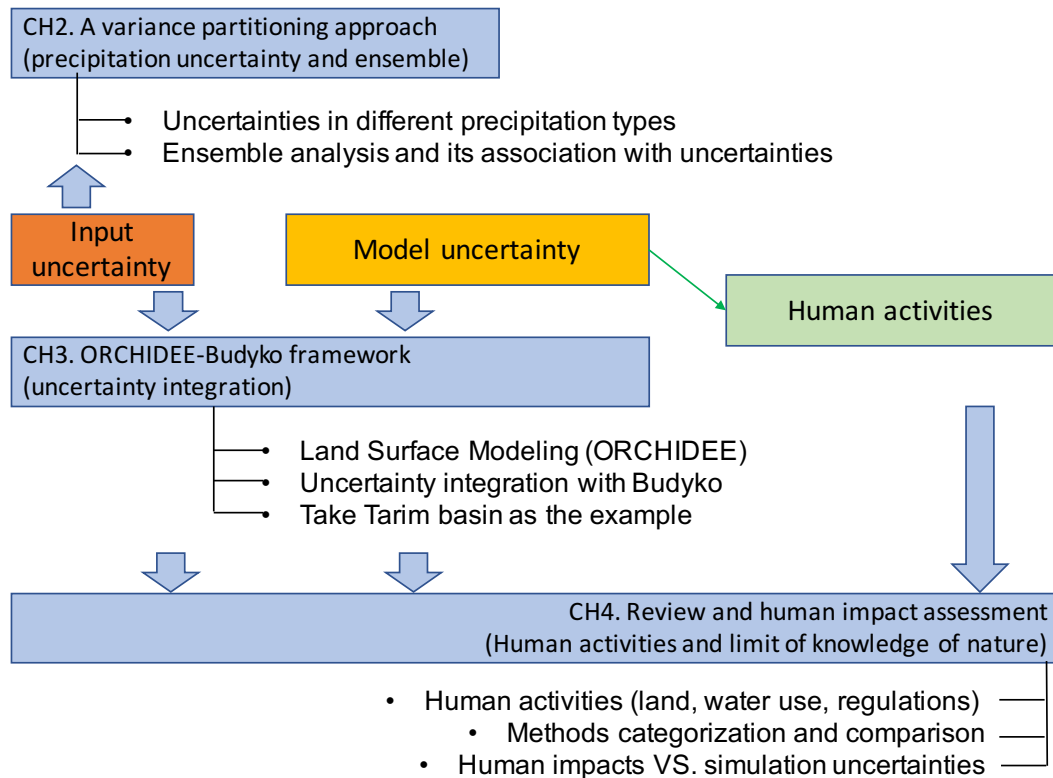


Figure 1.2 – Flow-chart of the thesis

The structure of the thesis is organized as follows (refer to the illustration in Figure 1.2).

In Chapter 1, the background of the research topics, the related literature, the scientific questions and the objectives of the thesis are introduced.

In Chapter 2, a new approach of partitioning the variances in an ensemble analysis is introduced and applied to precipitation datasets. The uncertainties of different types of precipitation are analyzed and associated with the uncertainty estimation with the newly proposed approach.

In Chapter 3, a framework named ORCHIDEE-Budyko, which can be used to attribute the model bias in discharge estimation to the uncertainties in model inputs and the model itself, is introduced. The Tarim basin is chosen as the example.

In Chapter 4, the recent literature about human activities, particularly in China, is reviewed in terms of understanding the impacts on hydrology. The methods that have been used to estimate the human impacts are also reviewed, and their peculiarities are compared between different approaches. The human impact identified by the difference between observed and naturalized river discharge is compared with the influence due to limitation of our knowledges of natural variables on the forcing variables and estimated water cycle.

In Chapter 5, the conclusions are summarized based on the previous chapters. The key points are further explained and discussed. The perspectives are provided on the basis of the results of the thesis.

# 2

## Assessment of the uncertainty in precipitation

### Contents

---

<b>2.1</b>	<b>Introduction</b>	<b>18</b>
<b>2.2</b>	<b>Methodology and datasets</b>	<b>19</b>
2.2.1	Mathematical Derivation	20
2.2.2	Study area and data descriptions	23
<b>2.3</b>	<b>Uncertainty in precipitation products</b>	<b>25</b>
2.3.1	Uncertainty between different precipitation groups	25
2.3.2	Uncertainties in space	29
2.3.3	Uncertainties across time	30
2.3.4	Variations in the time and space dimensions	32
<b>2.4</b>	<b>Variances in precipitation products</b>	<b>34</b>
2.4.1	Variances in three dimensions	34
2.4.2	Variance proportions in three dimensions	35
2.4.3	Deviations in three dimensions	38
<b>2.5</b>	<b>Uncertainty and metric comparisons</b>	<b>41</b>
2.5.1	Uncertainty and standard deviations	41
2.5.2	Decomposing the ensemble variance	42
2.5.3	Uncertainty with other metrics	43
<b>2.6</b>	<b>Discussion and Conclusion</b>	<b>44</b>

---

2.6.1	What is the uncertainty means among precipitation groups . . . . .	44
2.6.2	Features and applicability of the approach . . . . .	46
2.6.3	Conclusion . . . . .	46

---

In this chapter, we present a new approach which can be used to estimate uncertainties among multiple datasets. Precipitation is taken as the example variable to explain the features of the new approach. The uncertainty characteristics within multiple precipitation products of different types and their physical meanings are analyzed as well. The background of the uncertainties in precipitation and the trend of using multiple ensembles to reduce the uncertainty influence are introduced in section 2.1. The proposed three-dimensional approach is introduced in the methodological part (section 2.2). The general precipitation characteristics and the differences in different precipitation types are presented in section 2.3. The diagnostics of the precipitation with new approach are shown in section 2.4 and their comparisons discussed in section 2.5. Following is the section of discussion and conclusion (section 2.6).

## 2.1 Introduction

Precipitation is the dominant variable in the global water cycle. The amount of precipitation is vital in assessing the water resources of a specific place, and the accuracy determines the quality of water cycle modeling. The gauge measurements of precipitation are considered to have high data quality. However, the accuracy does not perform well in spaces with high spatial heterogeneity in mountainous areas and during storms (Hijmans et al. 2005; Roe 2005; Andermann et al. 2011). A few different interpolation methodologies were introduced to covert these point measurements to spatial datasets and therefore a few grid-based precipitation datasets have been released for grid-analysis (e.g., Harris et al. 2014; Scheff and Frierson 2015). With technologies supported by remote sensing and radar detection, the spatial distribution of precipitation can be obtained and then merged with the gauge observations for scientific and general usage (Zhao and Fu 2006; Adler et al. 2018; Sun et al. 2018). Datasets only driven by models are also available (e.g. General Circulation Models, GCMs) especially for the implementations in the historical period before measurements and the future (Li et al. 2011a; Chadwick et al. 2013; Wang and Chen 2014).

Because of the differences in the used information (e.g., observations from different gauges, different remote sensing products) and the methodologies (e.g., interpolation methods or climate model algorithms), there are differences between different precipitation products. The differences between the precipitation products are also called uncertainties. Many studies have attempted to understand and quantify the uncertainties of precipitation. Although the causes to the uncertainties have been generally summarized, quantification and removal of the uncertainties are still limited over large spaces. Using the ensembles consisting of multiple models to generate a weighed simulation have become popular in the climate-related research (Milly et al. 2005; Christensen and Lettenmaier 2006; Tebaldi et al. 2011; Yang et al. 2012a; Schewe et al. 2014). This method has been widely accepted and applied because it reduces the

requirements for understanding the uncertainties. It also reduces the dependence on a single dataset and the risk of large deviations in individual datasets. A few statistical metrics are used to quantify uncertainties among the multiple datasets for an ensemble.

The standard deviation is the most popularly used index to measure the extent of the deviation of a data group. It is most used for evaluating the results at different time steps for the spatial mean (Seneviratne et al. 2016; Shen et al. 2018) or seen as a map of the standard deviation for temporal means (Rocheta et al. 2014). However, the approach can provide only the deviation of results in only one of the spatiotemporal dimensions. It is unavoidable because the standard deviation approach only operates in one dimension. Similar to the standard deviation, the uncertainties can be taken in quantiles (e.g. 75%(25%) or 95%(5%) of the results, Orlowsky and Seneviratne 2014). The approach is especially applicable to the variables that are not normally distributed (e.g., precipitation). However, the standard deviation approach uses collapsed information in either the spatial or temporal dimension. It also needs a sufficient number of models for obtaining the quantiles.

If the number of models are sufficient, the consensus of multiple models is sometimes taken as the measurement of uncertainties. It is measured as the ratio of models agreeing on a certain conclusion to the whole number of models. For example, in Figure SPM.8-b in the IPCC report (Stocker et al. 2013), stipplings are used to indicate grid boxes where more than 90% of the members agreed on the sign of rainfall change while leaving as white where 66% of models do not agree on either increases or decreases in rainfall. It only evaluates the variation on the final conclusions but ignores the processes. It also requires quite a large number of models to generate a reliable number ratio so that the method is limited in applications with a large number of similar inputs (e.g. GCMs).

A few indices have been developed to quantify the uncertainties in results for the water cycle components (e.g. precipitation). These indices have disadvantages that they only evaluate the uncertainty in one dimension (time or space) with the other dimension collapsed by averaging. Because of the limitation, the temporal variations or the spatial heterogeneity is ignored in obtaining the uncertainty range. The uncertainty results thus cannot reveal the model variation based on spatiotemporal dimension as a whole. Moreover, a sufficient number of models is needed for these indices especially for the quantiles and consensus which restricts their applicability. In this study, we aim to introduce a new approach which can quantify the model variation over spatiotemporal dimensions without any aggregation in time or space. The uncertainty among the multiple ensemble products is also evaluated with the new approach. Examples for precipitation are provided for better understanding of the properties of the present approach.

## 2.2 Methodology and datasets

The coefficient of variation (Cv), also known as the relative standard deviation (a ratio of the standard deviation to the mean,  $\sigma^2/\mu$ ), is a standardized measure of dispersion of a probability distribution or frequency distribution (Everitt 2013). However, it works for one dimension as the previously introduced indices, leading to the fact that regional aggregation is

obligatory for generating the regional means or evaluating the temporal variation (McSweeney and Jones 2013). Scheffe (1999) introduced the grand variance that measures the total variations across time and space dimensions. Sun et al. (2010) partitioned the grand variance into temporal and spatial dimensions, named as time variance and space variance, respectively. The variance is closely associated with the variation at each time step (or at each grid), but it integrates the variation in the time dimension (or the space dimension) to evaluate the overall performance in this dimension. The relative amount of the variance determines the dominant dimension which contributes more to the data variation. For example, the space variance of global annual-average temperature is much larger than time variance since the temperature difference in regions (from the equator to polar) is generally larger than the differences among seasons in a specific region. Moreover, the temperature difference between latitude zones is more significant than that between time steps. The approach prevents aggregation before spatiotemporal analysis, and all the spatial and temporal variation remains for evaluation.

By analogy, when using multiple models as an ensemble, the grand variance of the whole dataset is therefore related to not only the spatial or temporal variations but also the variations among different models. The partitions of the total grand variance can expand to time variance, space variance and the third component "ensemble variance" which represents the intra-ensemble variations (namely the variation of the values in different models at the same time step and same grid point). For climatic variables, the temporal and spatial variations are inherent, while the ensemble variation is artificially induced by using multiple models. With a lower proportion of ensemble variance to the grand variance, the ensemble members are more consistent with each other, and the agreement level of the ensemble results is higher since less uncertainty comes from the model variations. It therefore can serve as an indicator of the agreement among ensemble members for regional analysis and measures uncertainty in the model ensemble output.

### 2.2.1 Mathematical Derivation

The dataset has to be organized in three dimensions of (1) time with a regular time interval (e.g. monthly or annual), (2) space with regular spatial units where all the grids are re-organized in a new dimension from the original latitude-longitude grids, (3) ensemble with different ensemble members regarded as the third dimension. Thus, the dataset array can be reformed as

$$\mathbf{Z} = [z_{ijk}] \quad (2.1)$$

with  $i$ -th time step ( $i = 1, 2, \dots, m$ ),  $j$ -th grid ( $j = 1, 2, \dots, n$ ), and  $k$ -th ensemble member or ensemble model ( $k = 1, 2, \dots, l$ ).

We define the three dimensions as time, space and ensemble dimension and the means for these three dimensions are called temporal mean, spatial mean and ensemble mean, respectively. The corresponding variances are named time variance, space variance and ensemble variance, respectively. The grand mean ( $\mu$ ), grand variance across time, space and

ensemble models ( $\sigma^2$ ) as well as the total sum of squares ( $SST$ ) are defined as.

$$\mu = \sum_{i=1}^m \sum_{j=1}^n \sum_{k=1}^l z_{ijk} / (mnl) \quad (2.2)$$

$$\sigma^2 = \frac{SST}{mnl - 1} \quad (2.3)$$

$$SST = \sum_{i=1}^m \sum_{j=1}^n \sum_{k=1}^l (z_{ijk} - \mu)^2 \quad (2.4)$$

The derivation starts from the third ensemble dimension. For a specific  $k^{th}$  ensemble member, the grand mean is formulated as  $\mu_{ts}[k] = \sum_{i=1}^m \sum_{j=1}^n z_{ijk} / (mn)$ , leading to the total squares rewritten as

$$SST = \sum_{i=1}^m \sum_{j=1}^n \sum_{k=1}^l (z_{ijk} - \mu_{ts}[k] + \mu_{ts}[k] - \mu)^2 \quad (2.5)$$

and then expanded and rearranged as

$$\begin{aligned} SST = & \sum_{i=1}^m \sum_{j=1}^n \sum_{k=1}^l (z_{ijk} - \mu_{ts}[k])^2 \\ & + 2 \times \sum_{k=1}^l (\mu_{ts}[k] - \mu) \underbrace{\left[ \sum_{i=1}^m \sum_{j=1}^n (z_{ijk} - \mu_{ts}[k]) \right]}_{=0} \\ & + \underbrace{\left[ \sum_{i=1}^m \sum_{j=1}^n \right]}_{=mn} \sum_{k=1}^l (\mu_{ts}[k] - \mu)^2 \end{aligned} \quad (2.6)$$

$$SST = \sum_{i=1}^m \sum_{j=1}^n \sum_{k=1}^l (z_{ijk} - \mu_{ts}[k])^2 + mn \sum_{k=1}^l (\mu_{ts}[k] - \mu)^2 \quad (2.7)$$

$$SST = (mn - 1) \sum_{k=1}^l \sigma_{ts}^2[k] + mn(l - 1)\sigma^2(\mu_{ts}) \quad (2.8)$$

Where  $\sigma^2(\mu_{ts})$  is the variance of the grand mean for each member of the ensemble, and  $\sigma_{ts}^2[k]$ , the grand variance in space and time for ensemble member  $k$ , can be split using the average of the space variance at each time step  $\sigma_s^2[k, :]$  and the variance of the spatial mean  $\sigma^2(\mu_s[k, :])$ , denoted as

$$\sigma_{ts}^2[k] = \frac{m(n-1)}{mn-1} \sigma_s^2[k, :] + \frac{n(m-1)}{mn-1} \sigma^2(\mu_s[k, :]) \quad (2.9)$$

One can refer to Sun et al. (2010) and Sun et al. (2012) or Supporting Information Text S1.1 for detailed derivations of  $\sigma_s^2[k, :]$  and  $\sigma^2(\mu_s[k, :])$ . Similarly,  $\sigma_{ts}^2[k]$  can also be split into the average of the time variance from all regions  $\sigma_t^2[:, k]$  and the space variance of the temporal

mean  $\sigma^2(\mu_t[:, k])$ , expressed as

$$\sigma_{ts}^2[k] = \frac{n(m-1)}{mn-1} \overline{\sigma_t^2[:, k]} + \frac{m(n-1)}{mn-1} \sigma^2(\mu_t[:, k]) \quad (2.10)$$

With Eq. (2.9) and Eq. (2.10), we can have

$$\sigma_{ts}^2[k] = \frac{1}{2} \left\{ \frac{m(n-1)}{mn-1} [\sigma^2(\mu_t[:, k]) + \overline{\sigma_s^2[k, :]}] + \frac{n(m-1)}{mn-1} [\sigma^2(\mu_s[k, :]) + \overline{\sigma_t^2[:, k]}] \right\} \quad (2.11)$$

Substituting Eq. (2.11) into Eq. (2.8) results in

$$\begin{aligned} SST = & \frac{m(n-1)}{2} \sum_{k=1}^l [\sigma^2(\mu_t[:, k]) + \overline{\sigma_s^2[k, :]}] \\ & + \frac{n(m-1)}{2} \sum_{k=1}^l [\sigma^2(\mu_s[k, :]) + \overline{\sigma_t^2[:, k]}] + mn(l-1)\sigma^2(\mu_{ts}) \end{aligned} \quad (2.12)$$

The first term on the right-hand side of Eq. (2.12) can be transformed to:

$$\frac{m(n-1)}{2} \sum_{k=1}^l [\sigma^2(\mu_t[:, k]) + \overline{\sigma_s^2[k, :]}] = lm(n-1) \left[ \frac{\overline{\sigma_{s-t}^2} + \overline{\sigma_s^2}}{2} \right] \quad (2.13)$$

where  $\overline{\sigma_{s-t}^2}$  is the average of space variance of the temporal mean across each ensemble member,  $\overline{\sigma_s^2}$  represents the grand mean of  $\sigma_s^2$ , the grand variance across time and ensemble dimensions. Then Eq.(2.12) becomes:

$$SST = lm(n-1) \left[ \frac{\overline{\sigma_{s-t}^2} + \overline{\sigma_s^2}}{2} \right] + ln(m-1) \left[ \frac{\overline{\sigma_{t-s}^2} + \overline{\sigma_t^2}}{2} \right] + mn(l-1)\sigma_e^2(\mu_{ts}) \quad (2.14)$$

where  $\overline{\sigma_{t-s}^2}$  is the average of time variance of the spatial mean across ensembles,  $\overline{\sigma_t^2}$  represents the grand mean of  $\sigma_t^2$ , the grand variance across space and ensemble dimensions.  $\sigma_e^2(\mu_{ts})$  represents the variance of the spatial-temporal means ( $\mu_{ts}$ ). Similarly, the derivation can start from any of the other two dimensions. The SSTs derived from time and space dimensions are formulated, respectively, as

$$SST = lm(n-1) \left[ \frac{\overline{\sigma_{s-e}^2} + \overline{\sigma_s^2}}{2} \right] + mn(l-1) \left[ \frac{\overline{\sigma_{e-s}^2} + \overline{\sigma_e^2}}{2} \right] + nl(m-1)\sigma_t^2(\mu_{se}) \quad (2.15)$$

$$SST = nm(l-1) \left[ \frac{\overline{\sigma_{e-t}^2} + \overline{\sigma_e^2}}{2} \right] + nl(m-1) \left[ \frac{\overline{\sigma_{t-e}^2} + \overline{\sigma_t^2}}{2} \right] + ml(n-1)\sigma_s^2(\mu_{et}) \quad (2.16)$$

Where each variable is defined in the Supporting Information Text S1.2. Averaging these three SSTs defined in Eqs. (2.14) - (2.16) leads to

$$\begin{aligned} SST = & \frac{nl(m-1)}{3} \left[ \frac{\overline{\sigma_{t-s}^2} + \overline{\sigma_{t-e}^2}}{2} + \overline{\sigma_t^2} + \sigma_t^2(\mu_{se}) \right] \\ & + \frac{lm(n-1)}{3} \left[ \frac{\overline{\sigma_{s-t}^2} + \overline{\sigma_{s-e}^2}}{2} + \overline{\sigma_s^2} + \sigma_s^2(\mu_{et}) \right] \\ & + \frac{mn(l-1)}{3} \left[ \frac{\overline{\sigma_{e-t}^2} + \overline{\sigma_{e-s}^2}}{2} + \overline{\sigma_e^2} + \sigma_e^2(\mu_{ts}) \right] \end{aligned} \quad (2.17)$$

With the total degree of freedom ( $m \times n \times l - 1$ ), the grand variance is expressed as

$$\begin{aligned} \sigma^2 = & \underbrace{\frac{nl(m-1)}{3(mnl-1)} \left[ \frac{\overline{\sigma_{t-s}^2} + \overline{\sigma_{t-e}^2}}{2} + \overline{\sigma_t^2} + \sigma_t^2(\mu_{se}) \right]}_{V_t} \\ & + \underbrace{\frac{lm(n-1)}{3(mnl-1)} \left[ \frac{\overline{\sigma_{s-t}^2} + \overline{\sigma_{s-e}^2}}{2} + \overline{\sigma_s^2} + \sigma_s^2(\mu_{et}) \right]}_{V_s} \\ & + \underbrace{\frac{mn(l-1)}{3(mnl-1)} \left[ \frac{\overline{\sigma_{e-t}^2} + \overline{\sigma_{e-s}^2}}{2} + \overline{\sigma_e^2} + \sigma_e^2(\mu_{ts}) \right]}_{V_e} \end{aligned} \quad (2.18)$$

where  $V_t$ ,  $V_s$  and  $V_e$  represent the time, space and ensemble variances, respectively. The partitions of the three dimensions are symmetrical. To facilitate the understanding of the partitioning results, a visual illustration of the present approach is shown in Figure 2.1.

Note that  $V_e$  is based on the combination of variance across the ensemble dimension of temporal and spatial values ( $\overline{\sigma_e^2}$ , zone B3), temporal mean ( $\overline{\sigma_{e-t}^2}$ , zone C3), spatial mean ( $\overline{\sigma_{e-s}^2}$ , zone C6) and the grand variance of the spatiotemporal mean for a single ensemble member ( $\sigma_e^2(\mu_{ts})$ , zone F3). These variances rely on different zones, which displays the symmetry of the partitioning results.

To explore the relative effects of the three parts, we can quantify the contribution of each part to the total grand variance. The variance proportions are therefore defined as:  $P_t = V_t/\sigma^2$  for time;  $P_s = V_s/\sigma^2$  for space and  $P_e = V_e/\sigma^2$  for ensemble dimension. Similar to the definition of standard variation and standard deviation, the deviation in this three dimensional approach can be quantified as the ratio of the square root of the variance to the grand mean (i.e.,  $U = \sqrt{V}/\mu$  for the grand variance,  $U_t = \sqrt{V_t}/\mu$  for the time dimension,  $U_s = \sqrt{V_s}/\mu$  for the spatial dimension and  $U_e = \sqrt{V_e}/\mu$  for the ensemble dimension). For the ensemble dimension, the  $P_e$  is a measurement of the variation among models which integrates the variations in time and space dimensions. The  $U_e$  is a measurement of the relative uncertainty among the models. Both the two metrics avoid any aggregation of spatiotemporal dimensions.

### 2.2.2 Study area and data descriptions

China is large in its area, and different climate types are encountered in the mainland (Kottek et al. 2006). To facilitate the comparisons and analysis that have spatial variations, ten different regions are defined in Figure 2.2 as the (1) Songhua River Basin, (2) Liao River Basin, (3) Hai River Basin, (4) Yellow River Basin, (5) Huai River Basin, (6) Yangtze River Basin, (7) Southeast China, (8) South China, (9) Southwest China, (10) Northwest China. The entire Chinese mainland is numbered as the 11<sup>st</sup> region. Most of the regions are natural river basins, and this definition is better in water resources analysis than definitions using longitude-latitude grids or that are based on administrative regions.

As shown in Table 2.1, thirteen precipitation datasets from different sources are collected

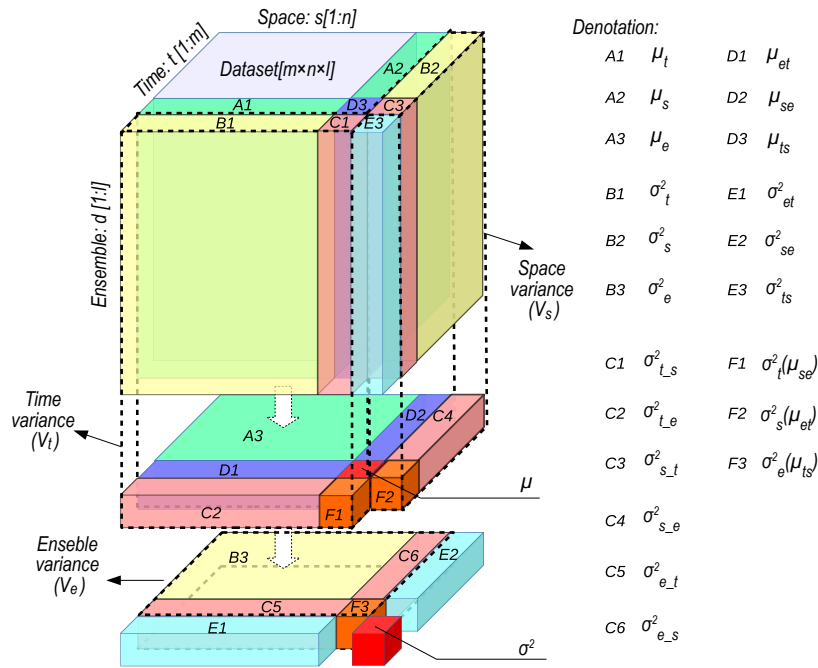


Figure 2.1 – The illustration of the partitioning time-space-ensemble variance method. The original dataset is organized in three dimensions of time, space and ensemble. The denotations of the zones are listed to the right. The grand variance is defined as  $\sigma^2$  and the grand mean  $\mu$ . The subscripts  $t$ ,  $s$ , and  $e$  represent time, space and ensemble, respectively. Zone A ( $\mu_i$ ) indicates the average mean in for  $i$  dimension; zone B ( $\sigma_i^2$ ) indicates the variance for  $i$  dimension; zone C ( $\sigma_{i,j}^2$ ) indicates the variation across  $i$  dimension of the average means of  $\mu_j$ ; zone D ( $\mu_{ij}$ ) indicates the average means across  $i$  and  $j$  dimensions; zone E ( $\sigma_{ij}^2$ ) indicates the variation across  $i$  and  $j$  dimensions; zone F ( $\sigma_i^2(\mu_{jk})$ ) indicates the variation across  $i$  dimension of the average means across  $j$  and  $k$  dimensions. The detailed definitions of these denotations can be found in Supporting Information Text S1.2.

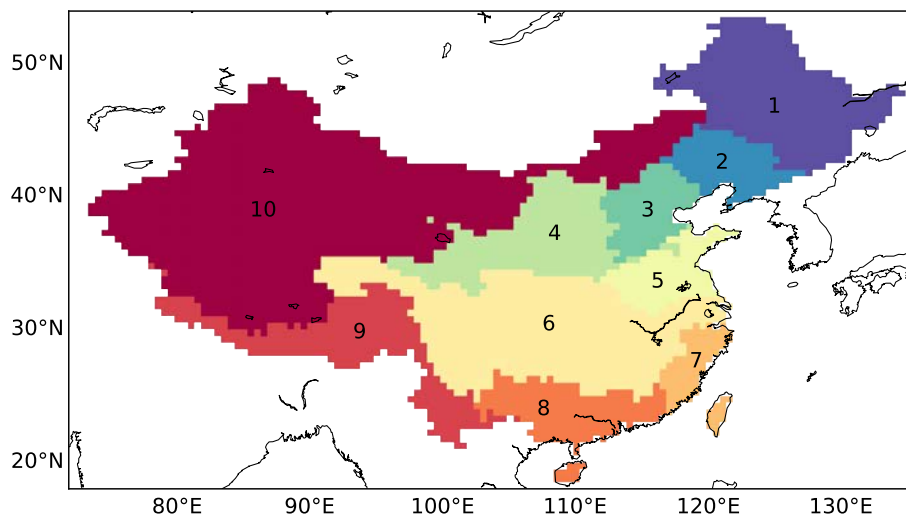


Figure 2.2 – The regions in China that defined in this chapter.

for comparison. All these datasets are categorized into three groups, i.e., gauge-based products, merged products and General Circulation Models (GCMs). The gauge-based products only rely on the gauge measurements, but the collected gauges and algorithms to generate the precipitation map are different among different products. CMA (China Meteorological Administration) dataset uses the densest gauges and probably has the best quality to capture the spatiotemporal variations of the precipitation. CMA is therefore chosen as the reference datasets for comparisons, and it is excluded when estimating the ensemble means of the gauge-based products.

The merged precipitation products rely on databases from many various sources including satellite remote sensing, radar radiation or re-analysis dataset. These datasets are also assimilated with gauge observations to correct potential biases. The GCMs precipitation is modeled without correction from any measurements. The difference among GCMs is therefore a result of the model differences (e.g., initial conditions, model algorithms, numerical simulations). They also have a different synoptic variability as they are not constrained to follow a specific trajectory in the manifold of all possible climatic solutions. There are more than 20 datasets of GCMs, while only four are randomly taken to match the number of gauge-based products and merged products. All the datasets have been interpolated to  $0.5^\circ$  spatial resolution. The overlap time span of all the datasets is from 1979 to 2005 for the maximum coverage of all products. Four different products are included in each precipitation group, which can explain more than 80% of the uncertainties when much more models are used. The details of the explanation is shown in the appendix A.

## 2.3 Uncertainty in precipitation products

### 2.3.1 Uncertainty between different precipitation groups

The ensemble means of the long-term annual precipitation (1979-2005) at each grid are estimated and mapped as Figure 2.3. The ensemble mean of the gauge-based products has excluded the CMA dataset. The ensemble means for the precipitation in three groups are obtained by averaging the datasets in corresponding group. The annual precipitation is 589.8 mm/yr (1.6 mm/day) in the China mainland with CMA data (Table 2.2). The absolute bias in other gauge-based products, merged products and GCM is -4.1, 63.1, 232.0 mm/yr (with the bias as -0.7%, +20.4% and +41.3%) respectively. The spatial pattern of the annual precipitation shows a decreasing trend from the southeast China (>1600 mm/yr) to the northwest China (<400 mm/yr) and all the ensemble means for the three groups capture the spatial gradient.

However, because of the deviation of precipitation in different groups, the land area with a certain magnitude of annual precipitation can change and shift in its locations. The annual precipitation is an important factor that determines the climate type in the Köppen-Geiger climate classification system (Kottek et al. 2006). For instance,  $2.66 \times 10^6 \text{ km}^2$  (28.2% of the China mainland area) has annual precipitation more than 800 mm/yr in CMA dataset, which can be categorized as the humid region (Table 2.2).  $3.88 \times 10^6 \text{ km}^2$  has annual precipitation less than 400 mm/yr, belonging to the dry area.  $2.89 \times 10^6 \text{ km}^2$  locates in the transition area, with annual precipitation between 400 and 800 mm/yr.

Table 2.1 – The precipitation datasets used in this chapter.

No	Type	Name	Long name	Version	Resol	Time-scale	Institute	Reference
1		CMA	China Meteorological Administration dataset	2018	0.5°	Daily	China Meteorological Administration	
2		GPCC	Global Precipitation Climatology Centre	v7	0.5°-2.5°	1901-present	the World Climate Research Programme (WCRP) and to the Global Climate Observing System (GCOS)	Schneider et al. (2017)
3	Gauge-based	CRU TS	Climatic Research Unit Series	3.24	0.5°	1901-2015	Climatic Research Unit (CRU) / Ian Harris, Phil Jones	Harris et al. (2014)
4		CPC	CPC Global Unified Gauge-Based Analysis of Daily Precipitation	Update Daily	0.5°	1979-present	NCEP/Climate Prediction Center	Xie et al. (2007)
5		UDEL	University of Delaware Air Temperature & Precipitation Global (land) precipitation and temperature	v4.1	0.5°	1900-2014	University of Delaware	Willmott and Matsuura (2012)
6		CMA	CPC Merged Analysis of Precipitation	V1808	2.5°	1979-2018	NOAA CPC	Xie et al. (2003)
7	Merged Products	GPCP	Global Precipitation Climatology Project	V2.3	2.5°	1979-2018	GSFC (NASA)	Adler et al. (2018)
8		MSWEP	Multi-Source Weighted-Ensemble Precipitation		0.1°	1979-2017	Princeton University, Princeton, NJ, USA	Beck et al. (2017)
9		ERA-I	ERA-Interim		~0.7°	1979-2012	European Centre for Medium-Range Weather Forecasts	Dee et al. (2011)
10		HadCM3	Hedley Centre Model Version 3	2011	3.75°×2.47°	1859-2005	Met Office Hadley Centre, UK	
11	GCMs	IPSL-CM5A-LR		2011	3.75°×1.825°	1850-2005	Institut Pierre Simon Laplace, Paris, France	
12		CMCC-CM		2011	0.75°×0.75°	1850-2005	Centro Euro-Mediterraneo per I Cambiamenti	
13		MIROC5		2011	1.4°×1.4°	1850-2005	AORI, Chiba, Japan, NIES, Ibaraki, Japan, JAMSTEC, Kanagawa, Japan	

For precipitation from other products, the statistics demonstrate the differences in climate pattern determined by annual precipitation. The spatial patterns of the gauge-based products are almost the same as that of the CMA data. The area of the dry area decreases by  $0.67 \times 10^6 \text{ km}^2$  in the merged products compared to that of the observations, while the transition and humid area increases by  $0.29 \times 10^6 \text{ km}^2$  and  $0.38 \times 10^6 \text{ km}^2$  respectively. The GCMs produce more precipitation than the other two groups, and the dry area decreases the most by 16.4% while the humid area increases by 53.7% compared to that identified by the observations. Although the change in the ratio within the transition area is very small (+3.1%), the area moves northward.

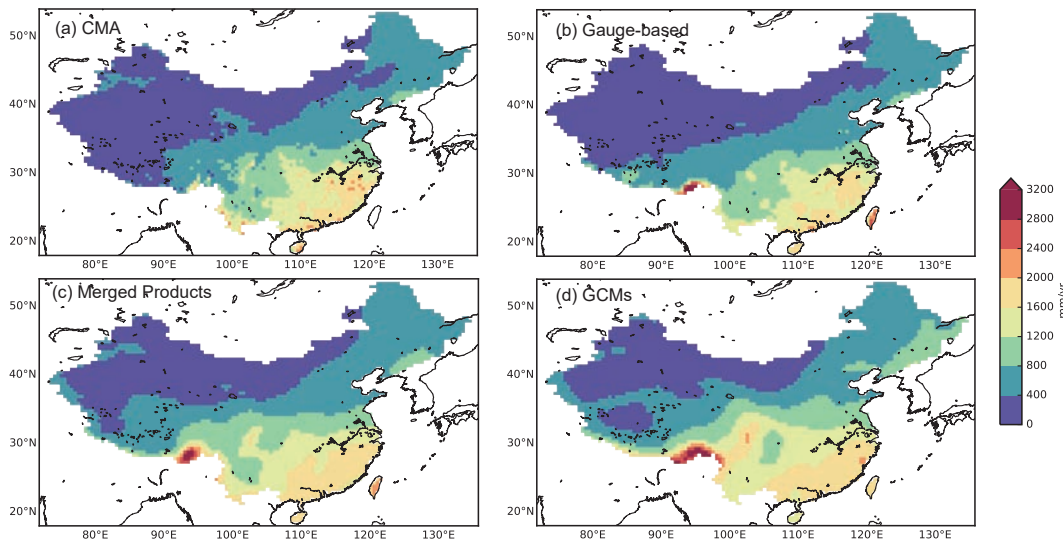


Figure 2.3 – Long-term (1979-2005) annual precipitation in different precipitation groups. (a) Annual precipitation of CMA dataset, (b) ensemble means of annual precipitation in gauge-based products excluding CMA, (c) ensemble mean of annual precipitation of all merged products, (d) ensemble man of annual precipitation of all GCMs. CMA has no observations in Taiwan.

Table 2.2 – The averaged annual precipitation (mm/yr) in different precipitation groups (i.e., CMA, gauge-based products, merged products and GCMs) and the area with different precipitation magnitudes as well as the proportion (Prop.) of the area to the whole China mainland. The unit of the area is  $10^6 \text{ km}^2$ . The area of Taiwan region is not included in the CMA dataset.

Datasets	CMA		Gauge-based		Merged		GCMs	
	Value	Bias	Value	Bias	Value	Bias	Value	Bias
Annual Precipitation	589.8	–	585.7	-4.1	710.2	120.4	833.1	243.3
Precipitation magnitude	Area	Prop.	Area	Prop.	Area	Prop.	Area	Prop.
<400 mm	3.88	0.410	3.87	0.409	2.80	0.296	2.26	0.239
400-800 mm	2.89	0.305	2.87	0.303	3.18	0.336	2.93	0.310
>800 mm	2.66	0.281	2.72	0.288	3.48	0.368	4.27	0.451

The differences in annual precipitation of gauge-based products from CMA dataset are within 200 mm/yr and 25% in ratio for the major part of the mainland (Figure 2.4-a,b).



### 2.3.2 Uncertainties in space

In addition to the precipitation difference found in the three precipitation groups when compared to the CMA, there are also differences among datasets within the same precipitation group. The spatial standard deviation (s.std) of the annual precipitation among different datasets is calculated. The ratio of the s.std to the annual precipitation in CMA dataset is also mapped in Figure 2.5.

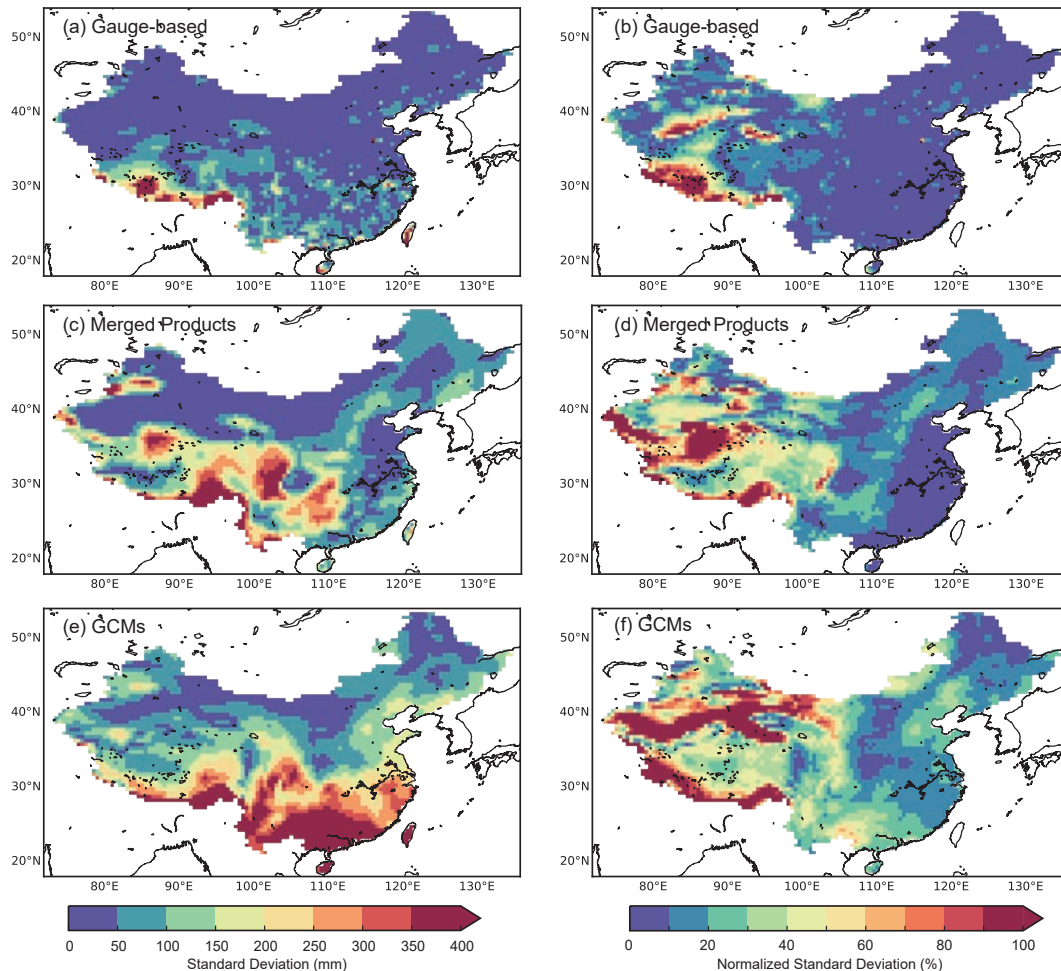


Figure 2.5 – The standard deviation (s.std) of the annual precipitation over China in each group and the normalized standard deviation by dividing by the annual precipitation of CMA.

Among the datasets based on gauge observations, the s.std is small in most of China (<50 mm/yr). It is higher in the south of China (50-100 mm/yr) although the area is not continuous in space. The highest s.std occurs along the Himalayas. The ratio of the s.std to the annual precipitation in CMA shows low values (<10%) in the east China. While the ratio is high in the west China especially in the Himalayas and the centre Tarim, where the annual precipitation is among the lowest in China. Regarding the merged precipitation, the s.std shows high values (>200 mm/yr) in the southwest China (e.g., the Tibet Plateau, Yunnan Province, Guangxi Province). Moderate s.std is found in the northeast China, north China and southeast China. The s.std ratio has the highest values (>100%) in the west around the north part of the Tibet Plateau. A moderate ratio (>40%) is found in the Tarim basin and other parts of the Tibet Plateau. There is a geophysical belt of the area where the s.std ratio is between

10% to 20% from the southwest China to the northeast China (Figure 2.5-d). Different from the gauge-based and merged products, the s.std among GCMs has the highest value (>400 mm/yr) in the south China (Figure 2.5-e). The s.std ratio to the annual means of CMA shows similar patterns in the west China to that of the merged products but with higher magnitudes. Moreover, the ratio is higher in the east as the small ratio (<10%) is only found in the northeast and the centre China.

The magnitude of the s.std demonstrates the variations among different precipitation products. The GCMs have the largest differences between models because there are no constraints of any forcing conditions and no measurements are used for bias correction in model simulations (Figure 2.4-f and 2.5-f). Different merged products have moderate variations between each other which might be induced by different means of precipitation measurements and the results are constrained with gauge observations. The differences among the gauge-based products are the smallest especially in the east China. The low density of the gauges and the orographic effect in the mountainous area are the main causes of the uncertainties between different datasets (Figure 2.4-b and 2.5-b).

### 2.3.3 Uncertainties across time

As discussed above, there are differences in the precipitation values between precipitation groups (Figure 2.3 and 2.4) and variations exist among the datasets within the same group. Both of the absolute differences and the spatial variations have significant spatial variations across the China mainland especially in the west China. In this section, the annual precipitation in ten different regions and the whole China mainland are analyzed to show the spatial heterogeneity of the quantity of precipitation (Figure 2.6).

The time length of the datasets varies from one group to the other (Table 2.1) and therefore the time length of the group is chosen as the overlap period of all datasets within that group. As shown in Figure 2.6, the annual precipitation of the GCMs is apparently higher than that of the gauge-based products or merged products for almost all regions, which agrees with the spatial patterns in Figure 2.4-f and the statistics in Table 2.2. The annual precipitation in the gauge-based products is similar to that of CMA except in the southwest China (Figure 2.6-i) for the overestimation along the Himalayas (Figure 2.4-b). The precipitation in merged products is higher in the southwest and northwest China, in accordance with Figure 2.4-d.

The standard deviation shown in Figure 2.6 represents the variations of the datasets within the same group at each time step. The normalized standard deviation facilitates the comparisons between different regions by comparing the width of the uncertainty range (shaded area) in the same scale of the y-axis. High deviations are found in all three precipitation groups in the southwest China (Figure 2.6-i) because of the large differences along the Himalayas. The deviations among the gauge-based products and the merged products in other regions are small and getting smaller along with time. It is mainly because the observations are used to control the data quality, more observations are integrated, and technologies improve with time. A large deviation is found in the merged products in 10-northwest China (Figure 2.6-j) and the 4-Yellow River Basin (Figure 2.6-d), where the annual precipitation is among the lowest and dry climate dominates. The model deviation of GCMs varies among regions as it is smallest

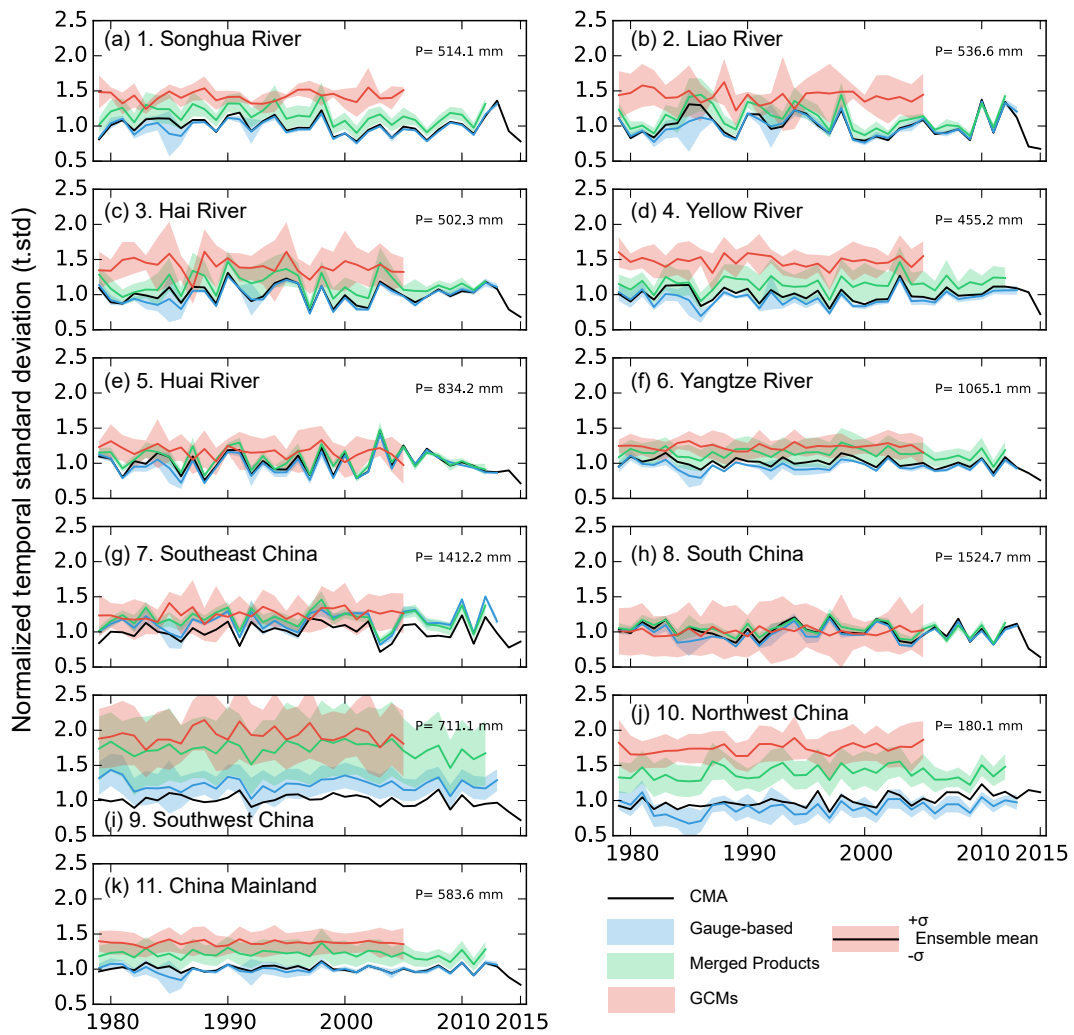


Figure 2.6 – The normalized temporal variations (to CMA annual means) of different precipitation groups and the standard deviation within the same dataset group. The value on the top right of each panel is the annual regional precipitation estimated in CMA dataset (1979-2015). All the regional average precipitation is normalized (divided by the annual precipitation). The shade represents the standard deviation of the annual precipitation in each year among the datasets within that group.

in the 1-Songhua River Basin (Figure 2.6-a) and the 6-Yangtze River Basin (Figure 2.6-f), while it is among the highest in the 8-south China and the west China (9,10), agreeing with the deviation maps in Figure 2.5.

The temporal variations of the gauge-based products and merged products agree well with that of the CMA dataset, while the temporal variation of GCMs ensemble is weaker and not well correlated with that of the CMA. The main reason is that GCMs are not constrained in their sub-decadal variability and the sequence of the wet and dry years can be very different from that of the observations. So a smoother result can be obtained when we build the ensemble means from the GCMs. While this is different for the gauge-based and merged products, as they have a strong co-variance and the ensemble mean preserves this co-variance.

For the entire Chinese mainland (Figure 2.6-k), the standard deviation remains stable for different precipitation groups. In contrast, the annual precipitation spans the largest difference in the mainland compared to those divided basins (Figure 2.3). However, the spatial variation has been collapsed when estimating the regional precipitation for temporal analysis. It is therefore interesting to see if the variations in the time dimension and in the space dimension can be compared or integrated with each other among the precipitation datasets.

### 2.3.4 Variations in the time and space dimensions

The precipitation varies in time and space. However, it is averaged either in the time dimension to compare the spatial patterns (Figure 2.3) or in space dimension to compare the temporal variations (Figure 2.6). The deviations in the time and space dimensions are therefore very rarely compared. Herein, the standard deviation of the temporal and spatial variations in annual precipitation datasets are compared in Figure 2.7 in ten regions and the Chinese mainland for different precipitation groups.

The gauge-based products provide similar annual regional precipitation to CMA over the China mainland and ten specific regions except for the region 7-southeast China (Figure 2.7-g). The regional precipitation is larger in merged products than that of observations. The spatial variations are the same for the GCMs, while the magnitude of the deviation in GCMs is even larger except in the region 8-south China (Figure 2.7-h). These results indicate the reduced ability of merged products and GCMs in reproducing the total value of the annual precipitation.

Regarding the variations in time and space dimensions, the 3-Hai River basin and 7-southeast China have the comparable values of temporal standard deviation (t.std) and spatial standard deviation (s.std). It is mainly because these two regions are relatively small so that the spatial heterogeneity is not strong in a given climate type. The t.std is also large in these regions (Figure 2.6). So that the t.std is similar to s.std. Larger s.std is found in the regions of 1-Songhua River basin, 2-Liao River basin, 5-Huai River basin and 8-South China. The area of these regions is larger than the previous two basins, and the spatial heterogeneity is therefore larger than that in the previous two basins. For the other four regions (i.e., 4-Yellow River basin, 6-Yangtze River basin, 9-southwest China, 10-northwest China) and the China mainland, the spatial variation is significantly larger than the variations in the time dimension. The main reason is that these large regions span areas with different climate types where the

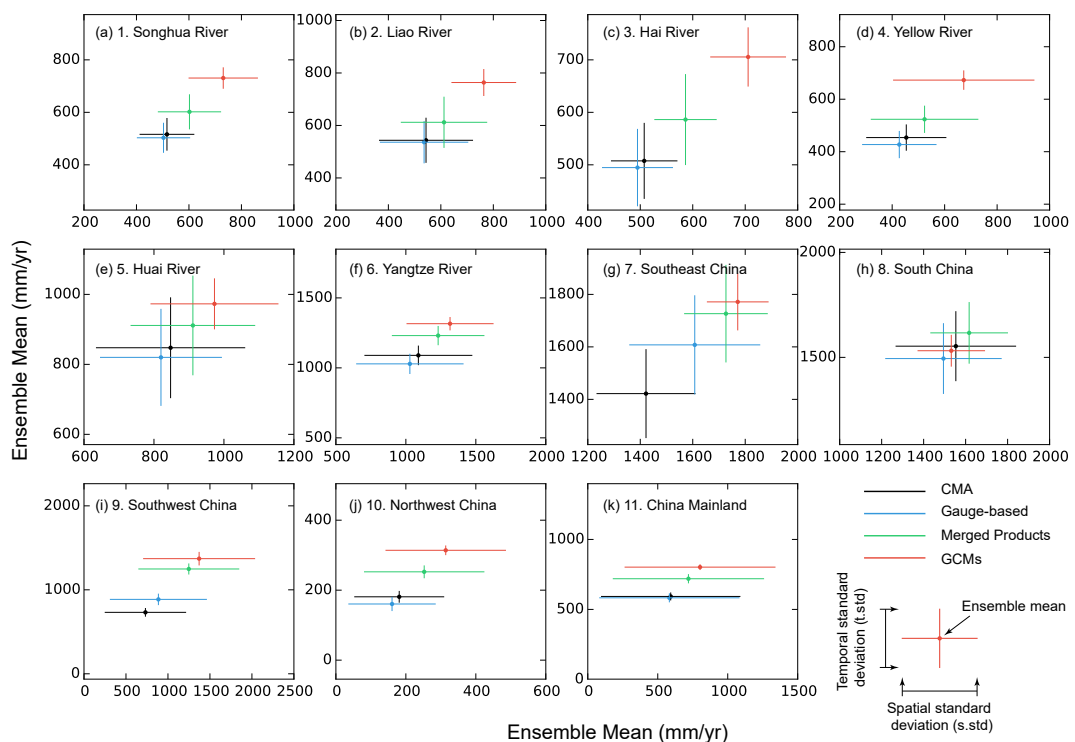


Figure 2.7 – The spatial standard deviation (s.std, horizontal) and temporal standard deviation (t.std, vertical) of the annual precipitation in different precipitation groups for ten regions and the mainland China. The cross centre represents the long-term means of the regional annual precipitation. The horizontal error bar represents the spatial standard deviation (spatial variation of the long-term annual precipitation at all the grids). The vertical error bar represents the temporal standard deviation (temporal variations of region-averaged annual precipitation in different years).

annual precipitation may be significantly different in the annual means. For example, in the CMA dataset, the annual precipitation over China mainland is  $592.6 \pm 25.0$  mm/yr in difference years, while it is  $592.6 \pm 494.5$  mm/yr at different grids in China. The very small ratio of the t.std to s.std ( $25.0/494.5=0.05$ ) indicates a higher reliability of annual regional precipitation in a specific year than the reliability of the annual precipitation at a specific grid point.

## 2.4 Variances in precipitation products

### 2.4.1 Variances in three dimensions

The standard deviations in either the space dimension or the time dimension in Figure 2.7 are estimated based on the ensemble means of the same precipitation group. The differences among datasets within that group (used to build the ensemble mean) are therefore not considered. On the other hand, although the standard deviation among the ensemble members can be compared with either the spatial means or the temporal means in Figure 2.5 and 2.6, it cannot evaluate the impact of ensemble variations on both the temporal dimension and spatial dimension together. It is therefore more difficult to compare the variation among the datasets together with the spatial variation and temporal variation by current approaches. A method which can integrate the variations together in the ensemble dimension, the temporal dimension and the spatial dimension is therefore needed for their comparisons.

As introduced in the methodology section, the ensemble variance can be estimated by the proposed three-dimensional partitioning approach. The input annual precipitation to the approach is organized into three dimensions as (1) time, 27 years from 1979 to 2005, (2) space, the number of  $0.5^\circ$  grids in a specific region and (3) ensemble, the number of the models in a same precipitation groups (4 models in all three groups).

The grand variance and the variances in three different dimensions (i.e., time, space and ensemble) for all the regions are mapped in Figure 2.8. It is similar for data groups of gauge-based products and the merged products for the grand variance (total value of the variance for all three dimensions, Figure 2.8-a,b,c), while the grand variance in GCMs is approximating twice the values of the grand variance in regions 9-south China and 10-southwest China. The differences are mainly constituted by the space variance and ensemble variance (Figure 2.8-i,l).

The time variance ( $V_t$ ) is the smallest of all three variance proportions, and there are very little differences of  $V_t$  in the north China (Figure 2.8-d,e,f).  $V_t$  in the gauge-based products is higher than that in the merged products and GCMs in regions 8-southeast China and 9-south China, indicating a relatively strong temporal variation in the annual precipitation series. For the space variance ( $V_s$ ), similar patterns are found in the gauge-based products and merged products (Figure 2.8-g,h), the 7-Yangtze River basin and 9-southwest China have the largest  $V_s$  because the precipitation significantly varies in space in these two regions.  $V_s$  is higher in the precipitation of GCMs especially in the 9-southwest China, indicating the strong spatial heterogeneity in the GCM models over the Himalayas (Figure 2.8-i). The ensemble variance ( $V_e$ ) is relatively small in most of the regions in gauge-based products (Figure 2.8-j), with the highest  $V_e$  occurring in 9-southwest China. It indicates that the model variation between

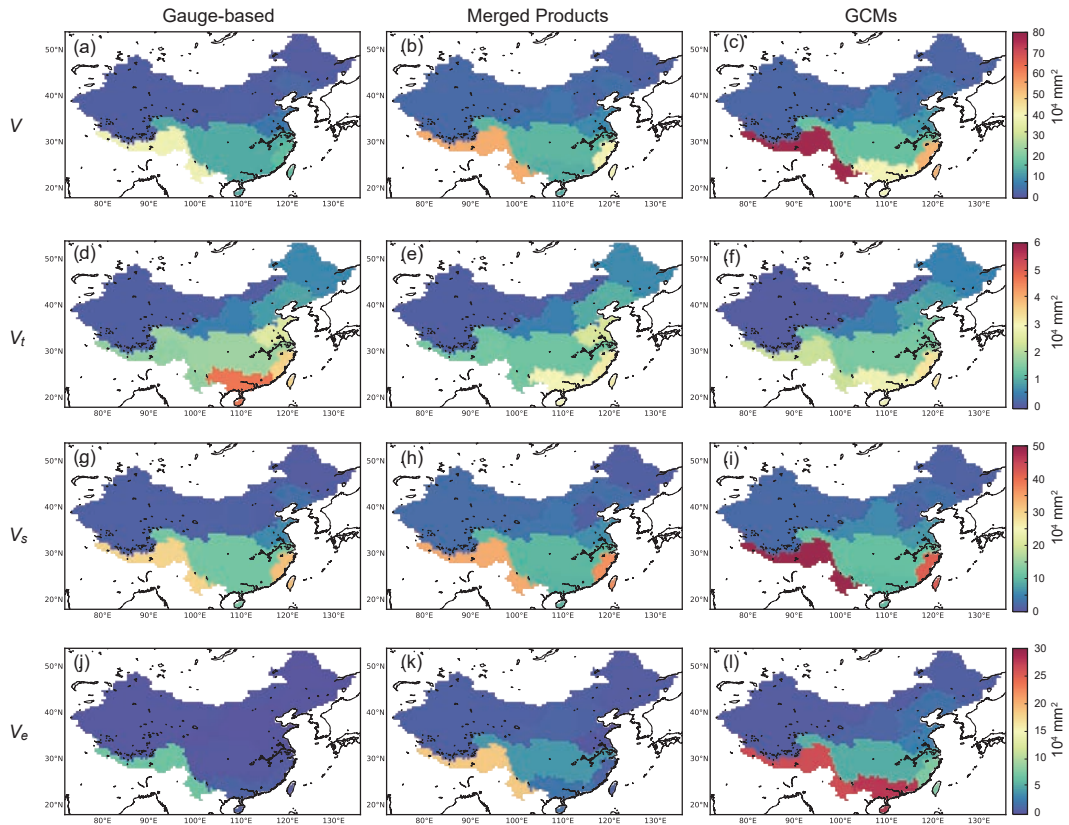


Figure 2.8 – The maps of the grand variance ( $V$ ) and variances in different dimensions ( $V_t$ ,  $V_s$ ,  $V_e$ ) for three different precipitation groups.

datasets in the observation group is small. Similar small values of  $V_e$  are found in the northern regions in merged products as well as in the GCMs for the regions in north China, while the intra-ensemble variations are large in the south especially the 9-southwest China and 8-south China in the GCMs (Figure 2.8-k,l).

In conclusion, the grand variance and variances in three different dimensions are generally larger in the dataset group consisting in GCMs. The variations for the gauge-based products and merged products are similar in values and spatial distribution. However, the statistics only show the total variances without consideration of the absolute regional means. The deviations which are estimated as the ratio of the square root of the variance to the mean (i.e.,  $U$ ,  $U_t$ ,  $U_s$ ,  $U_e$ ) should be evaluated to eliminate the systemic effect of the average means. Moreover, it is not easy to capture how the three variances vary with each other from Figure 2.8. The normalized variance proportion in time, space and ensemble dimensions  $P_t$ ,  $P_s$ ,  $P_e$  are therefore analyzed as well in the next sections.

### 2.4.2 Variance proportions in three dimensions

All of the variance proportions are normalized so that the comparison between variances in different dimensions becomes easy. As shown in Figure 2.9, the  $P_t$  is in general the smallest among the three variances and the  $P_s$  is the largest, which agrees with the standard deviation comparisons in Figure 2.7. The  $P_s$  is especially large in the 7-Yangtze River basin and 10-northwest China because the area is the largest and they span different climate zones

(Figure 2.9-d,e,f). The ensemble variance  $P_e$  is smaller than the  $P_t$  in the observation dataset group in the east China (Figure 2.9-g), which is probably because the gauge-based products are based on similar sets of observations to some degree and the orographic effect is not obvious in the east so that interpolation will not induce large uncertainties in the precipitation maps.  $P_e$  is generally lower than the  $P_s$  while an exception is found for the GCMs in the 8-southern China (Figure 2.9-i), indicating significant variations in different GCM models in estimating the precipitation. The model deficiency to represent the monsoonal flows in GCMs may result in the large differences.

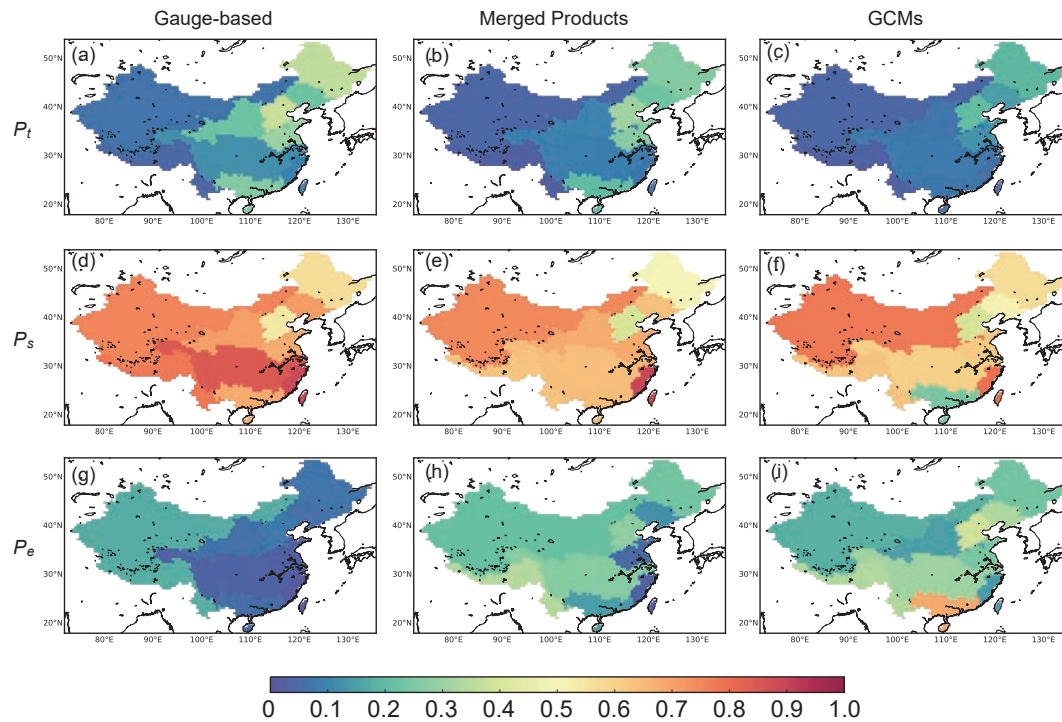


Figure 2.9 – The maps of variance proportion in different dimensions ( $P_t$ ,  $P_s$ ,  $P_e$ ) for three different precipitation groups.

The variance proportions are plotted in a ternary diagram in Figure 2.10. The scatter is distinguished in colours and shapes to represent three different precipitation groups. The numbers representing the regions are labelled near the scatter points. In general, the space variance proportion ( $P_s$ ) dominates the variances as it is larger than 0.5 in most of the regions in different precipitation groups (zone V and VI). The larger  $P_s$  agrees with the standard deviation in Figure 2.7 and  $P_s$  of regions of 4, 6, 9, 10, 11, which has very large space standard deviation in Figure 2.7 has the largest  $P_s$  in the right bottom corner of Figure 2.10.  $P_t$  is the largest among the three variance proportions for region 3, 1, 5 in gauge-based products as well as regions 3, 1, 5, 8 in merged products (zone III and IV in Figure 2.10), agreeing with the larger temporal deviation in Figure 2.7.

All the ensemble variance proportion  $P_e$  is lower than 0.2 for the precipitation group of gauge-based products, and the  $P_e$  is the highest in 9 of 10 regions (zone IV and V). The  $P_e$  in the merged products expands with the largest value of 0.35 in region 9. However, the  $P_e$  is still not the dominant variance since there are no values in the zone I and II, the  $P_e$  is larger than the temporal variance  $P_t$  in regions-4, 6, 9, 10, 11(zone VI).

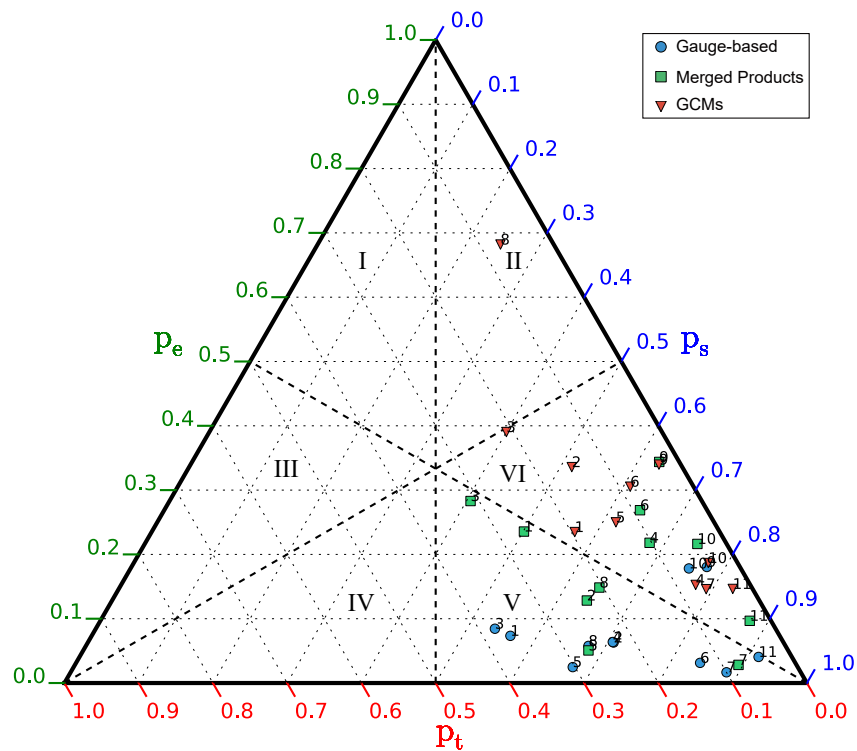


Figure 2.10 – Ternary diagram of the variance proportion in time, space and ensemble dimensions over the annual precipitation data. Six zones are divided in the diagram as (I) where  $P_e > P_t > P_s$ , (II) where  $P_e > P_s > P_t$ , (III) where  $P_t > P_e > P_s$ , and (IV) where  $P_t > P_s > P_e$ , (V)  $P_s > P_t > P_e$  and (VI) where  $P_s > P_e > P_t$ .

For the precipitation ensemble of GCMs, the  $P_e$  dominates the variances in region 8 where is the most affected by tropical cyclones. It shows the significant variations among different GCM models and the variation has exceeded both the temporal variation and spatial variation. Also, the  $P_e$  for other regions are not the dominated, it is larger than  $P_t$  which represents the temporal variation. The choice of GCMs becomes more critical since different GCMs provide results with high uncertainty compared to the temporal variations.

The lines which represent the ratios of the ensemble variance to other two variances  $K_{et} = P_e/P_t$  and  $K_{es} = P_e/P_s$  are added in Figure 2.11. Most of the scatter is located in the area with  $K_{es} < 1$ , indicating that the choice of precipitation products will not affect the results in spatial analysis (spatial heterogeneity). For the scatter in the area IV and V in Figure 2.10, the  $K_{et}$  is also smaller than 1.0, the dataset choice will not introduce significant differences in the temporal analysis (i.e., annual precipitation) as well. Half of the scatter for merged products and all GCMs is located in the area with  $K_{et} > 1$ . The  $K_{et}$  is even larger than 4 for regions of 8, 9, 10 and 11. It indicates that the choice of any dataset from the merged products or GCMs will have large uncertainty in the temporal analysis, that is, any of the single model among them has very low reliability on the temporal variations and obtaining ensemble means is highly recommended. While the choice of a single model will not affect the spatial analysis since the spatial patterns will be similar in any datasets in the group for the low  $K_{es}$ . For the scatters with high  $K_{es}$  and high  $K_{et}$  (e.g., region 8 for the GCMs), the spatial patterns may differ among datasets, but the spatial heterogeneity may also vary between different GCMs. An ensemble is needed for either the spatial analysis or the temporal analysis to avoid large bias in a single dataset.

### 2.4.3 Deviations in three dimensions

Opposite of the spatial patterns of the variances (Figure 2.8), the larger values of the deviation occur in the northwest, and lower values occur in southern China in general (Figure 2.12). It is because of the decreasing gradient of precipitation from the southeast to the northwest China (Figure 2.3). Although both the ensemble means and the variances are among the lowest in the northwest China, the total deviation ( $U = \sqrt{V}/\mu$ ) is the highest in this region ( $U=0.89$ , Figure 2.12-a,b,c) for all three groups.  $U$  is relatively small in the 1-Songhua River ( $U=0.27$ ) in the northeast and 8-South China ( $U=0.29$ ) for the gauge-based products and 6-Yangtze River has relatively lower  $U$  in the merged products and GCMs in the east part of China.

The variation in time and space dimension are inherent, and they show the temporal variation and spatial heterogeneity of the precipitation characteristics. It is found that the  $U_t$  is small and contributes very little to the total  $U$ , indicating the weak fluctuation of annual precipitation compared to spatial variations (Figure 2.12-d,e,f). The  $U_t$  values are the smallest for GCMs, in accordance with the temporal variations in Figure 2.6. The relative variance in space dimension ( $U_s$ ) contributes the most the total variance, especially in the northwest China ( $U_s=0.77$  for the gauge-based products, Figure 2.12-g). The high values indicate the strong spatial heterogeneity of precipitation in the region compared to the mean values. However, because the GCMs have difficulty to describe the spatial variation in the northwest, the

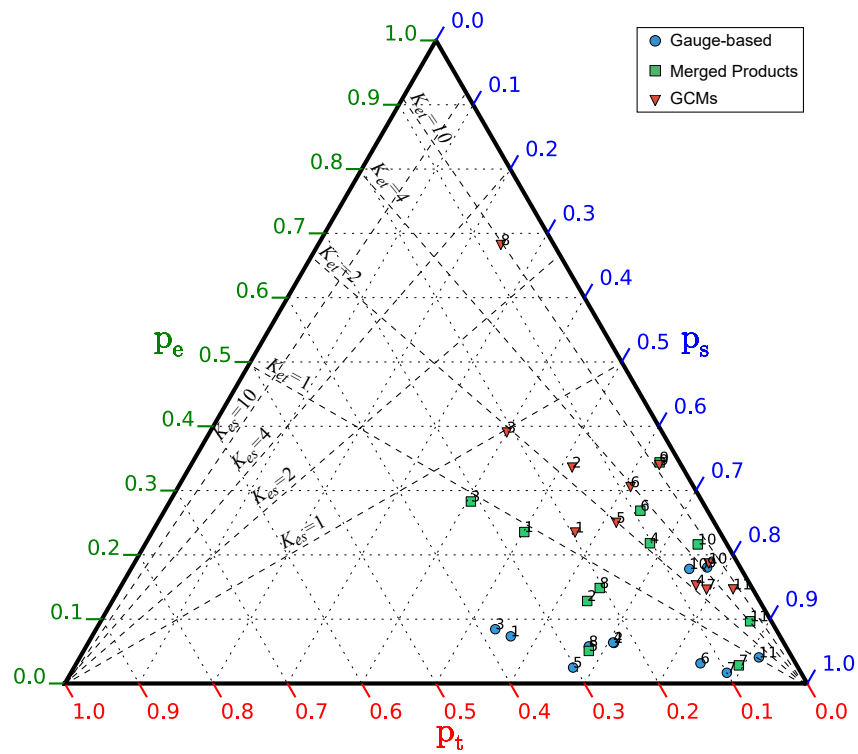


Figure 2.11 – Same as Figure 2.10 while the ratio of  $K_{et} = P_e/P_t$  and  $K_{es} = P_e/P_s$  is divided with ratios of 1, 2, 4 and 10.

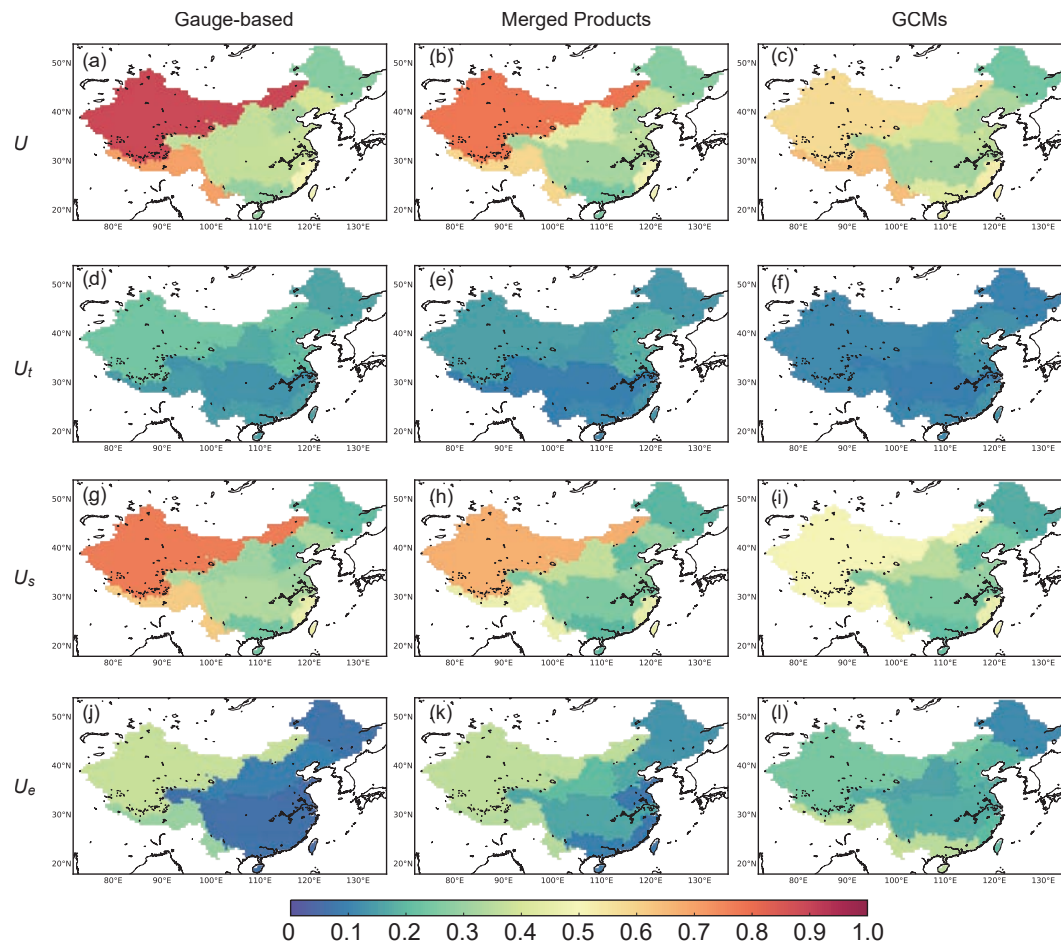


Figure 2.12 – The maps of deviations ( $U$ ,  $U_t$ ,  $U_s$ ,  $U_e$ ) estimated as the ratio of the square root of the corresponding variances (i.e.,  $V$ ,  $V_t$ ,  $V_s$ ,  $V_e$ ) to the regional mean ( $\mu$ ) for three different precipitation groups.

$U_s(=0.51)$  is smaller than that of the gauge-based and merged products.

As presented previously, the variations in time and space dimension are the inherent characteristics of the precipitation patterns, it is not the absolute value (i.e.,  $U_t$  or  $U_s$ ) but the deviation of the value to that of the observations show the ability of the products to represent the spatiotemporal patterns. The relative variance in the ensemble dimension ( $U_e$ ) shows the variations among different products in the same group. It thus can be called the "uncertainty" level as what is defined for the standard deviation. For the gauge-based products, the  $U_e$  is smaller than 0.1 for the regions in the east China, indicating that the model differences are small compared to the annual means. The  $U_e$  value is higher for the 9-southwest ( $=0.30$ ) and 10-northwest China ( $=0.37$ ), showing large variations even in the gauge-based products. The  $U_e$  is similar to that of the gauge-based products in the west China ( $=0.36$ ), while it is larger in the east especially for the 6-Yangtze River and 4-Yellow River (more than two times larger than  $U_e$  of the gauge-based products). For the GCM precipitation, the uncertainty increases for the eastern regions as expected, while it decreases in 10-northwest China ( $U_e=0.25$ ) compared to that of the other two groups. The result is different from the expectation that in the northwest, all the absolute bias (Figure 2.4-e,f), the spatial standard deviation (Figure 2.5-e,f) and the temporal standard deviation (Figure 2.6-j) are larger than that of the other two groups.

## 2.5 Uncertainty and metric comparisons

### 2.5.1 Uncertainty and standard deviations

As shown in equation 2.18, the ensemble variance is formulated as

$$V_e = \frac{mn(l-1)}{3(mnl-1)} \left[ \frac{\overline{\sigma_{e_t}^2} + \overline{\sigma_{e_s}^2}}{2} + \overline{\sigma_e^2} + \sigma_e^2(\mu_{ts}) \right] \quad (2.19)$$

It combines four elements which calculate the variation of different values across the ensemble dimension (i.e., the variance of original temporal and spatial values- $\overline{\sigma_e^2}$ , of the temporal mean- $\overline{\sigma_{e_t}^2}$ , of the spatial mean- $\overline{\sigma_{e_s}^2}$  and of the grand mean- $\sigma_e^2(\mu_{ts})$ ). Among which, the  $\overline{\sigma_{e_t}^2}$  is the average mean of the square of spatial standard deviation (s.std) in Figure 2.5-a,c,e for all grids in a specific region and  $\overline{\sigma_{e_s}^2}$  average mean of the square of the temporal standard deviation (t.std) in Figure 2.6 in each time step in a specific region. These are two classic metrics that are used to quantify model uncertainties.  $\overline{\sigma_e^2}$  and  $\sigma_e^2(\mu_{ts})$  are overall estimations of the spatiotemporal variations. The difference is only whether the averaging of across the time and space dimensions is before or after the variation calculation.

We will compare the uncertainty that quantified by the variance partitioning approach with the two classic metrics to better understand the similarities and differences of the new estimation. To facilitate the comparisons, we normalize the three metrics as the square root and divided by the mean. The uncertainty level which quantified with the variance is formulated as

$$U_e = \sqrt{(V_e)/\mu} \quad (2.20)$$

And the classic metrics are

$$N.t.std = \sqrt{\sigma_{e_s}^2} / \mu \quad (2.21)$$

$$N.s.std = \sqrt{\sigma_{e_t}^2} / \mu \quad (2.22)$$

The uncertainty metric is compared with the average mean of the normalized spatial standard deviation (N.s.std) for all grids in specific region and the average mean of the normalized temporal standard deviation (N.t.std) for each region (Figure 2.13).

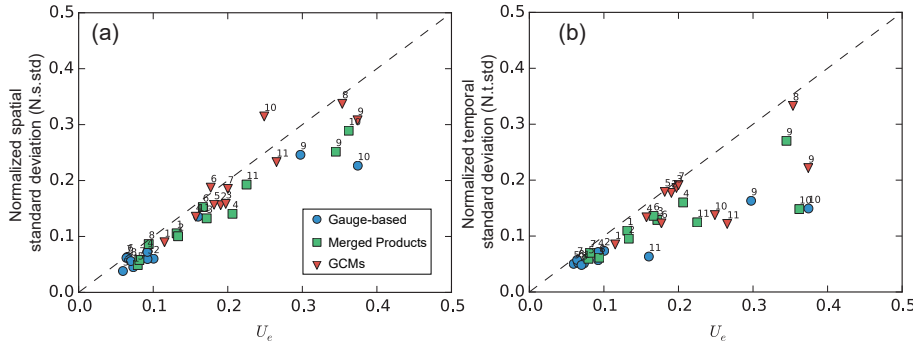


Figure 2.13 – The relation of the  $U_e$  to (a) the normalized spatial standard deviation - N.s.std and (b) the normalized temporal standard deviation - N.t.std.

The  $U_e$  is in line with both the N.s.std and N.t.std when the  $U_e$  is smaller than 0.2 where the regions from 1 to 8 are generally included for all three precipitation groups (Figure 2.13). The  $U_e$  is in general larger than the N.s.std and N.t.std for the products. It is simply because the variations of the other dimension have collapsed when calculating the spatial deviation (or temporal deviation). For the regions 6 and 10, the N.s.std is larger than the  $U_e$  due to the effect of variations in original dataset ( $\sigma_e^2$  and  $\sigma_e^2(\mu_{ts})$ , Figure 2.14). For the regions 9, 10 and 11, the values of the N.s.std and N.t.std deviate from the 1:1 line of the  $U_e$ . These regions feature with strongly space heterogeneities (Figure 2.5) as the spatial variation across space is extremely higher than the temporal variation. While the estimation of the two classic metrics needs to average one of the dimensions which can result in the loss of information of that dimension. Because the estimation of N.t.std needs the averaging in spatial dimension which may include more information than that in the time dimension, the deviation between N.t.std and  $U_e$  (Figure 2.13-b) is larger than that between N.s.std and  $U_e$  (Figure 2.13-a).

## 2.5.2 Decomposing the ensemble variance

By decomposing the equation 2.19, the contributions of the four components to the total value are shown in Figure 2.14. For all the three precipitation groups, the  $\sigma_e^2$  is the dominant component, simply because all the other components are estimated first by averaging the original data which is the most varying in either time or space dimension. The contributions differ in three precipitation groups as it is stable and around 0.65 for the gauge-based products, generally between 0.4 and 0.5 for the merged products and between 0.5 and 0.6 for the GCMs.

The other three components are similar in their values, with a limit of 0~0.3. For the gauge-based products, the variation of the ensemble means  $\sigma_e^2(\mu_{ts})$  is the smallest, indicating

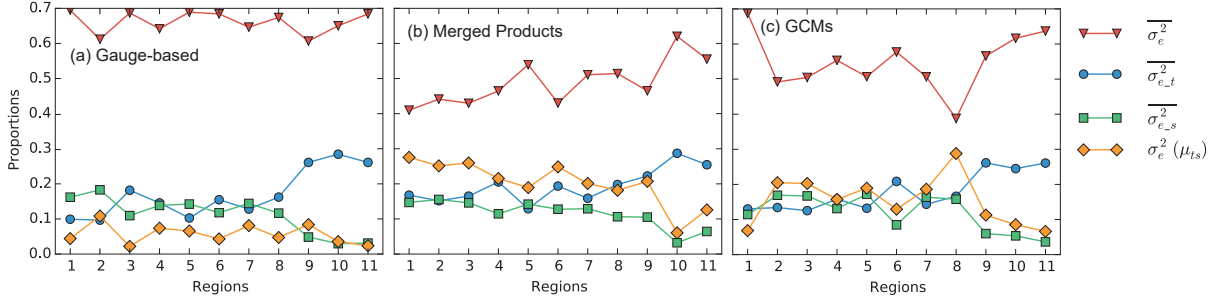


Figure 2.14 – The proportion of the four components in equation 2.19 to the  $V_e$  in three precipitation groups, (a) gauge-based products, (b) merged products and (c) GCMs. The contribution are normalized so that the sum of them is 1.0 for each region.

the least systematic uncertainty among different products. While, both the merged products and GCMs have large systematic uncertainty (bias in the mean values, also see Table 2.2). The proportions of the  $\overline{\sigma_{e-t}^2}$  and  $\overline{\sigma_{e-s}^2}$  slightly shift around 0.15 for regions from 1 to 8. While for the region 9, 10 and 11, the  $\overline{\sigma_{e-t}^2}$  increases, indicating that the spatial heterogeneity of the temporal means is significant for these regions. On the contrary, the  $\overline{\sigma_{e-s}^2}$  decreases because the spatial averaging has collapsed the spatial variations. The very small contribution of the  $\overline{\sigma_{e-s}^2}$  which is related to the N.t.std is the inherent reason that there is larger deviation between the N.t.std and the  $U_e$ .

Although all the variations are used as the metrics for evaluating the variations among multiple datasets, there are limitations for each of the variations. For the variation of temporal mean  $\overline{\sigma_{e-t}^2}$  and spatial mean  $\overline{\sigma_{e-s}^2}$ , the collapse of a dimension has ignored part of the information (also introduced in the Introduction). The variation of original data  $\overline{\sigma_e^2}$  cannot account for the systematic uncertainty while the variation of the grand mean  $\overline{\sigma_e^2(\mu_{ts})}$  has ignored both the temporal variability and spatial heterogeneity. Therefore, it is difficult to use any of these metrics to represent others either from the theory or the results (Figure 2.14). Integration of different components is therefore needed and able to represent other metrics to different degrees.

What is interesting is that the variability of the proportions of  $\overline{\sigma_{e-t}^2}$  and  $\overline{\sigma_{e-s}^2}$  (or  $\overline{\sigma_e^2}$  and  $\overline{\sigma_e^2(\mu_{ts})}$ ) are opposite and the sum of their proportions is stable around 0.3 (or 0.7). It is known that the variation in the time dimension and that in the space dimension should be considered together. In addition, the total ensemble variance ( $V_e$ ) is in proportion with the sum of variations in the two dimensions (time and space). Moreover, the ensemble variance ( $V_e$ ) is also in proportion with the sum of the variations in original data and that of the systematic uncertainty. As concluded, the ensemble variance ( $V_e$ ) shows an integrated variation from different aspects of multiple datasets and has better ability to demonstrate the uncertainties compared to other metrics.

### 2.5.3 Uncertainty with other metrics

To further verify the applicability of uncertainty metric  $U_e$  to represent uncertainties among multiple datasets, a few other coefficients (i.e., absolute bias in percentage-*apb*, Normalized Root Mean Square Error-*rmse\_nor*, correlation coefficient, Nash-Sutcliffe Efficiency-*NSE*)

are imported and compared with  $U_e$ . The coefficients are estimated between each single model in a group with the ensemble means of datasets in that group. These coefficients may to some degree indicate the deviations of the considered product to the ensemble means. Different coefficients reflect the similarities between two series from different angles. For example, the *apb* and *rmse\_nor* shows the value deviations from the other in one order and two orders. The correlation coefficient shows the similarity in the temporal variation, while *NSE* integrates the value deviations as well as the temporal variation.

For all the four coefficients, the  $U_e$  show a positive relation with the increasing of the deviations (i.e., higher *apb*, higher *rmse\_nor*, lower correlation and lower *NSE*), indicating that the ensemble means have changed in a larger degree from the original datasets with higher  $U_e$  (Figure 2.15). The spread of coefficients from different models in the same group indicates differences among the models because they have the same reference time series (i.e., ensemble means). The standard deviations of the coefficients for each dataset group for each region are plotted in Figure 2.16, and their linear regression relation identified by the regression lines. Known from Figure 2.16, the standard deviation of the coefficient increases with higher  $U_e$  either for single precipitation group (colored best-fit lines in Figure 2.16) or the total scatters (black best-fit line in Figure 2.16). Only the exception is the correlation coefficient for gauge-based datasets because the temporal variabilities are highly accorded with each other, and the difference is not large between different products (Figure 2.16-c). The positive correlation of the  $U_e$  with the increasing coefficients deviation still exist for the remaining scatters and for the total values. As concluded, the relation tests regarding the value of coefficients and the standard deviation among models indicate that the  $U_e$  is capable of representing the intra-ensemble variations.

## 2.6 Discussion and Conclusion

### 2.6.1 What is the uncertainty means among precipitation groups

This chapter estimates the uncertainties among precipitation products in different groups (i.e., gauge-based products, merged products and GCMs). Because the generation methods of these precipitation products are different, the uncertainties among products therefore show different physical meanings from one group to another. The gauge-based products (i.e., GPCC, CRU, CPC and UDEL) use observed data from global atmospheric gauges, while the density of ground observation gauges, the representatives of the gauges and the interpolation algorithms for converting the gauge observations to grids dataset vary from product to product (see Table 1 in Tapiador et al. 2012). Therefore, the uncertainties among the multiple products measure the differences caused by the difference of used gauge observations and the interpolation approaches.

Among the merged precipitation products, the CMAP, GPCP and MSWEP use different sources of precipitation data (e.g., gauge observations, satellite remote sensing, atmospheric model re-analysis). These different precipitation sources are averaged using different weights. Thus the differences among the three merged products are associated with the precipitation sources and the weight of the gauge observations. The ERA-Interim is re-analysis model

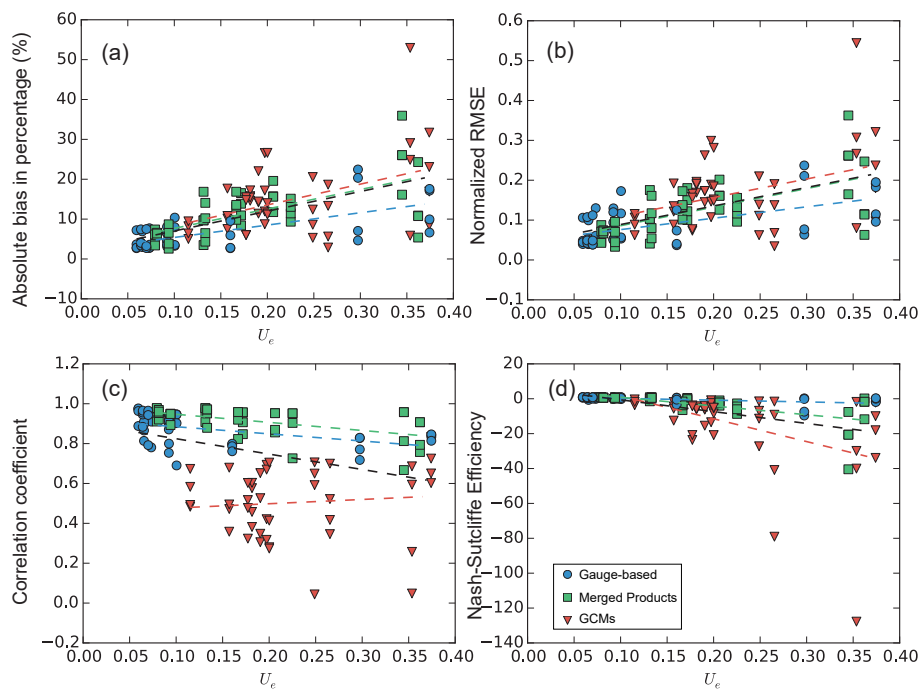


Figure 2.15 – The relation between the uncertainty  $U_e$  with other currently used coefficients (a) the absolute bias in percentage, (b) normalized root mean square error, (c) correlation coefficient, (d) Nash-Sutcliffe Efficiency. The dashed lines show the linear regression of the values in different dataset groups.

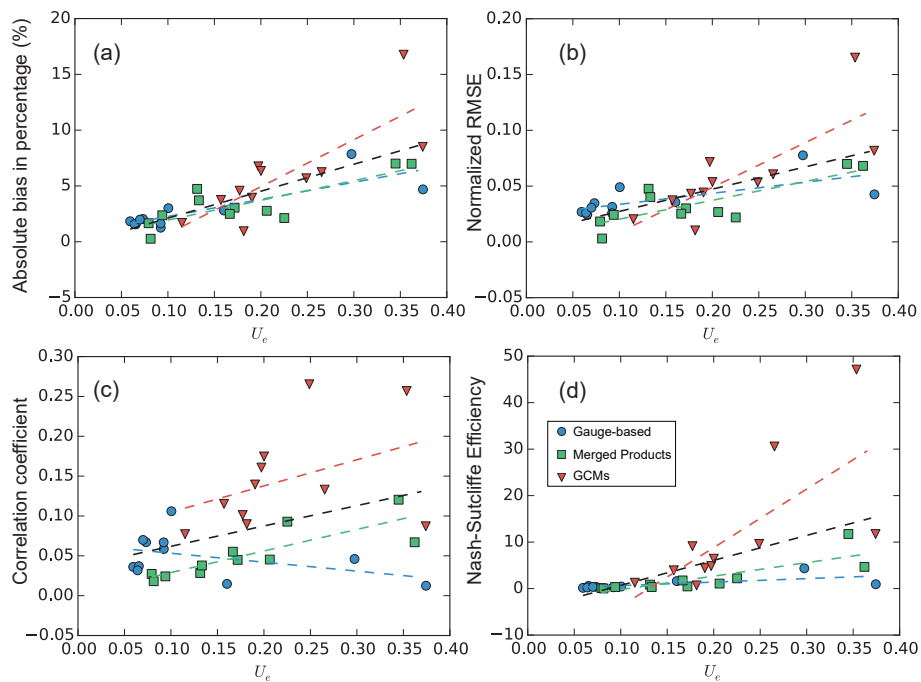


Figure 2.16 – The relation between the uncertainty  $U_e$  with the standard deviation coefficients for different datasets in a same precipitation group.

output, while it uses near-real-time assimilation with data from global observations (Dee et al. 2011). Thus the forecasting model is constrained to observations and forced to follow the real system to some degree. The temporal variability of the merged products is therefore consistent while the absolute values are different from the gauge-observed precipitation (Figure 2.6).

GCMs are precipitation estimations, and there are not any observations that constrain the simulation development. Therefore, the model algorithms will definitely affect the accuracy of models and the model errors have been validated in many studies over different places using the observations. In addition to inherent model, the initial condition of the GCMs will result in a spread of simulations as well. Kay et al. (2015) repeatedly run the same GCM with a very small difference in the initial conditions, and there is a spread of the model outputs after a number of time steps of running (see Figure 2 in Kay et al. 2015). Therefore, the uncertainty estimated by the proposed approach evaluates the model variations resulted from the differences in the model and the initial conditions. The uncertainty is also larger than the results of the other two precipitation groups which are constrained by observations.

## 2.6.2 Features and applicability of the approach

The proposed variance partitioning approach works in three dimensions, and it is able to use all of the information in the time and the space dimensions among the multiple ensemble members. Compared to the current commonly used metrics (e.g., standard deviation), the new estimation of uncertainty avoids aggregation in both temporal and spatial dimensions. The result of the new uncertainty is, in general, larger than the values which are estimated by old metrics.

The results of the partitioning approach can be affected by the choice of the time step intervals. For example, the time variation or time variance proportion will significantly increase if the time interval is chosen as one month. The inter-annual variation of precipitation will result in higher  $V_t$  and lower  $V_s$  or  $V_e$ . It depends how significant the inter-annual variability is compared to the intra-annual variations.

The present approach has a flexible structure that potentially deals with different problems from global to regional dimensions. The time dimension can consider intervals from daily, monthly, annual or to decadal analysis which corresponds to climate change scopes. The ensemble dimension is applicable from 2 members (i.e., model evaluation between simulations and observations) to any number of multi-models (consensus evaluation, Tebaldi et al. 2011; McSweeney and Jones 2013). The present approach is applicable to any variables that are organized in the three dimensions such as climatic variables (e.g., temperature, evaporation), hydrological variables (e.g., soil moisture, runoff) or environmental variables (e.g., drought index). Based on these advantages, the three-dimensional partitioning approach can widely be applied in the hydroclimatic analysis.

## 2.6.3 Conclusion

The uncertainties among multiple precipitation datasets are investigated over China in this chapter. Thirteen precipitation datasets are categorized as three groups (i.e., gauge-based

products, merged products and GCMs) in terms of the way the datasets were generated. A new three-dimensional partitioning approach is proposed to assess the model variation among different datasets in the same precipitation group. The ensemble variance ( $V_e$ ), the variance proportion ( $P_e$ ) and the deviation ( $U_e$ ) are estimated.  $P_e$  is a relative proportion of the ensemble variation to variations of other dimensions (i.e., time and space).  $U_e$  indicates the uncertainty level of the multiple datasets compared to the ensemble means. The  $U_e$  is compared with the current coefficients (e.g., standard deviation) to show its applicability. The main conclusions are listed as:

1. The magnitude of the intra-ensemble variations in three precipitation groups is different. The GCMs show the largest intra-ensemble variations in both the spatial dimension and the temporal dimension. The datasets based on gauge-based products have the least intra-ensemble variations among the three precipitation groups.
2. The model variation is larger in the south and west China especially in the mountainous area (e.g., the Himalayas and the Kunlun Mountains). It demonstrates the difficulty of precipitation measurement and modeling in these areas with strong orographic effects.
3. The spatial variation is generally larger than the temporal variation for the annual precipitation in different regions. The proposed new three-dimensional partitioning approach additionally estimates the ensemble variance among the multiple models. Although the ensemble variance is not the dominant proportion in the total (sum of the time, space, ensemble variances), it is larger than the temporal variance in some cases which means the ensemble will significantly change the temporal patterns of original datasets.
4. The metric  $U_e$  is estimated and used to represent the uncertainty level of the multiple datasets to the ensemble means. The  $U_e$  is higher in the northwest and the southwest regions where the topography weather dynamics are more complicated.
5. The uncertainty metric  $U_e$  is correlated with some other coefficients (e.g., standard deviation, correlation, Nash-Sutcliffe Efficiency) that are used to identify the similarities between models. The correlation proves that the  $U_e$  can be used as an indicator of intra-ensemble variations. The  $U_e$  is in the meantime superior to other metrics since it integrates the variation in both time and space dimensions.



# 3

## An ORCHIDEE-Budyko framework to attribute the discharge bias

### Contents

---

<b>3.1</b>	<b>Introduction</b> . . . . .	<b>51</b>
<b>3.2</b>	<b>Study area and hydro-meteorological characteristics</b> . . . . .	<b>53</b>
<b>3.3</b>	<b>Data and Models</b> . . . . .	<b>54</b>
3.3.1	Data and simulation description . . . . .	54
3.3.2	Land Surface Model-ORCHIDEE . . . . .	57
3.3.3	Main biases over the headwater catchments . . . . .	60
3.3.4	Budyko hypothesis . . . . .	62
3.3.5	Bias assessment with ORCHIDEE-Budyko framework . . . . .	63
<b>3.4</b>	<b>Results and discussion</b> . . . . .	<b>65</b>
3.4.1	Forcing and discharge comparison . . . . .	65
3.4.2	Evidence of the bias in estimated discharge for the headwater catchments . . . . .	71
3.4.3	Bias range and possibility analysis for the headwater catchments . . . . .	73
3.4.4	Human intervention in the lower oases . . . . .	78
<b>3.5</b>	<b>Conclusions</b> . . . . .	<b>78</b>

---

Known from the literature presented in Chapter 1, the Tarim basin in China is one of the regions where there are high uncertainties in both the meteorological observations and hydrological modeling. The precipitation is very light over the Tarim but with strong heterogeneity in space (see Chapter 2). The water source of the Tarim basin relies on glacier melt and thus it is sensitive to climate change, especially global warming over Central Asia. Human activities in the meantime play an important role in the Tarim basin by shifting the natural water cycle and discharge regimes in the lower oases. Therefore, the Tarim basin is a region where the climate change and human activities interact with high uncertainties due to the lack of data or model practices (see details in section 3.2). This chapter attempts to assess the factors that affect the model accuracy in hydrological modeling in the Tarim basin. Supplementary literature (section 3.1) and a new framework (ORCHIDEE-Budyko, section 3.3.1) are proposed for this purpose. The model bias is attributed to uncertainties in the forcing variables (especially the precipitation) and the model structure. The human impact on the discharge is also discussed in section 3.4. The chapter was published to the international journal *Hydrology and Earth System Science*.

Xudong Zhou et al. (2018). “Understanding the water cycle over the upper Tarim Basin: retrospectively the estimated discharge bias to atmospheric variables and model structure.” *Hydrology and Earth System Sciences* 22, Pages 6087–6108. DOI: [10.5194/hess-22-6087-2018](https://doi.org/10.5194/hess-22-6087-2018)

## Understanding the water cycle over the upper Tarim Basin: retrospectively estimating the discharge bias to atmospheric variables and model structure

Xudong Zhou<sup>1,2</sup>, Jan Polcher<sup>2</sup>, Tao Yang<sup>1</sup>, Yukiko Hirabayashi<sup>3</sup>, Trung Nguyen-Quang<sup>2</sup>

<sup>1</sup>State Key Laboratory of Hydrology-Water Resources and Hydraulic Engineering, Hohai University, 210098, Nanjing, China

<sup>2</sup>Laboratoire de Météorologie Dynamique du CNRS, IPSL, École Polytechnique, 91128, Paris, France

<sup>3</sup>Department of Civil Engineering, Shibaura Institute of Technology, Tokyo, Japan

### Abstract

The bias in atmospheric variables and that in model computation are two major causes of failures in discharge estimation. Attributing the bias in discharge estimation becomes difficult if the forcing bias cannot be evaluated and excluded in advance in places lacking qualified meteorological observations, especially in cold and mountainous areas (e.g., the upper Tarim Basin). In this study, we proposed an Organizing Carbon and Hydrology In Dynamic Ecosystems (ORCHIDEE)-Budyko framework which helps identify the bias range from the two sources (i.e., forcing and model structure) with a set of analytical approaches. The latest version of the land surface model ORCHIDEE was used to provide reliable discharge simulations based on the most improved forcing inputs. The Budyko approach was then introduced to attribute the discharge bias to two sources with prescribed assumptions. Results show that, as the forcing biases, the water inputs (rainfall, snowfall or glacier melt) are very likely underestimated for the Tarim headwater catchments (-43.2 % to 21.0 %). Meanwhile, the potential evapotranspiration is unrealistically high over the upper Yarkand and the upper Hotan River (1240.4 and 1153.7 mm yr<sup>-1</sup>, respectively). Determined by the model structure, the bias in actual evapotranspiration is possible but not the only contributor to the discharge underestimation (overestimated by up to 105.8 % for the upper Aksu River). Based on a simple scaling approach, we estimated the water consumption by human intervention ranging from  $213.50 \times 10^8 \text{ m}^3 \text{ yr}^{-1}$  to  $300.58 \times 10^8 \text{ m}^3 \text{ yr}^{-1}$  at the Alar gauge station, which is another bias source in the current version of ORCHIDEE. This study succeeded in retrospectively estimating the bias from the discharge estimation to multiple bias sources of the atmospheric variables and the model structure. The framework provides a unique method for evaluating the regional water cycle and its biases with our current knowledge of observational uncertainties.

### 3.1 Introduction

A failure of discharge estimation can easily happen to a researcher especially when exploring a new region. It is often attributed to model inapplicability to the region, and tuning the model parameters is a common way to eliminate the discharge bias (Refsgaard 1997; Westerberg et al. 2011). However, a hidden assumption is often ignored that the atmospheric variables (or named here forcing) are essentially correct, while it may fail in some regions

(Fekete et al. 2004; Adam et al. 2006). Without knowing the bias in forcing, the calibration becomes meaningless if the model parameters are tuned to values that are far from their physical meaning (Hernández and Francés 2014; Qin et al. 2018a; Qin et al. 2018b). Thus, an important step before applying a model to a new region is to understand where the bias sources lie and their relative relations (Renard et al. 2010).

In situ measurements are considered most reliable sources for atmospheric variables and thus can be used to evaluate or further correct the variables used to drive hydrological models (Wang et al. 2017b). However, larger uncertainties are still found in mountainous and arid areas due to the poor representativity of in situ observations (Adam et al. 2006; Harris et al. 2014; Yang and Lu 2014; Wang et al. 2018). For instance, the precipitation ( $P$ ) over the mountainous area is mostly underestimated due to rare observations at high altitude and orographic effects (Harris et al. 2014). A total of 20.2 % of the precipitation is underestimated over global orographically affected regions according to Adam et al. (2006). Arid areas receive less water input but have larger relative uncertainties in precipitation (Fekete et al. 2004), which are crucial to regional runoff ( $R$ ) generation. Meanwhile, the energy flux over arid regions varies significantly. Thus the potential evapotranspiration (PET) and the actual evapotranspiration (ET) are quite uncertain over those areas (Federer et al. 1996; Weiß and Menzel 2008); in the meanwhile, the PET and ET are variables unable to directly measure for a basin. Investigation of their errors and relations based on the model simulation becomes necessary.

Model efficiency needs to be verified firstly. The model performance is generally evaluated on the agreement of a single variable, and discharge is the most commonly used as it is the result of all the water–energy processes. It reveals the accuracy of the whole system while also accumulating all the errors from the forcing and the model. Therefore, a multivariable analysis based on the relation between variables is needed for overall evaluation (Kavetski et al. 2006). These relations represent typical climatic and regional characteristics; i.e., the aridity index ( $PET / P$ ) reveals the energy and water input over a specific region (Zomer et al. 2007; Zomer et al. 2008), and the ratio of evapotranspiration to precipitation ( $ET / P$ ) is relevant to the land cover conditions (Liu et al. 2003; Yang et al. 2008a). The Budyko hypothesis is a widely accepted empirical relation between  $ET / P$  and  $PET / P$  (Webster 1976). The shape of the optimal Budyko curve reflects local climatic and underlying characteristics (Ponce et al. 2000; Yang et al. 2007). Hence with a Budyko curve derived from land surface model simulations, biases of the water–energy components ( $P$ , ET or PET) can be assessed. For example, Adam et al. (2006) quantified the precipitation bias in orographically affected areas using the Budyko hypothesis, although their work attributed all the bias in discharge simulation to the forcing with an incorrect assumption that their model was perfect.

Most of the hydrological models, with either a lumped or a distributed concept, are dependent on the calibration. Because of the assumption that water input ( $P$ ) is correct and a very crude description of energy processes, the ET is the variables which can be adjusted to meet the water mass balance. Most of the bias is therefore assumed to derive from the ET. It may mislead the relations between  $PET / P$  and  $ET / P$ , which represents the climatic and regional characteristics (Liu et al. 2003; Zomer et al. 2007; Yang et al. 2008a; Zomer et al. 2008). Land surface models (LSMs) are almost independent of the calibration process, with

most of the model parameters obtained from multiple maps (e.g., land cover, land use, soil textures). Based on their substantial physically based modules, the LSMs have been widely used to estimate most of the components in the continental water cycle (Yu et al. 1999; Yu 2000; Pitman 2003; Trenberth et al. 2007; Renard et al. 2010). Although the LSMs do not necessarily provide good estimates of discharge (Giorgi and Francisco 2000; Fekete et al. 2004; Yu et al. 2006; Knutti et al. 2010), they prevent all the bias being revised by calibration. In return, the modeled discharge bias can reveal the biases related to model input or model structure, which have not attracted enough attention.

The Tarim Basin – located in the northwest of China, central Asia; surrounded by high mountains; and punctuated by oases in the center of deserts – is a region integrating the mountainous, arid and cold characteristics in different parts (Yang et al. 2015a; Yang et al. 2015b). The precipitation is mainly distributed over the upper mountainous area around the boundaries, and the snowmelt and glacier melt are major contributors to the local water resources (Gao et al. 2010; Pritchard 2017). However, the meteorologic observations on the water input components are sparse, and the gauges are not representative because the surface conditions are heterogeneous especially in the mountainous area (Shen et al. 2010). In the lower oases, intensive irrigation is developed, which is hugely reliant on the discharge flowing from the headwater catchments (Mamitimmin et al. 2014; Ren et al. 2018), causing considerable changes in the natural river discharge downstream of the area (Zhou et al. 2000; Tao et al. 2011). In reality, human intervention is very difficult to model as it is policy related and because of the lack of an efficient dataset. The anthropogenic effects on the water cycle, accompanying the climatic and topographic characteristics, make the Tarim one of the most challenging places to apply land surface models.

There are three major steps in this study, Firstly, we generated a best-possible forcing dataset for the Tarim domain which reduces as far as possible the biases using refined data sets. The refined forcing then drove an improved land surface model (Organizing Carbon and Hydrology In Dynamic Ecosystems: ORCHIDEE) to obtain the improved discharge estimations. Secondly, the estimated discharge was compared with in situ discharge observations (Sect. 3.4.1), and the evidence of their bias analyzed (Sect. 3.4.2). In the third step, the possible bias sources from the forcing and model structure were qualified with the Budyko hypothesis (Sect. 3.4.3), and their possibilities are discussed in Sect. 3.4.4. The model bias due to ignorance of human intervention is estimated based on the bias analysis over the headwater catchments in Sect. 3.4.5.

## 3.2 Study area and hydro-meteorological characteristics

The Tarim Basin locates in the northwest of China, surrounded by the Kunlun Mountains in the south, the Tianshan Mountain in the north and the Pamirs Plateau in the west (Fig. 3.1). Its U-shaped terrain blocks the westerly atmospheric water vapor transport that leads to relatively low precipitation inside the basin (Wu et al. 2012b). As simulated by Wu et al. (2012b), 63 % of the water vapor enters Tarim through the eastern passway, but it only happens in summer, contributing around 54 % of the total annual precipitation, leading to a strong

seasonality in precipitation (Tao et al. 2011). Combined with the glacier melt during warm summer, 70 % of the annual discharge is concentrated in the period from June to October (Liu et al. 2010b). The high seasonality implies a high risk of water deficit in dry seasons and endangers the ecosystem along the rivers (Döll et al. 2009), which requires human regulation to allow for efficient agriculture.

Despite the high interannual variability, the precipitation is heterogeneously distributed due to orographic effects (Wu et al. 2012b). It ranges from 200 to 500 mm yr<sup>-1</sup> in the mountainous area, while there is less than 50 mm in the central Tarim (Chen et al. 2007). The mountainous glacier melt/snowmelt occurs in the same place where precipitation is generated. The mountainous area contributes almost all the river runoff of the Tarim Basin, while the plains of Tarim contribute little to the water resource of the main Tarim (Yang et al. 2015b; Shi et al. 2016). In the upper Tarim, only three water systems (the Yarkand, the Hotan and the Aksu rivers; see Fig. 1) have natural hydraulic connections to the mainstream - the Tarim (Yang et al. 2015b). The water originating from the mountains flows through the oases where people live and allows intensive agriculture (Mamitimmin et al. 2014). As a consequence, a large proportion of the water is extracted for human utilization in the oases, so that only 8.7 %, 43.4 % and 30.6 % of the discharge from headwater regions of the Yarkand, Hotan and Aksu rivers can finally reach Tarim mainstream, respectively (25.3 % in overall in 1995; Zhou et al. 2000). The Kaxgar River is another major tributary of the Tarim, but it has already dried up before water could reach the mainstream due to natural evaporation/leakage and human intervention. Of all the water consumption, agriculture irrigation accounts for more than 95 % in the Tarim Basin (Zhou et al. 2000); hence the dominant human influence in the Tarim Basin is considered to be the irrigation influence.

There are 11 665 glaciers with a total area of 19 878 km<sup>2</sup> and a volume of 2313 km<sup>3</sup> distributed over the Tarim (Liu et al. 2006). The glacier melt is a critical contributor to the local water resource. According to Zhou et al. (2000) and Shangguan et al. (2009), the estimated glacier melt accounts for around 40 % of the total river runoff for the whole Tarim. However, due to the climate change, a large number of the glaciers were in retreat during the last 40 years (1960s–2001). In the upper Tarim, the Yarkand River has suffered the most significant glacier area changes (-205 km<sup>2</sup>) with a relative proportion of -6.1 %. The most significant retreat rate (-7.9 %) in glacier area occurs on the Pamirs Plateau in the west (Shangguan et al. 2009). All the changes in glaciers will result in the alteration in the river discharge and also the human interactions.

## 3.3 Data and Models

### 3.3.1 Data and simulation description

#### River discharge observations

River discharge is a very reliable and integrated observation of the continental water cycle which is always used as a validation variable (Yang et al. 2017). Over the headwater catchments, there are 13 hydrological gauges recorded in the Hydrological Yearbooks of

China issued by the Ministry of Water Resources, though only six gauges are selected with consideration of their locations and data completeness. Two gauges (1, 2) are in the upper Yarkand River, two (3, 4) are in the upper Hotan River, and two (5, 6) are in the upper Aksu River, while no gauge is found on the Kaxgar River. For the gauges in headwater catchments, the discharge is considered free of human intervention, i.e., irrigation or reservoir regulation, so to a large extent they represent the natural environment (Cui et al. 2018). This facilitates model validation. Moreover, on the mainstream of Tarim, one gauge (7, Alar) was selected at the junction of three upstream rivers (Fig. 3.1). Different from the headwater gauges, the river discharge at Alar has been significantly altered by human consumption after flowing through the irrigation area (Mamitimmin et al. 2014). Hence, the observations are no longer natural values but can be used to quantify the influence resulting from human activities.

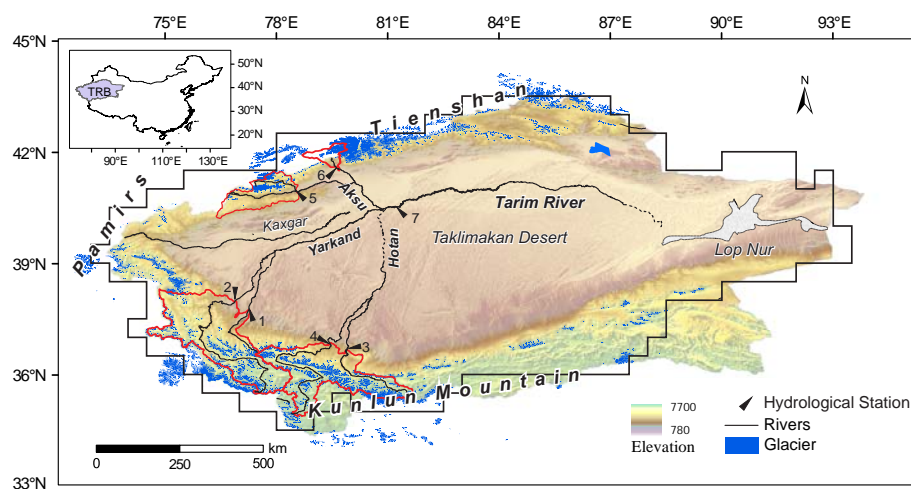


Figure 3.1 – The major rivers and the glacier distribution in the Tarim Basin. The upper Yarkand River catchment is defined by hydrological gauges 1 (JK) and 2 (KQ), the upper Hotan River catchment is defined by hydrological gauges 3 (TGZLK) and 4 (WLWT), and the upper Aksu River catchment is defined by hydrological gauges 5 (SLGLK) and 6 (XHL). The upper Tarim Basin is defined by hydrological gauge 7 (Alar).

### Near-surface atmospheric conditions

Near-surface atmospheric conditions are crucial to hydrological responses (Adam et al. 2006). However, both the model simulation and gridded forcing generated from observations are proven to have large uncertainties where observations are sparse and heterogeneity is strong (Harris et al. 2014; D’Orgeval et al. 2008), i.e., in the arid and mountainous area, so that, in practice, several forcing datasets are always used in parallel to generate an ensemble of climate conditions which hopefully tracks the uncertainties (Knutti et al. 2010; Tebaldi and Knutti 2007). Alternatively, when possible, regional datasets which contain more information than global datasets are used to move the forcing closer to true values (Ines and Hansen 2006). In this study, several sets of estimated forcing inputs based on WATCH (Water and Global Change Harding et al. 2011; Weedon et al. 2014) are developed and then used to drive the land surface model (Fig. 3.2). The best simulations among them will be used to analyze the accompanying bias with its driving forcing.

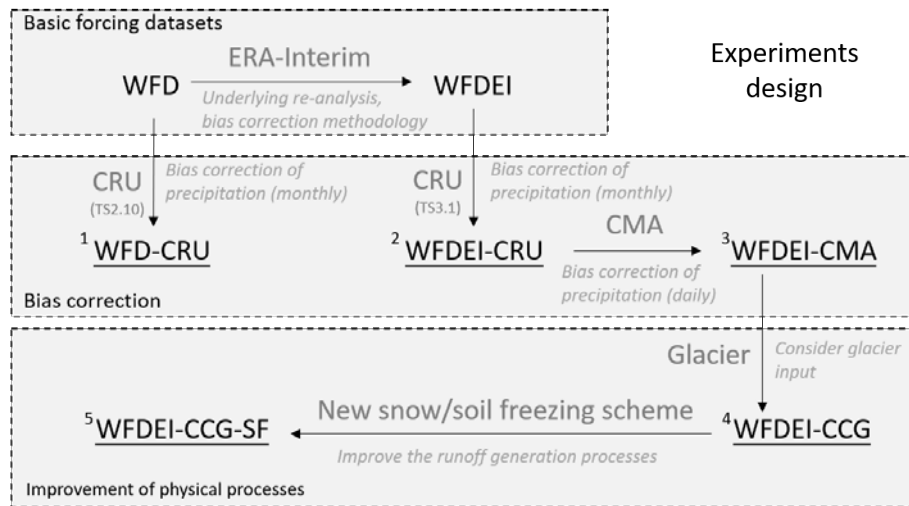


Figure 3.2 – The flowchart of the 5 experiments designed for driving the ORCHIDEE in this study. WFD and WFDEI are two basic forcing datasets. The underlined terms with numbers are five experiments while the grey arrows represent the development of the forcing compared to their previous ones.

A pair of reference forcing datasets are WFD (WATCH Forcing Data, 1958–2001; Weedon et al., 2010, 2011) and WFDEI (WATCH Forcing Data methodology applied to ERA-Interim data, 1979–2012, Weedon et al. 2014). They use the same methodologies but have slight differences in the basic data, processing and formatting (Weedon et al. 2014). In brief, WFDEI is an evolution of WFD where the underlying re-analysis is now ERA-Interim but using the same bias correction methodology. This product has been proven to be superior to WFD. CRU (Climate Research Unit) monthly total precipitation observations were used to biascorrect the precipitation in WFD and WFDEI datasets. However, the WFD uses a previous version CRU TS 2.10 before the CRU TS 3.1 used in WFDEI was released (Weedon et al. 2014). The two CRU datasets differ in the time period (CRU TS 2.10: 1901–2002; CRU TS 3.1: 1979–2009; Jones and Harris, 2013), in the stations used and in the methods employed; see Harris et al. (2014) for details. Hence, there are still some differences between the two which could further affect the hydrological responses. The two datasets are named WFD-CRU and WFDEI-CRU for later description, and the time step for all the forcing variables is 3 h.

The CRU datasets were constructed by monthly observations at meteorological stations across the world’s continents. The observations were then interpolated to  $0.5^\circ$  longitude - latitude grid cells. Though the CRU compares favorably to some other gridded datasets, it has significant deviations over regions and time periods with sparser observational data (Harris et al. 2014). Moreover, because only the monthly total precipitation was used to correct WFDEI and WFD, it cannot improve the temporal variabilities at smaller time steps (i.e., daily or sub-daily). However, the precipitation variations in a short period would result in different hydrological responses even in the condition of the total monthly amount remaining the same (Potter et al. 2005).

Hence, in addition, the WFDEI-CRU dataset was further corrected by the gridded daily precipitation data from the China Meteorological Administration (named CMA). The CMA precipitation product compiles 2416 national meteorological monitoring stations over China,

using the climatological optimal interpolation method to generate the gridded  $0.5^\circ$  precipitation field from 1951 to 2016 (Shen et al. 2010). PRISM (Parameter-elevation Regression on Independent Sloped Methods; Daly et al. 2008) was used to lessen the orographic effects (Shen et al. 2010). The density of meteorological stations used in the CMA is much higher than that used for CRU. For instance, there are only six gauges over the Tarim Basin in the CRU database, while 39 gauges are recorded in the CMA system (Tao et al. 2011) so that it can to a certain degree improve the data applicability where precipitation is spatially inhomogeneous compared to CRU datasets. Given that the CMA data provide the daily information, it also improves the temporal variations of precipitation rather than using the total monthly value in CRU datasets. The corrected atmospheric input dataset is hereafter referred to as WFDEI-CMA.

### Glacier melt dataset

As mentioned in Sect. 2, glacier melt is a vital water input to the Tarim. However, glacier runoff measurement is so difficult for such large regions that model-based estimates of the glacier melt are necessary. In general, a glacier module is not coupled in LSMs (Fraedrich et al. 2005). Hence, rather than building a separate glacier module, we use an independent daily glacier melt dataset obtained from the glacier model called HYOGA2 (meaning glacier in Japanese), which has been proven reliable over the globe (Hirabayashi et al. 2013). HYOGA2 is a temperature-index-based model utilizing an extensive global-scale glacier inventory and has several improvements compared to its first version (HYOGA) in model parameter simulation as well as the temporal extent. More details can be found in the original papers (Hirabayashi et al. 2010; Hirabayashi et al. 2013). The glacier melt is added to the rainfall series of WFDEI-CMA as an additional water flux to the system. The melt water hence participates instantaneously in the water cycle without delays such as stores in ice, glacier pack or groundwater recharge beneath the ice being considered. This method was chosen for its simplicity and the lack of knowledge on the details at the transition between the glacier and the soil. Daily values are uniformly distributed over the eight time steps per day of WFDEI. By adding the glacier melt, the fourth new forcing dataset is generated as WFDEI-CCG.

### 3.3.2 Land Surface Model-ORCHIDEE

The land surface model ORCHIDEE (Organizing Carbon and Hydrology In Dynamic Ecosystems) was developed by the Laboratoire de Météorologie Dynamique (IPSL-LMD) (Ducoudré et al. 1993; Rosnay and Polcher 1998; D'Orgeval and Polcher 2008). After more than 20 years of development, ORCHIDEE has been validated from the global scale (Alkama et al. 2010) to typical regional cases, e.g., tropical rainforest area (Amazon, Guimberteau et al. 2012a), semiarid regions (Western Africa, D'Orgeval et al. 2008) and middle-latitude regions (Europe, Tallaksen and Stahl 2014). Within ORCHIDEE, only SECHIBA (Schematisation des Echanges Hydriques l'Interface entre la Biosphere et l'atmosphère), which represents the energy and water fluxes between land surfaces and the atmosphere, is used in this study. The hydrological module in SECHIBA is based on developments by Rosnay et al. (2003) and D'Orgeval (2006). Thirteen types of vegetation are defined (D'Orgeval and Polcher 2008), and

dynamic leaf area index is computed to generate the interception and transpiration. The vertical soil water movement is represented by diffusion-type equations resolved on a fine vertical discretization (11 levels) and partitioning between infiltration and surface runoff through a time-splitting procedure (Rosnay et al. 2002; D'Orgeval and Polcher 2008; Guimberteau et al. 2012a). The routing is conducted based on a linear reservoir concept through redefined routing units which are different from the atmospheric grids (Guimberteau et al. 2012a). The ORCHIDEE version used in this study is available at <https://forge.ipsl.jussieu.fr/orchidee/> (Nguyen-Quang et al. 2018).

### Evapotranspiration simulation

On top of precipitation, evapotranspiration and potential evapotranspiration are two important fluxes, and their errors are key to the water cycle modeling. In ORCHIDEE, the evapotranspiration is calculated with energy balance and resistance concepts. The potential evapotranspiration is defined as “the amount of evapotranspiration that would occur if enough water was available at the surface”, as explained in Barella-Ortiz et al. (2013). The PET is computed as the sum of the potential soil evaporation and the potential transpiration from vegetation. For soil evaporation, the diffusive equations are taken with the ratio of the humidity gradient, the aerodynamic resistance and the air density. The virtual surface temperature is used instead of the actual one to compute the saturate humidity, while the virtual surface temperature is calculated through an unstressed surface energy balance. The method has been proven superior to other diffusive methods in the reference paper (Barella-Ortiz et al. 2013). The potential transpiration is driven by the potential evaporation between the evaporating surface and the overlying air but is limited by vegetation resistances. The maximal water loss under stress-free conditions is the potential transpiration (Guimberteau et al. 2012a). The actual evapotranspiration is a function of the potential evaporation but is modeled by a series of resistances (canopy and aerodynamics) of the surface layer. The details of the methods in simulating PET and ET can be found in D'Orgeval (2006), Guimberteau et al. (2012a), and Barella-Ortiz et al. (2013).

### Snow and soil freezing scheme

There is one key improvement which has been implemented in the current version of ORCHIDEE, that is, the snow and soil freezing scheme. Snow and soil freezing are two crucial water processes in cold regions; snow covers nearly half of land area (Wang et al. 2013b), and the frozen soils occupy 55 % to 60 % of the land surface of the Northern Hemisphere in winter (Zhang et al. 2003). Snow plays an important role in both the energy and water flux as the snow cover is first an insulation which prevents the heat loss from the soil. It also increases the thermal inertia of the surface by adding a new phase change and acts as a moisture reservoir which stores winter precipitation that is released in spring or early summer. In the old ORCHIDEE version, a constant density and very simple heat capacity are applied for the snow. The snowmelt directly feeds the runoff without refreezing, and the snow layer is mixed with the first soil layer so that they are equal in temperature. While in the new snow scheme, the snow layer is defined and separated from the soil layers. The snowpack

is represented in three layers which adequately resolve the snow thermal gradients between the top and base of the snow cover. The energy balance and the temperature of the snow body become more realistic. Refreezing of the snowmelt is allowed, which makes the energy changes more reliable. The snow properties are more detailed than before, i.e., the density, albedo and roughness. All the improvements have been validated over France and northern Eurasia and already implemented in the current ORCHIDEE (Wang et al. 2013b).

Soil freezing impedes water infiltration and drainage, thus leading to changes in hydrological responses (Woo and Marsh 2005). At small scales, the soil freezing alters the soil structure and therefore its water capacity, which has a consequence on the water flux between soil and atmosphere, as well as the water availability for plants (Pitman et al. 1999; Huang et al. 2018). On the other hand, the frozen soil changes the latent heat exchange, which delays the soil temperature signal (Boike et al. 1998). Soil thermal characteristics are also improved due to the different thermal properties of ice and water. In the old soil thermal equations, thermal advection and phase change of the water are not considered when resolving the latent heat exchanges (Gouttevin et al. 2012). The mechanical effects of soil freezing are therefore ignored. In the new soil freezing scheme, the apparent soil heat capacity can be increased by considering the ice content of the soil layer during a freezing-temperature window between 0 and -2 °C. A temperature correction is applied if any soil layer is entirely frozen or thawed. Moreover, the soil heat conductivity is changeable according to the ice content in the soil, which affects the thermal propagation in the vertical soil column. Finally, the hydraulic conductivity is reduced as a function of the ice content. Liquid water is not allowed to cross the frozen soil layers. Thus infiltration and drainage are forced to stop. Full descriptions of the new freezing soil equations and the parameterizations setting can be found in (Gouttevin et al. 2012).

### **Human intervention**

Irrigation is included in the current version of ORCHIDEE. The irrigation requirement is estimated as the deficit of the available water of the corresponding grid to the potential evapotranspiration. The irrigation extracts water from the local grid first and then its neighboring grids if necessary (Guimberteau et al. 2012a). This solution is acceptable for most of the humid regions at a 0.5° resolution since the rivers are very likely within 100 km. However, for dry regions, the Tarim for example, the irrigation area is concentrated, with controlled irrigation infrastructures. The nearby rivers are far from the irrigation area, and the irrigated water is not taken directly from the rivers but transported from upstream by channels. Due to the shortcoming of the scheme and the lack of knowledge on the local irrigation, we turned off the irrigation in ORCHIDEE. In the Tarim Basin, the irrigation accounts for more than 95 % of the consumed water (Zhou et al. 2000), so that the difference between the simulated discharge and observations can be attributed to neglecting irrigation in the model.

In conclusion, as shown in Fig. 3.2, four different forcing inputs are prepared to drive the ORCHIDEE simulations, two basic forcing datasets (WFD-CRU and WFDEI-CRU), one after correction by CMA (WFDEI-CMA) and then one after adding glacier melt (WFDEI-CCG). Among them, the input water amounts are different, while WFDEICMA and WFDEI-CCG

have the same other forcing variables as WFDEI-CRU. Additionally, the experiment with the newly developed snow and soil freezing scheme is named WFDEI-CCG-SF based on the forcing dataset WFDEI-CCG. Because the WFD covers the overlapping period 1901–2002, the WFDEI covers the period 1979–2014, CMA covers years 1951–2016 and the glacier melt dataset covers 1958–2001, all the simulations and analysis in this paper are over the overlap period 1979–2001. The monthly discharge measurements for those chosen hydrological gauges over 1979–2001 are then compiled. Spatial resolution for all the forcing inputs remains  $0.5^\circ$  (about 50 km at the Equator), and the time step is 3 h.

### 3.3.3 Main biases over the headwater catchments

In the water cycle, all the water entering a specific river basin will become ET back to the atmosphere and discharge (R) flowing out of the basin as long-term water storage changes are negligible. The underestimation of discharge is thus attributable either to the underestimation of water inputs or to overestimation of evapotranspiration. The possible biases from water inputs and the ET estimation are discussed in this section.

#### Bias in precipitation

The Tarim Basin is one of the areas where significant deviations exist among different modeled precipitation estimates and observation-derived datasets because of the sparse observations and orographic effects (Fekete et al. 2004; Wu et al. 2012b). Meanwhile, the precipitation bias might not be well addressed in the CMA system because the number of meteorological gauges is still too limited in the Tarim region to build a reliable interpolation climate field (Shen et al. 2010). Although Xie et al. (2007) have tried to use other gauges outside China, the density of the gauge distribution is extremely low around the boundaries of the Tarim Basin where most of the precipitation is generated. Furthermore, due to the orographic effects, the precipitation over the mountainous area is larger and with more significant heterogeneity than that in the plains (Daly et al. 2008; Chorley et al. 2003), while the center of the precipitation events is hard to observe for the nearby gauges. Adam et al. (2006) has pointed out that the orography could cause 41.6 % underestimation of the precipitation over the northwestern North American mountainous ranges, and the deviations are larger at higher altitude.

#### Bias in rainfall and snowfall repartition

The differences between WFDEI-CRU and WFDEI-CMA are not only in the total amount of precipitation but also in the proportion of rainfall and snowfall (Table 3.3). Compared to the rainfall, the snowfall is more difficult to observe and affected by a large uncertainty; hence in the CMA dataset, only the rainfall was recorded and then used to scale the CRU dataset but keeping the relative proportion of liquid and solid precipitation provided by WFDEI-CRU. The energy needs for phase change are considerably different for the liquid from the solid water. Berghuijs et al. (2014) suggested snow will lead to more runoff than rain in similar

conditions based on the observations over the US and China. The impact of the precipitation type on the evapotranspiration rate is affected by many factors and hard to measure.

### **Bias in glaciers melt**

HYOGA2 is a state-of-the-art global glacier model but has not been calibrated over the Tarim Basin. The general bias for global estimation is around -5.0 % compared to the available global glacier mass balance measurements (Hirabayashi et al. 2013). The estimated annual glacier melt amount is  $81.0 \times 10^8 \text{ m}^3 \text{ yr}^{-1}$  for the whole Tarim Basin (Table 3.3), significantly lower than previous estimations ( $133.4 \times 10^8 \text{ m}^3 \text{ yr}^{-1}$ , Yang 1991) and ( $144.16 \times 10^8 \text{ m}^3 \text{ yr}^{-1}$ , Gao et al. 2010). On the one hand, the difference in the forcing which drives the glacier melting model is probably one of the causes of the deviation. On the other hand, all the glacier melt is evenly distributed in a whole grid. It leads to a higher infiltration ratio and thus feeds more evaporation (Berger and Entekhabi 2001; Potter et al. 2005). This also artificially forces part of the glacier melt to flow out of the grid not belonging to the right basin. However, it is unable to eliminate this problem with the current gridded concepts. Finer spatial resolution in glacier dataset and model simulation is needed to lessen the impacts of discretization.

### **Bias in potential evapotranspiration estimation**

As described in Sect. 3.2.1, the PET estimation is independent of underlying conditions (e.g., topography, vegetation) because enough water is provided. It is therefore determined only by forcing conditions, especially the humidity gradient and aerodynamic conditions (e.g., radiation flux, wind). Temperature also plays a role in its estimation. Thus, the bias in PET is mainly propagated from various forcing variables.

### **Bias in actual evapotranspiration estimation**

Overestimation (underestimation) of the actual ET will also result in the discharge underestimation (overestimation). Many processes can cause ET errors either by the biases in PET or the stress functions which limit the potential evaporation. The vegetation fraction, vegetation type, surface slope and soil properties are all the uncertain sources affecting the final ET estimation.

### **Bias sources category**

With the main biases listed as above, we consider bias in any processes that changes  $P$  or PET as bias from forcing and bias in any processes that directly changes ET as bias caused by model structure. Although the shifts in forcing variables will change the ET estimation - for example, the  $P$  restricts the available water for ET - this shift still belongs to the forcing category since the relation is indirect. The biases which directly affect ET include biases in infiltration, soil water movement, snow processes, vegetation representation and many other model processes. And all these are considered as biases caused by model structures.

### 3.3.4 Budyko hypothesis

Budyko hypothesis is an empirical expression for the coupling of the water and energy balances at the surface. It uses the relation between the water and energy balance equation to partition  $P$  into ET and R. The Budyko curve is the analytical solution to the Budyko hypothesis, expressed as the evapotranspiration rate ( $ET/P$ ) being a function of the aridity index ( $PET/P$ , Webster 1976). Many forms of Budyko curves have been developed and can be categorized into a non-parameter group and parameter group depending on whether there is an adjustable parameter describing the Budyko shape (Table 3.1).

Table 3.1 – Different formulas of Budyko curves. Note that the aridity index is expressed as  $\theta = PET/P$ .

No.	Parameter	Formula	Reference
1	Non-parameter	$ET/P = 1 - e^{(-\theta)}$	(Schreiber 1904)
2	Non-parameter	$ET/P = \theta \tanh(1/\theta)$	(OL'DEKOP 1991)
3	Non-parameter	$ET/P = 1/(1 + (1/\theta)^2)^{0.5}$	(Pike 1964)
4	Non-parameter	$ET/P = \{[1 - e^{-\theta}] \cdot \theta \cdot \tanh(1/\theta)\}^{0.5}$	(Webster 1976)
5	Parameter n	$ET/P = 1/[1 + (1/\theta)^n]^{1/n}$	(Choudhury 1999) ; (Yang et al. 2008a)
6	Parameter $\varpi$	$ET/P = 1 + \theta - [1 + (\theta)^\varpi]^{1/\varpi}$	(Fu 1981)
7	Parameter $\varpi$	$ET/P = (1 + \varpi\theta)/(1 + \varpi\theta + 1/\theta)$	(Zhang et al. 2001)

The forms without parameters (formulas 1 to 4) are universal for most of the basins, while they are unable to capture the various landscape characteristics across regions (Yang et al. 2007). Regarding the effects of landscape characteristics, adjustable parameters and corresponding formulas were introduced as formula (5) to (8). Although they have different analytical expressions, the shape of these curves is quite similar (Gerrits et al. 2009) and their parameters are highly correlated (Yang et al. 2008a). Hence, from the formulas with parameters, Fu's equation (formula 6) is chosen in this study as it is more often used in the China region.

The ranges of the aridity index ( $PET/P$ ) correspond to the regional precipitation feeds and climate types (Table 3.2). For example, the precipitation for a semiarid region ranges from 400 to 800 mm yr<sup>-1</sup>, and the regional aridity index mostly ranges from 2 to 5. Moreover, the Budyko curve is a reflection of the landscape characteristics which can influence the water movement through different hydrological cycles (Dingman 2015) and thus changes the ET rate. Many surface conditions are related to the Budyko parameter setting. (1) Vegetation types and vegetation cover affect the ET rate. Transpiration accounts for about 42 % (25 %–64 % depends on different models) of global ET (Zhang et al. 2004). Regions that have a larger fraction of vegetation cover or are covered by vegetation with bigger leaves and deeper roots tend to have a larger transpiration rate as well as ET rate; i.e., the forested catchment tends to show a higher evaporation ratio than the grass-covered catchments (Zhang et al. 2004; Carmona et al. 2014). (2) Properties of soil determine infiltration rates and the amount of evapotranspirable water. Steeper slopes are more likely to shed surface water as runoff (Yang et al. 2007; Yu et al. 2014). Limit of infiltration ability also matters as intense precipitation rates (Berger and Entekhabi 2001; Potter et al. 2005) or freezing soils tend to

force the water into the surface runoff (the solid frozen soil limits the percolation of infiltrated water, Gouttevin et al. 2012). (3) The ability to transmit or retain infiltrated water of soil also determines the evapotranspiration rate; the soil with larger water conductivity is likely to release more subsurface water rather than evaporation (Yang et al. 2007). (4) The soil depth determines the ability to store infiltrated water. Rocky mountains or regions with thin soil would produce more runoff and less ET (Yang et al. 2008a; Dingman 2015).

Table 3.2 – The definition of climate types by precipitation and aridity index ((Ponce et al. 2000)).

Climatic types	$P$ (mm/yr)	Aridity index (PET/ $P$ )
Superarid	<100	>30
Hyperarid	100-200	12-30
Arid	200-400	5-12
Semiarid	400-800	2-5
Subhumid	800-1600	0.75-2
Humid	1600-3200	0.375-0.75
Hydrperhumid	3200-6400	0.1875-0.375
Superhumid	>6400	<0.1875

### 3.3.5 Bias assessment with ORCHIDEE-Budyko framework

The Budyko formulation relates the ET to PET and  $P$ . Both the biases from the water flux ( $P$ ) and energy flux (PET) will propagate to ET. The shape parameter of the Budyko curve is obtained by fitting the PET /  $P$  and ET /  $P$  relation; it is thus a reflection of the model if we use the simulated PET and ET fluxes (i.e., ORCHIDEE simulations in this study, red dots and red curve in Fig. 3.3). However, because of the existing bias in all the three variables, the relations of the three components may have been shifted to an unrealistic state (point A in Fig. 3.3). Therefore, the changes in  $P$ , PET or ET which can shift the system back to a reliable state are considered as the possible bias. The difference between the unrealistic state with their corrected values provides the estimation of how the forcing or the model would need to be changed for the model to produce the realistic discharge values. To separate the individual effect of the single water–energy component on the hydrologic cycle, three independent assumptions are made as follows, and the illustration can be found in Fig. 3.3.

The red dots in Fig. 3.3 represent the states of the PET /  $P$  and ET /  $P$  according to ORCHIDEE estimations and forcing inputs for each year. Point A represents the representative state, which is the average of the dots' locations. It reflects the current model and is probably in an unrealistic state because the modeled discharge ( $P$ -ET) may be with bias compared to the observations.

Assumption 1. Only the water input ( $P$ ) is uncertain. Because the model structure remains unchanged, the relation between ET /  $P$  and PET /  $P$  still follows the original Budyko line regardless of how  $P$  changes. The PET is assumed to be independent of  $P$ , while the ET is modified as a result of  $P$  changes. To meet the deviation between simulated discharge (RS) and the observed discharge (RO), the representative point (long-term “corrected” annual ET /  $P$  against long-term “corrected” annual PET /  $P$ ) should be shifted along the Budyko

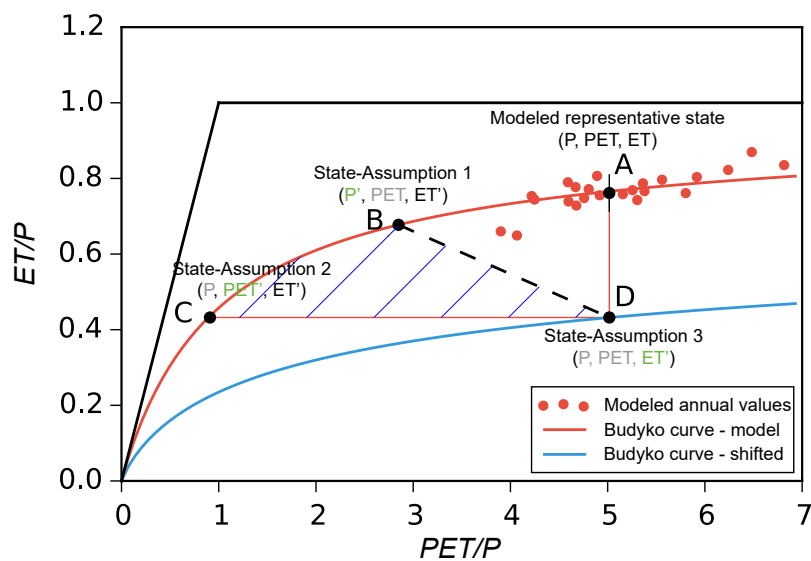


Figure 3.3 – The illustration of the ORCHIDEE-Budyko framework. Point A represents the average state among the modeled annual values (with land surface model-ORCHIDEE), and the red curve is the simulated Budyko curve following the modeled state. Point B, C, D represent the representative state with shifting the  $P$ ,  $PET$  and  $ET$  respectively with different assumptions to meet the discharge observations. A shifted Budyko curve (blue) is obtained crossing the point D which indicates a new state of model structure. The new points of B and C still stay on the original Budyko curve indicating that the model structure remain the same and the changes only relate to forcing variables. The shade area is the area among the three shifted states.

curve from current point “A” to the new point “B”, where the difference between the “true” precipitation ( $P'$ ) and the “true” evapotranspiration ( $ET'$ ) equals the observed discharge ( $P' - ET' = RO$ ). The possible maximum bias in  $P$  is calculated as

$$\text{Bias}(P) = (P - P')/P' \times 100\%. \quad (3.1)$$

Assumption 2. Only the PET is uncertain. The  $P$  remains the same, while  $ET$  changes because of the changes in PET. Under these conditions, the model structure still remains unchanged, and so does the Budyko curve. Then the representative point should be shifted along the Budyko curve to point “C” to decrease the  $ET$  ratio to meet the discharge observation ( $ET' = P' - RO$ ). The PET is changed to a “true” PET', and the possible maximum bias in PET is calculated as

$$\text{Bias}(\text{PET}) = (\text{PET} - \text{PET}')/\text{PET}' \times 100\%. \quad (3.2)$$

Assumption 3. Only the  $ET$  is uncertain.  $P$  and PET, which are mainly linked to the forcing, remain the same, while the  $ET$ , which is significantly affected by the model structure, is assumed biased. It is essentially relevant to the model processes rather than the forcing dataset. To compensate the discharge bias, the  $ET$  should be decreased to point “D” where the  $ET$  equals precipitation minus observed discharge ( $ET' = P' - RO$ ). The possible maximum bias in  $ET$  is calculated as

$$\text{Bias}(ET) = (ET - ET')/ET' \times 100\%. \quad (3.3)$$

With the target  $ET'$ , a new Budyko curve can be drawn for new relations between  $P$ , PET and the new  $ET$  (the blue lines in Fig. 3.3). However, all the assumptions are proposed in conditions of only one variable being uncertain, but in reality any of the three variables can be biased at the same time. The final probable “corrected” state may be located in the shaded area identified by the three states (Fig. 3.3).

## 3.4 Results and discussion

### 3.4.1 Forcing and discharge comparison

#### Forcing inputs comparison among experiments

We specify  $P$  as the sum of all the water inputs into the system, which include the atmospheric water flux (in its liquid and solid phases) and glacier melt. The precipitation for the three headwater catchments and the upper Tarim is listed in Table 3.3 for each simulation. The interannual variations and the intra-annual cycle of total precipitation over upper Tarim Basin are plotted for different forcing in Fig. 3.4.

The annual cycle of the two basic forcing datasets WFD-CRU and WFDEI-CRU are similar, while the precipitation in WFDEI-CRU is slightly larger in monthly values (Fig. 3.4a, red and blue lines). The deviation is the result of their expanding differences after 1990 (Fig. 3.4b). The precipitation difference is mainly due to the fact that two different versions of CRU

Table 3.3 – The five simulations in this study and basic diagnostics of the water inputs over three headwater catchments and the Upper Tarim basin. Units:  $10^8 \text{ m}^3 \text{ yr}^{-1}$ .

Subbasins	Area ( $\text{km}^2$ )	Simulations	Precipitation	Rainfall	Snowfall	Glacier
Yarkand	55637	WFD-CRU	80.19	11.16	69.03	-
		WFDEI-CRU	82.04	20.82	61.22	-
		WFDEI-CMA	117.73	92.35	25.38	-
		WFDEI-CCG	141.21	104.09	25.38	11.74
		WFDEI-CCG-SF				
Hotan	34557	WFD-CRU	31.83	6.63	25.20	-
		WFDEI-CRU	33.34	4.37	28.97	-
		WFDEI-CMA	82.71	72.13	10.58	-
		WFDEI-CCG	137.34	99.45	10.58	27.31
		WFDEI-CCG-SF				
Aksu	31982	WFD-CRU	76.11	49.06	27.05	-
		WFDEI-CRU	78.03	41.83	36.19	-
		WFDEI-CMA	106.38	72.22	34.16	-
		WFDEI-CCG	120.23	79.15	34.15	6.93
		WFDEI-CCG-SF				
Tarim	359022	WFD-CRU	435.94	221.55	214.39	-
		WFDEI-CRU	473.31	246.35	226.96	-
		WFDEI-CMA	649.71	524.08	125.63	-
		WFDEI-CCG	758.74	578.60	125.62	54.52
		WFDEI-CCG-SF				

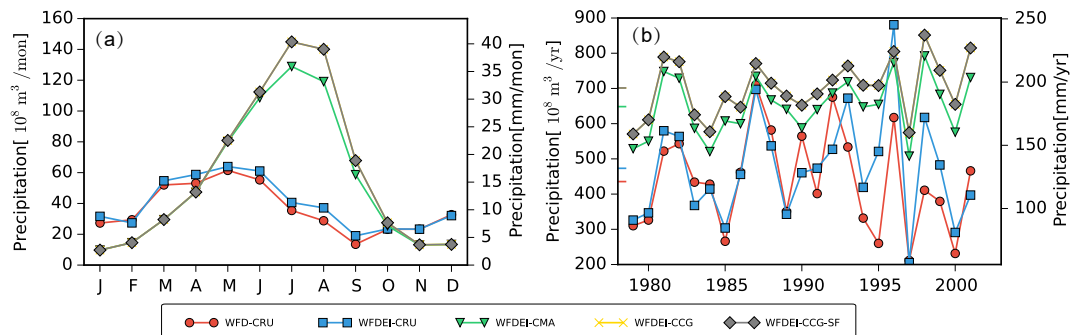


Figure 3.4 – The inter-annual cycle and intra-annual series of the precipitation (including rainfall, snowfall and glacier) in difference simulations for the Upper Tarim basin.

(CRU TS 2.10 and CRU TS 3.1) are used for precipitation correction in WFD and WFDEI (See subsection 3.1.2 or Weedon et al. 2014). The precipitation difference between the two CRU datasets is relatively small, while the CMA dataset increases the precipitation to a large extent, by 37.3 %, compared to CRU for the upper Tarim Basin (Table 3.3). The changes mostly occur during summer when the peak of CMA precipitation is more than twice as large as precipitation in CRU. The shape of the annual cycle changes greatly as the timing of the peak is shifted from April to July. However, the precipitation amount in winter (DJF) decreases in CMA, to which the decrease in snowfall is the major contributor. The changes in rainfall and snowfall are similar in all three headwater catchments (Table 3.3) and the upper Tarim Basin.

Adding the glacier melt leads to negligible changes during winter and spring but large increases in the total water inputs in summer (JJA) when the temperature is higher. The estimated glacier melt is 9.1 %, 25.8 % and 6.1 % to the total water inputs for the upper Yarkand River, upper Hotan River and upper Aksu River. It significantly increases after 1990 (Fig. 3.5; the trend is  $+3.8 \times 10^8 \text{ m}^3 \text{ yr}^{-2}$ ,  $p = 0.024$ ), being consistent with its ratio to the total water input ( $r = 0.918$ ,  $p < 0.001$ ). The trend is mainly caused by climate warming as the glacier melt is highly correlated with the summer temperature ( $r = 0.852$ ,  $p < 0.001$ ). The increasing trend has also been documented in glacier runoff observations (Shangguan et al. 2009).

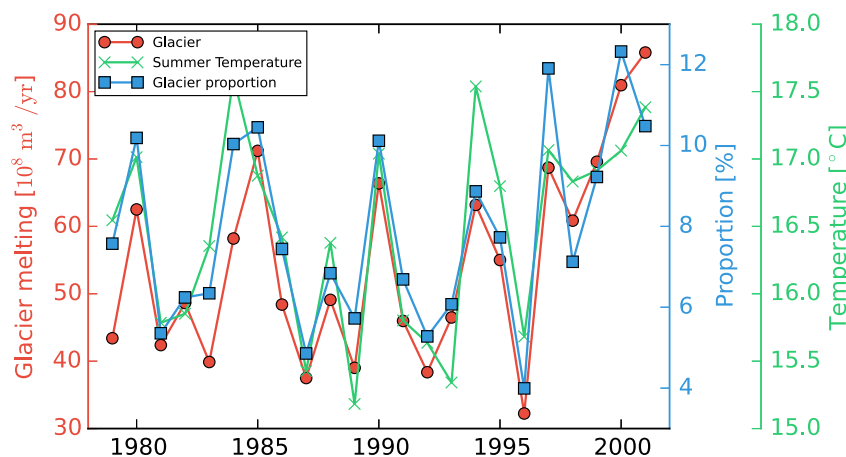


Figure 3.5 – The temporal variations of the glacier melt, the proportion of glacier melt in the water input and the average summer temperature over the Upper Tarim basin. They are in good correlation and have a consistent increasing trend after 1990.

### Assessment of the discharge estimations with observations

Evaluating the bias in precipitation over meteorological rain gauges is not convincing as most gauges are located at lower altitude, which makes it difficult to capture regional patterns as intensive precipitation occurs over higher mountains. Instead, the discharge measurement can serve as a better reference since it integrates the net water flux over the entire basin. Therefore, driven by the forcing, ORCHIDEE was used to simulate the river discharge and for comparison to in situ observations (Fig. 3.6). The corresponding assessment using criteria for

the three headwater catchments are plotted in Fig. 3.7. For the three headwater catchments where most of the discharge of the Tarim Basin is generated, the discharge is significantly underestimated, with the underestimation ratio reaching 90 % (Figs. 3.6b, d, f, 3.7a) for CRU datasets. Discharge increases after the precipitation is corrected by the CMA dataset, with the absolute bias decreasing to around 80 %. Adding glacier melt also increases the discharge but by a relatively small amount. Changes in the model structure (new snow and soil freezing scheme) further decrease the bias, especially for the Aksu River. The final biases of the discharge for the three subbasins are -71.1 %, -47.8 % and -49.4 %. The gradual improvements and corresponding magnitude changes are visible in the annual discharge variability in Fig. 3.6b, d and f.

Besides the increase in the annual mean discharge, the amplitude of the interannual cycle of the discharge is also improved by the progressive changes. The estimated discharge peaks have been shifted from April in CRU simulations to the summer (July or August) by CMA correction and adding glaciers (Fig. 3.6a, c, e). Correspondingly, the correlation of the annual variability between the estimated and observed discharge has increased above 0.9 for all the three subbasins with the WFDEI-CCG forcing (Fig. 3.7b). However, contrary to the upper Yarkand River and the upper Hotan River, the introduction of the new snow and soil freezing scheme decreases the discharge correlation for the upper Aksu River from 0.91 to 0.42. An early discharge peak exists in May, while not enough runoff is generated in the summer period (Fig. 3.6e). Although the correlation decreases, it does not mean the model/simulation deteriorates because correlation only evaluates the similarity of temporal variation but ignores the fact that the discharge amount has been better estimated (Figs. 3.6e and 3.7a).

By extracting the observed discharge in the first and last 5 years from the whole period, we can notice there is an obvious shift of the discharge peak from August to July in the three headwater catchments (Fig. 3.6a, c, e). The regional precipitation changes largely cause the shift, but the increasing temperature also allows the snow/glacier to melt at a higher rate in the most recent period. Furthermore, increasing trends are detected after the 1990s (Fig. 3.6b, d, f), as the increasing trend is  $1.43 \times 10^8 \text{ m}^3 \text{ yr}^2$  (or  $0.77 \times 10^8 \text{ m}^3 \text{ yr}^2$ ,  $1.78 \times 10^8 \text{ m}^3 \text{ yr}^2$ ) for the upper Yarkand (or Hotan, Aksu) River. The increasing trends are consistent with the glacier melt, glacier proportion in water input and summer temperature in the same period (Fig. 3.5).

The trends in the estimated discharge are also calculated and compared with the observed trends, expressed as the ratio of the trend in estimation to that in observations (Fig. 3.7c). For CRU simulations, no increasing trend is detected since the ratio is less than 0. The CMA correction increases the ratio for all three subbasins to around 0.3, which means the precipitation accounts for only around 30 % of the discharge increase. Adding the glacier melt increases the ratio from 0.35 to 0.54 for the upper Hotan River and from 0.31 to 0.76 for the upper Aksu River; the improvement of the glacier melting is comparable to the CMA correction. However, no apparent changes are detected for the upper Yarkand River. By comparing the criteria between WFDEI-CMA and WFDEI-CCG, we find that, although adding the glacier melt does not change much the absolute amount of discharge or the correlation, the increased trend in discharge has been considerably improved. The increasing glacier melt is, therefore, one of the contributors to the discharge trend in the Tarim. The modification of the snow and soil freezing scheme increases the trend ratio in the upper Aksu River up to 0.72,

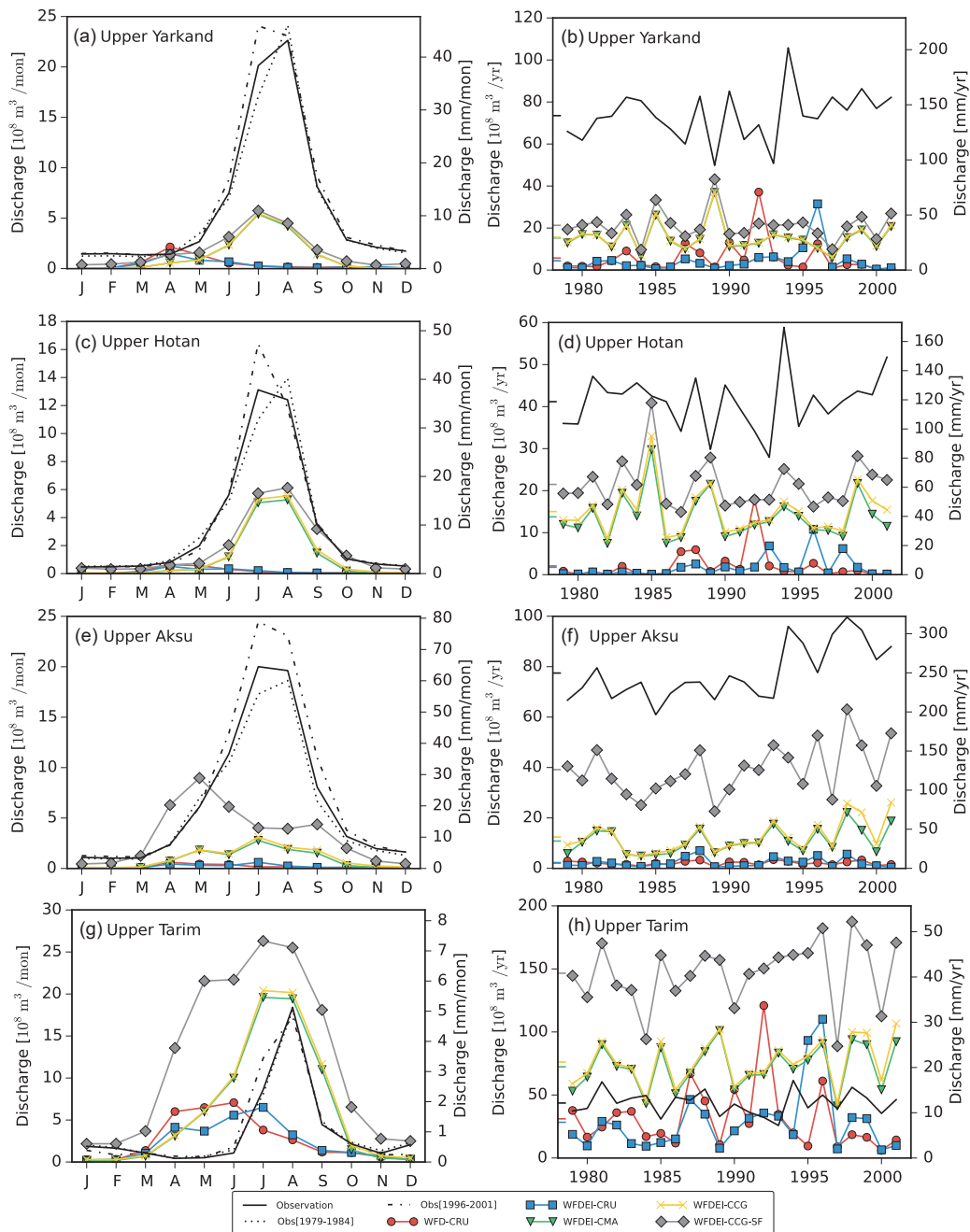


Figure 3.6 – The inter-annual cycle and intra-annual series of the discharge simulation for three headwater catchments and the Upper Tarim basin, a,b-Yarkand, c,d-Hotan, e,f-Aksu and g,h for the Upper Tarim. Observed discharge for each subbasin was aggregated by the measurements at separated discharge gauges and shown as the black solid line. The simulated discharges at the corresponding grids were extracted from each experiment and plotted as the color lines with markers. The dotted line and dotdash line in the inter-annual cycle plots represent the observed discharge in different periods.

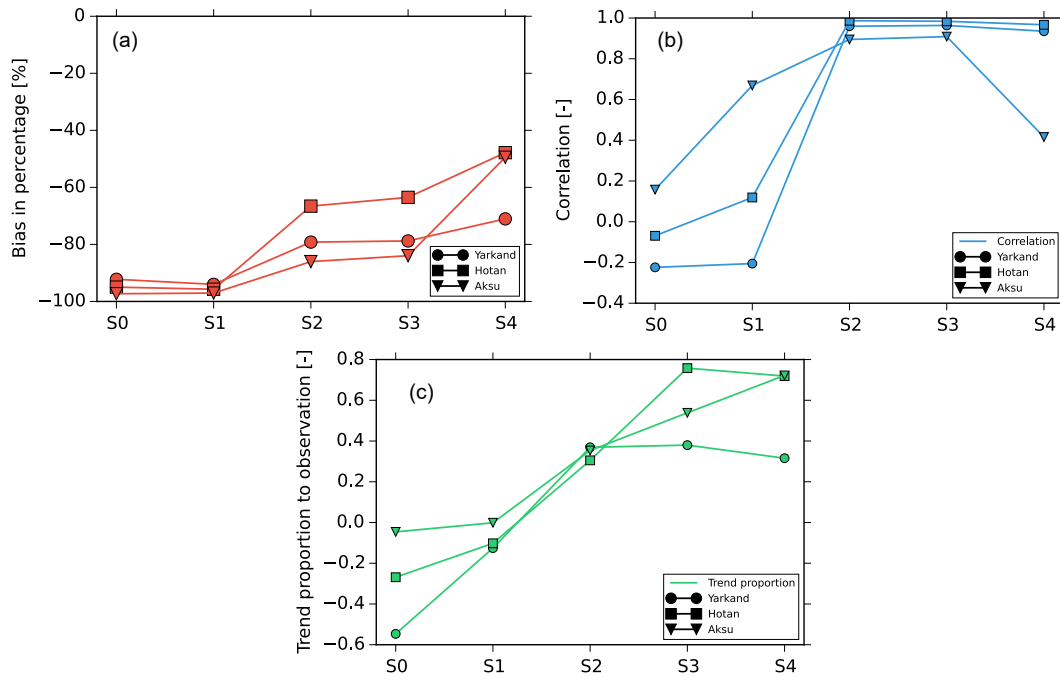


Figure 3.7 – The discharge diagnostics of different experiments for three catchments (round-Yarkand, square-Hotan and triangle-Aksu). a) represents the absolute bias in percentage, b) represents the correlation of the inter-annual cycle and c) represents the ratio of the trend in estimated discharge to that in observed discharge for period 1990-2001. S0 to S4 correspond to the experiments WFD-CRU, WFDEI-CRU, WFDEI-CMA, WFDEI-CCG and WFDEI-CCG-SF respectively.

while slightly decreasing it for the two other catchments.

In brief, the gradual refinement of the forcing datasets (from WFD-CRU to WFDEI-CRU to WFDEI-CMA to WFDEI-CCG) is effective for improving the model performance using different criteria (bias, correlation, proportion to the trend) to compare the observed discharge. The three criteria are independent as they stand for the averages, the variation and the trend, which can capture the various aspects of the model agreement to the observations. The responses are similar for different catchments, but at different magnitude at different stages. The correction of the CMA dataset is the most significant improvement to all the criteria. The role of glaciers melting is critical for the trend analysis. The modification in the snow and soil freezing scheme increases the total discharge amount but could lead to adverse responses in the correlation and trend simulation. However, the impact of the modification of the model structure is not larger than changes resulting from the forcing biases. From the previous analysis, we can conclude that the simulations of WFDEI-CCG and WFDEI-CCG-SF are comparable in the correlation and trend analysis, while WFDEI-CCG-SF is better regarding the water quantity. Therefore, the further study on the bias is all based on the WFDEI-CCG-SF simulation.

### 3.4.2 Evidence of the bias in estimated discharge for the headwater catchments

Although the simulations with WFDEI-CCG-SF are better than other experiments, there are still biases compared to the observations (Fig. 3.7a). In this section, we aim to find evidence of the biases. The annual mean water balance components (rainfall, snowfall, glacier melt, estimated ET and discharge RS) of the three upper catchments are plotted as bars with their relations quantified by comparison to the discharge observations (RO, red lines in Fig. 3.8a, c, e) in WFDEI-CCGSF. Their annual cycles are also plotted as Fig. 3.8b, d and f over the three headwater catchments. Over a long enough period, the changes in terrestrial water storage are assumed negligible compared to the water fluxes, so that the water input into the system either returns to the atmosphere through ET or flows out of the basin as RS.

From the left panels of the Fig. 3.8, we have a visual impression of the relative amount of different water inputs and their contribution to the ET or discharge. Note that the sum of the ET and RS is not exactly equal to  $P$  because in ORCHIDEE the discharge is represented at the outflow of the grid and not at the confluence point of the analyzed catchment with other tributaries. The largest bias is 8 % for the upper Yarkand River (Fig. 3.8a,  $ET / P + RS / P = 0.92$ ), while it matches exactly for the upper Aksu River. The bias can be added to the current RS if necessary.

Among the three headwater catchments, the upper Hotan River has the best discharge simulation compared to the observations ( $RS / RO = 0.52$ ). The annual cycle of the water also matches well as all the  $P$ , ET and discharge RO or RS have the synchronous peaks in summer (Fig. 3.8d). There are also deviations between  $P$  and E, which represent the net water inputs to the system and the estimated discharge (the shaded area with blue lines in Fig. 3.8d). The deviation implies the regional water storage changes; in summer the soil moisture increases to store the abundant water inputs, which are later released in autumn and winter when the drainage rate is larger than infiltration. The water storage decreases as a result by then. It is the natural adjustment to the strong seasonality in water inputs.

As the neighboring catchment of the upper Hotan River, the upper Yarkand River has similar phases of estimated flux ratios ( $ET / PET$ ,  $ET / P$ ,  $RS / P$ ) and interannual variations. However, the estimated discharge rate is smaller ( $RS / RO = 0.29$ ) than that of the upper Hotan River. Underestimation in water inputs in summer and autumn is possibly the reason as there is no obvious water storage gaining in the summer period and the ratio of observed discharge to regional precipitation is unrealistically high ( $> 0.9$ , Fig. 3.8b).

The upper Aksu River has different characteristics from the other two regions since it lies in the northern part of the Tarim. It has a larger snowfall proportion in the precipitation. Meanwhile, it has the largest ratio of estimated  $ET / PET$ , the largest runoff generation ratio ( $RS / P = 0.35$ ) and the least discharge simulation error ( $RS / RO = 0.51$ ). However, there is certainly large bias in the regional precipitation as the discharge has exceeded the precipitation input in the summer period (July and August). The estimated annual cycle of discharge diverges from the observations (Fig. 3.8f), as its peak advances by 2 months and the discharge estimation significantly exceeds the observations in spring (MAM). The runoff generation ratio in the summer period is also unrealistically low.

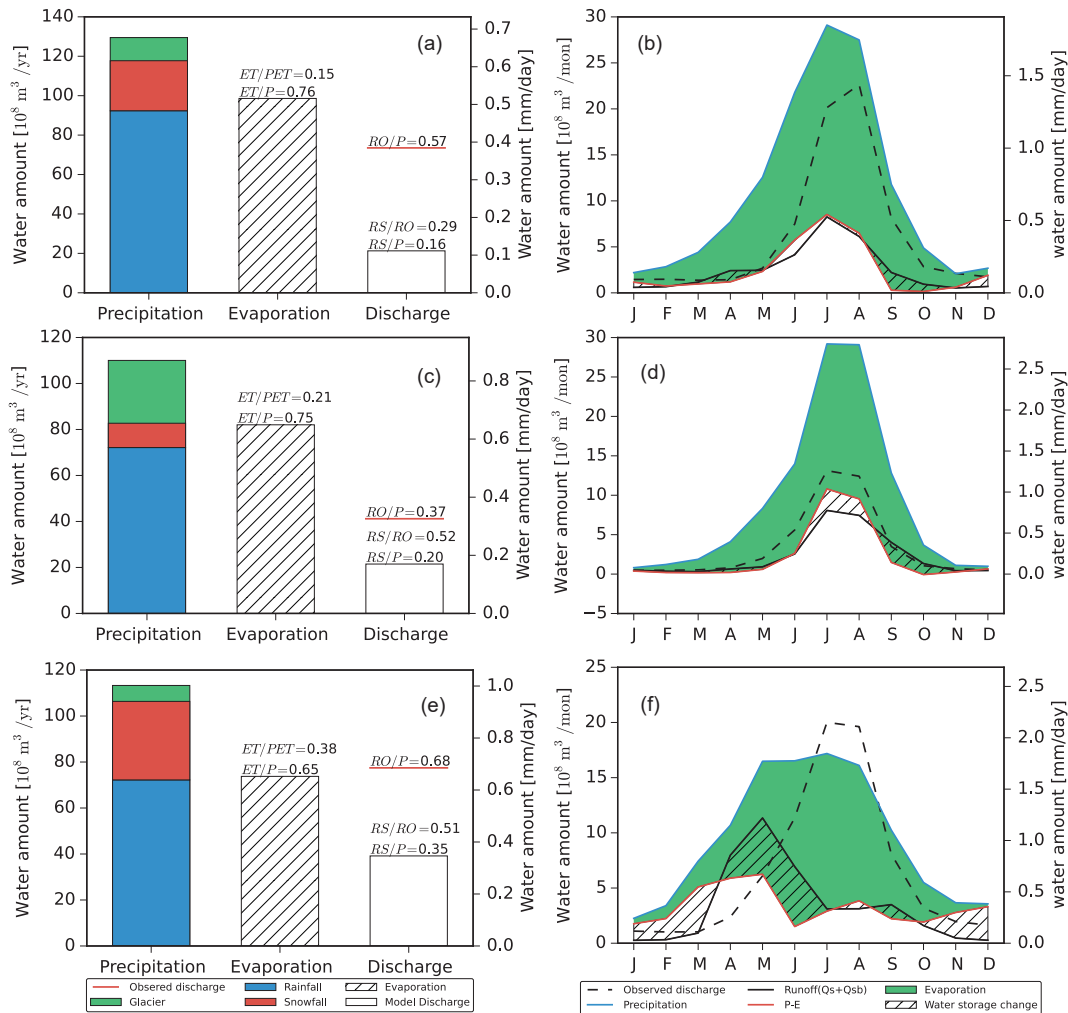


Figure 3.8 – The water input components (rainfall, snowfall, glacier melt), evapotranspiration and discharge for three headwater catchments (a-Yarkand, c-Hotan and e-Aksu from the top to the bottom) in the WFDEI-CCG-SF simulation. In the left panels, the amounts of different variables are plotted as bars, while the average mean of the observed discharge (RO) is plotted as the red line. *RS* denotes the simulated discharge by ORCHIDEE. In the right panels, the annual cycle of the water inputs (blue line), evapotranspiration (green shadow), estimated discharge (runoff plus drainage, solid black line), observed discharge (dashed black line) and the changes in terrestrial water storage (TWS, slashed area) changes are plotted as b,d and f. The green slashed area represents decreasing in TWS and the white one slashed area represents increasing in TWS.

In summary, the biases in discharge estimation exist in terms of the total amount and the annual cycle. Precipitation is one of the largest bias sources, which makes the bias analysis in models more difficult.

### 3.4.3 Bias range and possibility analysis for the headwater catchments

Although either  $P$  or PET or ET can cause final underestimation of discharge over the three headwater catchments, quantifying the bias in each flux is challenging and impractical due to the lack of direct measurements and the strong heterogeneity over the mountainous area. To separate the individual bias, we use the Budyko hypothesis by assuming only one variable is uncertain, while the other two are assumed to have negligible errors, with which we “correct” the model simulation to meet the discharge observation and obtain the possible bias range. Then we evaluate the possibility of rejecting the assumption to find the most likely bias source by checking the status of the water system (i.e., amount of the water–energy components and their relations) in indirect ways. The water–energy components used in the Budyko analysis are all ORCHIDEE outputs of the most satisfactory simulation, WFDEI-CCG-SF. The corresponding characteristics of the water–energy components for three headwater catchments are listed in Table 3.4.

Table 3.4 – The water-energy components for the headwater catchments in WFDEI-CCG-SF simulation. Units:  $\text{mm yr}^{-1}$ .

	Precipitation	Rainfall	Snowfall	Glacier	$ET$	$RS$	$PET$	$RO$
Yarkand	247.3	198.8	48.5	22.4	188.3	59.1	1240.4	140.4
Hotan	317.8	287.2	30.6	78.9	236.9	81.3	1153.7	118.9
Aksu	365.8	255.5	110.3	22.4	238.1	128.0	631.8	250.1

#### Bias ranges estimated by the ORCHIDEE-Budyko framework

The ORCHIDEE-estimated evapotranspiration rate ( $ET / P$ ) against the estimated aridity index ( $PET / P$ ) over each subbasin in each year is scattered as red points in Fig. 3.9. Point A represents the Budyko relation between long-term average annual  $ET / P$  and the long-term average annual  $PET / P$ . According to the categories introduced by Ponce et al. (2000), all three catchments belong to semiarid climate zones by the definition of the annual average precipitation (Table 3.2). Hence the aridity index is supposed to range from 2 to 5. Regarding the high elevation and cold temperature, the PET rate is likely to be smaller than the representative climate of this aridity index. Thus the aridity index for the three catchments is supposed to be lower than expected. It is realistic for the upper Hotan River and the upper Aksu River as their aridity is 3.63 and 1.73, respectively. While the aridity index for the upper Yarkand River is 5.02, which can be categorized as a semiarid or arid region, this is not very likely since the upper Yarkand River is providing water resources for the irrigated area over the lower Yarkand oases (Zhou et al. 2000; Mamitimmin et al. 2014).

However, because there is still a bias in the ORCHIDEE discharge estimations with the observations, the current state A is not correct. Based on the assumptions introduced in Sect.

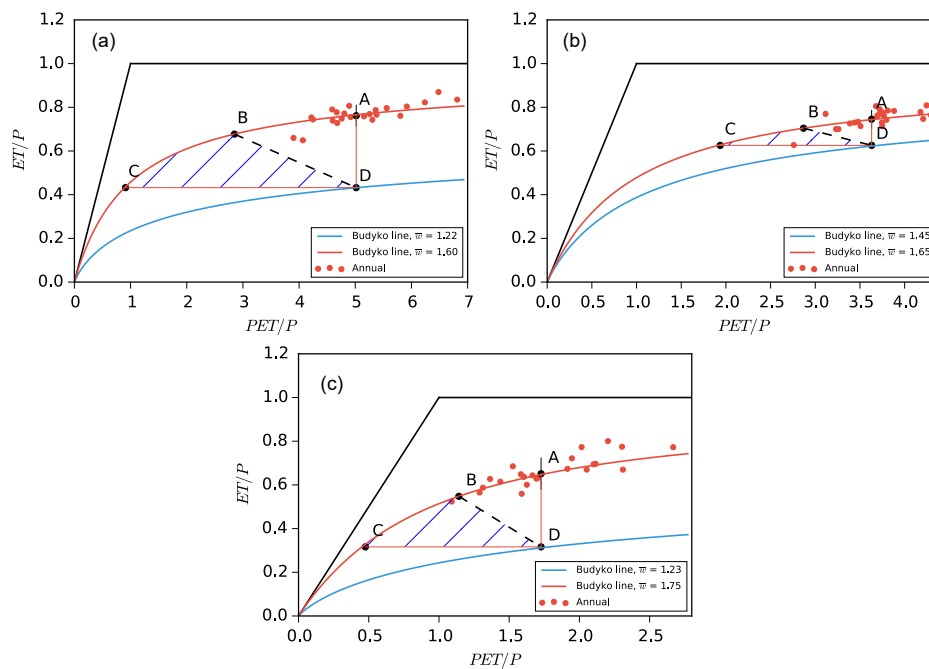


Figure 3.9 – Budyko relation for three headwater catchments (a-Yarkand, b-Hotan, c-Aksu). The red points represent the values for each year, the  $P$  is obtained from the forcing, while  $ET$  and  $PET$  are obtained from the model. Point A represents the long-term average Budyko relation and red lines are the optimal fitted Budyko line. Either the water input  $P$ , the potential evapotranspiration  $PET$  or the actual evapotranspiration  $ET$  can be modified to meet the observed discharge, which correspondingly shift the representative points from A to B, C or D. B and C stay in the original Budyko curve while a new optimal fitted Budyko curve through point D can be built after the changes in  $ET$ . The shaded area is the most likely area when not only single variable is changing.

3.5, the three possible “corrected” states by shifting the  $P$ , PET and ET are shown in Fig. 3.9 for the three headwater catchments. Taking the upper Yarkand River as an example (Fig. 3.9a), if we consider only  $P$  to be biased (assumption 1), the  $P$  has to be shifted from 247.3 to 435.4 mm yr<sup>-1</sup>. PET remains the same, and the ET changes accordingly, but the relation between ET /  $P$  and PET /  $P$  still follows the Budyko curve. The state is shifted from point A to point B with the  $P$  change ratio as 76.1 %. Reversely, the possible bias of  $P$  is -43.2 % ((247.3–435.4)/247.3 × 100 %). Similarly, to change the PET in order to shift the state to correct (point C, assumption 2), the PET has to be shifted from 1240.4 to 225.0 mm yr<sup>-1</sup>. The possible bias in PET is 451.2 %. To change the ET in order to shift the state to correct (point D, assumption 3), the ET has to be shifted from 188.3 to 106.9 mm yr<sup>-1</sup>, and the possible bias in ET is 76.1 %. The route is the same for the other two catchments, and their results are listed in Table 3.5.

Table 3.5 – The annual average values for different water-energy components ( $P$ ,  $ET$ ,  $PET$ ; units in mm yr<sup>-1</sup>) and their relations ( $P-ET$ ,  $PET/P$  and  $ET/P$ ) for the three upstream subbasins. The scenarios correspond to the diagnostics of current model (A) and three bias assumptions list above from B to D. The bold values are the main factors changed within the three basic water-energy components. The changing ratio (C.R.) indicates the ratio of the changing value to the original value (unit in %). While the bias range (B.R.) implies the bias of the values in the current variables compared to the values they should be (unit in %).

		$P$	PET	ET	$P-ET$	$PET/P$	$ET/P$	Factor	C.R.	B.R.
Yarkand	A	247.3	1240.4	188.3	59.0	5.02	0.76	-	-	-
	B	<b>435.4</b>	1240.4	<b>294.9</b>	140.5	2.85	0.68	$P$	76.1	-43.2
	C	247.3	<b>225.0</b>	<b>106.9</b>	140.4	0.91	0.43	$PET$	-81.9	451.2
	D	247.3	1240.4	<b>106.9</b>	140.4	5.02	0.43	$ET$	-43.2	76.1
Hotan	A	317.8	1153.7	236.9	80.9	3.63	0.75	-	-	-
	B	<b>402.3</b>	1153.7	<b>283.3</b>	119.0	2.85	0.70	$P$	26.6	-21.0
	C	317.8	<b>615.2</b>	<b>198.8</b>	118.9	1.94	0.63	$PET$	-46.7	87.5
	D	317.8	1153.7	<b>198.8</b>	118.9	3.63	0.63	$ET$	-16.1	19.1
Aksu	A	365.8	631.8	238.1	127.7	1.73	0.65	-	-	-
	B	<b>553.3</b>	631.8	<b>303.1</b>	250.2	1.14	0.55	$P$	51.3	-33.9
	C	365.8	<b>174.1</b>	<b>115.7</b>	250.1	0.48	0.32	$PET$	-72.4	262.4
	D	365.8	631.8	<b>115.7</b>	250.1	1.73	0.32	$ET$	-51.4	105.8

The previous analysis is based on the assumptions that the  $P$  and PET are independent and only a single variable is uncertain, which might be invalid in reality. However, the three assumptions provide the bias boundaries of each variable, and the final system reproducing observed RO is likely to be located within the shaded area shown in Fig. 9. Taking the Hotan River as an example, to meet the discharge observation, the final changes in  $P$  will be 0 %–26.6 %, the decrease in PET will be 0 %–46.7 % and the decrease in ET will range 0 %–16.1 %. While in turn, we also conclude that the  $P$  is underestimated by 0 %–21.0 %, the PET is overestimated by 87.5 % at most and the ET is overestimated by 19.1 % at most. If we know the bias for any single variable, the feasible ranges will be narrower than at present.

### Ranking the bias possibility

Although the Budyko approach provides us with possible ranges for the bias of each variable, it is still difficult to determine the bias source without proper bias measurements for each of the forcing variables. We alternatively compare the regional diagnostics with nearby regions or regions with similar climatic and regional characteristics which have qualified observations in an indirect way. In doing so, we can generally rank the occurrence possibility of an uncertain variable.

From multiple-model analysis based on CMIP5 general circulation models (GCMs), the estimated PET over the western boundary of the Tarim Basin is about the same as over the Tibetan Plateau (Scheff and Frierson 2015). However, because of the unpredictable biases in GCMs, the absolute values are not highly reliable in their simulation. Nevertheless, the equivalent relation provides us with the ranges of PET over the Tarim headwater catchments by referring to the observations over the Tibetan Plateau, where the topography changes are relatively small and the observations are more abundant. According to (Chen et al. 2006), who used site observations from 101 stations over the Tibetan Plateau, the annual average PET over the plateau ranges from 580 to 720 mm yr<sup>-1</sup>. Hence the PET over the upper Yarkand River and the upper Hotan River is probably overestimated (1240.4 and 1153.7 mm yr<sup>-1</sup>). Therefore, only changes in  $P$  or ET are not satisfactory because the PET is unchanged. For the upper Yarkand River, the PET is not the only error source, because, to match the discharge deviation by only decreasing PET, the PET should be decreased to 225 mm yr<sup>-1</sup>, which exceeds the referenced PET range. Moreover, because Yarkand and Hotan are neighboring regions which have similar climates, the PET should be a similar amount in each (615.2 mm yr<sup>-1</sup> if only PET is uncertain in the upper Hotan River, while 225 mm yr<sup>-1</sup> in the Yarkand River). The estimated PET over the Aksu River is realistic since the PET is 631.8 mm yr<sup>-1</sup> for the current scenario, but it would decrease to 174.1 mm yr<sup>-1</sup> if only the PET changed, which is too low. Besides the absolute value of PET, the ratio PET /  $P$  also shifts when PET changes, which means the climatic types can be changed. Only decreasing the PET in the upper Yarkand and the upper Aksu River would cause significant decreases in the aridity index (from 5.02 to 0.91 for the upper Yarkand, from 1.73 to 0.48 for the upper Aksu River), which are not realistic for these regions.

ET computation is sensitive to the climatic conditions and the surface conditions; hence the absolute value of ET significantly varies in time and space, and its bias very difficult to quantify. The evapotranspiration ratio to precipitation (ET /  $P$ ) is typical for specific climatic types or regions with similar land cover types (Yang et al. 2007). (Liu et al. 2003) estimated the evapotranspiration ratio to precipitation using a remote-sensing approach over regions of Canada. They concluded that the ratio ET /  $P$  is 32 % for barren land and 18 % for snow/ice land. In general, most of the catchment area of the three headwater catchments consists of barren and snow/ice land. Because of its lower latitude, the ET ratio could be higher but still below the rate for cropland (67 %). Therefore, only changes in  $P$  are not very likely for Yarkand and Hotan (ET /  $P$  is 0.68 for Yarkand and 0.70 for Hotan after the correction). Higher  $P$  for the upper Aksu River is likely to maintain a realistic ET /  $P$  ratio.

The biases of the three variables ( $P$ , ET, PET) have relatively weak dependence because

they are governed by different processes.  $P$  and PET are quite independent because they relate to different forcing variables. Although the ET amount is linked to two other variables, the ET bias is weakly dependent, and it also comes more from the surface conditions and model biases. The chances of biases arising from each variable are about the same in theory. However, based on the analysis of the model output and the assumed bias-corrected scenarios, there are some priorities for the bias sources over each subbasin. The possibility of biases and the supporting arguments are listed in Table 3.6 for each headwater catchment. For instance, for the upper Yarkand subbasin, an increase in  $P$ , especially the glacier melt, is necessary because of the lower glacier melt ratio compared to the Hotan basin (Sect. 5.1.2.3) and the small trend in model discharge compared to the discharge observation (Sect. 4.2). However, only increasing the precipitation is not sufficient because the current PET is very likely too high compared to the surrounding regions (PET = 1240.4 mm yr<sup>-1</sup>, while PET ranges 580-720 mm yr<sup>-1</sup> over the Tibetan Plateau). Meanwhile, only decreasing the PET without changing other variables would cause a very low PET rate (225 mm yr<sup>-1</sup>) and low aridity index (PET /  $P$  = 0.91), which is not realistic for this region. Modification in ET is possible but not adequate due to the overestimated PET. Hence, this error analysis reveals that increasing precipitation over the upper Yarkand subbasin is quite necessary, the overestimation of PET is very likely and modification in ET estimation is possible but not fundamentally necessary. For the upper Hotan River, the most likely biases come from the overestimation of PET, while the two other variables are possible sources. An increase in precipitation and changes in temporal variability are necessary for the upper Aksu subbasin, but they are not the only causes, as either the PET or ET, or both, is overestimated.

Table 3.6 – Summary of the possible causes of the underestimation in discharge and the corresponding arguments. Three levels of the possibility are presented as Yes: with direct argument, likely: with indirect argument, No: with negative argument.

Subbasin	Variable	Is it a factor?	Is it the only factor?
Yarkand	$P$ underestimation	YES: Glacier (low glacier ratio, smaller trend in discharge simulation)	Likely NO (very high PET=1240.4 mm yr <sup>-1</sup> ; high ET/ $P$ = 0.68)
	PET overestimation	Likely YES: Very high PET=1240.4 mm yr <sup>-1</sup>	NO (very low PET=225.0 mm/yr; low PET/ $P$ =0.91)
	ET overestimation		Likely NO (very high PET=1240.4 mm yr <sup>-1</sup> ; high PET/ $P$ =5.02)
Hotan	$P$ underestimation		Likely NO (very high PET=1153.7 mm yr <sup>-1</sup> ; high ET/ $P$ =0.70)
	PET overestimation	Likely YES: Very high PET=1153.7 mm yr <sup>-1</sup>	
	ET overestimation		Likely NO (very high PET=1153.7 mm yr <sup>-1</sup> )
Aksu	$P$ underestimation	YES: $P < R$ in summer	Likely NO (low PET/ $P$ =1.14)
	PET overestimation		NO (very low PET=174.1 mm yr <sup>-1</sup> , very low PET/ $P$ =0.48)
	ET overestimation		

### 3.4.4 Human intervention in the lower oases

The current ORCHIDEE version does not yet take into account the intensified evapotranspiration caused by human activities especially through irrigation, which is a major process in the hydrological cycle transferring water to the atmosphere. As a consequence, in the lower oases the simulated discharge at the Alar station is significantly larger than the observations (Fig. 3.6g, h;  $146.59 \times 10^8 \text{ m}^3 \text{ yr}^{-1}$  in WFDEI-CCG-SF simulation to  $43.34 \times 10^8 \text{ m}^3 \text{ yr}^{-1}$  in observation). However, because the biases of the upstream discharge will propagate to the Alar station, the catchment of which includes the three basins discussed above, the currently estimated discharge is thus underestimated compared to the potential river flow at Alar, which is the natural river flow without human intervention.

We use two simple approaches to estimate this underestimation. In the first one, according to the work of (Tao et al. 2011), all the water increment of the Alar gauge station is caused by the water changes from the three headwater catchments. Hence the underestimation of the discharge to the potential river flow at Alar equals the underestimation of discharge from those three catchments. The increment at Alar should be  $110.25 \times 10^8 \text{ m}^3 \text{ yr}^{-1}$  (observed  $192.15 \times 10^8 \text{ m}^3 \text{ yr}^{-1}$  from the three headwater catchments minus simulated  $81.9 \times 10^8 \text{ m}^3 \text{ yr}^{-1}$ ), so that the potential river flow at Alar should be  $256.84 \times 10^8 \text{ m}^3 \text{ yr}^{-1}$  ( $= 146.59 + 110.25$ ), and the influence of human activities on the increase of ET can be estimated as  $213.50 \times 10^8 \text{ m}^3 \text{ yr}^{-1}$  ( $= 256.84 - 43.34$ ), 83.1 % of discharge.

A second simple scaling approach to obtaining the potential river flow at Alar is that we assume the model bias for the whole upper Tarim Basin is constant over space. The scaling factor is 2.35 ( $= 192.15 / 81.9$ ); hence the potential discharge at Alar should be  $343.92 \times 10^8 \text{ m}^3 \text{ yr}^{-1}$  ( $= 146.59 \times 2.35$ ). And the influence of human activities on the increase of ET is estimated as  $300.58 \times 10^8 \text{ m}^3 \text{ yr}^{-1}$  ( $= 343.92 - 43.34$ ), 87.4 % of the discharge. The overestimation over the discharge observation is the amount caused by additional human intervention, especially the irrigation-caused evapotranspiration.

To validate the proposed values, we collected the irrigation area over the Tarim Basin using the FAO Global Map of Irrigation Areas (Siebert et al. 2013), according to which the total irrigated area for the upper Tarim Basin is  $13548.5 \text{ km}^2$ . In addition, Zhou et al. (2000) provides the gross irrigation quota as  $1.77 \times 10^6 \text{ m}^3 \text{ km}^{-2}$ ; hence the total irrigation water consumption will be  $239.80 \times 10^8 \text{ m}^3 \text{ yr}^{-1}$ . Hence the results of the two approaches assessing human net abstraction are -11 % and 25 % ( $213.50 \times 10^8 \text{ m}^3 \text{ yr}^{-1}$  and  $300.58 \times 10^8 \text{ m}^3 \text{ yr}^{-1}$ , respectively) in relation to the consumption data, which are acceptable figures because of the unknown biases in irrigation area as well as the gross irrigation quota. The proportion of the consumed water (83.1 %– 87.4 %) is higher than the estimation (74.7 %) in 1995, which could be explained by the intra-annual variation of inflow and abstraction.

## 3.5 Conclusions

In this work, we proposed an ORCHIDEE-Budyko framework which is used to attribute the modeled discharge bias to different sources as the forcing and model structure. Bias in the precipitation ( $P$ ) and any processes related to the potential evapotranspiration (PET) is

considered as bias from forcing and bias in any processes affecting the actual evapotranspiration (ET) estimation is considered as bias from model structures. The discharge simulation was provided by the land surface model ORCHIDEE with latest developments in its modules and driven by the most improved forcing inputs (WFDEI-CCG-SF). However, underestimation in the discharge still exists over the three Tarim headwater catchments, where the biases of  $P$ , PET and ET are analyzed with a Budyko analytical approach. With a set of assumptions, we isolated the biases in three variables, and their possibilities were assessed with information from nearby and hydroclimatically similar regions. Results show that precipitation (here considered as the sum of rainfall, snowfall and glacier melt) underestimation is highly likely for the upper Yarkand River and the upper Aksu River, while the overestimation of PET is likely to affect the upper Yarkand River and the upper Hotan River. The overestimation in ET is possible but not likely the only cause for the discharge underestimation for all headwater catchments. In the lower oases, humans consume 83.1 %–87.4 % of the discharge for irrigation, which is also a bias source in the current version of model. Thus, inclusion of detailed human modules is needed for any large-scale model.

In this attempt to analyze the performance of a complex land surface model over the Tarim Basin, large biases are found in the discharge estimation. Our finding that the bias is most likely caused by the forcing variables rather than the model is probably the reason for the failures of other models in specific regions as well. Our work provides more information about the Tarim Basin's water cycle and guidance for future studies that the bias in forcing variables should firstly be assessed and reduced in order to perform pertinent analysis of the regional water cycle. Land surface models are a recommended tool for water cycle analysis because of their independence of calibration and good ability to simulate most variables of the water cycle and their interplay, which facilitates the identification of bias sources. This kind of application along with the improvements of forcing data is also important for predicting water resources in the Tarim as well as other high-altitude basins in central Asia in a changing climate.

## **Acknowledgement:**

This study was supported by the National Natural Science Foundation of China (grant nos. 41561134016 and 51879068); the CHINA-TREND-STREAM French national project (ANR grant no. ANR-15-CE01-00L1-0L); the National Key Research and Development Program (2018YFC0407900); the Global Environmental Research Fund (S-14) of the Ministry of the Environment, Japan; and the China Scholarship Council (CSC, 201506710042). The work was supported by computing resource of the IPSL ClimServ cluster at École Polytechnique, France. We also thank the editor and two anonymous reviewers for their contribution to the improvement of this paper.



# 4

## Human impact on river discharge in China regions - a review

### Contents

---

<b>4.1</b>	<b>Introduction</b>	<b>82</b>
<b>4.2</b>	<b>How humans change river discharge</b>	<b>83</b>
4.2.1	Land-use change (LUC)	83
4.2.2	Water consumption	89
4.2.3	Dams and dam regulation	93
4.2.4	Summary	95
<b>4.3</b>	<b>Quantification methodologies of the human impacts</b>	<b>96</b>
4.3.1	Indirect approaches	97
4.3.2	Direct approaches	101
4.3.3	Towards integrating human impacts at high resolution	104
<b>4.4</b>	<b>Comparisons of human impacts to other uncertainties</b>	<b>106</b>
4.4.1	Data and gauge introduction	106
4.4.2	Quantification of human impacts	107
4.4.3	Uncertainties due to limitation of knowledge on the nature	111
4.4.4	Results	113
<b>4.5</b>	<b>Summary</b>	<b>118</b>

---

Chapter 2 introduces a new approach which estimates the uncertainties in the atmospheric variables. Chapter 3 introduces a ORCHIDEE-Budyko framework which aims to attribute the model bias in river discharge to both uncertainties in atmospheric variables and the model itself. This chapter will then focus on the human activities which act as the third uncertainty source in hydrological modeling (see section 1.2.2). Different kinds of human activities and their impact on river discharge over Chinese regions are introduced in section 4.2. The methodologies for quantification of the human impact are introduced and compared in section 4.3. Finally, the magnitude of the human impact estimated at a number of river discharge gauges is compared with the uncertainties in precipitation among multiple products. The impact of model simulation on the uncertainty changes through hydrological processes is also discussed in section 4.4.

## 4.1 Introduction

China is experiencing rapid growth in its population after the People's Republic of China was founded in 1949, and the economy is exploding after China's reform and opening in 1978 (Liu et al. 2014a). Along with the increasing population and economy, the needs for land and water have also increased for different purposes such as residence, food and industries (Liu et al. 2014b; Xu and Luo 2015). Transitions from forests to cropland and urban areas occurred in large parts of China with different patterns and different magnitudes (Liu et al. 2008; Liu and Tian 2010). The land cover transition is an important factor that changes land surface properties. Water consumption<sup>1</sup> has significantly increased in different sectors which has resulted in uneven water pressures in different places across China. To better manage the rivers and increase electricity production, a large number of dams was built and used to regulate the river discharge to optimize benefits (Yang and Lu 2014). All the human activities finally exert impacts on river discharge, though the effective ways, the places, the temporal scale and the magnitude of the impact vary among different human activities (Piao et al. 2010; Wang et al. 2011a; Yang et al. 2015a; Li et al. 2016c). In this chapter, three major human activities (i.e., land-use change, water consumption and dam construction) are reviewed regarding their evolutions in China and their impacts on river discharge in the literature. The methods that are proposed to quantify the human impact on discharge are also reviewed. The methods are divided into two groups (i.e., indirect approaches and direct approaches) depending on whether the human impact is estimated directly or in an indirect way. The peculiarities of these methods are discussed based on their estimations and existing studies.

Human impact is estimated with different magnitudes over regions because the human interferences vary over space (Zhao et al. 2014; Jiang and Wang 2016; Li et al. 2016c; Guo et al. 2018). The abundance of water at local regions also affect the relative impact of humans. As we have shown in previous chapters, there are various uncertainty sources in hydrological

---

<sup>1</sup>Water consumption: the actual amount of water used for different products. It equals to water withdrawal from natural water bodies minus the water return to the water system including the evapotranspiration to the atmosphere and return water to rivers, lakes, soil, groundwater.

modeling, and the uncertainty will finally propagate to affect the accuracy of model predictions (e.g., the discharge). The question is whether the uncertainty in a model simulation due to the different uncertainties is larger than the magnitude of human impact that is defined as the alteration of discharge by humans. If the modeled uncertainties caused by the various sources are larger than that can be affected by humans, the assessment of human impact will lack credibility since it is difficult to ensure the modeled changes in discharge are only associated with human activities. Therefore, in this chapter, the human impacts are estimated as the difference between observed and naturalized river discharge at some available gauges. The discharge differences caused by humans are compared with the uncertainties in the modeled river discharge caused by other sources.

## 4.2 How humans change river discharge

### 4.2.1 Land-use change (LUC)

Land-use change (LUC) is one of the major factors that change the river discharge, and humans play the dominant role in recent rapid LUC evolutions (Liu and Tian 2010). LUC does not directly change the river flow, but it alters the water cycle processes (e.g. infiltration, evapotranspiration, lateral flow) through changes in surface and soil properties. The impact of LUC on discharge varies in regions as the LUC varies in space and time (Liu et al. 2003; Liu and Tian 2010) and the types of LUC (e.g. urbanisation, deforestation, reforestation) affect the discharge in different ways. The magnitude of LUC impacts depends on its type as well as its density in specific regions.

China experienced a rapid loss of forest of 38.4 million ha (hereafter Mha, 21.8%) from 1700 to 2005, while the cropland and urban area increased by 39.7 Mha and 17.1 Mha, respectively (Liu and Tian 2010). The changing trend was not stable during the historical period as the forest kept decreasing until its minimum area around 90 Mha in the 1950s and then rapidly increased to ~140 Mha in 2000 (Figure 4.1). 77.0% of the forest degraded to woodland, and the woodland showed an opposite trend to that of the forest. Cropland increased slowly before the 1930s, while it accelerated to its historical maximum of 152 Mha in 1950s. It then decreased at a low rate until 135 Mha in 2005. The urban area increased at a stable speed after 1950 until 18.8 Mha in 2005.

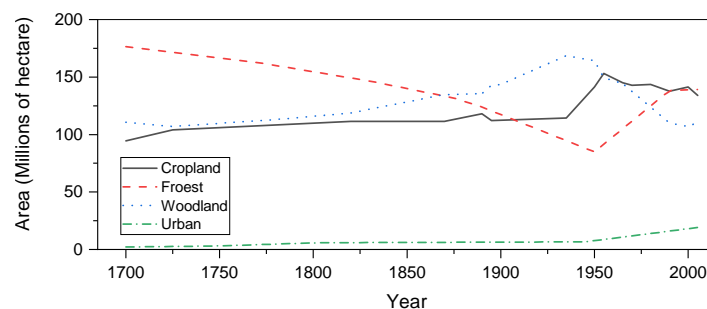


Figure 4.1 – Changes in total area of cropland, urban, forest and woodland in China during 1700-2005 (Liu and Tian 2010).

LUC varies in basins and a significant loss of forest occurred in the northeast (e.g., the Songhua River basin, Liao River basin; Figure 4.2) and the southwest (e.g., upper and middle of the Yangtze River basin) during the last three centuries (1700-present, Liu and Tian 2010). The deforestation is concentrated in the recent century (1900-present, Figure 4.3). The Songhua River and the Yangtze River are the most affected river basins before the mid-1950s (Liu et al. 2008). The Pearl River and the Yellow River were suffering deforestation during 1945-1955 (Liu et al. 2008). No apparent changes are found in the Haihe River, Huai River, the Southwest Basin and the Continental Basin, while the forest significantly increased by 2.5 Mha in the Southeast during the last century (Liu et al. 2008).



Figure 4.2 – The map of China and the main rivers (same as Figure 1.1).

After the 1950s, the cropland decreased especially after the China's reform and opening up in 1978. During the 1980s to 2000, 46.0% of the area with decreased cropland was used for urban construction, and the ratio increased to 55.4% during 2000-2010 (Liu et al. 2014b). The urban area increased from 6.59 Mha in 1949 to 19.8 Mha in 2016 according to national statistics. The eastern plain and southeastern China, which include provinces of Beijing, Shanghai, Guangdong, Zhejiang, Jiangsu, Shandong and Tianjin, occupy the largest urban area (12.5 Mha) and have the largest increasing ratio in history (Liu and Tian 2010) (Figure 4.4). Most of the remaining area with decreased cropland were used for ecological construction (i.e., afforestation), accounting for 34.54% of the total decreased cropland (Liu et al. 2014b). From 1990, the forest/grass-based vegetation restoration projects, especially the "Grain for Green project", stimulated the afforestation, especially in ecologically fragile regions (e.g., the Loess Plateau). 28.0 Mha of plantations established from 2001 to 2007 (Chazdon 2008)

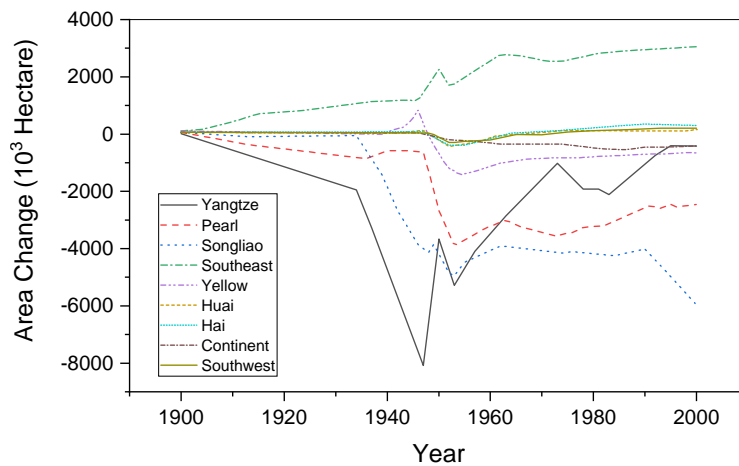


Figure 4.3 – Changes in forest area for each river basin during 1900–2000 based on reconstructed historical land-use data (unit: 1,000 ha) (Liu et al. 2008)

and the forest area has increased from 174.9 Mha in 2004 to 207.7 Mha in 2016 for the whole China, of which 33.4% is afforestation.

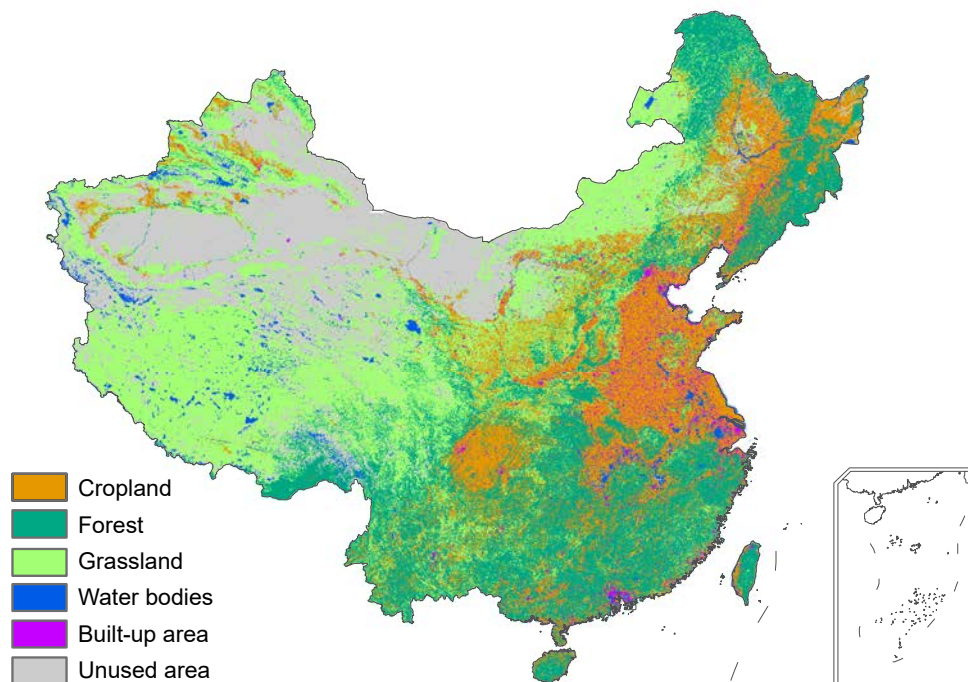


Figure 4.4 – The land use map (1 km resolution) in China in 2015.

Different types of LUC will change the surface conditions and further affect the water cycle. However, their impacts on the river discharge are different in terms of the magnitude of LUC itself and the ways it changes the water cycle. The characteristics of the affected area also affect the relative impact of the LUC. In the following three subsections, the impacts of deforestation, urbanisation and afforestation on the hydrological components (i.e., evapotranspiration and

water yield<sup>2</sup>) are introduced, respectively. The introduction below reviews the different types of land-use change and the impact of LUC on the hydrological elements through literature.

### Deforestation

Deforestation is one of the major LUC patterns in the period of population expansion and economic growth. Despite the degradation from forest to woodland, most of the deforestation area was transformed to cropland for food production (Liu and Tian 2010). The shift mainly changes the surface conditions (e.g., roughness, albedo ratio) and soil properties (e.g. cohesion, soil moisture content, water holding capacity) (Sirajul Haque et al. 2014). It then affects the evapotranspiration (*ET*) rate and the water yield finally changes the river discharge.

The *ET* is simulated to decrease over the deforested area in most studies (Twine et al. 2004; Mao and Cherkauer 2009). The main causes include (1) the water retention capacity decreases because the reduced soil cohesion in the deforested area decreases the residence time of soil moisture and the soil ability to hold water (Chen et al. 2009). (2) the evapotranspirable water decreases because of the decrease in root depth and drier soil (Jiang et al. 2014). (3) the changes in surface conditions decreases the *ET* rate with lower Leaf Area Index (LAI, Liu et al. 2013a), higher albedo ratio (Myhre and Myhre 2003) and lower surface roughness (Mao and Cherkauer 2009). However, because some of the forest areas were converted to paddy land where the *ET* is significantly high during the crop growth, opposite trend of the total *ET* is estimated especially in the east and south China (Liu et al. 2008).

The change of water yield due to LUC is opposite to that of the *ET* because of the water balance law as the total amount of water yield is estimated to increase in the deforested area in southern China (Wang et al. 2015). The runoff coefficient (ratio of water yield to the precipitation) is also increased either in simulations or field experiments (El Kateb et al. 2013). The flood risk increases as higher flood peaks are predicted in deforested area mainly because of the reduced retention of water storage in soils (Liu et al. 2008). Evidence also shows that in developing countries where the largest deforestation is ongoing, the flood risk and severity increased in terms of the flood duration, the victims and people forced to move as well as the economic damage (Hattermann et al. 2017; Zong and Chen 2000). Similar to the trend in the *ET*, there are a few studies that indicate the opposite trends in water yield with deforestation (Liu et al. 2008).

The availability of hydrological data restricts research on the deforestation impact on river discharge in China as very few gauges have discharge measurements before the 1950s, and the large-scale decrease in the forest has taken place before that (Figure 4.3). In the recent half-century after the 1950s, the deforestation impact has been investigated over regions with different climate types. (Cui et al. 2007) stated that the transpiration decreases and the runoff increases in the Tibet Plateau in deforestation scenario simulation. The annual runoff increases by about 1.4% (12.6 mm) in the deforestation scenario over the East River in southern China (warm and wet, Niu and Sivakumar 2014). The similar conclusion is found in the dry area in the north China (Wang et al. 2017a) and cold area the northeast China (Zhang et al. 2014).

---

<sup>2</sup>Water yield: the total amount of water generated by precipitation, snow and glacier melt and groundwater. It consists of surface runoff, subsurface drainage and groundwater recharge. And it equals the precipitation over a catchment minus the evapotranspiration back to the atmosphere in area free of glaciers.

However, it is difficult to evaluate the net impact of deforestation because the impact is generally too small to discern from the natural climate variability and change (Sitch et al. 2005). In the simulations based on scenarios, the other factors except the forest area are considered unchanged, which it is not realistic (Cui et al. 2007; Niu and Sivakumar 2014) as climate change takes place anytime and anywhere. On the other hand, although the deforestation will decrease the *ET*, *ET* can increase due to irrigation over the new cropland and higher atmospheric demand produced by climate change (Liu et al. 2008). The offsetting impact on the discharge change increases the difficulty in identifying the deforestation impact on a long-term scale. Therefore, in most of the studies, deforestation is only explained as a reason for the increase of water yield in specific regions without robust quantification.

### **urbanisation**

The direct impact of urbanisation compared to the natural area is the increase of the impervious surface. The annual *ET* in the urban area is estimated to decrease because of the decline in vegetation cover and less soil exposure with an increase in impervious surface (Liu et al. 2008). The urbanisation has the only a slight impact on annual water yield (Du et al. 2012; Zhou et al. 2013) on a regional level probably because the urban area still accounts for only a small proportion of the whole. However, remarkable changes are found in the flood events in cities. The impervious surface redistributes the ratio of surface runoff and the subsurface drainage because infiltration is restrained (Xu and Zhao 2016). The runoff coefficient increases especially during flood events (Shi et al. 2007; Xu and Zhao 2016). The flood peak discharge increases and the peak time advances because the residence time is short on the impervious surface (Shi et al. 2007; Zhou et al. 2013). The river network has been partly replaced by built-up areas so that the ability of water to flow is reduced, which increases the risk of waterlogging in the urban area (Deng et al. 2015; Xu et al. 2014; Wu et al. 2018).

The studies of the urbanisation impact on the water cycle are mainly local and in developed areas. One of the regions which experienced significant expansion in the urban area is the Pearl River Delta in the south China. Weng (2001) stated that there is an increase of 8.1 mm in annual runoff depth due to the growing urban area during 1989-1997 over the Pearl River Delta. Jia et al. (2015) stated that the runoff coefficient increased by 13.4% and the flood peaks increased by 12.9% in Shenzhen city (south China) due to the urbanisation. In the Yangtze River Delta in the middle of China, Du et al. (2012) stated that the annual runoff increased slightly while the flood peaks increased more significantly (2.3% to 13.9% in estimation) in the Qinhuai Basin (Nanjing). Chen et al. (2009) estimated that the peak discharge for flooding with the recurrence interval of 100 years would increase by 2.3% and the total runoff increases by 3.0% if the current urban proportion increased from 9.2% to 17% in a future scenario over the Taihu basin (lower Yangtze River Basin). The similar conclusion is also found in the north China as Zhang et al. (2015) stated that decreases of the green cover are associated with an increasing runoff coefficient in Beijing. However, studies on the relation between urbanisation and runoff are fewer in northern China than that in southern China, probably because the cities in the south are experiencing a rapid expansion of urban area and the risk of heavy rain is also higher. The occurrence of city floods has been increased in the large cities

(e.g., Guangzhou, Shenzhen, Nanjing, Wuhan) with the interactions of climate change (e.g., sudden heavy storms, long-lasting rains).

### Afforestation

In general, the impact of afforestation on the water cycle is the opposite to that of deforestation. Increasing in the *ET* and decreasing in water yield are found in observed data as well as in some simulated cases (Dijk and Keenan 2007; Niu and Sivakumar 2014; Zhang et al. 2017; Li et al. 2018). The impact on the water cycle varies in space, and it is more apparent in the water-limited area (e.g., northern China) than in the energy-limited area (e.g., southern China) (Zhang et al. 2017). In some tropical areas, the afforestation impact on water yield is less significant because changes in the underlying conditions do not change the soil moisture much (Farley et al. 2005; Li et al. 2007). The influence on the seasonality of hydrology is similar across different climates as the flood peaks decrease and the low flow in dry seasons increases (Liu et al. 2014c). Increased soil moisture and the increasing capacity for soil water storage are considered as the explanations.

Afforestation aims to control soil erosion and restore the sustainability of local ecosystems (Song et al. 2014). Although it has achieved these goals in many afforested areas, a new problem is found in some places: excessive afforestation exerts negative impacts on the local environment. Revegetation needs water for the new plantation and creates conflicts between the demand and available soil water (Feng et al. 2016). The soil moisture rapidly decreases because of the high potential evapotranspiration of the forest (Jia et al. 2017). The water yield has decreased to a low level which is difficult to maintain the water demands downstream (Zhang et al. 2008). The most typical case is the afforestation in the Loess Plateau (Figure 4.5).



Figure 4.5 – The area of the afforestation in the Yellow River basin. (Feng et al. 2016)

From 2001, the “Grain for Green Project” started with a total investment of USD 8.7 billion and 32 Mha has been planned for the afforestation area until 2010 (Cao et al. 2011), for which nearly half of the afforestation area is in the middle of the Yellow River, leading to

an increase of vegetation cover by 25% in the Loess Plateau over the last decade (Feng et al. 2016; Zhang et al. 2018). With the increasing forest, average water yield decreased by 50 mm/yr in the Loess plateau, accounting for 50% of its natural level (Sun et al. 2006). The soil moisture deficit increased, and the available soil water decreased to 8-10 m which is difficult for the new vegetation to reach (Wang et al. 2011b). The decreased soil moisture, in turn, restricts the sustainability of forest growth, leading to stunted or “small old” trees, and even plant mortality (McVicar et al. 2007).

There should be an equilibrium vegetation cover which can ensure the ecological function of the forest with the least negative impact on other sectors (Zhang et al. 2018). Zhang et al. (2018) suggested a value for the equilibrium vegetation cover fraction of 0.43 on average over the Loess Plateau while the current average forest cover has reached 0.48. Therefore, vegetation restoration solutions must be tailored to the water availability and other ecological conditions in a region (Chen et al. 2015; Normile 2007). Further revegetation on the Loess Plateau and any other environmentally fragile areas should be applied with caution (Zhang et al. 2018).

#### 4.2.2 Water consumption

Water is the most important element for human beings, food production and economic development. Humans take water for domestic, agricultural and industrial sectors from the water cycle (e.g. surface water, groundwater). According to the latest bulletin of water resources in China in 2016 (Ministry of Water Resources 2016), the total gross water use<sup>3</sup> is 604.02 km<sup>3</sup>, among which the irrigation water use is 376.80 km<sup>3</sup> (62.4%). The domestic and industrial water use accounts for 13.6% (82.16 km<sup>3</sup>) and 21.6% (130.80 km<sup>3</sup>) of the total, respectively. The total water use accounts for 18.6% of the total water resources (3247.4 km<sup>3</sup>) in 2016, which is a large proportion that can affect the hydrograph.

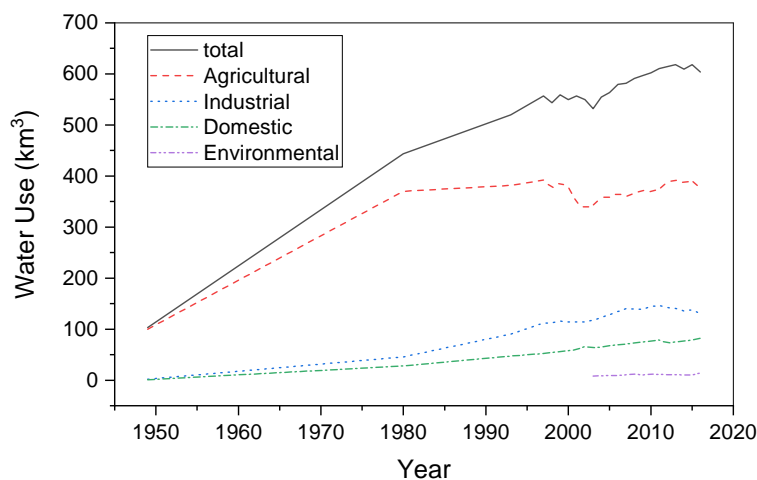


Figure 4.6 – The gross water use in China historical period (1949-2016).

<sup>3</sup>Water use: gross water taken from water bodies. It includes water used for different products, evapotranspiration to the atmosphere and return water to the land system (e.g., rivers, lakes, soil, groundwater).

The gross water use in China has exploded in the last half-century as the total water use in the year 1949 is estimated as  $103.1 \text{ km}^3$ , and 97% of which was used for agriculture (Figure 4.6). In 1980, the total water use rapidly increased and reached  $443.7 \text{ km}^3$ . Among which the water used for agriculture increased to quadruple its level in 1949. The ratio of domestic and industrial water usage sharply increased to 16.6% of the total. In the 1990s, the agricultural water use became stable, while the use for domestic and industrial purposes kept increasing and doubled in the end of 20th century based on the level in the 1980s. From 1997 to 2016, when the national reports were introduced, the water use in different sectors is available with good reliability. The total water use increased by 8.5% in total. The industrial, domestic and agricultural water use changed by 16.7%, 56.5% and -4.8%, respectively. The water usage structural has improved as the water taken for agriculture decreased from 70.4% in 1997 to 62.4% in 2016 (Ministry of Water Resources 2016).

Part of the water taken for different purposes will be consumed (e.g., stored in food or industrial products) and the left will return to rivers or groundwater aquifers or evaporate to the atmosphere. The ratio of the water consumption to the gross water use is around 0.64 for agriculture, 0.25 for industrial and domestic sectors, 0.8 for environmental water. The total water consumption accounts for 53% of the total water use and thus the reduction of water accounts for around 9.8% of the total water resources for the China mainland. Although the water consumption data is not available before 1997, the magnitude of the water consumption can easily get with a proportion of the gross water use since the efficiency of water usage was not significantly changed.

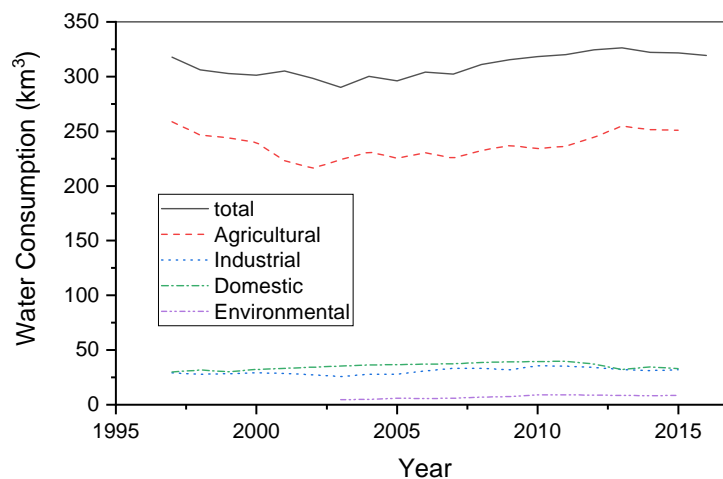


Figure 4.7 – The gross water consumptions in China historical period (1997-2016).

The effect of water consumption to the river change is direct as water is withdrawn from water bodies (e.g. rivers, reservoirs, lakes, groundwater) and transferred to different sectors (e.g. farms, factories, residences) over space. The discharge in rivers or the storage in the water reservoirs (i.e. dam-formed reservoirs, lakes, groundwater) immediately decreases due to the abstraction of water. The magnitude of the hydrograph change depends on the amount of water demand and the proportion to the available water at the extraction point. Although part of the water returns to the land-water system, there is a time lag, and the effects are not at

the point where the water is abstracted.

The change due to domestic and industrial demand is about the same in each month and is always taken as the monthly average of the annual total in model simulations (Hanasaki et al. 2006). The impact of domestic and industrial water consumption is sometimes ignored because these two types account for a small proportion of the total water usage and they are not consumptive water use (Haddeland et al. 2006) as more than 80% of the taken water returns to the rivers (Neverre et al. 2016). The irrigation water demand varies by month according to the crop growth period which peaks in the late spring and early summer. The demand is also related to the available water at the local scale, since the demand decreases in wet years because more demand can be satisfied by local water rather than requesting water from water bodies far away.

Regarding the irrigation water consumption in China, 7.4% of the total water resources is consumed for irrigation, while the proportion varies in different places: only 4.0% (0.9%-5.3%) is consumed in the four southern river basins (i.e., Yangtze, Southeast, Pearl and Southwest), while 23.9% (17.1%-37.3%) is consumed in northern river basins (i.e., Songhua, Liao, Hai, Yellow, Huai, Northwest) (Table 4.1). Hai river has the largest proportion of irrigation water consumption (37.3%) which is probably a basin with a significant irrigation impact on river discharge. The Northwest area is another basin which deserves attention because the agricultural consumption is high (39.7 km<sup>3</sup>, next to the Yangtze) and the irrigation water consumes 93.9% of the total water consumption. Moreover, less water returns to rivers because of the dry continental climate in the northwest China. Therefore, the impact of irrigation is significant as irrigation reduced the surface runoff by more than 80% in the Tarim River (Hao et al. 2015; Zhou et al. 2018), much higher than the average level (26.1%) shown in Table 4.1. Consideration of the water consumption, especially the irrigation water, is thus very necessary in northern China.

Despite the water consumption, cross-basin water transfer across basins is also directly changing the hydrographs. The South-to-North water diversion project, the largest water diversion project in China, transfers 2.39 km<sup>3</sup> per year from the Han River and 8.9 km<sup>3</sup> per year from the Yangtze River to the north each year at the current stage (Kong et al. 2018) and is planned to transfer 44.8 km<sup>3</sup> per year in total by 2050 (Zhang 2009). The impact on the river discharge over places where water is removed is limited to within 1% since the abstracted water only accounts for a small proportion of the original river flow (Gu et al. 2012; Wang et al. 2016). While the transferred water may exert more significant changes of hydrographs in areas receiving water as the natural water resources of Hai River is 38.8 km<sup>3</sup> in 2016 (Table 4.1). However, quantitative assessment on the hydrological impact in areas receiving water is very little probably because the water distribution along the transfer route and among the different sectors is not precise. Assessment of the eco-environmental effects of the water transfer project is now more popular than the assessment of the impact on the hydrograph (Yan et al. 2012).

Table 4.1 – The water consumption in different sectors and their proportion to the total water consumption in different regions in 2016. Since the water consumption values for each river basin is not available in the bulletin, the water consumption is estimated by multiplying the water use and the average water consumption efficiency. It takes 0.64 for agricultural water, 0.25 for industrial and domestic water, 0.8 for environmental water. The unit of the water consumption is km<sup>3</sup>, and the unit for the proportion (Prop.) is %. T. W.C. is the abbreviation of total water consumption; T. W.R. is the abbreviation of total water resources; W.C. Prop. is the abbreviation of the ratio of total water consumption of the total water resources; Agri. W.C. Prop. is the abbreviation of the ratio of agricultural water consumption to the total water resources.

Basins	Agricultural		Industrial		Domestic		Environmental		T. W.C.	T. W.R.	W.C. Prop.	Agri. W.C. Prop.
	Amount	Prop.	Amount	Prop.	Amount	Prop.	Amount	Prop.				
National	241.2	78.9	32.7	10.7	20.5	6.7	11.41	3.73	305.8	3246.6	9.4	7.4
North (6)	133.7	85.8	7.1	4.5	6.9	4.4	8.14	5.23	155.8	559.3	27.9	23.9
South (4)	107.4	71.6	25.6	17.1	13.7	9.1	3.26	2.18	150.0	2687.4	5.6	4.0
Songhua	26.6	90.0	1.0	3.4	0.7	2.5	1.20	4.06	29.6	148.4	19.9	17.9
Liao	8.4	80.1	0.7	6.6	0.8	7.5	0.62	5.89	10.5	49.0	21.3	17.1
Hai	14.5	74.8	1.2	6.2	1.6	8.2	2.08	10.76	19.3	38.8	49.8	37.3
Yellow	17.5	82.1	1.4	6.5	1.2	5.5	1.25	5.87	21.3	60.2	35.3	29.0
Huai	27.2	82.4	2.3	7.0	2.2	6.6	1.34	4.05	33.0	101.0	32.7	26.9
Yangtze	62.0	68.9	18.4	20.4	7.8	8.7	1.84	2.04	90.0	1194.7	7.5	5.2
Southeast	8.7	64.5	2.5	18.8	1.7	12.3	0.60	4.43	13.5	311.3	4.3	2.8
Pearl	31.5	77.4	4.5	11.0	3.9	9.7	0.74	1.83	40.6	592.9	6.9	5.3
Southwest	5.2	90.3	0.2	3.8	0.3	4.5	0.08	1.38	5.8	588.4	1.0	0.9
Northwest	39.7	93.9	0.5	1.1	0.4	1.0	1.67	3.96	42.2	162.0	26.1	24.5

### 4.2.3 Dams and dam regulation

China has the largest number of dams in the world (Lehner et al. 2011; Yang and Lu 2014; Ministry of Water Resources 2016). The total number of the dams exceeded 96000 in 2016 (Ministry of Water Resources 2016). There were very few dams on record in China before the 1950s as there were only 22 dams located in China among the global 5268 dams recorded in the Global Reservoir and Dam (GRanD) database (Lehner et al. 2011). Most of the dams were built after the 1950s (Figure 4.8a). The number of the dams increased dramatically during 1950s-1970s as there have been 72131 dams recorded in documents. The number kept increasing at a high rate to 86900 sites around the year 1982. The total number then decreased by 4.6% until 1990 because the removal of small and old dams. The dam number increased after that but at a low rate. The total number of large dams<sup>4</sup> kept increasing after the 1970s. It increased from 283 dams in 1973 to 639 dams in 2016 (Ministry of Water Resources 2016). Both the capacity of all reservoirs or of the large reservoirs increased from the 1970s, and the increase of the total capacity is mainly owing to the large dams (Figure 4.8b). After 2003, the rate of reservoir capacity reached a high level because a few mega dams<sup>5</sup> were built (e.g. the Three Gorges Dam-TGD, 39.3 km<sup>3</sup>, 2003-2009; Xiaowan Dam, 15.1 km<sup>3</sup>, 2002-2010; Xiluodu Dam, 12.8 km<sup>3</sup>, 2005-2013).

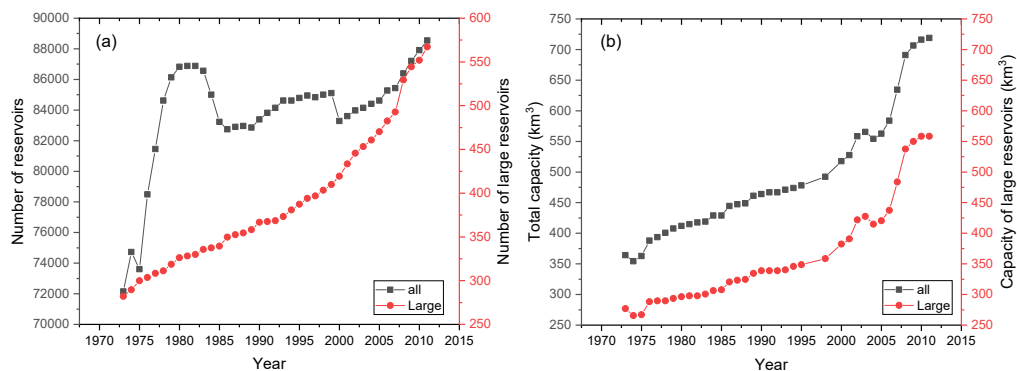


Figure 4.8 – The development of the (a) number of dams in China and (b) the total capacity of the reservoirs in China (Yang and Lu 2014). The black lines represent the total dams, and the red lines represent the large dams with a capacity larger than 10<sup>8</sup>m<sup>3</sup>.

The estimated total storage capacity of all the reservoirs in China exceeded 794 km<sup>3</sup>, accounting for 24.5% of the annual water resources in 2016 (Yang and Lu 2014; Ministry of Water Resources 2016). All the dams act as a huge regulator of land surface water resources and the amount of water stored in the dams varies by year. For example, the actual water stored in the dams at the end of 2016 was 395.4 km<sup>3</sup> (49.8% of the total storage capacity and 12.2% of the total water resources). Dams directly alter the inter-annual river discharge through regulation, and the dam's impact on discharge is determined by their designed purposes. In general, the flood peaks decrease because dams store water amounts associated with extreme high floods to reduce the downstream flood risk. The low flow in dry seasons increases

<sup>4</sup>Large dams: dams with a storage capacity larger than 10<sup>8</sup>m<sup>3</sup>

<sup>5</sup>Mega dams: dams with a storage capacity larger than 10 km<sup>3</sup>.

because dams release their stored water when the river discharge reduced to a very low level. The dams built mainly for flood control have a higher impact on flood peaks; the dams built for water supply change more the low flow and increase the reliability of water supply during drought; the dams mainly designed for hydropower generation change the discharge mainly after flooding season. For the dams which are the critical projects in a region with multiple objectives (e.g. the TGD in the Yangtze River, Xiaolangdi Dam in the Yellow River), the dam impact on river discharge is more complicated.

The analysis of the dam impacts is generally conducted by comparing the discharge before and after the dam's construction with observed or simulated data. Yu et al. (2011) estimated that the discharge in the wet season (May to October) decreased by 10.3% (from 280.3 km<sup>3</sup> in 2003-2008 to 251.5 km<sup>3</sup> in 1953-1980) at Yichang hydrological gauge (right after the TGD) after the TGD started to store water in 2003. The discharge increased by 8.0% for the rest of the months after 2003. Chen et al. (2016) estimated that 30-43% of the increment in January-March arise from the releases from the TGD. Although the change in discharge is not only the result of the dam regulation, the climate change may also change the discharge, the sudden change of the runoff ratio in the wet season and other months around 2003 indicates the influence from dam construction. Regardless of the natural climate variation, the proportion of the discharge in the wet season decreased by 4% which indicates that part of the water in the wet season has been stored in the dams (Yu et al. 2011). According to the report from the Three Gorges Company, the TGD decreased the flood by 83.1 km<sup>3</sup> in the flood seasons and increased by more than 120.4 km<sup>3</sup> the water in the dry season in total during 2010-2015 that helped to overcome the flood and drought risk in downstream area (China Three Gorges Corporation 2016).

The alteration in the seasonality of hydrological cycle is apparent in the wet regions where the water consumption is small compared to the water resources, and the dams are mainly built for electricity production (e.g. the Yangtze River, the Pearl River, Wu et al. 2012a; Yu et al. 2011). The conclusion is different in the Yellow River basin where the built dams are mainly regulated for increasing water availability (Yang et al. 2008b). Although the released river discharge may increase in the dry season for a single dam, the overall impact of the cascades is negative in that more water is used as a result of the dams regulation (Ouyang et al. 2011). The variability of annual cycle did not change a lot because the phases of river discharge and water demand are similar in seasons.

Except for the inter-annual cycle changes of discharge, the dams may reduce the annual total stored water. Yang et al. (2015a) estimated that 0.3 km<sup>3</sup>/yr (0.77% of the water stored in the TGD) is lost due to the increased evaporation over water surface of the TGD (~1084 km<sup>2</sup>). Together with the initial filling of the TGD, the water discharge decreased by 3-14 km<sup>3</sup> yr<sup>-1</sup> (0.25%-1.17% of the total annual water resource of the Yangtze River). The loss can be significantly high in China as the total surface area of all dams at designed water level reaches 26870 km<sup>2</sup>, which is 32.7% of the current lake surface area (Yang and Lu 2014). On the other hand, as the dam regulation increases the availability of water usage, more agricultural demand is satisfied and the lost water increases because a large proportion of agricultural water evaporates to the atmosphere. However, the contribution of dams to the increased evapotranspiration through irrigation is not well evaluated currently in China.

The dam influence on discharge will cause other ecological problems over the lakes downstream. The Dongting Lake and Poyang Lake are the two largest lakes that are still naturally connected with the Yangtze River. The lake storage is therefore affected by the water level in the Yangtze River. Because the Three Gorges Dam, which is upstream to the outlets of the two lakes, reduces the release in flood season especially at the end of the flood season, the water level downstream at the outlets of the two lakes becomes lower than normal (decreased by at most 2.0-2.8 m). The release from the two lakes therefore increases because there are no sluices for the water exchanges. The water storage in the two lakes decreases which threatens the ecosystems and the water availability in the lake area (Lai et al. 2014a; Lai et al. 2014b). The river-lake interactions with dam regulation and whether the two lakes need gate controlling are a subject of debate among the researches, public and government.

Moreover, because China has the largest density of dams in the Yangtze and the Yellow River, the cumulative effect of the cascaded dams on the discharge becomes another topic of study for hydrologists (Ouyang et al. 2011). The single dam effect is amplified through the cascades, e.g., the maximum difference between the inlet and outlet of Long-Liu section (from Longyangxia Dam to Liujiaxia Dam), with three large dams and a few small dams, decreased from 430 to 115 m<sup>3</sup> s<sup>-1</sup> (Ouyang et al. 2011). The cascaded dams also increase the residence time of water (Vörösmarty et al. 1997). The response of the river discharge to the precipitation in the Yangtze River has changed from one month in the 1980s to two months in the past decade as determined by isotopic approaches (Li et al. 2016a). The delayed residence time reduces the speed of land water refreshing and in the meanwhile increases the risk of environmental problems. The cumulative dam effect is more associated with the water quality or the ecosystem rather than the flow regime (Kibler and Tullos 2013).

#### 4.2.4 Summary

In conclusion, this section reviewed three major human activities that change river discharge and the related studies in Chinese regions. The Land-use change, mainly consisting of deforestation, urbanisation and afforestation, indirectly alters the river discharge since land-use change alters the properties of the land surface. The altered properties will then change the water yield through changes in water processes such as infiltration and evapotranspiration. The water consumption in three sectors, domestic, industrial and agricultural water use, directly change the river discharge by withdrawing water from water bodies. Dams affect the river discharge through regulation by controlling the dam release with certain regulation rules to maximize the benefits.

The different Land-water use and dam regulation take place in different places, and their impacts on the river discharge regimes vary in magnitudes (Figure 4.9). Forest change (i.e., deforestation and afforestation) change both the total value of water yield and the extremes of river discharge (i.e., flood peaks and low flow). Urban area expansion increases the flood peak and decreases the flood residence time in cities. It also increases the total value of water yield due to less evaporation. Water used for domestic and industrial purposes change little the river discharge (2.0% in average for China), while agricultural water consumption decreases the total water yield by 7.4% (in average for China). The water consumption has very little impact

on the discharge extremes, while the dam regulation mainly changes the inter-annual cycle by decreasing the high floods and increasing the low flow. The total water amount slightly decreases due to dams because of the increases in water surface and human water usage.

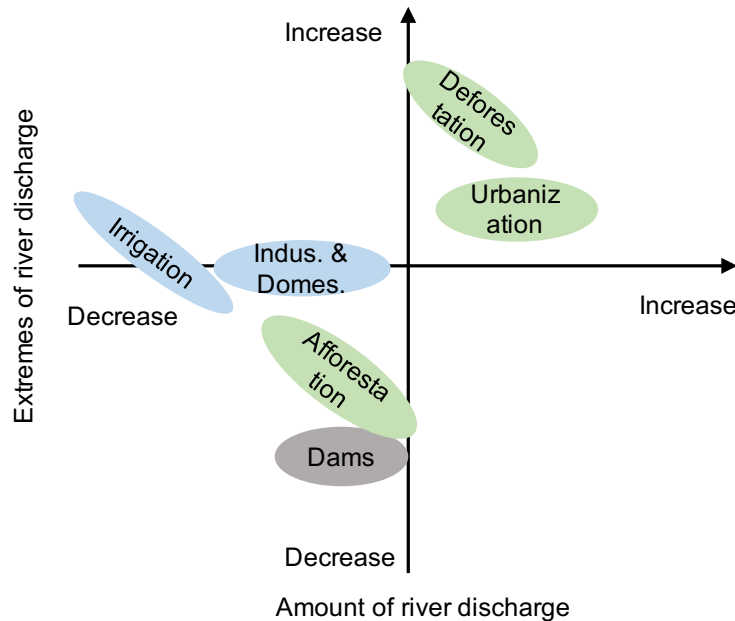


Figure 4.9 – The illustrative summary of the impact of land and water use as well as the dams on river discharge.

Recognizing the impacts of human activities and their magnitudes are necessary for understanding how and how much human beings are affecting the natural river discharge. It is a mean of evaluating the hydrological impacts of current engineering projects (e.g., dams, agricultural irrigation projects, water-transfer projects), economic developments (e.g., urbanisation, GDP increasing) and policies (e.g., "Green for Grain" projects). The results of scenario analysis also provide guidance for future policies and adaptation actions.

### 4.3 Quantification methodologies of the human impacts

As described in the above section, the impacts of human activities are various in time and space. The magnitude and the direction of the impacts on the means of river discharge and the extremes are also different. Quantifying the impacts is needed to understand the human interventions. On the other hand, these human activities may also occur together and interact with each other in specific regions. Climate change also takes place with human interventions which make the quantification more complicated. Therefore, separating the impacts out of the climate variabilities and isolating the individual human impact is with difficulty.

There have been a few approaches designed for this purpose and a large number of implementations on global catchments. Two review papers (Dey and Mishra 2017; Wang and Chen 2014) have reviewed those approaches although they mainly focused on the indirect approaches (i.e., estimate the human impact in an indirect way) but paid very little attention to direct quantitative technologies. Here, this section will give a brief introduction of those

indirect approaches but emphasize the direct approaches. The corresponding implementations in Chinese regions and the peculiarities of the two types of approacher are discussed.

### 4.3.1 Indirect approaches

#### Basic concepts

The indirect approaches estimate the human impacts on river discharge indirectly. These methods assume that the changes in any hydrological components are a result of combined effect from climate change and human activities.

$$\Delta Q = \Delta Q^c + \Delta Q^h \quad (4.1)$$

where the  $\Delta Q$  is the total change in discharge, and  $\Delta Q^c$  and  $\Delta Q^h$  are the changes induced by climate change and human activities, respectively. The impact of human activities can be obtained if the impact of climate change is estimated and excluded from the total. Therefore, the indirect approaches mainly aim at quantifying the impacts of climate change with different strategies.

The primary assumption of these indirect methods is that there is a natural period when the human impacts are considered negligible. Statistical analysis (e.g., Mann-Kendall test, Pettitt test, Double-mass curve test) is applied to the discharge to find the change-point that separates the pre-effect and post-effect periods. Various models (equation 4.2) are set-up and calibrated with hydroclimatic observations ( $Q_{pre}$ ) in the pre-effect period. Only the variables that are free of human interventions can be used as the variables ( $x_i^c$ ) in the model (e.g., precipitation, temperature, discharge in the natural state).

$$\hat{Q}_{pre} = f(x_1^c, x_2^c, \dots, x_i^c, \dots, x_n^c), i = 1, 2, \dots, n \quad (4.2)$$

In the post-effect period, both the climate change and human interventions exert influence on the river discharge, and the impact (changes compared to the pre-effect period) can be quantified as the averaged discharge measurement in the post-effect period ( $\overline{Q_{post}}$ ) minus the averaged pre-effect discharge ( $\overline{Q_{pre}}$ , see equation 4.3).

$$\Delta \overline{Q} = \Delta \overline{Q}^c + \Delta \overline{Q}^h = \overline{Q_{post}} - \overline{Q_{pre}} \quad (4.3)$$

The impact of climate change on the river discharge is mainly caused by the alteration in the forcing variables (e.g., precipitation, temperature, radiation, wind, etc.). These alterations are driven by large-scale atmospheric dynamics and are not affected by human interventions. With the model set-up in the pre-effect period (equation 4.2) and the new climate in the post-effect period ( $x_{i,post}^c$ ), the discharge response to the only climate change is estimated as

$$\hat{Q}_{post}^c = f(x_{1,post}^c, x_{2,post}^c, \dots, x_{i,post}^c, \dots, x_{n,post}^c), i = 1, 2, \dots, n \quad (4.4)$$

The impact of climate change ( $\Delta \overline{Q}^c$ ) is then estimated as the difference between the model estimation driven by the new climate in post-effect period ( $\hat{Q}_{post}^c$ ) and the discharge in pre-effect

period ( $\overline{Q_{pre}}$ ) (see equation 4.5). In some cases, the discharge measurement  $Q_{pre}$  is replaced by its estimation  $\hat{Q}_{pre}$ .

$$\Delta\overline{\hat{Q}^c} = \overline{\hat{Q}_{post}^c} - \overline{Q_{pre}} \quad (4.5)$$

The impact of human activities ( $\Delta\overline{\hat{Q}^h}$ ) can thus be estimated as the difference between  $\Delta\overline{Q}$  and  $\Delta\overline{\hat{Q}^c}$  or by subtracting the estimated discharge in new climate without human impacts ( $\overline{\hat{Q}_{post}^c}$ ) from discharge in post-effect period ( $\overline{Q_{post}}$ ).

$$\Delta\overline{\hat{Q}^h} = \Delta\overline{Q} - \Delta\overline{\hat{Q}^c} = \overline{Q_{post}} - \overline{\hat{Q}_{post}^c} \quad (4.6)$$

The contribution of climate change ( $\eta^c$ ) and human activities ( $\eta^h$ ) to the total changes is estimated as

$$\begin{cases} \eta^c = \Delta\overline{\hat{Q}^c} / \Delta\overline{Q} \\ \eta^h = \Delta\overline{\hat{Q}^h} / \Delta\overline{Q} \end{cases} \quad (4.7)$$

### Different approaches and case studies

The key to the indirect approaches is to estimate the river discharge in the post-effect period only considering climate variabilities without human activities. It requires that the model settings in the pre-effect period only depend on climate forcing or other variables free of human interventions (equation 4.2). According to the variables and strategies used for building the model, these approaches can be categorized into the following two groups.

- Constructing the models by forcing inputs. It is the most used way of modeling, and there have been many kinds of methods to set-up such models. For example, the regression model (Miao et al. 2011) and Neural Networks (Liu et al. 2010a) based on the observed discharge and forcing components are effective approaches to obtain a rainfall-runoff relationship. The precipitation ( $P$ ) is the dominant variable for the water cycle. Temperature ( $T$ ) or the potential evapotranspiration ( $PET$ ) are often accounted for in the models since they are related to the actual evapotranspiration ( $ET$ ) back to the atmosphere. Elastic models relate the increments of observed discharge with the changes in forcing components (Jiang et al. 2011). The discharge changes due to climate change in the post-effect period can be directly estimated by the increments of the climate variables (e.g.,  $P$ ,  $T$ ,  $PET$ , radiation). These statistical methods strongly rely on the data, but they require a very low understanding of physical mechanisms. Budyko-related methods are also statistical approaches, but they relate  $P$ ,  $ET$  and  $PET$  by an empirical Budyko curve (Yuan et al. 2016). The contribution of climate change will be firstly estimated from the curve according to the shift of the representative points which represent the system in different statuses. The remaining difference from the observations represents the impact of human activities. Moreover, there are many kinds of hydrological models and land surface models driven by the climate forcing (Lu et al. 2015). These models are improved compared to the statistical approaches in terms of the representation of physical mechanisms (e.g., infiltration, evaporation, runoff generation). The underlying conditions (e.g., soil types, land cover) are considered as well. The

climate impacts in the post-effect period are estimated with the new forcing, but other underlying conditions remain as the pre-effect conditions. The human impacts are then estimated by subtracting the climate impacts.

- Constructing a model of discharge free of human interventions as paired comparisons. For a few regions with sparse data and complex surface conditions (e.g., mountains, deserts), the models are difficult to build, and the accuracy of forcing variables are probably not acceptable for the model set-up. The discharge model can be established with discharge measurements at reference gauges where the human interventions are negligible. One approach links the downstream discharge with the discharge at upstream gauges (Tao et al. 2011). The upstream gauges are considered free of human impacts in both pre-effect and the post-effect period. The climate change is considered to be the same for both the upstream and downstream areas. In this case, the estimated downstream discharge with a relation from the pre-effect period and upstream discharge in post-effect period is the result of a climate-effect scenario, and the remaining part results from the influence of human activities. For example, there is very little human interventions in the source catchments of the Tarim basin (see Chapter 3), while the large area of the human activities (mainly the irrigation) is between the source catchments and the lower target gauge (Alar, see Figure 3.1). The climate change is considered to be the same for both the upstream and downstream area over the whole period. The climate impact on the downstream gauge in the post-effect period is estimated by the established model driving by measured discharge at the upstream gauge in the same period. The difference between the estimated discharge and the measurements at the downstream gauge can be recognized as the human impacts. The other approach is to establish the model with a similar basin nearby and free of human activities in the whole period which acts as the upstream area in the previous method. A few studies that used these indirect approaches are listed in Table 4.2.

Table 4.2 – Implementations of the indirect approaches in quantifying human impacts on river discharge.

	Methods	References
Regression	Linear Regression	Kong et al. (2016), Miao et al. (2011), and Wang et al. (2012a)
	Multi Regression	Jiang et al. (2011) and Xu et al. (2004)
	Neural Network	Liu et al. (2010a)
	Paired comparison	Tao et al. (2011)
Elasticity		Jiang et al. (2011)
Budyko		Jiang et al. (2015), Yuan et al. (2016), and Zhao et al. (2014)
Hydrological Models		Lu et al. (2015) and Ye et al. (2013)

### Advantages and Disadvantages

These indirect approaches are widely applied in many case studies in the globe at different spatial scales because of their simple concepts and low data requirements. Comparison among

models in order to analyze the uncertainties and possible physical explanations of the discharge change is easy because of a large number of different approaches in the group.

However, these indirect approaches are short in the following aspects,

- The primary assumption of the indirect approaches is that the human impact is considered negligible in the pre-effected period while because the two periods are mainly separated through the discharge time series, only the time with intensive human activities which immediately change the discharge can be detected (e.g. dam construction, land cover fast change such as forest fires). Other activities (e.g., land use change with deforestation, afforestation, urbanisation) which take a long time to cast measurable impacts on discharge are difficult to detect. The detection based on discharge is also sometimes not perfect since climate may dominate the changes in discharge so that the separation indicates the point of changes in climate rather than the human impact.
- The indirect approaches estimate the human impacts ( $\eta^h$ ) on the changes of river discharge in the post-effect period compared to the pre-effected period ( $\Delta\bar{Q}$ , equation 4.3). When the assumption that the human impact is negligible in the pre-effect period is valid, the  $\Delta\hat{Q}^h$  represents the total impact due to human interference. While the assumption is not always valid in reality because the human activities (e.g., land and water use) in the defined pre-effect period have already existed and therefore the impacts. The  $\Delta\bar{Q}$  only evaluates the human impacts due to changes in human activities rather than the absolute impact because the human impact in the pre-effect period is considered as natural variability. The separation of the periods is therefore related to the point where the human activities have changed the most significantly.
- The model ability in estimating the river discharge is overvalued in the post-effect period because the model is not validated with the new climate and human impact in the post-effect period. The estimation of the human impact is made by extracting the discharge estimation with only the climate change from the observed discharge will attribute the model bias to the impact of human activities.
- The human impact is a sum of the impact from all kinds of human activities. The impact of individual human activity cannot be disentangled with these indirect approaches. Therefore, there is a need to develop models which can separate the impact of individual human activities.
- These indirect methods are unable to project the future human impacts because they use observed discharge as a result of combined impacts by human activities and climate change. Only the climate change impacts can be obtained from model estimation, and the human impacts cannot be obtained because of the lack of observed discharge (see equation 4.6).

### 4.3.2 Direct approaches

#### Basic concepts

The direct approaches, namely, are the approaches that estimate the human impacts directly rather than subtracting the climate impacts from the total (equation 4.6). A qualified model is set-up to estimate the discharge based on different variables ( $x_i^c, x_j^h$ ) and models ( $f(x)$ ),

$$\bar{Q} = f(x_1^c, x_2^c, \dots, x_i^c, \dots, x_n^c; x_1^h, x_2^h, \dots, x_j^h, \dots, x_m^h), i = 1, 2, \dots, n; j = 1, 2, \dots, m \quad (4.8)$$

The impact of any human activities ( $\hat{Q}^h$ ) is estimated by the difference between simulations with human interventions ( $\hat{Q}$ ) and without such activities ( $\hat{Q}^{-h}$ , equation 4.9).

$$\hat{Q}^{-h} = f(x_1^c, x_2^c, \dots, x_i^c, \dots, x_n^c), i = 1, 2, \dots, n \quad (4.9)$$

$$\hat{Q}^h = \hat{Q} - \hat{Q}^{-h} \quad (4.10)$$

Compared to the models for indirect approaches (equation 4.2), the variables used in the direct approaches are not limited to the climatic variables ( $x_i^c$ ). The variables ( $x_j^h$ ) and processes related to human interventions (e.g., water consumption amount, irrigation, dam regulation) are also included. These approaches estimate the absolute value of human impact ( $\hat{Q}^h$ ) rather than the human impacts to the changes ( $\Delta\hat{Q}^h$ ). Therefore, there is no need to separate the pre-effect and post-effect periods. The impacts of human activities that took place in the pre-effect period can be evaluated as well. The length of the period is not limited while the statistical analysis of the change-point needs a relatively long period for the indirect approaches.

#### Different approaches and case studies

There have also been many kinds of approaches that can estimate the human impact directly, only if the models are integrated with the modules and variables that represent the human activities.

- The impacts of land use change have been able to be modeled in many hydrological models or land surface models (Liu et al. 2008; Liu et al. 2013b; Niu and Sivakumar 2014). Different types of land use are represented in models with different parameters (e.g. the root depth, the infiltration rate, the leaf area index, the roughness, the albedo ratio). Knowing the spatial distribution of land-use in different periods, the discharge affected by human activities is obtained, and the discharge difference versus the simulation with the land use scenario and scenario with its natural state (e.g., forest) gives the impact of the land use. The method is the same for evaluating human impacts of deforestation, urbanisation or afforestation, as long as these land-use change patterns can be represented in the model. Niu and Sivakumar (2014) assessed the land use change by different scenarios of deforestation and afforestation at different rates in the East River Basin with the VIC model. Chen et al. (2009) estimated the urbanisation

impact on storm-runoff generation with scenarios with different urban area proportions (9.2%, 14% and 17%) in Taihu Lake with the HEC-HMS model. While Du et al. (2012) used different land cover maps in 1988 and that planned in 2018 to predict the urbanisation impact in Qinhuai Basin with the HEC-HMS model.

- The water consumption can be considered in models in either an independent or a coupled way. Water consumption for domestic and industrial purposes are human-dominated and mainly independent of the hydrological processes (Hanasaki et al. 2006). These demands are always estimated using quota methods according to the population and Gross Domestic Product for each small model unit (e.g., lon-lat grids, administration unit) (Wada et al. 2017). The irrigation demand is calculated as the insufficient water between potential transpiration to the actual transpiration over the croplands (Guimberteau et al. 2012b). These demands take water from the water system and thereby change the hydrographs. The hydrological impact of the water consumption is evaluated as the differences between estimations with and without consideration of these water consumptions.
- Dam regulation is considered in studies which focus more on the inner-annual cycle of discharge. Such models include the dam regulation rules to represent the dams' function in altering the dam inflow. Despite case studies which have detailed regulation rules for each dam, the generalisation of the dam regulation is the main difficulty for large-scale studies. The dam release was estimated simply as (Meigh et al. 1999).

$$Q_{out} = k_r \times S_r \left( \frac{S_r}{S_{r,max}} \right)^{1.5} \quad (4.11)$$

Where  $Q_{out}$  is the dam release,  $k_r$  is the outflow coefficient,  $S_r$  is the current dam storage and  $S_{r,max}$  is the maximum value active storage capacity. However, the complexity of the dam release is higher in reality as the dam has to balance the dam release and the water left in dams to meet the downstream water demands (Hanasaki et al. 2006) and other purposes (e.g. hydropower generation and the flood control Haddeland et al. 2006) in the future. Two major groups of dam regulation are proposed for large-scale modeling in the current literature. The first one is based on Hanasaki et al. (2006) for which dams only serve the water consumption needs and the release is estimated by a set of given equations and parameters. The other group is developed from Haddeland et al. (2006) in which the dam release is optimized to satisfy multiple objectives (e.g. water consumption need, hydropower, flood control). The later model is retrospective as the inflow in the future year (12 months) is known and used to determine the dam release. It therefore has high uncertainties if used for future projections.

The implementations of direct approaches to determine water consumption and dams are rare in the large Chinese regions. The difficulties inherent in setting up a reliable large-scale hydrological or land surface model and the difficulties to establish the module to represent human activities restrict the implementations of the direct approaches.

### Advantages and disadvantages

Compared to the indirect approaches, the human impact on discharge is directly estimated by comparing the results with and without activating the modules that represent human processes (equation 4.10). The advantages of the direct approaches include

- The direct approaches evaluate the pure impacts of the human activities on river discharge, rather than the contribution to the discharge changes between two separate periods. The results of the impact analysis therefore provide more insights for practical water management.
- The separation of pre-effect and post-effect periods is not needed so that the human impacts in the whole period can be assessed. The results are not affected by the accuracy of the estimation of the change-point, and the bias in the results is therefore only induced by the model abilities rather than other processes.
- The human activities are represented in more detail in the direct models using physical mechanisms. The division of a single human process and the understanding of factors that affect single human activities becomes possible with the direct approaches.

Two major problems limit the development and implementation of the direct approaches. They are the accuracy of the model simulation either for the natural water cycle or the human activities and the complexity of the models.

- The ability of the modules to represent the natural water cycle and human activities determines the accuracy of the impact assessment. However, because these models are mainly implemented in large-scale regions, there are many uncertainty sources which affect the final results. Bias in forcing inputs has been shown to play an important role in the model uncertainty (see Chapter 2 and 4). However, the forcing bias is difficult to assess and to remove in the current stage for large-scale analysis.
- The generation of the water management may introduce extra uncertainties to the model results and the implementation of such parameterisation is difficult as we do not have the natural flow to see if the results produced by the model is correct. For example, the dam regulation rules are considered to be the same for the dams with the same main purpose in the current implementations, while the dam regulation in reality also takes into account the local situation. The real action of the regulation is also affected by the dam managers. Because we cannot assess the forcing errors, but the parameterisation can easily be tuned, the representation of the human processes can compensate the errors in rainfall and the evaporation formulation.
- The spatial and time resolution is sacrificed to reduce the computing consumptions in large-scale analysis. The locations of the human impacts as well as the impact in a short period cannot be considered as a result. The interactions between the human activities and nature and that among different human activities are simplified to some degree and generalized to decrease the model complexity as well as the simulation cost.

However, this disadvantage is not fundamental and can be solved with the improvement of our understanding about the physical processes and the advances of technologies.

### 4.3.3 Towards integrating human impacts at high resolution

In the real world, the human activities have interacted with the natural water cycle. The amount of available water limits the total consumption for different sectors. The amount of soil moisture together with the climate determines the crop water needs and irrigation amount for the agriculture. The irrigated water then infiltrates to the soil and part of it is absorbed by the plants and transpired to the atmosphere. The rest of the water either evaporates or joins the water cycle as return water. How much the water can be used and how much the water returns depend on irrigation methods and the soil properties. The dams regulate the river discharge and change the seasonal water availability especially in the dry period. The shift in the discharge regimes further changes the amount of water that can be used for different social-economic sectors. The amount of water availability, the way the plants use irrigation water, and the return-water effect on the river system may differ in different models, and the interactions among these processes differ from model to model.

The interactions between the human water use and natural processes are considered in different ways between models (e.g., PCR-GLOBWB, H08 and LPJmL) which are shown in Figure 4.10. The sources of water consumption in the three models are different. In PCR-GLOBWB, the water consumption withdraws water from sources such as the surface water, groundwater and desalized water. In H08, the water consumption withdraws water from the surface water, the medium-size reservoirs and then the nonrenewable and nonlocal blue water (NNBW), among which the NNBW is assumed as unlimited. In the LPJmL, the consumption withdraws water from the river discharge and then lakes and reservoirs. If the water demand is not satisfied, the model will search water from neighbouring grids for available water. Reservoirs in the LPJmL provides water for the downstream within five grids. In H08 and LPJmL, the dam release is determined by the dam regulation rules, and it is also affected by the downstream water demands.

However, there are a few limitations when these models account for the water interactions. The locations of the water consumption (i.e., agriculture, residence, factories) are not specified in the unit of the model simulation (approximating  $0.5^\circ$  in the lat-lon grid). The water demands at specific locations are summed and considered as a whole for water supply. The locations of the water sources relative to these demands are also not precise. Moreover, there are no reliable river networks (not the routing route in the models at coarse resolution) identified in the models, and thus the water demands only consume water from the total amount of surface water or the reservoirs of specific grids. However, water is often pumped from the nearest river in reality. On the other hand, the abstracted water is not distributed to the points where the water is needed but evenly distributed over the grid space. The evapotranspiration rate may also differ from reality because of the added water. The influence range of the reservoirs is prescribed by users, but this range is not easy to be assessed in the natural system and it varies from dam to dam. Neverre et al. (2016) introduced a new strategy to find the demand-reservoir associations based on a "least cost" function, which considers the distance

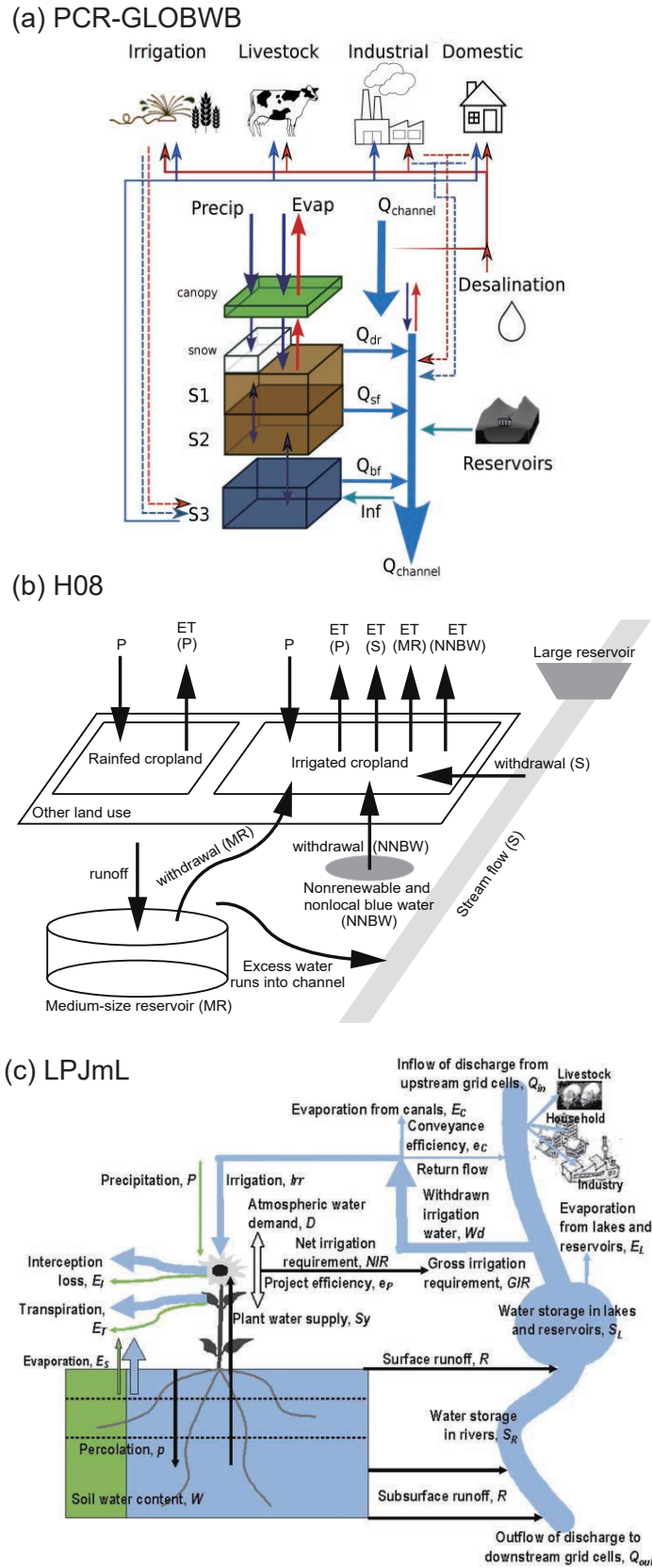


Figure 4.10 – The illustration of the interactions between land surface processes and human activities in three global hydrological models (a) PCR-GLOBWB (PCRaster GLOBal Water Balance Sutanudjaja et al. 2017), (b) H08 (Hanasaki et al. 2010) and (c) LPJmL model (Lund-Potsdam-Jena managed Land, Rost et al. 2008).

of the water demand to the dam and uphill height from the path. This links the water demand with the water sources by practical experience and have been validated in the north Africa. However, these links are still virtual as there are no real connections such as rivers or channels between them.

The above limitations mainly result from the lower spatial resolution in the global hydrological models which are in turn constrained by the resolution of the forcing variables. Compared to the spatial heterogeneity of the forcing variables, the spatial heterogeneity of the river channels is more significant, and the river surface only accounts for a very small proportion of the land area. The location of water abstraction should be more accurate than that dealt with in these models. More detailed topographic information has become available (e.g., 1 km in HydroSHEDS) and routing approaches based on such high-resolution topography have been developed in (Nguyen-Quang et al. 2018; Zhou et al. 2018). The integration of human interventions and the interactions between human water management and natural water processes should be further improved.

## 4.4 Comparisons of human impacts to other uncertainties

From the previous literature review, we know that the human impacts on the water cycle vary in space. The magnitude of the impact is also different for human activities and in different places. Therefore, in this section, we will quantify the human impacts on river discharge by analyzing the census data (observed discharge and naturalized discharge). The significance of human impacts is then compared to the uncertainties in precipitation datasets and uncertainties caused by models. The purpose of this section is to find whether our knowledge on the forcing is sufficient to attribute the human impact, and where the condition can be satisfied.

### 4.4.1 Data and gauge introduction

The dataset involves 84 available gauges over the Chinese mainland. The locations of these gauges with their corresponding upstream area are shown in Figure 4.11. Most of the gauges are located along the Yellow River (middle China), Songhua River (Northeastern China), Pearl River (Southwestern China), Hai River basin (Northern China near Beijing) and part of the Huai River basin (Eastern China). The colour shows the number of gauges that can monitor the discharge of the region. Among the five large basins, the upper Yellow river is monitored by the most gauges (5 gauges), while most of the upstream area is monitored by one or two gauges. There are a few gauges which do not belong to these five large basins.

The period of the dataset covers the years from 1956 to 2000. All the discharge is collected at a monthly interval. The observed discharge is measured at corresponding gauges. The natural river discharge has been interfered with by humans as they withdraw water through pipes, regulate the water through dams, and transfer water across basins through different projects. The differences between the observed discharge, which has been altered, and its natural state is the effect of human interference.

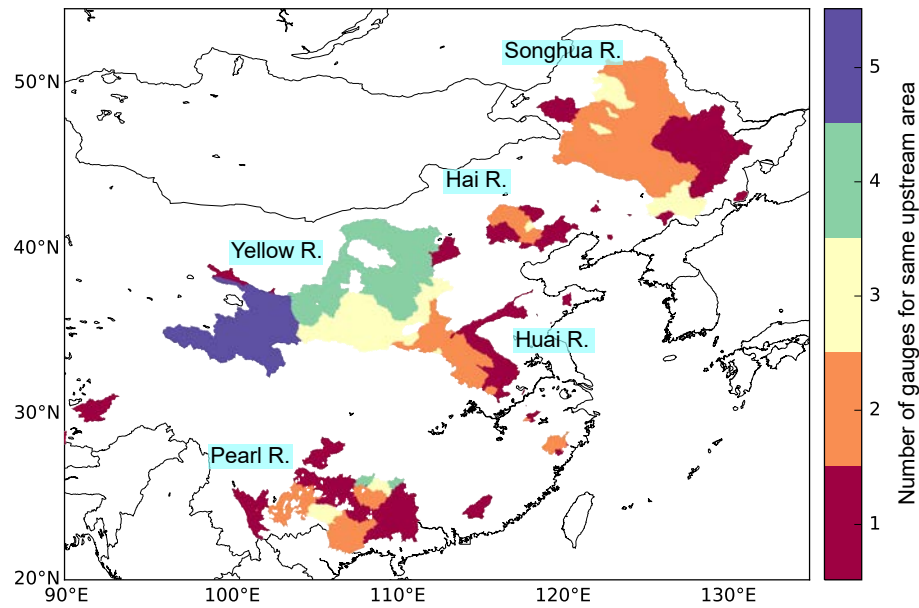


Figure 4.11 – The upstream area of all the 84 hydrological gauges. The number corresponding to the area represents the number of the gauges having same upstream area.

The estimation of the natural river discharge is challenging because there are human water usage is scattered and consists of many sectors. The data is collected through different departments and it is difficult to access for the public. Model estimation is an alternative way to estimate all the water consumption but the processes to build and validate the model also require quite a large amount of data. Thus, the naturalized river discharge used in this section is obtained from basin managers. They have statistical data in good quality and covering all the kinds of water consumption. The statistical data for different water sectors (e.g., agriculture, domestic and industrial water) is added to the observed discharge. The changes resulting from the cross-basin water projects and the changes in water storage in dams are also considered to estimate the naturalized discharge:

$$Q_{nat} = Q_{obs} + Q_{agr} + Q_{ind} + Q_{dom} \pm Q_{pro} \pm Q_{store} \quad (4.12)$$

Where  $Q_{nat}$  is the naturalized discharge,  $Q_{obs}$  is the discharge observed at the corresponding gauge.  $Q_{agr}$ ,  $Q_{ind}$ ,  $Q_{dom}$  denote the discharge that transports for water usage in agriculture, industry and domestic sectors, respectively.  $Q_{pro}$  denotes the discharge related to the amount of water exchange through water transfer projects. Finally,  $Q_{store}$  denotes the changes in dams that can regulate the natural river discharge. The difference between the naturalized river discharge from the observed river discharge is that caused by human intervention, and the ratio of this difference to the naturalized discharge is regarded as the human impact.

#### 4.4.2 Quantification of human impacts

The human impacts on river discharge are shown in two different aspects. On the one hand, water consumption for various purposes directly decreases the naturalized river discharge. On the other hand, human regulation, especially the dams, alters the discharge phases (annual cycle, seasonality). Therefore, the quantification of the human impacts at those gauges is

conducted from two aspects.

### Alteration in discharge amount

The map of the observed discharge flux is shown in Figure 4.13-a. The three largest basins have a different magnitude of discharge values, as the averaged discharge exceeds  $6000 \text{ m}^3 \text{ s}^{-1}$  in the Pearl River (Figure 4.12-a, Wuzhou). It is around  $2000 \text{ m}^3 \text{ s}^{-1}$  in the Songhua River (Figure 4.12-b, Jiamusi) while it is below  $1000 \text{ m}^3 \text{ s}^{-1}$  in the Yellow River (Figure 4.12-c, Lijin). The Hai River has the least amount of discharge since there is not much precipitation in addition to significant human water consumption. The observed discharge is less than  $800 \text{ m}^3 \text{ s}^{-1}$  for those small river basins. The spatial pattern of the naturalized river discharge is quite similar to that of the observed river discharge (Figure 4.13-b). The largest difference is on the lower reaches of the Yellow River ( $\sim 1000 \text{ m}^3 \text{ s}^{-1}$ , Figure 4.13-c, Figure 4.12-c). The water consumption is significant from the middle of the Yellow River and in the tributary of the Yellow River (i.e., Han River, Wei River). For the Songhua River and the Pearl River, the humans consume  $300\text{-}400 \text{ m}^3 \text{ s}^{-1}$  in the lower mainstream.

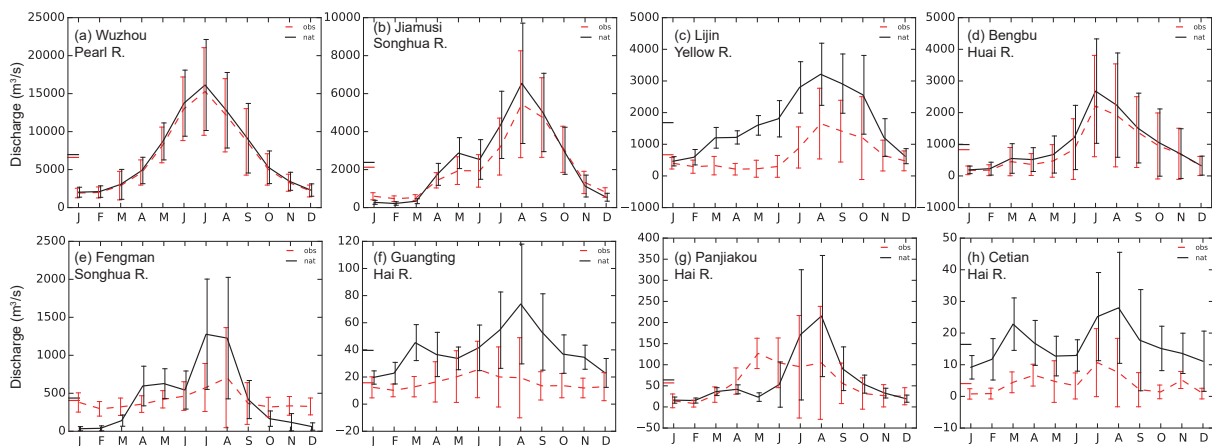


Figure 4.12 – The samples of a few gauges in the dataset.

The proportion of discharge difference to the naturalized river discharge shows the magnitude of the human water consumption to the natural river discharge (Figure 4.13-d). The proportion is small, within in  $-10\%$ , for the tributaries of the Songhua River basin, the headwater catchment of the Yellow River basin and the whole Pearl River basin. The water consumption accounts for  $10\%\text{-}20\%$  of the naturalized discharge in the lower Songhua River. The ratio of the water consumption to the river discharge increases to  $30\%\text{-}40\%$  in the Hai River, where the Beijing area relies heavily on the nearby water supply. The largest alteration is at the gauges of reservoirs (i.e., Guanting Reservoir,  $-60.1\%$ , Figure 4.12-f; Cetian Reservoir,  $-73.3\%$ , Figure 4.12-h). In the Huai River basin, the alteration of the river discharge is within  $30\%$ , and most of it is used for agriculture (Figure 4.12-d). In the Yellow River basin, significant alteration of the river discharge is monitored except for the upstream (up Lanzhou gauge). The water consumption accounts for  $\sim 33.8\%$  in the middle Yellow (Huayankou gauge) and  $55\%$  in the lower Yellow River (Lijin gauge, Figure 4.12-c).

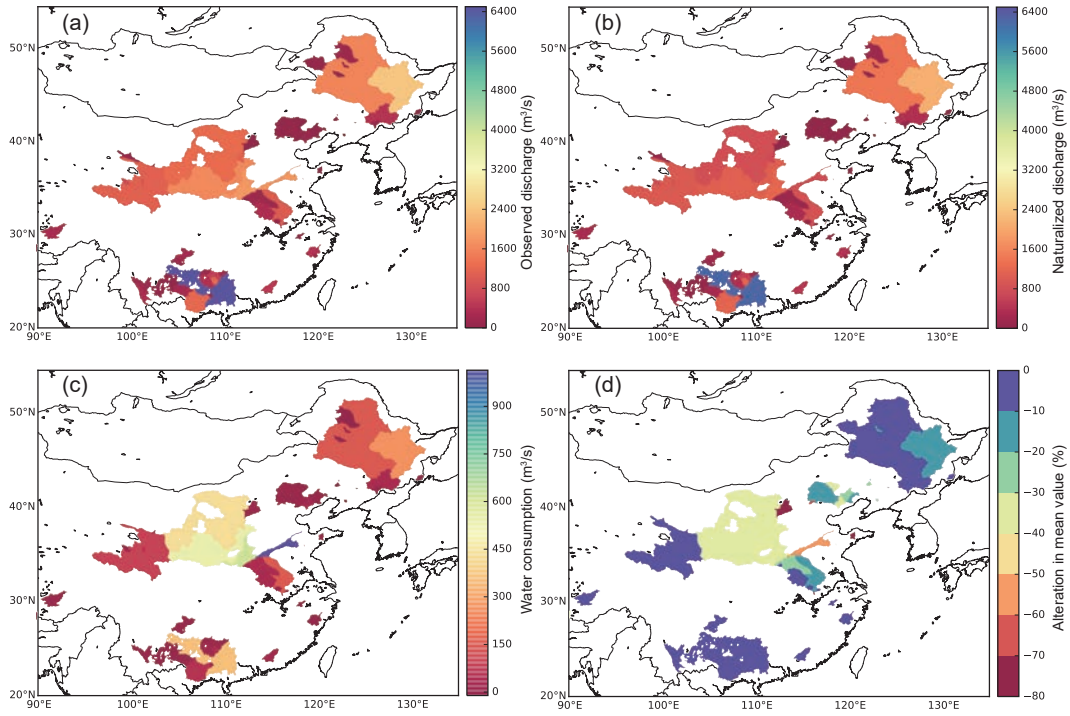


Figure 4.13 – Different discharge characteristics at the gauges (a) observed discharge, (b) naturalized discharge, (c) difference of the observed discharge from the naturalized discharge and (d) the proportion of the difference to the naturalized discharge.

### Alteration in discharge variability

Another alteration of the river discharge is the shift of its seasonality. The discharge varies within a year, and a large proportion of the discharge concentrates in the flood season. The concept of concentration period ( $C_p$ ) and concentration degree ( $C_d$ ) (Jiang et al. 2005; Li et al. 2008; Li et al. 2011b) is modified to evaluate the annual distribution of the river discharge and its changes due to human intervention.

The monthly discharge is represented as a vector with its quantity and the direction for a year that can be seen as a circle ( $360^\circ$ , Figure 4.14).

$$Q_{i,x} = Q_i \times \cos(\theta_i) \quad (4.13)$$

$$Q_{i,y} = Q_i \times \sin(\theta_i) \quad (4.14)$$

$$Q_x = \sum_{i=1}^{12} Q_{i,x} \quad (4.15)$$

$$Q_y = \sum_{i=1}^{12} Q_{i,y} \quad (4.16)$$

$$C_p = \frac{\arctan(Q_y/Q_x)}{2\pi/12} \quad (4.17)$$

$$C_d = \sqrt{Q_x^2 + Q_y^2} / \sum_{i=1}^{12} Q_i \tag{4.18}$$

where  $Q_i$  is the monthly discharge at the  $i$ -th month.  $\theta_i$  is the angle of the corresponding month, with  $30^\circ$  in January,  $60^\circ$  in February, ...,  $360^\circ$  in December.  $Q_{i,x}$  is the decomposition of the monthly discharge in the x-axis and  $Q_x$  is the sum of all the months.  $Q_{i,y}$  and  $Q_y$  are along the y-axis.  $C_p$  is the concentration period but has been transferred to a monthly value.  $C_d$  denotes the concentration degree of the discharge.

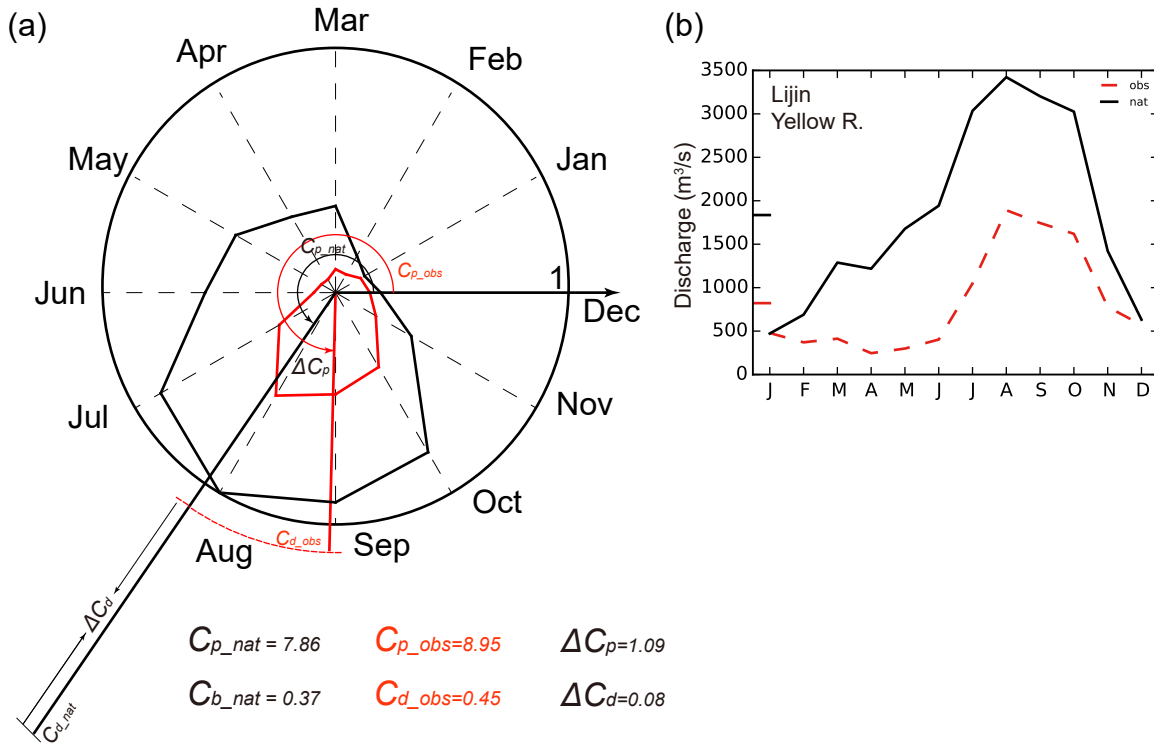


Figure 4.14 – (a) The illustration of the simulation of concentration period ( $C_p$ ) and concentration degree ( $C_d$ ). The discharge at (b) Lijin gauge in the lower Yellow River is taken as the example. The discharge has been normalized by dividing the maximum monthly value of the naturalized discharge. The  $C_d$  is enlarged in the graphic a with a ratio of  $\sum_{i=1}^{12} Q_i$  for better illustration.

The concentration period ( $C_p$ ) for the observed river discharge and the naturalized discharge, as well as their difference, are shown in Figure 4.15.  $C_p$  for the Pearl River for the naturalized river discharge (Figure 4.15-b) is mainly between 7.0 and 7.5 (early July), and there are a few gauges with  $C_p$  in June. The  $C_p$  for the northern basins are mainly located between 7.5 and 8.0 (late July). There are no significant differences between different gauges. While  $C_p$  for the observed discharge (Figure 4.15) has larger differences for the Yellow River, the lower Yellow has the latest  $C_p$  in September and a  $C_p$  for the middle Yellow is in August. The concentration period for the Hai River ranges from early June to late August. Moreover, the Hai River is where the  $C_p$  is shifted in advance by the most significant degree (1.4 months, Figure 4.15-c, Figure 4.12-g). It is caused by the dam regulation that increases the dam release in the spring but decreases the peak discharge in the flood period for water storage. The most delayed  $C_p$

occurs in the lower Yellow River (1.0 month at Lijin gauge, Figure 4.12-c) and in the middle Yellow River (0.9 months at Longmen gauge).

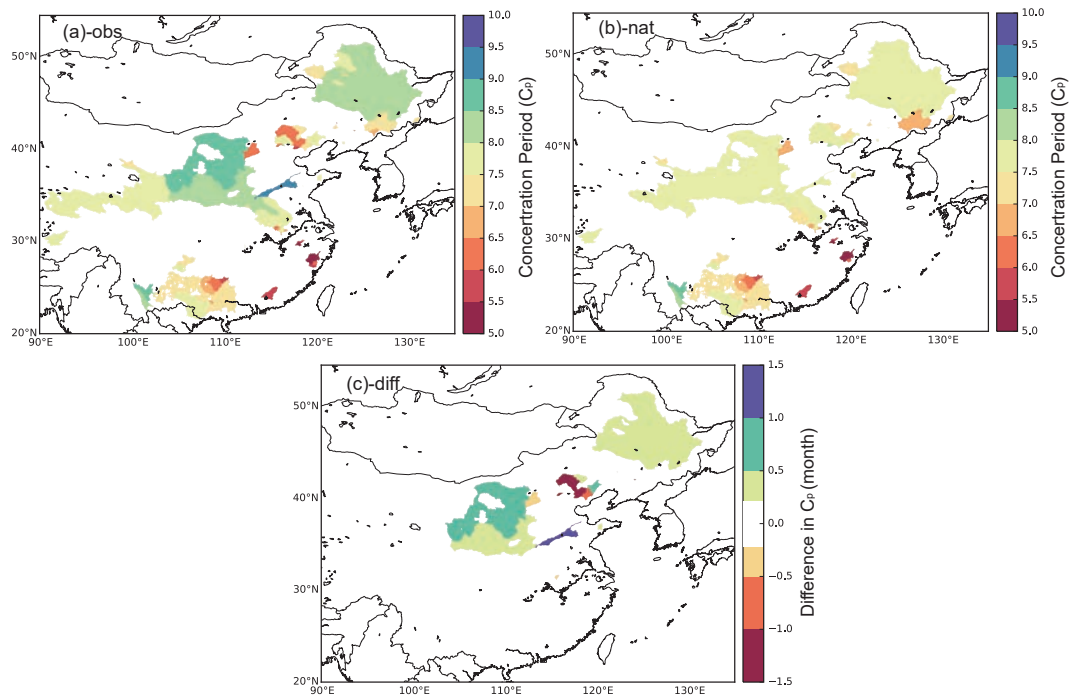


Figure 4.15 – Concentration period ( $C_p$ ) for the annual (a) observed discharge (b) naturalized discharge and (c) the  $C_p$  difference of the observed discharge from that of the naturalized discharge ( $\Delta C_p$ ). The regions with changes less than 0.25 month ( $\sim$  one week) are not shown in the subplot c.

The concentration degree ( $C_d$ ) for the observed and naturalized discharge is shown in Figure 4.16. A higher  $C_d$  represents a more concentrated discharge around the concentration period ( $C_p$ ) while a lower  $C_d$  indicates a more even distribution of the river discharge over the whole year. As shown in Figure 4.16-b,  $C_d$  for the naturalized river discharge is higher than 0.5 in the Songhua River basin and the Hai River basin. Its value is between 0.4-0.5 in the Pearl River basin, Huai River basin and the up-middle of the Yellow River basin. For the lower Yellow, the natural river discharge is more evenly distributed as the  $C_d$  is within 0.3 and 0.4. Most of the  $C_d$  decreases are for the observed river discharge which is modified by humans (Figure 4.16-c). The most significant decrease occurs in the Fengman reservoir (-0.42) in the Songhua River basin, and in the middle of the Yellow River (-0.23).  $C_d$  for these gauges has decreased among 0.1-0.2 (Figure 4.16-a, Figure 4.12-e), which means there is a very low fluctuation of the river discharge in the annual cycle after human interventions.

#### 4.4.3 Uncertainties due to limitation of knowledge on the nature

As shown in Chapter 2 and Chapter 3, there are uncertainties in different products of forcing variables because the representation of the nature variability differs from different product providers. The differences are due to our limits in knowing the natural variables. Applying the products to model simulations will further cause a shift of the model output from its real status. This shift can also be caused by applying different models which indicates

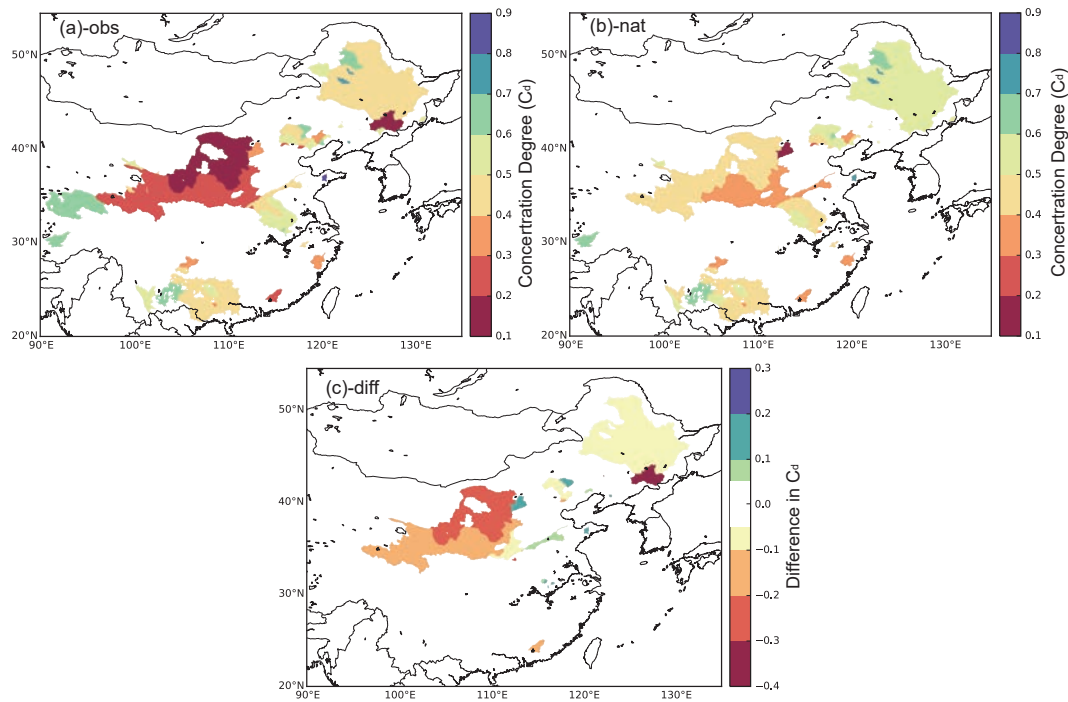


Figure 4.16 – Concentration degree ( $C_d$ ) for the annual (a) observed discharge (b) naturalized discharge and (c) the  $C_d$  difference of the observed discharge from that of the naturalized discharge ( $\Delta C_d$ ). The regions with changes less than 0.05 are not shown in the subplot c.

that our knowledge on the model processes is also limited.

However, the shift due to the knowledge limitation can not be measured directly because the real status is unknown. The alternative way is to compare the differences between descriptions on the same objects from independent sources. The larger the differences among different descriptions are, the more significant our limitation on the knowledge of the natural variability is. On the contrary, we have good confidence if there is only very little differences between independent descriptions.

In hydrological simulations, if the difference in estimated river discharge due to limitation of knowledge on the nature is smaller or much smaller than the shift in river discharge due to human activities, the results are with high significance. The limitation will not change the assessment of human impact a lot. While on the contrary, if the difference due to limitations is larger than human impact, we cannot make sure the estimation of human impact is reliable because something we do not know has been attributed to the human impact. And the bias in human impact assessment can be higher than the human impact itself.

In this study, we use four different sets of forcing inputs (Table 4.3). Among the four forcing products, the WFDEI\_CMA and WFDEI\_CRU products are gauge-based (interpolation from gauge observations), and their spatial resolution is  $0.5^\circ$ . The ITPCAS and E2O are reanalysis products with the spatial resolution as  $0.1^\circ$  and  $0.25^\circ$ . Since the WFDEI\_CMA dataset uses the most gauges in the Chinese region, it is used as a reference. The four forcing products are used to drive ORCHIDEE to provide other variables in the water cycle (e.g. potential evapotranspiration, river discharge). The regional precipitation or the estimated variables driven by the forcing is compared with that of the WFDEI\_CMA and the differences are considered to be the difference due to our knowledge on natural variability.

Table 4.3 – The four different precipitation products used for comparing the uncertainties.

Name	Spatial resolution	Data type	Provider
WFDEI_CMA	0.5°	Gauge-based	WFDEI corrected with CMA precipitation (China Meteorological Administration)
ITPCAS	0.1°	Reanalysis product	Institute of Tibetan Plateau Research Chinese Academy of Sciences
E2O	0.25°	Reanalysis product	Earth2Observe project
WFDEI_CRU	0.5°	Gauge-based	WFDEI corrected with CRU precipitation (Climatic Research Unit)

The difference can be explained by three indicators as the same as those used for identifying the shift of river discharge due to human activities in the previous subsection. The difference in the mean value ( $\Delta\mu$ ) represents the changes in the average state, the difference in concentration period ( $\Delta C_p$ ) and concentration degree ( $\Delta C_d$ ) represent the changes in the phase of the river discharge. The comparisons between the difference due to our limitation on knowledge and the shift due to human activities are conducted for the discharge, precipitation and potential evapotranspiration, respectively.

#### 4.4.4 Results

##### Knowledge on estimated river discharge

Driven by the four sets of forcing inputs, the ORCHIDEE provides the estimations of river discharge at all the gauges for each forcing. The difference between the simulations of a certain forcing is compared to that driven by WFDEI\_CMA and shown in the y-axis in Figure 4.17. The shift of the observed discharge due to human activities on the mean value and phases is shown in the x-axis. We can find in Figure 4.17a, for most of the catchments, human consumes water and reduces the natural river discharge by a ratio ranging  $[-50\%, 0\%]$ . There are a few gauges (e.g., Hai R. and Huai R.) where human activities have reduced the natural river discharge by more than 50%. While for the concentration period ( $\Delta C_p$ , Figure 4.17b), the shift of  $\Delta C_p$  is within  $[-0.5, 0.5]$ , representing a relatively small change. While the gauges in Hai R. (●) are experiencing an advancing concentration period with  $\Delta C_p$  less than  $-0.5$ , which indicates that the water consumption ratio to the river discharge in the Hai River is higher in winter season rather than the spring or summer. It is mainly because the irrigation water usage, which mainly occurs before summer, is not dominant in the water usage for those gauges. On the contrary, the concentration period in the Yellow River (▼) is delayed with  $\Delta C_p$  larger than 0.5, indicating that the water consumption ratio is higher before the peaks, showing a higher water demand in spring and early summer, especially for irrigation. In addition, the concentration degree shows the magnitude of the even distribution of river discharge. We can find that most of the catchments show a small shift within  $[-0.1, 0.1]$ . There is a sharp decrease of  $C_d$  for Yellow River (▼) which shows the observed discharge has become flat compared to the naturalized. An increase of  $C_d$  is found for Songhua River (+), showing an increasing in its high-flow concentration because the water consumption in low-flow seasons

is higher in the ratio to river discharge. The shift of  $C_d$  for other catchments is not apparent.

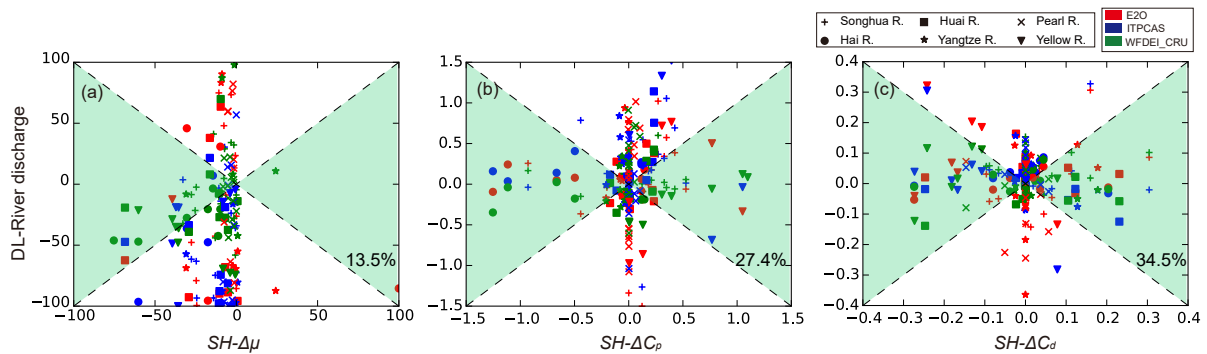


Figure 4.17 – Comparison of the shift due to human impacts on river discharge (SH) and the difference due to the limitation of knowledge on the natural variability (DL) of the estimated river discharge. The three columns indicate different human activities as the shift in the mean value- $\Delta\mu$ , in the concentration period- $\Delta C_p$  and in the concentration degree- $\Delta C_d$ . The green area represents where the DL is smaller than SH. The number in percentage represents the ratio of the points that located in the green area to the total. Different colors represent results of different forcing inputs to the reference forcing (WFDEI\_CMA) and different shapes represent different catchments. Note that the bias ( $\Delta\mu$ ) in some of the catchments has exceeded 100% so that they are not shown in the graphic.

In terms of the difference between estimated river discharge of a certain forcing to that of the reference WFDEI\_CMA (y-axis), we can find a large spread of the scatter on the mean values (Figure 4.17a). Ignoring the points that show a 100% bias, the ITPCAS underestimates the river discharge compared to that of the WFDEI\_CMA. The difference between simulations of E2O and that of the WFDEI\_CMA is also large since there are very few points showing a bias within 50%. The simulation of WFDEI\_CRU is better consistent with the results of WFDEI\_CMA than the other two forcing inputs since only the precipitation differs. The spread of the difference due to forcing difference is higher for most of the catchments and forcings (white area), especially when the shift due to human impact is relatively small. The ratio of the points that located in the green area where the DL is smaller than SH is only 13.5%, indicating the difference between estimations of river discharge driven by two different forcing inputs is larger than the shift of river discharge on mean values for most of the catchments. In which the mean value is not suggested to be used as an indicator to attribute the human impact.

In terms of the phasing, the spread of the differences in estimations is smaller for  $\Delta C_p$  and  $\Delta C_d$  than that for the mean values  $\Delta\mu$ , especially for the catchments having large shift due to human impacts (e.g., Hai River and Yellow River). Thus, for the assessment of these catchments with strong human intervention, it is sufficient to use the concentration period as the metric. However, the metric is not performing well for the regions with small human intervention (with  $\Delta C_p$  less than 0.3) as higher DL than the SH is found. The overall ratio of the points is thus increased but limited to 27.4%. The ratio is higher for the concentration degree ( $\Delta C_d$ ) as 34.5%, showing a higher possibility that the difference due to our limitation of knowledge is less than the shift due to human impact. Therefore, compared to the mean values, the concentration period and concentration degree which represent the phasing of the river discharge are better to be used to attribute the human impact. Compared to the

concentration period ( $C_p$ ), the  $C_d$  is better for catchments where the shift due to human impact is not strong, while on contrary the  $C_p$  is better for catchments where human impact has reached a strong level. The shift on the concentration degree ( $\Delta C_p$ ) has spatial features which are related to the dominant way of human water use (e.g., advancing for the Hai River, and delayed for the Yellow River). But it is not shown for the concentration degree and the mean values. Thus, we suggest that we use the concentration period ( $C_p$ ), which representing the phase of river discharge, to attribute the human impact instead of using the mean value ( $\mu$ ) and the concentration degree ( $C_d$ ).

### Knowledge on the forcing variables

Our limitation of the knowledge on the natural system (i.e., deviation of the estimated river discharge from simulations driven by different forcing) can be resulted from the forcing input or the model processes. Thus we do the same routine but compare the difference of precipitation between a certain forcing and that in the reference forcing (WFDEI\_CMA), which is shown in Figure 4.18. In general, the coverage of the catchments, where the precipitation difference is less than the shift due to human impact, is higher than that of the river discharge shown in Figure 4.17. The spread of the DL on the precipitation is also smaller than that of the river discharge, which together indicate that we have better knowledge of the precipitation than of the estimated river discharge.

The E2O precipitation has a systemic error as the mean value is generally higher than the precipitation in WFDEI\_CMA. While the systemic error is not shown apparently in the phasing metrics. The spread of the mean values are obviously higher than that for either the concentration period or the concentration degree. And the spread for the concentration degree ( $\Delta C_p$ ) is very small, especially for the regions where the human impact is higher. The comparison between Figure 4.18b and Figure 4.17b shows that we already have good knowledge to capture the phase (concentration degree) of the precipitation in different forcing products, the spread in the estimated river discharge is therefore dominated by the amplification of the models. The conclusion is relatively valid for the concentration degree but both the precipitation and the model are contributing to the spread of estimated river discharge in terms of the mean values.

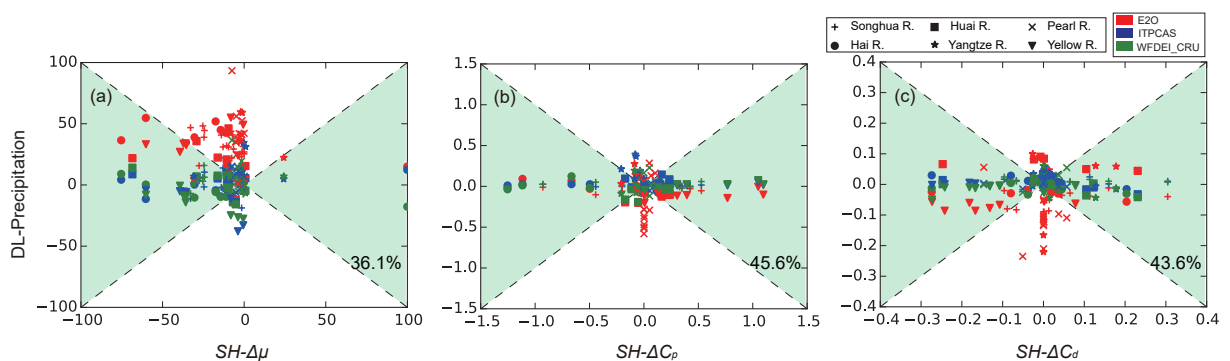


Figure 4.18 – Same as Figure 4.17, but the y-axis is represented as the differences in the precipitation between a certain forcing with the reference forcing.

The same routine is done for the potential evapotranspiration ( $PET$ ) which are shown

in Figure 4.19. The distribution of the scatter and the coverage are similar to that of the precipitation (Figure 4.18). As discussed in the Chapter 3, the estimation of  $PET$  is more related to the forcing variables except the precipitation. Thus, together with the conclusions made on the precipitation, we can conclude that, we already have good knowledge on the phasing of the forcing variables. The spread between the DL in estimated river discharge is mainly caused by the models. Therefore, there is still a need to improve the model ability to predict the phase of the discharge. Compared to the mean values, the phase ( $C_p$  and  $C_d$ ) are more suitable for attributing the human impacts. While we are limited by the ability to measure and estimate the water fluxes.

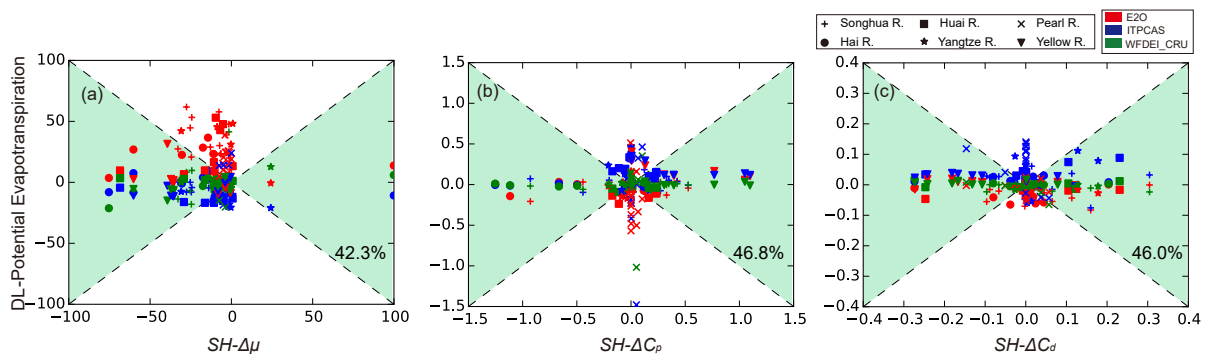


Figure 4.19 – Same as Figure 4.17, but for potential evapotranspiration.

### Catchments that are marked by three metrics

The previous discussion mainly focuses on an overall evaluation of the three metrics (mean value, concentration period, concentration degree) over all the catchments. The proportion of the catchments that met the condition, that difference due to limitation of knowledge on the natural system is smaller than the shift due to human impact, is calculated. We plot the locations of these catchments to show where the three metrics can be used for attributing the human impact.

As shown in Figure 4.20a, the catchments that met the condition are mainly the Songhua River and the mid-up stream of the Yellow River for the mean values. While the Hai River and Huai River can be remarked if concentration period is used as the metric. This is more realistic since the human water usage and its shift on the natural river discharge have been well identified for these two river basins. More catchments are identified using concentration degree compared to that identified using concentration period, and the number for the catchments is larger for concentration degree than that for the concentration period. This has been shown in the proportion of the catchments that met the condition ( $DL < SH$ ) in Figure 4.17. Though, because the spread of the concentration period ( $C_p$ ) for the precipitation and for the river discharge is smaller than that of the concentration degree ( $C_d$ ), concentration period ( $C_p$ ) is better suitable for attributing human impacts, especially for the regions that are strongly affected by human activities.

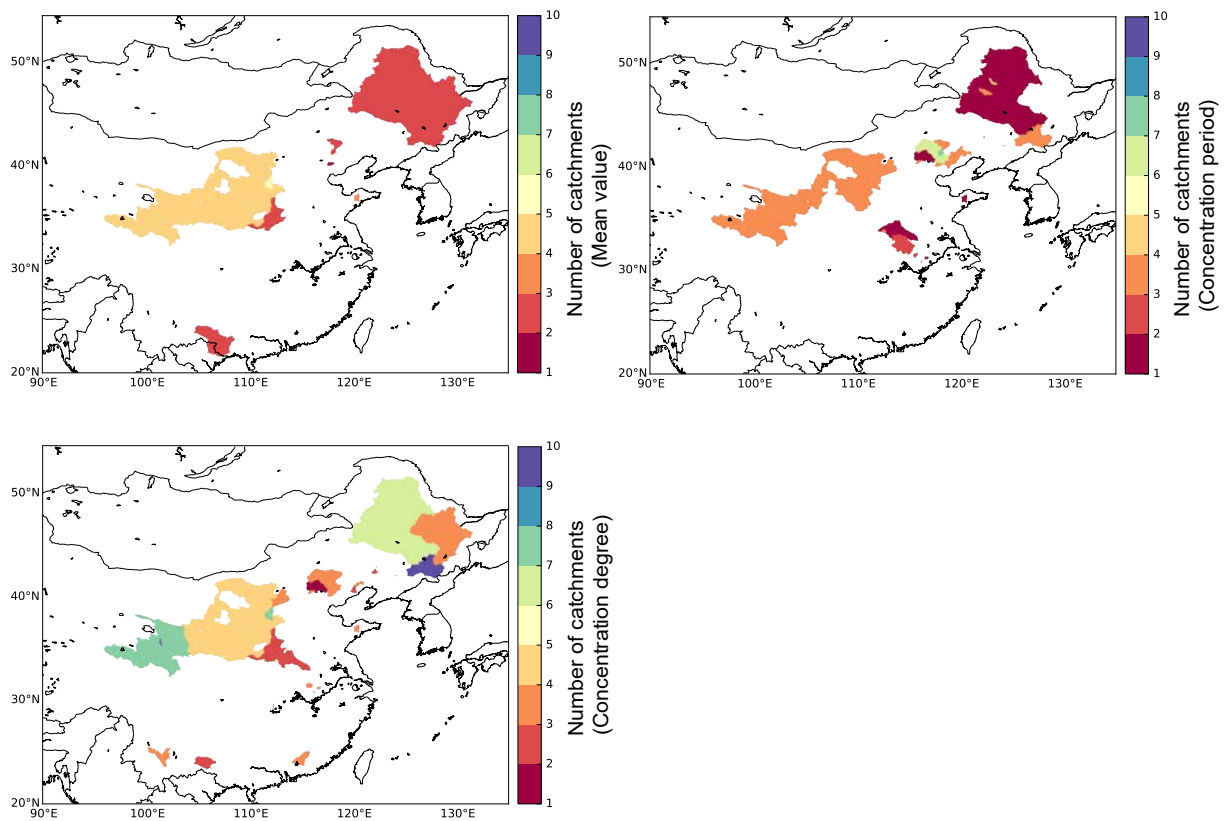


Figure 4.20 – The catchments that met the conditions that the difference due to limitation of knowledge on the natural system is smaller than the shift due to human impact in terms of (a) mean values -  $\Delta\mu$ , (b) concentration period -  $\Delta C_p$  and (c) concentration degree -  $\Delta C_d$ . The numbers indicate the total number of catchment that met the conditions in any forcing inputs.

## 4.5 Summary

Human activity has become one of the major factors that affect natural hydrological cycle in the world. It is even dominant in some basins as it significantly changes the total available water resources and the flow regimes in the annual cycle, which will further affect the agricultural, domestic and industrial sectors. Therefore, there is an urgent need to understand the roles of human activities in altering discharge and how much the impacts are in river basins.

In China, land-use change is ongoing although the rate has slowed down. The decreasing of cropland and increasing of forest and urban areas are the predicted trends in the near future. The reverse impact of significant afforestation and the impact of changes in the equilibrium vegetation cover over regions need further study. The increasing risk of city floods with rapid urbanisation also requires more investigations. The water consumption in different sectors has been stable for a decade, and more attention is needed better understanding the impact on the spatial heterogeneity over the large scale in China especially in places where the irrigation is intensively developed (e.g., the middle Yellow River, the Tarim Basin in the northwest China). The cumulative impact of the cascaded dams has received very little attention in the past, most probably because of the limit of technologies. Research has to focus on the overall impact of the huge number of dams in China in the future.

There are two groups of approaches that can quantify the human impact on the water cycle depending on whether the human impact is directly estimated. Because different human activities may take place together and interact with each other, indirect approaches have inherent difficulties to separate the impact of the individual human activity. Direct approaches with modules that particularly designed for the human activity are appropriate for such a purpose, but they need improvements in order to better describe the human intervention with interactions and at a higher spatial resolution.

The difference between the observed and the naturalized river discharge is caused by human intervention. The difference can be explained as the shift of the mean values ( $\Delta\mu$ ), concentration period ( $\Delta C_p$ ) and concentration degree ( $\Delta C_d$ ) which represent the magnitude and the phase of the river discharge. In general, the human impact is significant in northern China in the regions where agriculture is highly developed or domestic demand is high (e.g., the Yellow River basin, the Hai River basin and the northeast Songhua River basin), but the water resource is limited. The deviation of the river discharge from its reality can be also caused by the limitation of our knowledge on the natural system. The impact of the limitation is quantified as the difference between simulations driven by four different forcing inputs and is compared with the shift due to human impact on river discharge. Results show that we have better knowledge on the phasing of the forcing variables (e.g., precipitation, potential evapotranspiration) than that of the mean values. Concentration period ( $\Delta C_p$ ), representing the peak of the high-flow season, is the best suitable metric for attributing the human impact, because the spread of  $\Delta C_p$  is smaller than that of the other two metrics, especially for the catchments where human impact is higher. However, the deviation of river discharge on the phasing is mainly contributed by the models and therefore, there is still a need to improve the model ability to predict the phase of the river discharge. A larger effort is needed to improve

the ability of measuring and estimating the water fluxes either in the forcing variables or the models.



# 5

## Conclusions and perspectives

### Contents

---

<b>5.1 Conclusions</b> . . . . .	<b>122</b>
<b>5.2 Perspectives</b> . . . . .	<b>124</b>

---

This thesis focuses on the uncertainties that can affect our understanding and prediction of the regional water cycle and impact our assessment of climate change and human activities on river discharge. We reviewed the current studies about the uncertainties and developed new approaches to quantify and compare the uncertainties from different sources. Based on the results and arguments in the previous chapters, we conclude this thesis by answering a few questions (not only the scientific questions) and give our perspectives on this topic and the future work we will continue to do.

## 5.1 Conclusions

### *Why we study uncertainty?*

1. *There are many sources of uncertainties.* Three major sources of uncertainty can be identified when modeling the response of river discharge to climate change and human activities. Uncertainty exists along with measurements of the atmospheric variables and parameterisation of models that describe natural processes. These uncertainties are mainly induced because of our limitations in measurement accuracy and understanding of the real world. Uncertainties also increase when the point measurements are converted to space for model usage as interpolation approaches cannot perfectly represent the spatial heterogeneities of natural variables.
2. *Uncertainties are difficult to measure.* The uncertainties among different forcing products and models are difficult to measure since the "true" values/states of nature are not known. These uncertainties may occur together in the modeling, and the interaction increases the difficulty in attributing different uncertainties. The understanding of the physical meanings of uncertainties and associated approaches also need development to measure the uncertainty.
3. *Uncertainty analysis increases the credibility of results.* By simply using a few sets of datasets or simulations (e.g., multiple precipitation products in Chapter 2, ORCHIDEE and Budyko methods in 3, multiple model simulations with different forcing inputs in Chapter 4), the possible ranges are obtained for variables of interest. Although it is still possible that the state to meet the observations is outside of the uncertainty range, the uncertainty analysis (or sensitivity test) increases the credibility of results. Therefore, uncertainty analysis is very necessary for the studies of natural processes.

### *How significant are the uncertainties?*

1. The uncertainties and their magnitude depend on the datasets and the models used. For example, the uncertainties in the gauge-based precipitation products are smaller than that of the merged products or GCMs (Chapter 2). The uncertainty among gauge-based products is induced by the density of gauge used and the conversion of point measurement to space. While merging with other products (e.g., satellite and re-analysis data) increases the variations among different merged products. The GCMs are run without the constraints of observed data. Thus the uncertainty caused by the differences in models and initial conditions becomes large.
2. The uncertainties in the land surface model structure is probably smaller than that of the atmospheric variables in the Tarim basin (e.g., precipitation, Chapter 3). Retrospective approaches show that the precipitation and the potential evapotranspiration (associated

with atmospheric conditions) are further from the "true" state than the difference of actual evapotranspiration (associated with models) and its "true" values. The orographic effect and spatial heterogeneity of the forcing variables are the main causes of uncertainties in atmospheric variables.

3. The magnitude of the human impact on river discharge is higher in the northern river basins where there is intensive irrigated agriculture. The uncertainty caused by ignoring human water management in models is therefore larger than uncertainties in precipitation (Chapter 4). While the human impact is relatively small in other regions especially in southern China, the uncertainties in precipitation will dominate the final results. The uncertainties are higher in the mean values of the estimated river discharge or the forcing variables. While, the uncertainties for the phasing, e.g., the concentration period and concentration degree, are less than that of the water fluxes.

### ***What has been done and is useful to the research community?***

1. The thesis proposes a new three-dimensional variance partitioning approach which can estimate the variances and the uncertainty among multiple datasets (Chapter 2). The uncertainty estimation integrates variations in the original dataset, the temporal means, the spatial means and the overall means for each dataset (see equation 2.19). It uses all information across the temporal and spatial dimensions and is the first method which avoids the collapse of dimensions in assessing uncertainties among multiple datasets with temporal and spatial variations. The presented approach can be further utilized for data with three dimensions in other specific fields.
2. The thesis proposes an ORCHIDEE-Budyko framework which can be modified to assess the reliability of simulations by any other hydrological or land surface models (Chapter 3). The framework also provides an example to trace back the discharge bias to multiple uncertainty sources of the atmospheric variables and the model itself. The Budyko hypothesis is empirical but strongly associated with climatic and geographic characteristics, and therefore reference studies can be helpful for analysing the uncertainties of the study area with similar climatic or geographic features.
3. The thesis reviews the major human activities that occur in China in different time periods and over different places (Chapter 4). It helps readers find the most significant type of human impact over the area of their interest. The thesis also reviews a collection of approaches for quantifying human impact on river charge. The characteristics of these approaches and their advantages/disadvantages are discussed for easier selection by readers.
4. The thesis quantifies human impact (mainly by human water consumption and regulation) at the available gauges (84 gauges) by analyzing the difference between observed river discharge and naturalized river discharge (Chapter 4). The relative magnitude of the human impact and the deviation of estimations from the reality due to the limitation

of knowledge on the natural system are compared. Results inspire that the phasing metrics are better than the mean values to attribute the human impact. And ignoring uncertainties analysis is not appropriate for human impact assessment over those regions with a relatively small human impact (e.g., southern China).

## 5.2 Perspectives

1. *Dealing with human activities.* Human activities especially the water consumption and dam regulation are changing the natural river discharge. Although there are already a few approaches and attempts to assess the human impact, the interactions of human intervention with natural river system are cursory in modeling and need to be strengthened. The spatial resolution of atmospheric forcing is being developed (from degrees to at most  $0.1^\circ$ ), which requires corresponding adaptations to consider human interventions at a higher resolution. The adaptations which will be further discussed in my Chinese thesis (coming in six months) which mainly includes:

- *a higher resolution routing scheme.* The resolution of a routing scheme is limited mainly by forcing resolution and thus is very coarse for most of the land surface models. Also, there is not a concept of river network in those grid-to-grid routing and even in the old ORCHIDEE routing because the LSMs put more attention on the vertical water fluxes than the horizontal fluxes. Therefore, a new routing scheme will be developed based on the old ORCHIDEE routing to better define the routing units their connections and the routing strategy.
- *new strategy of locating the water use, water abstraction and dams.* The location of the water use, water abstraction and dams are simply put into a single grid without taking into account their exact locations at coarse spatial resolutions. The water is exchanged within the grid or between a few grids nearby. For models at higher spatial resolution, the locations of water use, rivers, dams become more precise, so the strategy should be improved to find reliable abstraction points from nearby water bodies (e.g., rivers, dam reservoir).
- *near-real water abstraction strategies and dam regulation rules.* The priority of various water demand (e.g., agricultural, domestic, industrial water) is different. The gross water use for different purposes can be simply summed up and distributed water to sectors from higher priority to the lower. The strategies should be improved in high-resolution models as the water demand changes with different distance to the water bodies. The distribution of water among demands from upstream to downstream should be considered, in addition to the return water. The dam regulation needs also improvement from those used for coarse resolution because the locations become more precise, the linkages become more clear, and the routing timestep is shortened. The function of dam regulation is supposed to be more important in higher-resolution modeling, since the exchanges between grids to grids are more significant in higher resolutions.

2. *Dealing with uncertainty.* There are big difficulties in a short time to improve the accuracy of all atmospheric products or the algorithms/parameters in all models. Therefore, uncertainty analysis or sensitivity test with multiple different forcing inputs and models (types or model settings) is highly recommended for studies related to the climate-hydrology modeling. In further analyzing the human impact, the sensitivity of the estimated human impact will need to be assessed to ensure the credibility of the results.





## Submitted paper II

The submitted paper to *Earth System Dynamics* is based on the same methodology introduced in Chapter 2. The main difference in this study from that presented in Chapter 2 is that this paper mainly deals with the variance (an estimation of the variations among multiple datasets) while Chapter 2 focuses on the uncertainty (the variation compared to the average means). This paper uses only the precipitation in GCMs to explain the features of the variance proportion approach. The propagation of uncertainties from atmospheric variables to the modeled land surface variables (e.g., evapotranspiration, runoff, soil moisture) are further discussed with support of the CMIP5 and GLDAS products.

# Quantifying ensemble variance across a multi-model dataset

Xudong Zhou<sup>1,2</sup>, Jan Polcher<sup>2</sup>, Tao Yang<sup>1</sup>, Ching-Sheng Huang<sup>1</sup>

<sup>1</sup>State Key Laboratory of Hydrology-Water Resources and Hydraulic Engineering, Hohai University, 210098, Nanjing, China

<sup>2</sup>Laboratoire de Météorologie Dynamique du CNRS, IPSL, École Polytechnique, 91128, Paris, France

## Abstract

Model variation indicates the reliability of ensemble results from multi-model ensemble analysis. This study develops a three-dimensional partitioning approach that is applied to quantify the model variation in hydroclimatic variables from different models in projects CMIP5 and GLDAS. Results suggest the ensemble variance ( $P_e$ ), which indicates variations in model predictions, agrees to the indication of model similarity evaluated by commonly used model performance coefficients. The contribution of forcing inputs to the variations in hydrological variables (e.g. runoff, soil moisture) is comparable to that resulted from model variations. In addition, the increasing  $P_e$  across land surface processes also indicates land surface models are inducing uncertainties to the water system in every step of hydrological simulation. With flexible structures, the present approach avoids collapse of spatial and temporal information in the analysis and is widely applicable to climate studies or environmental fields for inter-models comparisons.

## A.1 Introduction

Due to coordinated efforts from various institutions and individuals in more recent years, a wide range of datasets has been available for climatic analysis and land surface variables (e.g. General Circulation Models-GCMs, Global Land Data Assimilation Systems-GLDAS) (Meehl et al. 2007; Greve et al. 2014). Model estimations vary in space and time because of differences in their initial conditions, algorithms and parameter sets (Knutti et al. 2010; Getirana et al. 2011). Therefore, scientists prefer using multiple datasets to obtain ensemble means and reduce the dependence on a single dataset when model sensitivity is not well understood and the bias is not well addressed (Yang et al. 2011; Yang et al. 2012a; Chadwick et al. 2013). An uncertainty criterion associated with the reliability of multi-model estimations always relies on the ensemble means.

Model variation can be visualized as the uncertainty range of the results. Smaller uncertainty range infers stronger model agreement on the final ensemble means. The uncertainty range is generated at each time step by quantiles commonly regarded as 5% and 95% with sufficient models or by the standard variation with few models. This method is always taken for long-term analysis at annual scale and ignores the temporal processes and the extremes within a short time interval (e.g. monthly variability). Moreover, spatial aggregation for the target region is required in advance, leading to the loss of spatial heterogeneity information in regional analysis.

There are some performance coefficients, the algorithms of which involve temporal processes and extremes (e.g. correlation coefficient, Nash-Sutcliffe efficiency coefficient). Each coefficient cannot however evaluate the variation among multiple models because its output relies on two inputs of data series. Similar to the uncertainty range analysis, spatial aggregation is also obligatory to generate the spatial mean for regional evaluation. The difference between them is that performance coefficient gives one value for the entire period while the other generates several values at each time step.

Alternatively, model agreement can be defined as the ratio of the number of models agreeing on a certain conclusion to the total model number. For example, the IPCC applied stipplings to indicate grid boxes where more than 90% of the members agree on the sign of rainfall change while leaving as white where 66% of models do not agree on increase or decrease in rainfall (IPCC 2013, Figure SPM.8-b). This method evaluates the variation on the final conclusions but ignores the processes. It also requires a quite large number of models to generate a reliable number of the ratios, which is limited to a large number of similar inputs (e.g. GCMs). Moreover, it is always applied in grids analysis rather than regional analysis.

As concluded, the quantification of model variation is necessary in climatic analysis and there have been a few criteria proposed for this purpose. However, there is a lack of critical quantification means that prevents regional analysis from aggregation in the spatial or temporal scales. This study aims to build a new approach designed with three dimensions for quantifying variations among multiple models. The present approach is compared with commonly used performance coefficients in evaluating model similarity. The properties of the present approach are discussed by means of implementations related to climatic fluxes and hydrological variables provided by the Coupled Model Intercomparison Project Phase 5 (CMIP5) and the Global Land Data Assimilation System (GLDAS).

## A.2 Methodology

### A.2.1 Method development

The coefficient of variation (Cv) is designed to describe the data variation (Everett and Watson 1998). It works for one dimension, leading to the fact that regional aggregation is required to generate the regional mean and evaluate the temporal variation (McSweeney and Jones 2013). Scheffe (1999) introduced the grand variance that measures the total variations across time and space scales. Sun et al. (2010) partitioned the grand variance into temporal and spatial dimensions, named time variance and space variance, respectively. It can determine the dominant dimension in the analysis of data variability. For example, the space variance of global annual-average temperature is much larger than the time variance since the difference in regional temperatures (from the equator to polar) is generally greater than the difference among seasons in a specific region. Temperature difference between latitude zones is more significant than that between time steps. Their approach prevents aggregation from spatiotemporal analysis. All the spatial and temporal variation in other words remains in the analysis.

With regarding multiple models as an ensemble by analogy, the total grand variance can

expand to time variance, space variance and the third component "ensemble variance" that represents the inter-ensemble variations. The variation of the whole dataset is therefore related to not only the spatial or temporal variation but also the variations among different models. For climatic variables, the temporal and spatial variations are inherent while the ensemble variance results from the use of multiple models. With a smaller ratio of ensemble variance to the grand variance, the ensemble members are more consistent with each other, and the agreement level of the ensemble results is higher with less uncertainty. The ratio can therefore serve as an indicator of the agreement among ensemble members for regional analysis.

## A.2.2 Mathematical Derivation

The dataset has to be organized in three dimensions of (1) time with a regular time interval (e.g. monthly or annual), (2) space with regular spatial units where all the grids are re-organized in a new dimension from the original latitude-longitude grids, (3) ensemble with different ensemble members regarded as the third dimension. Thus, the dataset array can be reformed as

$$\mathbf{Z} = [z_{ijk}] \quad (\text{A.1})$$

with  $i$ -th time step (i.e.,  $i = 1, 2, \dots, m$ ),  $j$ -th grid (i.e.,  $j = 1, 2, \dots, n$ ), and  $k$ -th ensemble member or ensemble model (i.e.,  $k = 1, 2, \dots, l$ ).

We define the three dimensions as time, space and ensemble dimension and the means for these three dimensions are called temporal mean, spatial mean and ensemble mean, respectively. The corresponding variances are named time variance, space variance and ensemble variance, respectively. The grand mean ( $\mu$ ), grand variance across time, space and ensemble models ( $\sigma^2$ ) as well as the total sum of squares ( $SST$ ) are defined as.

$$\mu = \sum_{i=1}^m \sum_{j=1}^n \sum_{k=1}^l z_{ijk} / (mnl) \quad (\text{A.2})$$

$$\sigma^2 = \frac{SST}{mnl - 1} \quad (\text{A.3})$$

$$SST = \sum_{i=1}^m \sum_{j=1}^n \sum_{k=1}^l (z_{ijk} - \mu)^2 \quad (\text{A.4})$$

The derivation starts from the third ensemble dimension. For a specific  $k$ th ensemble member, the grand mean is formulated as  $\mu_{ts}[k] = \sum_{i=1}^m \sum_{j=1}^n z_{ijk} / (mn)$ , leading to the total squares rewritten as

$$SST = \sum_{i=1}^m \sum_{j=1}^n \sum_{k=1}^l (z_{ijk} - \mu_{ts}[k] + \mu_{ts}[k] - \mu)^2 \quad (\text{A.5})$$

and then expanded and rearranged as

$$\begin{aligned}
SST = & \sum_{i=1}^m \sum_{j=1}^n \sum_{k=1}^l (z_{ijk} - \mu_{ts}[k])^2 \\
& + 2 \times \sum_{k=1}^l (\mu_{ts}[k] - \mu) \underbrace{\left[ \sum_{i=1}^m \sum_{j=1}^n (z_{ijk} - \mu_{ts}[k]) \right]}_{=0} \\
& + \underbrace{\left[ \sum_{i=1}^m \sum_{j=1}^n \right]}_{=mn} \sum_{k=1}^l (\mu_{ts}[k] - \mu)^2
\end{aligned} \tag{A.6}$$

$$SST = \sum_{i=1}^m \sum_{j=1}^n \sum_{k=1}^l (z_{ijk} - \mu_{ts}[k])^2 + mn \sum_{k=1}^l (\mu_{ts}[k] - \mu)^2 \tag{A.7}$$

$$SST = (mn - 1) \sum_{k=1}^l \sigma_{ts}^2[k] + mn(l - 1)\sigma^2(\mu_{ts}) \tag{A.8}$$

Where  $\sigma^2(\mu_{ts})$  is the variance of the grand mean for each ensemble member, and  $\sigma_{ts}^2[k]$ , the grand variance in space and time for ensemble member  $k$ , can be split using the average of the space variance at each time step  $\overline{\sigma_s^2[k, :]}$  and the variance of the spatial mean  $\sigma^2(\mu_s[k, :])$ , denoted as

$$\sigma_{ts}^2[k] = \frac{m(n-1)}{mn-1} \overline{\sigma_s^2[k, :]} + \frac{n(m-1)}{mn-1} \sigma^2(\mu_s[k, :]) \tag{A.9}$$

One can refer to (Sun et al. 2010; Sun et al. 2012) or Supporting Information Text S1.1 for detailed derivations of  $\overline{\sigma_s^2[k, :]}$  and  $\sigma^2(\mu_s[k, :])$ . Similarly,  $\sigma_{ts}^2[k]$  can also be split into the average of the time variance from all regions  $\overline{\sigma_t^2[:, k]}$  and the space variance of the temporal mean  $\sigma^2(\mu_t[:, k])$ , expressed as

$$\sigma_{ts}^2[k] = \frac{n(m-1)}{mn-1} \overline{\sigma_t^2[:, k]} + \frac{m(n-1)}{mn-1} \sigma^2(\mu_t[:, k]) \tag{A.10}$$

With Eq. (A.9) and Eq. (A.10), we can have

$$\sigma_{ts}^2[k] = \frac{1}{2} \left\{ \frac{m(n-1)}{mn-1} [\sigma^2(\mu_t[:, k]) + \overline{\sigma_s^2[k, :]}] + \frac{n(m-1)}{mn-1} [\sigma^2(\mu_s[k, :]) + \overline{\sigma_t^2[:, k]}] \right\} \tag{A.11}$$

Substituting Eq. (A.11) into Eq. (A.8) results in

$$\begin{aligned}
SST = & \frac{m(n-1)}{2} \sum_{k=1}^l [\sigma^2(\mu_t[:, k]) + \overline{\sigma_s^2[k, :]}] \\
& + \frac{n(m-1)}{2} \sum_{k=1}^l [\sigma^2(\mu_s[k, :]) + \overline{\sigma_t^2[:, k]}] + mn(l - 1)\sigma^2(\mu_{ts})
\end{aligned} \tag{A.12}$$

The first term on the right-hand side of Eq. (A.12) can be transformed to:

$$\frac{m(n-1)}{2} \sum_{k=1}^l [\sigma^2(\mu_t[:, k]) + \overline{\sigma_s^2[k, :]}] = lm(n-1) \left[ \frac{\overline{\sigma_{s-t}^2} + \overline{\sigma_s^2}}{2} \right] \tag{A.13}$$

where  $\overline{\sigma_{s-t}^2}$  is the average of space variance of the temporal mean across each ensemble member,  $\overline{\sigma_s^2}$  represents the grand mean of  $\sigma_s^2$ , the grand variance across time and ensemble dimensions. Then Eq.(A.12) becomes:

$$SST = lm(n-1) \left[ \frac{\overline{\sigma_{s-t}^2} + \overline{\sigma_s^2}}{2} \right] + ln(m-1) \left[ \frac{\overline{\sigma_{t-s}^2} + \overline{\sigma_t^2}}{2} \right] + mn(l-1)\sigma_e^2(\mu_{ts}) \quad (\text{A.14})$$

where  $\overline{\sigma_{t-s}^2}$  is the average of time variance of the spatial mean across ensembles,  $\overline{\sigma_t^2}$  represents the grand mean of  $\sigma_t^2$ , the grand variance across space and ensemble dimensions.  $\sigma_e^2(\mu_{ts})$  represents the variance of the spatial-temporal means ( $\mu_{ts}$ ). Similarly, the derivation can start from any of the other two dimensions. The SSTs derived from time and space dimensions are formulated, respectively, as

$$SST = lm(n-1) \left[ \frac{\overline{\sigma_{s-e}^2} + \overline{\sigma_s^2}}{2} \right] + mn(l-1) \left[ \frac{\overline{\sigma_{e-s}^2} + \overline{\sigma_e^2}}{2} \right] + nl(m-1)\sigma_t^2(\mu_{se}) \quad (\text{A.15})$$

$$SST = nm(l-1) \left[ \frac{\overline{\sigma_{e-t}^2} + \overline{\sigma_e^2}}{2} \right] + nl(m-1) \left[ \frac{\overline{\sigma_{t-e}^2} + \overline{\sigma_t^2}}{2} \right] + ml(n-1)\sigma_s^2(\mu_{et}) \quad (\text{A.16})$$

Where each variable is defined in the Supporting Information Text S1.2. Averaging these three SSTs defined in Eqs. (A.14) - (A.16) leads to

$$\begin{aligned} SST = & \frac{nl(m-1)}{3} \left[ \frac{\overline{\sigma_{t-s}^2} + \overline{\sigma_{t-e}^2}}{2} + \overline{\sigma_t^2} + \sigma_t^2(\mu_{se}) \right] \\ & + \frac{lm(n-1)}{3} \left[ \frac{\overline{\sigma_{s-t}^2} + \overline{\sigma_{s-e}^2}}{2} + \overline{\sigma_s^2} + \sigma_s^2(\mu_{et}) \right] \\ & + \frac{mn(l-1)}{3} \left[ \frac{\overline{\sigma_{e-t}^2} + \overline{\sigma_{e-s}^2}}{2} + \overline{\sigma_e^2} + \sigma_e^2(\mu_{ts}) \right] \end{aligned} \quad (\text{A.17})$$

With the total degree of freedom ( $m \times n \times l - 1$ ), the grand variance is expressed as

$$\begin{aligned} \sigma^2 = & \underbrace{\frac{nl(m-1)}{3(mnl-1)} \left[ \frac{\overline{\sigma_{t-s}^2} + \overline{\sigma_{t-e}^2}}{2} + \overline{\sigma_t^2} + \sigma_t^2(\mu_{se}) \right]}_{V_t} \\ & + \underbrace{\frac{lm(n-1)}{3(mnl-1)} \left[ \frac{\overline{\sigma_{s-t}^2} + \overline{\sigma_{s-e}^2}}{2} + \overline{\sigma_s^2} + \sigma_s^2(\mu_{et}) \right]}_{V_s} \\ & + \underbrace{\frac{mn(l-1)}{3(mnl-1)} \left[ \frac{\overline{\sigma_{e-t}^2} + \overline{\sigma_{e-s}^2}}{2} + \overline{\sigma_e^2} + \sigma_e^2(\mu_{ts}) \right]}_{V_e} \end{aligned} \quad (\text{A.18})$$

where  $V_t$ ,  $V_s$  and  $V_e$  represent the time, space and ensemble variances, respectively. The partitions of the three dimensions are symmetrical. To facilitate the understanding of the partitioning results, a visual illustration of the present approach is shown in Figure A.1.

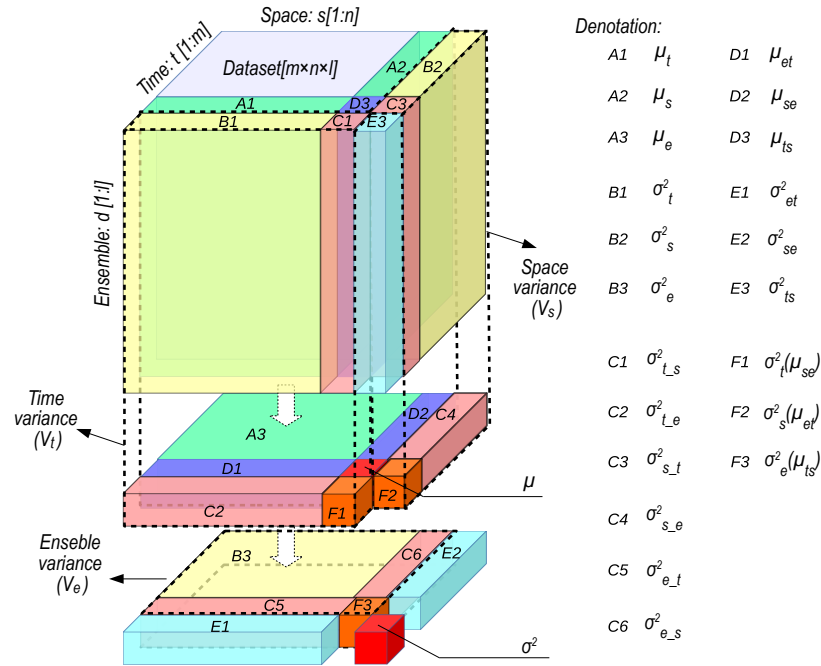


Figure A.1 – The illustration of the partitioning time-space-ensemble variance method. The original dataset is organized in three dimensions of time, space and ensemble. The denotations of the zones are listed in the right. The grand variance is defined as  $\sigma^2$  and the grand mean  $\mu$ . The subscripts  $t$ ,  $s$ , and  $e$  represent time, space and ensemble, respectively. Zone A ( $\mu_i$ ) indicates the average mean in for  $i$  dimension; zone B ( $\sigma_i^2$ ) indicates the variance for  $i$  dimension; zone C ( $\sigma_{i_j}^2$ ) indicates the variation across  $i$  dimension of the average means of  $\mu_j$ ; zone D ( $\mu_{ij}$ ) indicates the average means across  $i$  and  $j$  dimensions; zone E ( $\sigma_{ij}^2$ ) indicates the variation across  $i$  and  $j$  dimensions; zone F ( $\sigma_i^2(\mu_{jk})$ ) indicates the variation across  $i$  dimension of the average means across  $j$  and  $k$  dimensions. The detailed definitions of these denotations can be found in Supporting Information Text S1.2.

Note that  $V_e$  is based on the combination of variance across the ensemble dimension of temporal and spatial values ( $\overline{\sigma_e^2}$ , zone B3), temporal mean ( $\overline{\sigma_{e_t}^2}$ , zone C3), spatial mean ( $\overline{\sigma_{e_s}^2}$ , zone C6) and the grand variance of the spatiotemporal mean for a single ensemble member ( $\sigma_e^2(\mu_{ts})$ , zone F3). These variances rely on different zones, which displays the symmetry of the partitioning results.

To explore the relative effects of the three parts, we can quantify the contribution of each part to the total grand variance. The variance proportions are therefore defined as:  $P_t = V_t/\sigma^2$  for time;  $P_s = V_s/\sigma^2$  for space and  $P_e = V_e/\sigma^2$  for ensemble. The  $P_e$ , a measurement of the variation among models, avoids any aggregation of spatiotemporal scales.

## A.3 Model application

### A.3.1 Data and data pre-processing

Atmospheric fluxes and the land surface variables are featured with significant spatial and temporal variabilities (Chadwick et al. 2013) that are difficultly captured in models. The magnitudes of model variations vary because of different inputs and algorithms. Quantifying the variance magnitude can therefore understand how the model similarities change with different physical processes.

The Coupled Model Intercomparison Project Phase 5 (CMIP5) provides a set of outputs with coupled atmosphere-ocean general circulation models and land surface models. Among all the variables, precipitation dominates the land surface processes. We therefore investigate the variances in precipitation among 20 General Circulation Models (GCMs, Table A.1) in CMIP5 project. Each of the variables from CMIP5 (e.g. precipitation, evapotranspiration, runoff, and soil moisture) is then compared with that from the Global Land Data Assimilation System (Rodell et al. 2004, GLDAS) for examining the difference in the variances predicted by the two ensembles. All the data are interpolated to  $1^\circ \times 1^\circ$  grids using a bilinear interpolation as suggested by (Wang et al. 2012b). Thirty largest river basins calculated by TRIP (Oki and Sud 1998) are chosen (see Figure A.5 and Table A.2) for regional analysis. The total basin area accounts for 38.2% of the global land area.

### A.3.2 Partitioning ensemble variance of precipitation among GCMs

The variance partitioning adopts monthly precipitation for the historical period of 1991-2000 using 20 GCMs. The size of the space dimension is determined by the basin size at  $1^\circ$  resolution. The original spatial grids (latitude-longitude grids) are re-organized to one dimension with the spatial heterogeneity. The size of the dataset for each basin thus amounts to 120 months with a certain number of spatial units and 20 ensemble members.

The variance proportions of ensemble  $P_e$ , space  $P_s$  and time  $P_t$  for all basins are mapped in Figure A.2. In general, the  $P_e$  is not the major contribution to the grand variance as  $P_e < 0.5$ . The magnitude of  $P_e$  is relevant to local climate types as the largest values distribute in the dry basins (e.g. Sahara and South-eastern Australia). The precipitation over these basins has very low space variance (Figure A.2-b), which indicates weak spatial heterogeneity

in the precipitation compared to the variation across models. Moderate  $P_e$  (0.25-0.40) is found in north America and central Asia where the dominant climate is temperate continental. The  $P_e$  for other basins is lower in spite of different magnitudes of space variance ( $P_s$ ) and time variance ( $P_t$ ). For example,  $P_t$  is the highest for basins over eastern and northeastern Asia where there is a transition from maritime to continental climate. Similar magnitude of space variance proportion  $P_s$  or  $P_t$  is found in the south America and middle and south Africa with typical tropical climate. The  $P_s$  for the Nile river basin (No. 2) is the highest because the basin covers a wide range of climate types from tropical to dry climate. Thus, the magnitude of  $P_e$  reveals the ability of the models to reproduce the atmospheric water cycle in different climate types. The basins covering different climate types have a larger  $P_e$  than those in relatively uniform climate zones. Improving the model ability across climate types can decrease the variances among different model members and increase the applicability of GCMs for large-scale analysis.

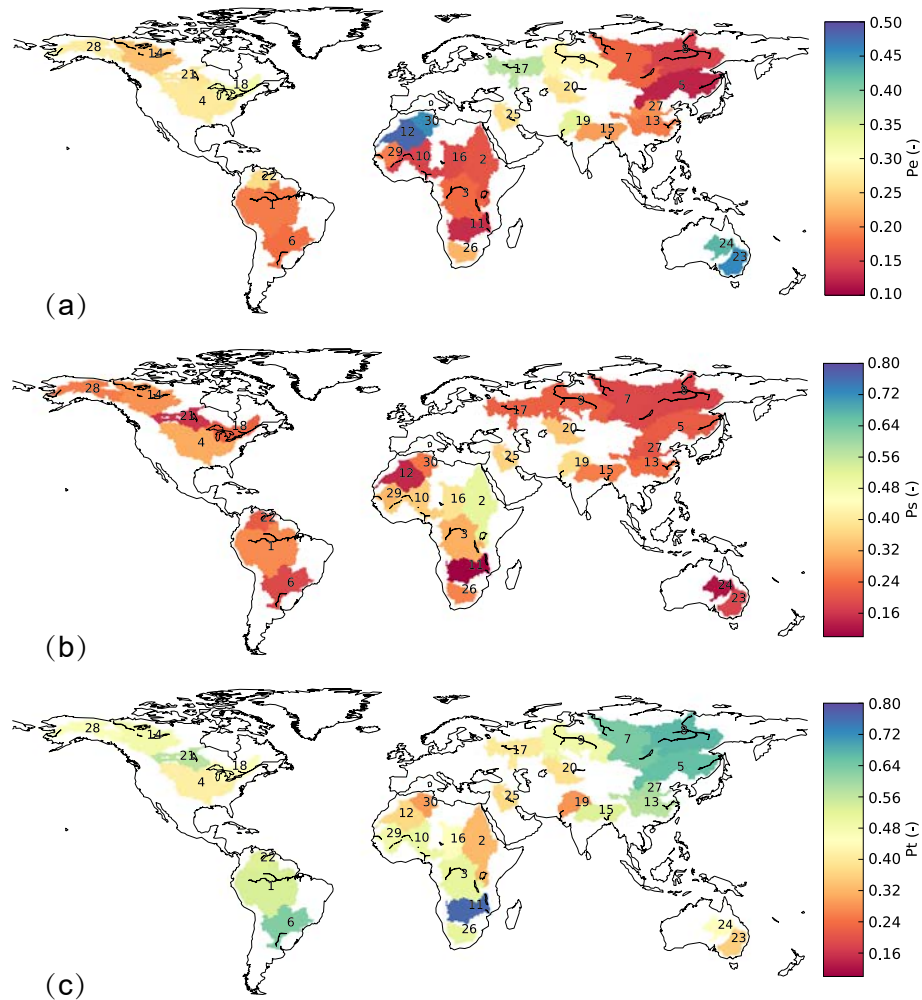


Figure A.2 – The global maps for (a) ensemble variance proportion- $P_e$ , (b) space variance proportion- $P_s$  and (c) time variance proportion- $P_t$  over the global 30 largest basins of the monthly precipitation among 20 GCMs during the period 1991-2000. The full maps of other variances and their proportions can be found in Figure A.10 of the Supporting Information.

The partitioning method is data-based; thus, the results may be affected by the dataset size. We therefore conducted sensitivity tests to the number of GCMs, the spatial resolution

and the time length of the datasets (Figure A.6-A.9). With the increasing number of GCMs,  $P_e$  increases with declining uncertainty range (Figure S2). The results for most of the basins become stable when 10 models are used, and removing one model from them leads to insignificant effect on the results (Figure S3). The increase in the spatial resolution (from  $2^\circ \times 2^\circ$  to  $0.5^\circ \times 0.5^\circ$ ) does not change the priorities of all the variances although it slightly decreases the space variance proportion  $P_s$  (Figure A.8). The change in the time length of the dataset (from 15 years to 5 years) has insignificant impacts on the results. In addition, the dataset at  $1^\circ$  resolution and 10 years can capture all the necessary features from the time and space scales.

### A.3.3 Comparison of precipitation in GCMs and GLDAS

Four land surface models (i.e., Noah, CLM, VIC and Mosaic) are integrated in GLDAS, and their precipitations are the same as these models are forced by the Global Meteorological Forcing Dataset from the Princeton University. The precipitation in GCMs is compared with the GLDAS precipitation in terms of absolute bias, correlation, Nash-Sutcliffe coefficient and the ratio of Root Mean Square Error (RMSE) to the average mean of the observations (i.e., RMSE/obs) referred to normalized RMSE (Figure A.3). Each boxplot represents the variations for each basin with different GCMs. The aggregation of the spatial means at each time step is required to calculate these coefficients.

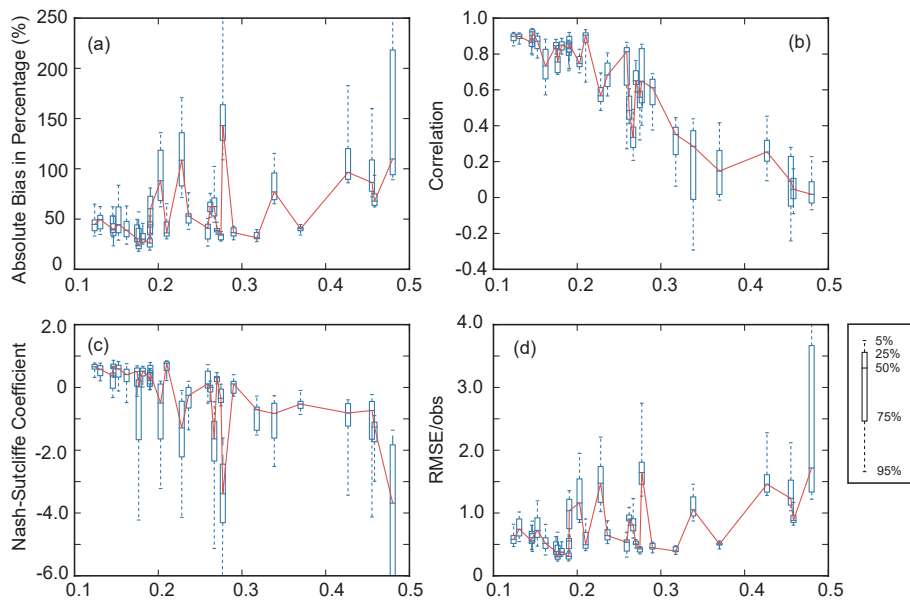


Figure A.3 – The global maps for (a) ensemble variance proportion- $P_e$ , (b) space variance proportion- $P_s$  and (c) time variance proportion- $P_t$  over the global 30 largest basins of the monthly precipitation among 20 GCMs during the period 1991-2000. The full maps of other variances and their proportions can be found in Figure A.10 of the Supporting Information.

With increasing  $P_e$ , the absolute bias increases especially when  $P_e > 0.3$ . The variation of the absolute bias for different basins also increases with  $P_e$  although the relation is not apparent for  $0.2 < P_e < 0.3$ . The change of the correlation coefficient indicates a systematic decrease of correlation with increasing  $P_e$  (Figure A.3-b). With a higher  $P_e$ , the correlation of the data between models becomes lower, indicating lower similarities and larger variations between models. The range of the correlation coefficient increases because of larger variations among basins. The median value for the Nash-Sutcliffe coefficient also decreases with increasing  $P_e$  with its maximum value around 0.8 at the minimum  $P_e$  of 0.12. Similarly, the normalized RMSE shows lower model quality with a higher  $P_e$ , indicating large variations among the whole ensemble members. In general, the model quality decreases with increasing  $P_e$  due to larger variations among GCMs. This result is applicable to other models in addition to GCMs, and a greater  $P_e$  leads to lower quality and larger uncertainty among models.

### A.3.4 Comparison of other variables between CMIP5 and GLDAS

Other than the dominant precipitation, CMIP5 provides extra variables in the water cycle although they are driven by different precipitation datasets. The variations in model outputs are partly due to the precipitation differences. With GLDAS, we can see how the variances are distributed by other processes because of the same precipitation for different GLDAS models. The variables in GLDAS and CMIP5 are progressed in the same way as the precipitation in CMIP5 for all the 30 basins.

The grand variance for the basins in GLDAS models is smaller than that of the CMIP5 because less models are used and the variance for precipitation is zero which deduces the model uncertainty for other variables. The  $P_e$  for each forcing variable is also zero as expected. The  $P_e$  for land surface variable is thus directly attributable to the land surface models, while  $P_e$  for each variable in CMIP5 is interacted by the forcing and the models.

As show in Figure A.4-a, the ensemble variance for evapotranspiration (Evap) increases from 0.06 in GLDAS to 0.32 in CMIP5 due to the forcing variations. This indicates the model diversity insignificantly affects evapotranspiration while the forcing plays more critical role in determining the evapotranspiration variations between models. The magnitudes of the variances caused by forcing and models are similar for runoff (RF,  $\sim 0.18$ ) and land soil moisture (SM,  $\sim 0.47$ ). A very large  $P_e$  is found for the soil moisture ( $\sim 0.94$ ). This is caused by the combination of the forcing difference, model variations and the different definitions of the soil moisture in the models. The depth of soil layers and their pedological characteristics vary from one model to another. In this case, soil wetness Index (SWI), normalized by the maximum and minimum soil moistures, is adopted and its ensemble variance indicates comparable spreads caused by the definitions and the forcing or model variations. Therefore, it is necessary to uniform the definition of soil moisture across models if multiple model ensembles are used.

The results also show the model is inducing variations or uncertainties in every step of the water cycle processes as the ensemble variance increases from precipitation to evapotranspiration, runoff and the soil moisture. The contribution of the forcing difference to the ensemble variances is amplified because of model variations. On the other hand, there

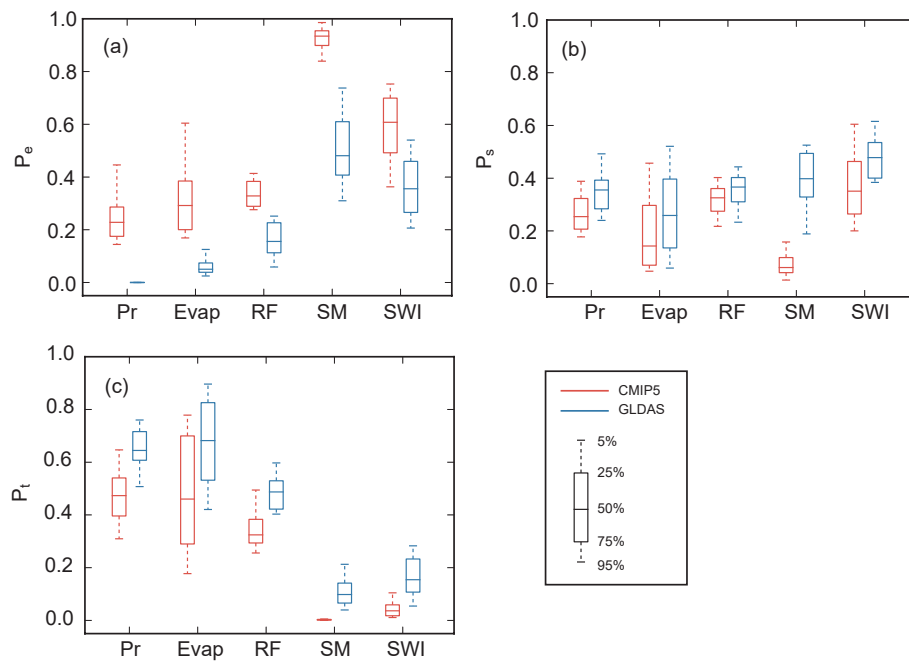


Figure A.4 – The comparisons of the variances ( $P_e$ ,  $P_s$ ,  $P_t$ ) for different variables of precipitation (Pr), evapotranspiration (Evap), runoff (RF), soil moisture (SM) and soil wetness index (SWI) provided by CMIP5 and GLDAS. The diagnose of each variance proportion is plotted as boxplot with the ranges (i.e., 5%, 25%, 75% and 95%) representing the spread of the basins.

is useful information revealed by the space variance proportion  $P_s$  and the time variance proportion  $P_t$  (Figure A.4-b and A.4-c). The runoff has a larger  $P_s$  than the precipitation and evapotranspiration, indicating the runoff generation increases the spatial heterogeneity of water distribution. The soil moisture has the largest  $P_s$  in GLDAS, indicating a more heterogeneous distribution of underground water resources. Opposite to the space variance trend among the variables, the  $P_t$  decreases after the hydrological processes. The soil moisture has the least time variation among the variables. With the comparison of the variance proportion, we can therefore conclude that the land surface processes will increase the spatial heterogeneity of water resources but act as a buffer in the time scale.

## A.4 Discussion and conclusion

This study presents a new three-dimensional partitioning approach to quantify model variation among multiple models in ensemble analysis. Compared to the two-dimensional space-time partitioning approach introduced by (Sun et al. 2010), the present approach offers a third dimension that quantifies the model variations in the spatiotemporal analysis. Moreover, our approach can reduce to a two-dimensional approach when one of the three dimensions is set to an identical unit. The previous approach for grid-based analysis is therefore the special case of ours. The superiority of the present approach is to consider all information across time, space and ensemble dimensions and to avoid aggregation of spatial or temporal variation which is vital information for climatic analysis (Giorgi and Francisco 2000). It is particularly applicable to regional studies (e.g. river basins, climatic zones or nations). The deterministic

variance proportion  $P_e$  is proposed for quantifying the variations among multiple models for all the grids and the whole time period, preventing decision making from a large number of coefficients at all the grids.

The present approach is tested with monthly precipitation among 20 GCMs. The findings suggest the ensemble variance proportion  $P_e$  is closely related to climate types. The  $P_e$  is higher in dry zones with temperate continental climate while it is lower in the area controlled by maritime climate. The comparison of precipitations estimated by the GCMs and the GLDAS shows  $P_e$  is highly correlated with model performance coefficients (e.g. correlation and Nash-Sutcliffe coefficient). A higher  $P_e$  agrees to the degradation of model similarity (lower correlation and lower Nash-Sutcliffe coefficient). Further application of the present approach to the land surface models demonstrates the model is inducing uncertainties to the water system in every step of the hydrological process. The ensemble variance due to GCMs forcing is comparable to that caused by the model variations. In order to obtain more reliable ensemble model results, future research should be alerted to the forcing bias in water cycle simulation.

The present approach has a flexible structure that potentially deals with different problems from global to regional scale. The time dimension can consider intervals from daily analysis to monthly, annual or decadal analysis which corresponds to climate change scopes. The ensemble dimension is applicable from 2 members (i.e., model evaluation between simulations and observations) to any number of multi-models (consensus evaluation, McSweeney and Jones 2013; Tebaldi et al. 2011). The present approach is applicable to any variables that are organized in the three dimensions such as climatic variables (e.g. temperature, evaporation), hydrological variables (e.g. soil moisture, runoff) or environmental variables (e.g. drought index). Based on these advantages, the three-dimensional partitioning approach can widely be applied in hydroclimatic analysis.

### Acknowledgements

The work was jointly supported by grants from the National Natural Science Foundation of China (41561134016, 51879068), National Key Research and Development Program (2018YFC0407900), and the CHINA-TREND-STREAM French national project (ANR Grant No. ANR-15-CE01-00L1-0L). We acknowledge the World Climate Research Programme's Working Group on Coupled Modelling, which is responsible for CMIP, and we thank the climate modelling groups (listed in Table A.1 of the Supplementary Information) for producing and making available their model outputs. The GLDAS LSM data used were acquired as part of the mission of NASA's Earth Science Division and archived and distributed by the Goddard Earth Sciences (GES) Data and Information Services Center (DISC). This work was supported by computing resource of the IPSL ClimServ cluster at École Polytechnique, France.

## Supplementary materials

In this chapter, the supporting information has included the necessary details about the equations and the definitions of different variables.

### S1.1 Model description

The derivation method here is similar to the work of (Sun et al. 2010) rather than the definition of variables. For a specific dataset  $k$ , the grand mean  $\mu_{ts}$  through space-time scale is

$$\mu_{ts}[k] = \frac{1}{m \times n} \sum_{i=1}^m \sum_{j=1}^n z_{ijk} \quad (\text{A.19})$$

The total squares for difference from the grand mean is

$$SST[k] = \sum_{i=1}^m \sum_{j=1}^n (z_{ijk} - \mu_{ts}[k])^2 \quad (\text{A.20})$$

while the grand variance  $\sigma_{ts}^2$  is

$$\sigma_{ts}^2[k] = \frac{1}{m \times n - 1} \sum_{i=1}^m \sum_{j=1}^n (z_{ijk} - \mu_{ts}[k])^2 \quad (\text{A.21})$$

If the derivation is started from spatial scale, equation A.20 can be rewritten by incorporating the spatial mean of each time step  $\mu_s[k, i] = \sum_{j=1}^n z_{ijk} / n$

$$SST[k] = \sum_{i=1}^m \sum_{j=1}^n (z_{ijk} - \mu_s[k, i] + \mu_s[k, i] - \mu_{ts}[k])^2 \quad (\text{A.22})$$

It can be expanded and then rearranged as

$$\begin{aligned} SST[k] &= \sum_{i=1}^m \sum_{j=1}^n (Z_{ijk} - \mu_s[k, i])^2 \\ &+ 2 \times \sum_{i=1}^m (\mu_s[k, i] - \mu_{ts}[k]) \times \underbrace{\left[ \sum_{j=1}^n (Z_{ijk} - \mu_s[k, i]) \right]}_{=0} \\ &+ \underbrace{\left[ \sum_{j=1}^n \right]}_{=n} \sum_{i=1}^m (\mu_s[k, i] - \mu_{ts}[k])^2 \end{aligned} \quad (\text{A.23})$$

$$SST[k] = \sum_{i=1}^m \sum_{j=1}^n (Z_{ijk} - \mu_s[k, i])^2 + n \sum_{i=1}^m (\mu_s[k, i] - \mu_{ts}[k])^2 \quad (\text{A.24})$$

$$\begin{aligned} SST[k] &= (n-1) \sum_{i=1}^m \sigma_s^2[k, i] + n(m-1) \sigma^2(\mu_s[k, :]) \\ &= (n-1) \overline{\sigma_s^2[k, :]} + n(m-1) \sigma^2(\mu_s[k, :]) \end{aligned} \quad (\text{A.25})$$

$$\sigma_{ts}^2[k] = \frac{m(n-1)}{mn-1} \overline{\sigma_s^2[k, :]} + \frac{n(m-1)}{mn-1} \sigma^2(\mu_s[k, :]) \quad (\text{A.26})$$

Here  $\overline{\sigma_s^2[k, :]}$  is the average of the spacial variance at each time step and  $\sigma^2(\mu_s[k, :])$  is the variance of the spatial mean. Or, the grand variance can be split using the average of the temporal variance from all regions  $\sigma_t^2[:, k]$  and the spatial variance of the temporal mean  $\sigma^2(\mu_t[:, k])$  if we started from temporal scale.

$$\sigma_{ts}^2[k] = \frac{n(m-1)}{mn-1} \overline{\sigma_t^2[:, k]} + \frac{m(n-1)}{mn-1} \sigma^2(\mu_t[:, k]) \quad (\text{A.27})$$

The equation A.26 and A.27 are used in the formal paper as equation 8 and 9.

## S1.2 Definition of the variables

Zone A:

A1:

$$\mu_t[s, e; n \times l]; \mu_t[j, k] = \frac{1}{m} \sum_{i=1}^l z_{ijk}$$

A2:

$$\mu_s[e, t; l \times m]; \mu_s[k, i] = \frac{1}{n} \sum_{j=1}^l z_{ijk}$$

A3:

$$\mu_e[t, s; m \times n]; \mu_e[i, j] = \frac{1}{l} \sum_{k=1}^l z_{ijk}$$

Zone B:

B1:

$$\sigma_t^2[s, e; n \times l]; \sigma_t^2[j, k] = \frac{1}{m-1} \sum_{i=1}^l (z_{ijk} - \mu_t[j, k])^2$$

B2:

$$\sigma_s^2[e, t; l \times m]; \sigma_s^2[k, i] = \frac{1}{n-1} \sum_{j=1}^l (z_{ijk} - \mu_s[k, i])^2$$

B3:

$$\sigma_e^2[t, s; m \times n]; \sigma_e^2[i, j] = \frac{1}{l-1} \sum_{k=1}^l (z_{ijk} - \mu_e[i, j])^2$$

Zone C:

C1:

$$\sigma_{t_s}^2[e; l]; \sigma_{t_s}^2[k] = \sigma^2(\mu_s[k, :])$$

C2:

$$\sigma_{t_e}^2[s; n]; \sigma_{t_e}^2[j] = \sigma^2(\mu_e[:, j])$$

C3:

$$\sigma_{s_t}^2[e; l]; \sigma_{s_t}^2[k] = \sigma^2(\mu_t[:, k])$$

C4:

$$\sigma_{s_e}^2[t; m]; \sigma_{s_e}^2[i] = \sigma^2(\mu_e[i, :])$$

C5:

$$\sigma_{e_t}^2[s; n]; \sigma_{e_t}^2[j] = \sigma^2(\mu_t[j, :])$$

C6:

$$\sigma_{e_s}^2[t; m]; \sigma_{e_s}^2[i] = \sigma^2(\mu_s[:, i])$$

Zone D:

D1:

$$\mu_{et}[s; n]; \mu_{et}[j] = \frac{1}{l \times m} \sum_{k=1}^l \sum_{i=1}^m z_{ijk}$$

D2:

$$\mu_{se}[t; m]; \mu_{se}[i] = \frac{1}{n \times l} \sum_{j=1}^n \sum_{k=1}^l z_{ijk}$$

D3:

$$\mu_{ts}[e; k]; \mu_{ts}[k] = \frac{1}{m \times n} \sum_{i=1}^m \sum_{j=1}^n z_{ijk}$$

Zone E:

E1:

$$\sigma_{et}^2[s; n]; \sigma_{et}^2[j] = \frac{1}{l \times m - 1} \sum_{k=1}^l \sum_{i=1}^m (z_{ijk} - \mu_{et}[j])^2$$

E2:

$$\sigma_{se}^2[t; m]; \sigma_{se}^2[i] = \frac{1}{n \times l - 1} \sum_{j=1}^n \sum_{k=1}^l (z_{ijk} - \mu_{se}[i])^2$$

E3:

$$\sigma_{ts}^2[e; l]; \sigma_{st}^2[k] = \frac{1}{m \times n - 1} \sum_{i=1}^m \sum_{j=1}^n (z_{ijk} - \mu_{ts}[k])^2$$

Zone F:

F1:

$$\sigma_t^2(\mu_{se}) = \frac{1}{m-1} \sum_{i=1}^m \left( \frac{1}{n \times l} \sum_{j=1}^n \sum_{k=1}^l z_{ijk} - \frac{1}{m} \sum_{i=1}^m \left( \frac{1}{n \times l} \sum_{j=1}^n \sum_{k=1}^l z_{ijk} \right) \right)^2$$

F2:

$$\sigma_s^2(\mu_{et}) = \frac{1}{n-1} \sum_{j=1}^n \left( \frac{1}{l \times m} \sum_{k=1}^l \sum_{i=1}^m z_{ijk} - \frac{1}{n} \sum_{j=1}^n \left( \frac{1}{l \times m} \sum_{k=1}^l \sum_{i=1}^m z_{ijk} \right) \right)^2$$

F3:

$$\sigma_e^2(\mu_{ts}) = \frac{1}{l-1} \sum_{k=1}^l \left( \frac{1}{m \times n} \sum_{i=1}^m \sum_{j=1}^n z_{ijk} - \frac{1}{l} \sum_{k=1}^l \left( \frac{1}{m \times n} \sum_{i=1}^m \sum_{j=1}^n z_{ijk} \right) \right)^2$$

### S1.3 Coefficient estimation

The equations for estimating the model performance coefficients in subsection A.3.3 and Figure A.3 in manuscript are listed here. Aggregation in the space dimension is necessary for conducting the estimations.

$$P1_k[i] = \sum_{j=1}^n P_k[i, j] \quad (\text{A.28})$$

$$P2[i] = \sum_{j=1}^n P_{GLDAS}[i, j] \quad (\text{A.29})$$

Where  $P_k[i, j]$  denote the precipitation value of the  $k$ -th GCM model precipitation at time step  $i$  and space unit  $j$ ,  $P1_k[i]$  denotes the spatial mean at time step  $i$ ,  $P_{GLDAS}$  denotes the GLDAS precipitation at time step  $i$  and space unit  $j$ ,  $P2[i]$  denotes the spatial mean at time step  $i$ .

The coefficients of the precipitation in the  $k$ -th GCM model and GLDAS are therefore estimated as

The absolute bias in percentage:

$$PAB_k = \left( 1 - \frac{\sum_{i=1}^m P1_k[i]}{\sum_{i=1}^m P2[i]} \right) \times 100\% \quad (\text{A.30})$$

The correlation coefficient:

$$COR_k = \frac{m \sum_{i=1}^m (P1_k[i] \times P2[i]) - \sum_{i=1}^m P1_k[i] \times \sum_{i=1}^m P2[i]}{\sqrt{m \sum_{i=1}^m P1_k[i]^2 - (\sum_{i=1}^m P1_k[i])^2} \sqrt{m \sum_{i=1}^m P2[i]^2 - (\sum_{i=1}^m P2[i])^2}} \quad (\text{A.31})$$

The Nash-Sutcliffe Efficiency coefficient:

$$NSE_k = 1 - \frac{\sum_{i=1}^m (P1_k[i] - P2[i])^2}{\sum_{i=1}^m (P2[i] - \overline{P2[i]})^2} \quad (\text{A.32})$$

The Normalized RMSE:

$$NRMSE_k = \frac{\sqrt{\frac{1}{m} \sum_{i=1}^m (P1_k[i] - P2[i])^2}}{\overline{P2[i]}} \quad (\text{A.33})$$

## Supplementary figures

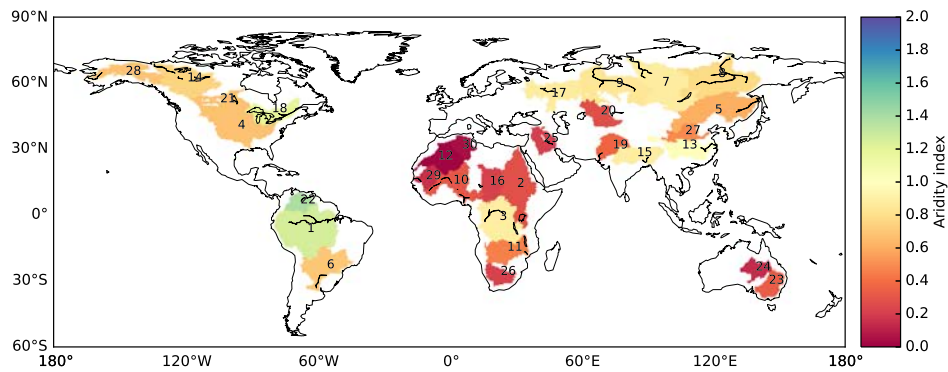


Figure A.5 – The global 30 largest regions with their regional average Aridity index.

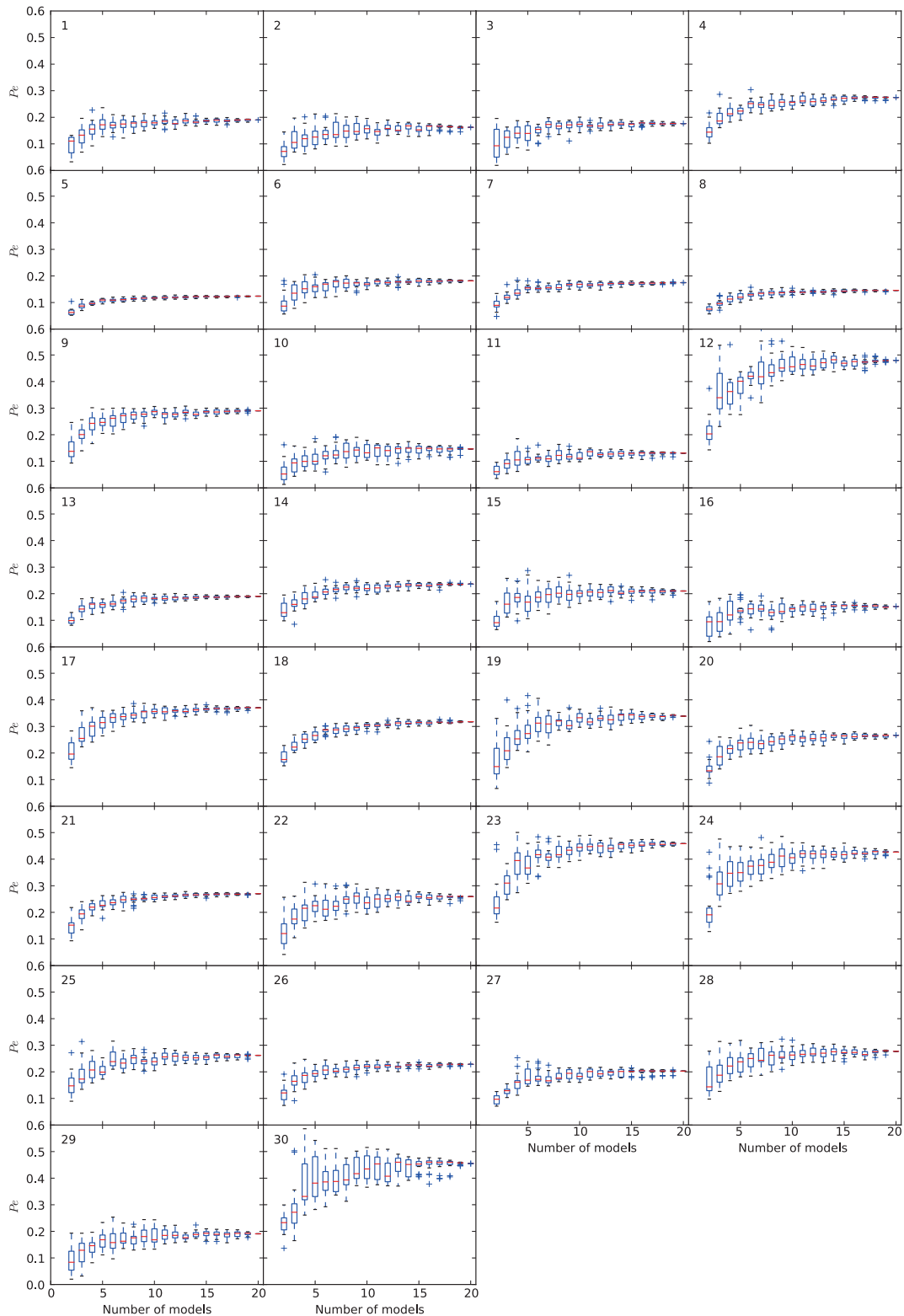


Figure A.6 – The sensitivity test of the number of selected models. At each number  $N$  ( $2 \geq N \leq 20$ ),  $N$  models are randomly selected out from the total 20 models for 40 times. The range (5% to 95%) of the variance estimation is plotted as boxplot with the mean value as the red line.

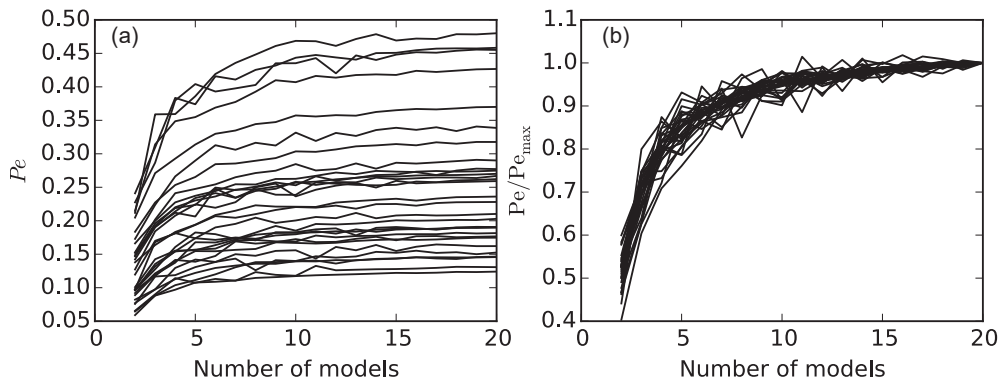


Figure A.7 – (a) The collection of the mean value for the  $P_e$  over the 30 basins in the sensitivity test. (b) Same as (a), while the  $P_e$  is divided by the maximum  $P_e$  which is the value with 20 models.

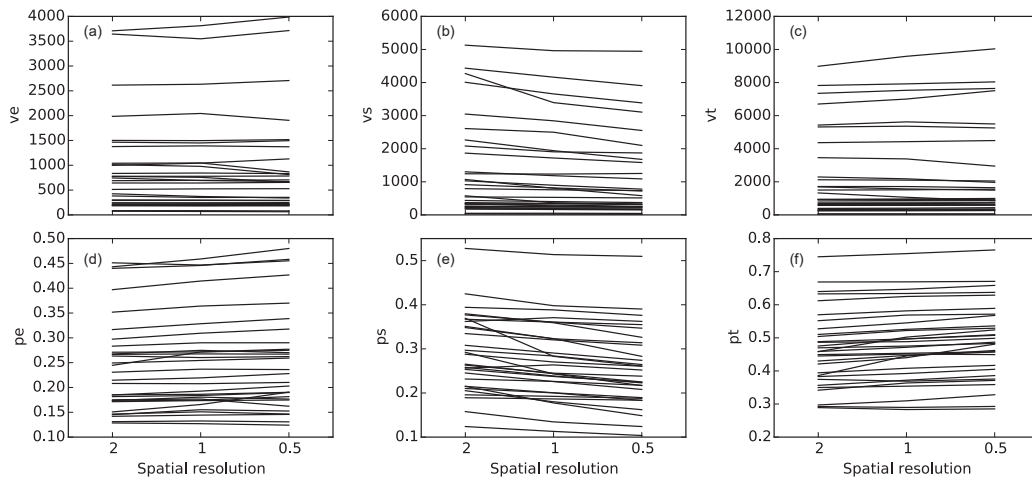


Figure A.8 – The changes of different variances and proportions for all the basins at different spatial resolution of  $2^\circ \times 2^\circ$ ,  $1^\circ \times 1^\circ$  and  $0.5^\circ \times 0.5^\circ$ .

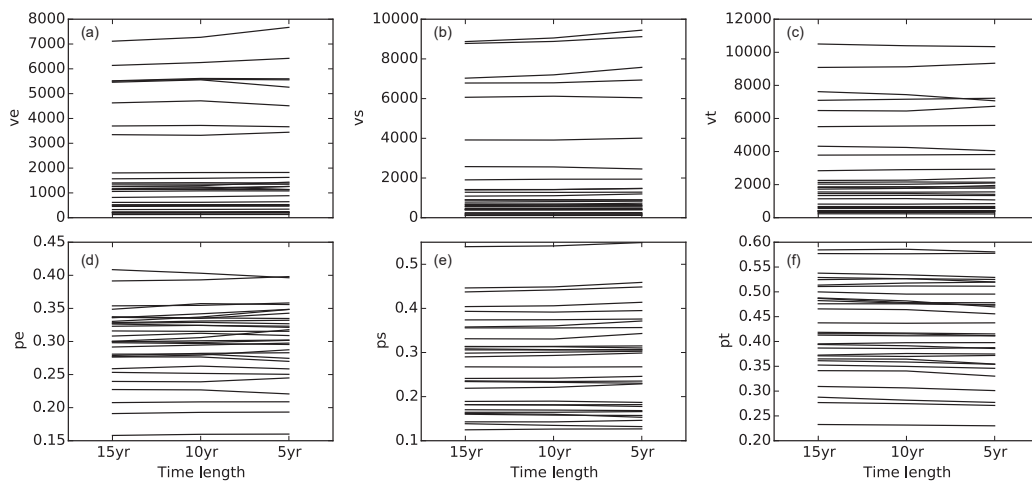


Figure A.9 – The changes of different variances and proportions for all the basins with different time length for 15 years, 10 years and 5 years.

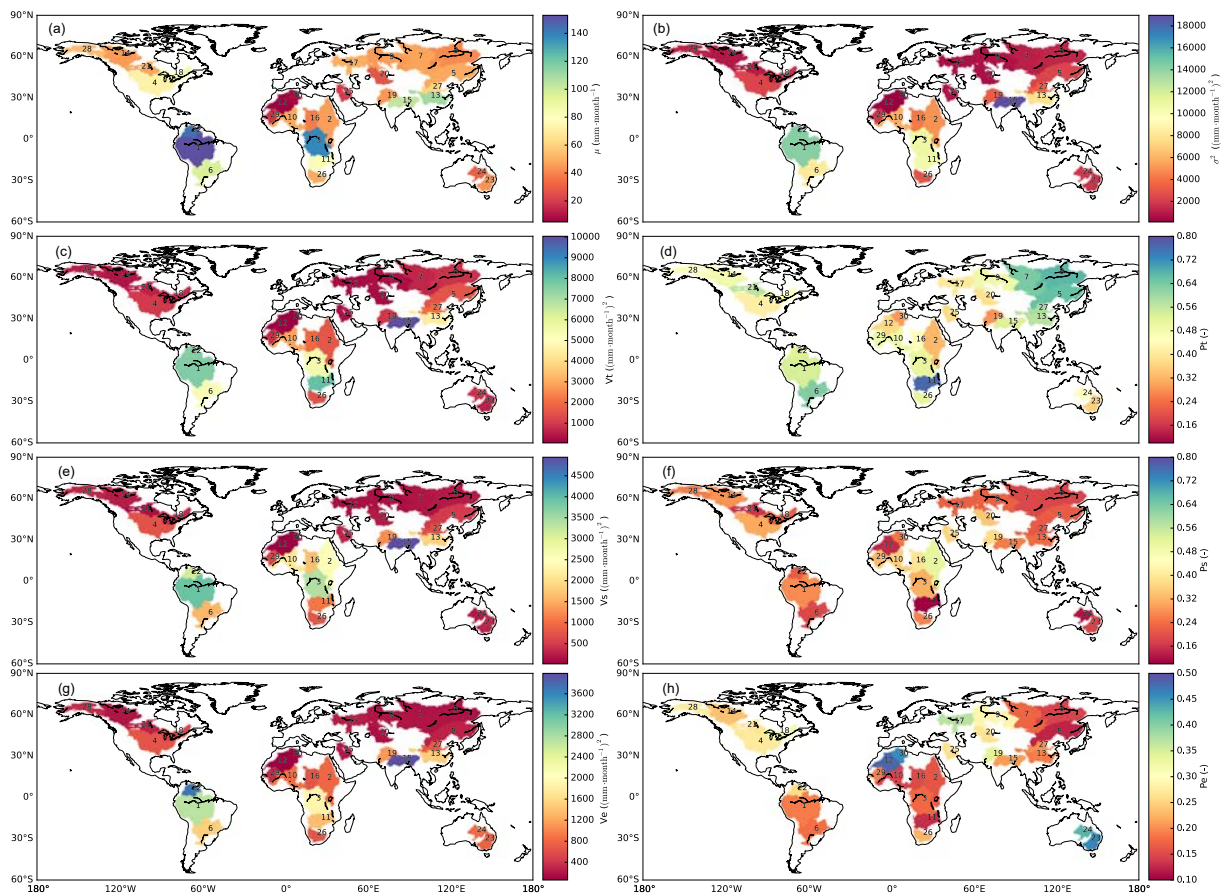


Figure A.10 – The global map for (a) grand mean- $\mu$ , (b) grand variance- $\sigma^2$ , (c) the time variance- $V_t$ , (d) the time variance proportion- $P_t$ , (e) the space variance- $V_s$ , (f) the space variance proportion- $P_s$ , (g) the ensemble variance- $V_e$  and (h) the ensemble variance proportion- $P_e$  for the selected 30 largest basins in the historical period (1991-2000).

Table A.1 – The general circulation climate models (GCM) and the descriptions used in the manuscript.

No.	GCM Name	Latitude resolution	Longitude resolution	Institution
1	CMCC-CESM	3.75	3.75	Centro Euro-Mediterraneo per i Cambiamenti Climatici,
2	CMCC-CM	0.75	0.75	Bologna, Italy
3	CMCC-CMS	1.875	1.875	
4	CNRM-CM5	1.4063	1.4063	Centre National de Recherches Météorologiques, Toulouse, France
5	CNRM-CM5-2			
6	FGOALS-g2	2.828	3.0	Institute of Atmospheric Physics, Chinese Academy of Sciences, Beijing, China
7	HadCM3	3.75	2.5	Met Office Hadley Centre, Devon, UK
8	HadGEM2-CC	1.875	1.25	
9	HadGEM2-ES	1.875	1.25	
10	inmcm4	2	1.5	Institute for Numerical Mathematics, Moscow, Russia
11	IPSL-CM5A-LR	1.8750	3.75	Institut Pierre-Simon Laplace, Paris, France
12	IPSL-CM5A-MR	2.5	1.25	
13	IPSL-CM5B-LR	1.8750	3.75	
14	MIROC4h	0.5625	0.5625	AORI (Atmosphere and Ocean Research Institute, The University of Tokyo, Chiba, Japan), NIES (National Institute for Environmental Studies, Ibaraki, Japan), and JAMSTEC (Japan Agency for Marine-Earth Science and Technology, Kanagawa, Japan)
15	MIROC5	0.5625	0.5625	
16	MIROC-ESM-CHEM	2.8125	2.8125	
17	MIROC-ESM	2.8125	2.8125	
18	MPI-ESM-LR	1.8750	1.8750	
19	MPI-ESM-MR			
20	MPI-ESM-P			

Table A.2 – The information for the global largest 30 rivers with their rank, name, upstream area and regional aridity index. The basins are sorted by their upstream area.

No	River name	Area (10 <sup>3</sup> km <sup>2</sup> )	Aridity index
1	Amazon	5852	1.25
2	Nile	3825	0.29
3	Zaire	3697	0.89
4	Mississippi	3202	0.68
5	Amur	2902	0.61
6	Parana	2658	0.71
7	Yenisei	2581	0.88
8	Lena	2417	0.78
9	Ob	2312	0.85
10	Niger	2239	0.32
11	Zambezi	1988	0.46
12	Sahara	1818	0.02
13	Yangtze	1794	1.01
14	Mackenzie	1712	0.75
15	Ganges	1628	0.90
16	Chari	1571	0.22
17	Volga	1454	0.88
18	Great lakes	1240	1.18
19	Indus	1143	0.37
20	Syr-Darya	1070	0.28
21	Nelson	1047	0.68
22	Orinoco	1039	1.38
23	Murray	1031	0.34
24	Great Artesian	977	0.14
25	Shatt al-Arab	967	0.21
26	Orange	943	0.22
27	Yellow	893	0.50
28	Yukon	852	0.69
29	Senegal	847	0.16
30	Chott_Jerid	842	0.05



# B

## List of abbreviations

---

LMD	Laboratoire de Météorologie Dynamique
CNRM	Centre National de Recherches Météorologiques
CEH	Centre for Ecology & Hydrology
LSCE	Le Laboratoire des Sciences du Climat et de l'Environnement
HHU	Hohai University
CMA	China Meteorological Administration
CMCC	Canadian Memorial Chiropractic College
CMIP5	Coupled model intercomparison project phase 5
CRU	Climatic Research Unit
E2O	Earth2Observe
ERA-I	ERA-Interim
GCM	Global Circulation Model
GPCC	Global Precipitation Climatology Centre
GPCP	Global Precipitation Climatology Project
HadCM	Hedley Centre Coupled Model Version
IPCC	Intergovernmental Panel on Climate Change
IPSL	Institut Pierre Simon Laplace
ITPCAS	Institute of Tibetan Plateau Research Chinese Academy of Sciences
LUC	Land Use Change
MIROC	Model for Interdisciplinary Research On Climate
MSWEP	Multi-Source Weighted-Ensemble Precipitation
N.s.std	Normalized spatial standard deviation
N.t.std	Normalized temporal standard deviation
ORCHIDEE	Organizing Carbon and Hydrology In Dynamic EcosystEms
RCM	Regional Circulation Model
s.std	spatial standard deviation
t.std	temporal standard deviation
UDEL	University of Delaware
VIC	Variable Infiltration Capacity
WFDEI	WATCH Forcing Data ERA-Interim
WFDEI_CMA	WFDEI corrected with CMA precipitation
WFDEI_CRU	WFDEI corrected with CRU precipitation

# Bibliography

- Adam, Jennifer C. et al. (2006). “Correction of global precipitation products for orographic effects.” *Journal of Climate* 19.1, Pages 15–38. DOI: [10.1175/JCLI3604.1](https://doi.org/10.1175/JCLI3604.1).
- Adler, Robert F. et al. (2018). “The Global Precipitation Climatology Project (GPCP) monthly analysis (New Version 2.3) and a review of 2017 global precipitation.” *Atmosphere* 9.4. DOI: [10.3390/atmos9040138](https://doi.org/10.3390/atmos9040138).
- Alkama, Ramdane, Masa Kageyama, and Gilles Ramstein (2010). “Relative contributions of climate change, stomatal closure, and leaf area index changes to 20th and 21st century runoff change: A modelling approach using the Organizing Carbon and Hydrology in Dynamic Ecosystems (ORCHIDEE) land surface model.” *Journal of Geophysical Research Atmospheres* 115.17, Page D17112. DOI: [10.1029/2009JD013408](https://doi.org/10.1029/2009JD013408).
- Andermann, C., S. Bonnet, and R. Gloaguen (2011). “Evaluation of precipitation data sets along the Himalayan front.” *Geochemistry, Geophysics, Geosystems* 12.7. DOI: [10.1029/2011GC003513](https://doi.org/10.1029/2011GC003513).
- Ballio, Francesco and Alberto Guadagnini (2004). “Convergence assessment of numerical Monte Carlo simulations in groundwater hydrology.” *Water Resources Research* 40.4, Pages 1–5. DOI: [10.1029/2003WR002876](https://doi.org/10.1029/2003WR002876).
- Barella-Ortiz, A. et al. (2013). “Potential evaporation estimation through an unstressed surface-energy balance and its sensitivity to climate change.” *Hydrol. Earth Syst. Sci.* 17.11, Pages 4625–4639. DOI: [10.5194/hess-17-4625-2013](https://doi.org/10.5194/hess-17-4625-2013).
- Beck, Hylke E. et al. (2017). “Global-scale evaluation of 22 precipitation datasets using gauge observations and hydrological modeling.” *Hydrology and Earth System Sciences* 21.12, Pages 6201–6217. DOI: [10.5194/hess-21-6201-2017](https://doi.org/10.5194/hess-21-6201-2017).
- Berger, Karen Plaut and Dara Entekhabi (2001). “Basin hydrologic response relations to distributed physiographic descriptors and climate.” *Journal of Hydrology* 247.3-4, Pages 169–182. DOI: [10.1016/S0022-1694\(01\)00383-3](https://doi.org/10.1016/S0022-1694(01)00383-3).
- Berghuijs, W. R., R. A. Woods, and M. Hrachowitz (2014). “A precipitation shift from snow towards rain leads to a decrease in streamflow.” *Nature Climate Change* 4.7, Pages 583–586. DOI: [10.1038/nclimate2246](https://doi.org/10.1038/nclimate2246).
- Beven, K J and Prophecy (1993). “Reality and Uncertainty in Distributed Hydrological Modelling.” *Advances in Water Resources* 16, Pages 41–51.
- Beven, Keith and Jim Freer (2001). “Equifinality, data assimilation, and uncertainty estimation in mechanistic modelling of complex environmental systems using the GLUE methodology.” *Journal of Hydrology* 249.1-4, Pages 11–29. DOI: [10.1016/S0022-1694\(01\)00421-8](https://doi.org/10.1016/S0022-1694(01)00421-8).
- Biemans, H. et al. (2009). “Effects of Precipitation Uncertainty on Discharge Calculations for Main River Basins.” *Journal of Hydrometeorology* 10.4, Pages 1011–1025. DOI: [10.1175/2008JHM1067.1](https://doi.org/10.1175/2008JHM1067.1).
- Boike, Julia, Kurt Roth, and Pier Paul Overduin (1998). “Thermal and hydrologic dynamics of the active layer at a continuous permafrost site (Taymyr Peninsula, Siberia).” *Water Resources Research* 34.3, Pages 355–363. DOI: [10.1029/97WR03498](https://doi.org/10.1029/97WR03498).
- Cao, Shixiong et al. (2011). “Excessive reliance on afforestation in China’s arid and semi-arid regions: Lessons in ecological restoration.” *Earth-Science Reviews* 104.4, Pages 240–245. DOI: [10.1016/j.earscirev.2010.11.002](https://doi.org/10.1016/j.earscirev.2010.11.002).
- Carmona, Alejandra M. et al. (2014). “Regional patterns of interannual variability of catchment water balances across the continental U.S.: A Budyko framework.” *Water Resources Research* 50.12, Pages 9177–9193. DOI: [10.1002/2014WR016013](https://doi.org/10.1002/2014WR016013).

- Chadwick, Robin, Ian Boutle, and Gill Martin (2013). "Spatial patterns of precipitation change in CMIP5: Why the rich do not get richer in the tropics." *Journal of Climate* 26.11, Pages 3803–3822. DOI: [10.1175/JCLI-D-12-00543.1](https://doi.org/10.1175/JCLI-D-12-00543.1).
- Chang, Jianxia et al. (2016). "Dynamic changes of sediment load and water discharge in the Weihe River, China." *Environmental Earth Sciences* 75.12. DOI: [10.1007/s12665-016-5841-9](https://doi.org/10.1007/s12665-016-5841-9).
- Chazdon, Robin L. (2008). "Beyond deforestation: Restoring forests and ecosystem services on degraded lands." *Science* 320.5882, Pages 1458–1460. DOI: [10.1126/science.1155365](https://doi.org/10.1126/science.1155365).
- Chen, Jie, François P. Brissette, and Robert Leconte (2011). "Uncertainty of downscaling method in quantifying the impact of climate change on hydrology." *Journal of Hydrology* 401.3-4, Pages 190–202. DOI: [10.1016/j.jhydrol.2011.02.020](https://doi.org/10.1016/j.jhydrol.2011.02.020).
- Chen, Jing et al. (2014). "Variability and trend in the hydrology of the Yangtze River, China: Annual precipitation and runoff." *Journal of Hydrology* 513, Pages 403–412. DOI: [10.1016/j.jhydrol.2014.03.044](https://doi.org/10.1016/j.jhydrol.2014.03.044).
- Chen, Jing et al. (2016). "Changes in monthly flows in the Yangtze River, China - With special reference to the Three Gorges Dam." *Journal of Hydrology* 536, Pages 293–301. DOI: [10.1016/j.jhydrol.2016.03.008](https://doi.org/10.1016/j.jhydrol.2016.03.008).
- Chen, Shenbin, Yunfeng Liu, and Thomas Axel (2006). "Climatic change on the Tibetan Plateau: Potential evapotranspiration trends from 1961-2000." *Clim. Change* 76.3-4, Pages 291–319. DOI: [10.1007/s10584-006-9080-z](https://doi.org/10.1007/s10584-006-9080-z).
- Chen, Ya ning et al. (2007). "Effects of climate change on water resources in Tarim River Basin, Northwest China." *Journal of Environmental Sciences* 19.4, Pages 488–493. DOI: [10.1016/S1001-0742\(07\)60082-5](https://doi.org/10.1016/S1001-0742(07)60082-5).
- Chen, Ying, Youpeng Xu, and Yixing Yin (2009). "Impacts of land use change scenarios on storm-runoff generation in Xitiaoqi basin, China." *Quaternary International* 208.1-2, Pages 121–128. DOI: [10.1016/j.quaint.2008.12.014](https://doi.org/10.1016/j.quaint.2008.12.014).
- Chen, Yiping et al. (2015). "Balancing green and grain trade." *Nature Geoscience* 8.10, Pages 739–741. DOI: [10.1038/ngeo2544](https://doi.org/10.1038/ngeo2544).
- China Three Gorges Corporation (2016). *Social Report of the Three Gorges company, China*. Technical report.
- Chorley, Roger G. Barry, and Richard J (2003). *Atmosphere, Weather and Climate*. CUP Archive, Page 328. DOI: [doi:10.4324/9780203871027](https://doi.org/10.4324/9780203871027).
- Choudhury, Bhaskar J. (1999). "Evaluation of an empirical equation for annual evaporation using field observations and results from a biophysical model." *Journal of Hydrology* 216.1-2, Pages 99–110. DOI: [10.1016/S0022-1694\(98\)00293-5](https://doi.org/10.1016/S0022-1694(98)00293-5).
- Christensen, N and D P Lettenmaier (2006). "A multimodel ensemble approach to assessment of climate change impacts on the hydrology and water resources of the Colorado River Basin." *Hydrology and Earth System Sciences* 3.4, Pages 3727–3770. DOI: [10.5194/hessd-3-3727-2006](https://doi.org/10.5194/hessd-3-3727-2006).
- Clark, Martyn P. et al. (2008). "Framework for Understanding Structural Errors (FUSE): A modular framework to diagnose differences between hydrological models." *Water Resources Research* 44.12, Pages 1–14. DOI: [10.1029/2007WR006735](https://doi.org/10.1029/2007WR006735).
- CNCCP (2007). *Report of China's National Climate Change Program*. Technical report.
- Cui, Tong et al. (2018). "Assessment of the impact of climate change on flow regime at multiple temporal scales and potential ecological implications in an alpine river." *Stochastic Environmental Research and Risk Assessment* 32.6, Pages 1849–1866. DOI: [10.1007/s00477-017-1475-z](https://doi.org/10.1007/s00477-017-1475-z).
- Cui, Xuefeng et al. (2007). "Hydrological impacts of deforestation on the southeast Tibetan Plateau." *Earth Interactions* 11.15, Pages 1–18. DOI: [10.1175/ei223.1](https://doi.org/10.1175/ei223.1).
- Daly, Christopher et al. (2008). "Physiographically sensitive mapping of climatological temperature and precipitation across the conterminous United States." *Int. J. Climatol.* 28, Pages 2031–2064. DOI: [10.1002/joc.1688](https://doi.org/10.1002/joc.1688).
- Dee, D. P. et al. (2011). "The ERA-Interim reanalysis: Configuration and performance of the data assimilation system." *Quarterly Journal of the Royal Meteorological Society* 137.656, Pages 553–597. DOI: [10.1002/qj.828](https://doi.org/10.1002/qj.828).

- Deng, Xiaojun et al. (2015). "Impacts of urbanization on river systems in the Taihu Region, China." *Water (Switzerland)* 7.4, Pages 1340–1358. DOI: [10.3390/w7041340](https://doi.org/10.3390/w7041340).
- Dey, Pankaj and Ashok Mishra (2017). "Separating the impacts of climate change and human activities on streamflow: a review of methodologies and critical assumptions." *Journal of Hydrology* 548, Pages 278–290. DOI: [10.1016/j.jhydrol.2017.03.014](https://doi.org/10.1016/j.jhydrol.2017.03.014).
- Dijk, Albert I J M van and Rodney J. Keenan (2007). "Planted forests and water in perspective." *Forest Ecology and Management* 251.1-2, Pages 1–9. DOI: [10.1016/j.foreco.2007.06.010](https://doi.org/10.1016/j.foreco.2007.06.010).
- Dingman, S Lawrence (2015). *Physical hydrology, Third Edition*. Waveland press. DOI: [10.1177/030913337800200111](https://doi.org/10.1177/030913337800200111).
- Döll, P., K. Fiedler, and J. Zhang (2009). "Global-scale analysis of river flow alterations due to water withdrawals and reservoirs." *Hydrology and Earth System Sciences* 13.12, Pages 2413–2432. DOI: [10.5194/hess-13-2413-2009](https://doi.org/10.5194/hess-13-2413-2009).
- D'Orgeval, T., J. Polcher, and P. De Rosnay (2008). "Sensitivity of the West African hydrological cycle in ORCHIDEE to infiltration processes." *Hydrology and Earth System Sciences* 12.6, Pages 1387–1401. DOI: [10.5194/hess-12-1387-2008](https://doi.org/10.5194/hess-12-1387-2008).
- D'Orgeval, Tristan (2006). "Impact du changement climatique sur le cycle de l'eau en Afrique de l'Ouest : Modélisation et incertitudes, PhD thesis." Doctoral dissertation. Paris 6, Page 187.
- D'Orgeval, Tristan and J. Polcher (2008). "Impacts of precipitation events and land-use changes on West African river discharges during the years 1951-2000." *Climate Dynamics* 31.2-3, Pages 249–262. DOI: [10.1007/s00382-007-0350-x](https://doi.org/10.1007/s00382-007-0350-x).
- Du, Jinkang et al. (2012). "Assessing the effects of urbanization on annual runoff and flood events using an integrated hydrological modeling system for Qinhua River basin, China." *Journal of Hydrology* 464-465, Pages 127–139. DOI: [10.1016/j.jhydrol.2012.06.057](https://doi.org/10.1016/j.jhydrol.2012.06.057).
- Duan, Kai and Yadong Mei (2014). "Comparison of Meteorological, Hydrological and Agricultural Drought Responses to Climate Change and Uncertainty Assessment." *Water Resources Management* 28.14, Pages 5039–5054. DOI: [10.1007/s11269-014-0789-6](https://doi.org/10.1007/s11269-014-0789-6).
- Ducoudré, Nathalie I., Katia Laval, and Alain Perrier (1993). *SECHIBA, a New Set of Parameterizations of the Hydrologic Exchanges at the Land-Atmosphere Interface within the LMD Atmospheric General Circulation Model*. DOI: [10.1175/1520-0442\(1993\)006<0248:SANSOP>2.0.CO;2](https://doi.org/10.1175/1520-0442(1993)006<0248:SANSOP>2.0.CO;2).
- Duethmann, Doris et al. (2016). "Projections for headwater catchments of the Tarim River reveal glacier retreat and decreasing surface water availability but uncertainties are large." *Environmental Research Letters* 11.5, Page 054024. DOI: [10.1088/1748-9326/11/5/054024](https://doi.org/10.1088/1748-9326/11/5/054024).
- Ehsani, Nima et al. (2016). "A neural network based general reservoir operation scheme." *Stochastic Environmental Research and Risk Assessment* 30.4, Pages 1151–1166. DOI: [10.1007/s00477-015-1147-9](https://doi.org/10.1007/s00477-015-1147-9).
- El Kateb, Hany et al. (2013). "Soil erosion and surface runoff on different vegetation covers and slope gradients: A field experiment in Southern Shaanxi Province, China." *Catena* 105, Pages 1–10. DOI: [10.1016/j.catena.2012.12.012](https://doi.org/10.1016/j.catena.2012.12.012).
- Everett, Jim and John Watson (1998). "Small business failure and external risk factors." *Small Business Economics* 11.4, Pages 371–390.
- Everitt, B.S. (2013). *The Cambridge Dictionary of Statistics*. Volume 53. 9. Cambridge University Press, Pages 1689–1699. DOI: [10.1017/CB09781107415324.004](https://doi.org/10.1017/CB09781107415324.004).
- Farley, Kathleen A., Esteban G. Jobbágy, and Robert B. Jackson (2005). "Effects of afforestation on water yield: A global synthesis with implications for policy." *Global Change Biology* 11.10, Pages 1565–1576. DOI: [10.1111/j.1365-2486.2005.01011.x](https://doi.org/10.1111/j.1365-2486.2005.01011.x).
- Federer, C. A., C. Vörösmarty, and B. Fekete (1996). "Intercomparison of methods for calculating potential evaporation in regional and global water balance models." *Water Resources Research* 32.7, Pages 2315–2321. DOI: [10.1029/96WR00801](https://doi.org/10.1029/96WR00801).
- Fekete, Balázs M. et al. (2004). "Uncertainties in precipitation and their impacts on runoff estimates." *Journal of Climate* 17.2, Pages 294–304. DOI: [10.1175/1520-0442\(2004\)017<0294:UIPATI>2.0.CO;2](https://doi.org/10.1175/1520-0442(2004)017<0294:UIPATI>2.0.CO;2).

- Feng, Xiaoming et al. (2016). “The role of climatic and anthropogenic stresses on long-term runoff reduction from the Loess Plateau, China.” *Science of the Total Environment* 571, Pages 688–698. DOI: [10.1016/j.scitotenv.2016.07.038](https://doi.org/10.1016/j.scitotenv.2016.07.038).
- Fraedrich, Klaus et al. (2005). “The Planet Simulator: Towards a user friendly model.” *Meteorologische Zeitschrift* 14.3, Pages 299–304. DOI: [10.1127/0941-2948/2005/0043](https://doi.org/10.1127/0941-2948/2005/0043).
- Fu, B.P. (1981). “More on the calculation of average total evaporation (in Chinese).” *Sci. Atmos. Sin.* 5.1, Pages 23–31.
- Gao, P. et al. (2013). “Impact of climate change and anthropogenic activities on stream flow and sediment discharge in the Wei River basin, China.” *Hydrology and Earth System Sciences* 17.3, Pages 961–972. DOI: [10.5194/hess-17-961-2013](https://doi.org/10.5194/hess-17-961-2013).
- Gao, Xin et al. (2010). “Glacier runoff variation and its influence on river runoff during 1961–2006 in the Tarim River Basin, China.” *Science China Earth Sciences* 53.6, Pages 880–891. DOI: [10.1007/s11430-010-0073-4](https://doi.org/10.1007/s11430-010-0073-4).
- Gates, Lydia Dümenil, Stefan Hagemann, and Claudia Golz (2000). “Observed historical discharge data from major rivers for climate model validation.” *MPI-Report* 307.
- Gaume, Eric, Jean Pierre Villeneuve, and Michel Desbordes (1998). “Uncertainty assessment and analysis of the calibrated parameter values of an urban storm water quality model.” *Journal of Hydrology* 210.1-4, Pages 38–50. DOI: [10.1016/S0022-1694\(98\)00171-1](https://doi.org/10.1016/S0022-1694(98)00171-1).
- Gerrits, A. M.J. et al. (2009). “Analytical derivation of the Budyko curve based on rainfall characteristics and a simple evaporation model.” *Water Resources Research* 45.4, Pages 1–15. DOI: [10.1029/2008WR007308](https://doi.org/10.1029/2008WR007308).
- Gerten, Dieter et al. (2008). “Causes of change in 20th century global river discharge.” *Geophysical Research Letters* 35.20. DOI: [10.1029/2008GL035258](https://doi.org/10.1029/2008GL035258).
- Getirana, A. C V et al. (2011). “Assessment of different precipitation datasets and their impacts on the water balance of the Negro River basin.” *Journal of Hydrology* 404.3-4, Pages 304–322. DOI: [10.1016/j.jhydrol.2011.04.037](https://doi.org/10.1016/j.jhydrol.2011.04.037).
- Giorgi, Filippo and Raquel Francisco (2000). “Evaluating uncertainties in the prediction of regional climate change.” *Geophysical Research Letters* 27.9, Pages 1295–1298. DOI: [10.1029/1999GL011016](https://doi.org/10.1029/1999GL011016).
- Gouttevin, I. et al. (2012). “Multi-scale validation of a new soil freezing scheme for a land-surface model with physically-based hydrology.” *Cryosphere* 6.2, Pages 407–430. DOI: [10.5194/tc-6-407-2012](https://doi.org/10.5194/tc-6-407-2012).
- Greve, Peter et al. (2014). “Global assessment of trends in wetting and drying over land.” *Nature Geoscience* 7.10, Pages 716–721. DOI: [10.1038/ngeo2247](https://doi.org/10.1038/ngeo2247).
- Gu, Wenquan, Dongguo Shao, and Yufang Jiang (2012). “Risk Evaluation of Water Shortage in Source Area of Middle Route Project for South-to-North Water Transfer in China.” *Water Resources Management* 26.12, Pages 3479–3493. DOI: [10.1007/s11269-012-0086-1](https://doi.org/10.1007/s11269-012-0086-1).
- Guimberteau, M. et al. (2012a). “Discharge simulation in the sub-basins of the Amazon using ORCHIDEE forced by new datasets.” *Hydrology and Earth System Sciences* 16.3, Pages 911–935. DOI: [10.5194/hess-16-911-2012](https://doi.org/10.5194/hess-16-911-2012).
- Guimberteau, Matthieu et al. (2012b). “Global effect of irrigation and its impact on the onset of the Indian summer monsoon.” *Climate Dynamics* 39.6, Pages 1329–1348. DOI: [10.1007/s00382-011-1252-5](https://doi.org/10.1007/s00382-011-1252-5).
- Guo, Leicheng et al. (2018). “How have the river discharges and sediment loads changed in the Changjiang River basin downstream of the Three Gorges Dam?” *Journal of Hydrology* 560, Pages 259–274. DOI: [10.1016/j.jhydrol.2018.03.035](https://doi.org/10.1016/j.jhydrol.2018.03.035).
- Haddeland, Ingjerd (2002). “Influence of spatial resolution on simulated streamflow in a macroscale hydrologic model.” *Water Resources Research* 38.7, Pages 1–10. DOI: [10.1029/2001WR000854](https://doi.org/10.1029/2001WR000854).
- Haddeland, Ingjerd, Thomas Skaugen, and Dennis P. Lettenmaier (2006). “Anthropogenic impacts on continental surface water fluxes.” *Geophysical Research Letters* 33.8, Pages 2–5. DOI: [10.1029/2006GL026047](https://doi.org/10.1029/2006GL026047).

- Hagemann, S. et al. (2013). "Climate change impact on available water resources obtained using multiple global climate and hydrology models." *Earth System Dynamics* 4.1, Pages 129–144. doi: [10.5194/esd-4-129-2013](https://doi.org/10.5194/esd-4-129-2013).
- Hanasaki, Naota, Shinjiro Kanae, and Taikan Oki (2006). "A reservoir operation scheme for global river routing models." *Journal of Hydrology* 327.1-2, Pages 22–41. doi: [10.1016/j.jhydrol.2005.11.011](https://doi.org/10.1016/j.jhydrol.2005.11.011).
- Hanasaki, Naota et al. (2010). "An estimation of global virtual water flow and sources of water withdrawal for major crops and livestock products using a global hydrological model." *Journal of Hydrology* 384.3-4, Pages 232–244. doi: [10.1016/j.jhydrol.2009.09.028](https://doi.org/10.1016/j.jhydrol.2009.09.028).
- Hao, Zhenchun et al. (2015). "Quantitative assessment of the impacts of irrigation on surface water fluxes in the Tarim River, China." *Hydrology Research* July, nh2015215. doi: [10.2166/nh.2015.215](https://doi.org/10.2166/nh.2015.215).
- Harding, Richard et al. (2011). "WATCH: Current Knowledge of the Terrestrial Global Water Cycle." *J. Hydrometeorol.* 12.6, Pages 1149–1156. doi: [10.1175/JHM-D-11-024.1](https://doi.org/10.1175/JHM-D-11-024.1).
- Harris, I. et al. (2014). "Updated high-resolution grids of monthly climatic observations - the CRU TS3.10 Dataset." *International Journal of Climatology* 34.3, Pages 623–642. doi: [10.1002/joc.3711](https://doi.org/10.1002/joc.3711).
- Hattermann, F. F. et al. (2017). "Cross-scale intercomparison of climate change impacts simulated by regional and global hydrological models in eleven large river basins." *Climatic Change* 141.3, Pages 561–576. doi: [10.1007/s10584-016-1829-4](https://doi.org/10.1007/s10584-016-1829-4).
- Hernández, Mario R and F Francés (2014). "On the Influence of Error Model in the Good Performance of the Hydrological Model for the Right Reasons." *International Conference on Hydroinformatics*.
- Hijmans, Robert J. et al. (2005). "Very high resolution interpolated climate surfaces for global land areas." *International Journal of Climatology* 25.15, Pages 1965–1978. doi: [10.1002/joc.1276](https://doi.org/10.1002/joc.1276).
- Hirabayashi, Yukiko, Petra Döll, and Shinjiro Kanae (2010). "Global-scale modeling of glacier mass balances for water resources assessments: Glacier mass changes between 1948 and 2006." *Journal of Hydrology* 390.3-4, Pages 245–256. doi: [10.1016/j.jhydrol.2010.07.001](https://doi.org/10.1016/j.jhydrol.2010.07.001).
- Hirabayashi, Yukiko et al. (2013). "Projection of glacier mass changes under a high-emission climate scenario using the global glacier model HYOGA2." *Hydrological Research Letters* 7.1, Pages 6–11. doi: [10.3178/hr1.7.6](https://doi.org/10.3178/hr1.7.6).
- Hong, Yang et al. (2006). "Uncertainty quantification of satellite precipitation estimation and Monte Carlo assessment of the error propagation into hydrologic response." *Water Resources Research* 42.8, Pages 1–15. doi: [10.1029/2005WR004398](https://doi.org/10.1029/2005WR004398).
- Huang, Ching Sheng, Tao Yang, and Hund Der Yeh (2018). "Review of analytical models to stream depletion induced by pumping: Guide to model selection." *Journal of Hydrology* 561, Pages 277–285. doi: [10.1016/j.jhydrol.2018.04.015](https://doi.org/10.1016/j.jhydrol.2018.04.015).
- Huntington, Thomas G. (2006). "Evidence for intensification of the global water cycle: Review and synthesis." *Journal of Hydrology* 319.1-4, Pages 83–95. doi: [10.1016/j.jhydrol.2005.07.003](https://doi.org/10.1016/j.jhydrol.2005.07.003).
- Immerzeel, Walter W, Ludovicus P H van Beek, and Marc F P Bierkens (2010). "Climate change will affect the Asian water towers." *Science (New York, N.Y.)* 328.5984, Pages 1382–5. doi: [10.1126/science.1183188](https://doi.org/10.1126/science.1183188).
- Ines, Amor V M and James W. Hansen (2006). "Bias correction of daily GCM rainfall for crop simulation studies." *Agric. For. Meteorol.* 138.1-4, Pages 44–53. doi: [10.1016/j.agrformet.2006.03.009](https://doi.org/10.1016/j.agrformet.2006.03.009).
- IPCC (2013). *Summary for Policymakers. In: Climate Change 2013: The Physical Science Basis. Contribution of Working Group I to the Fifth Assessment Report of the Intergovernmental Panel on Climate Change [Stocker T.F., D. Qin, G.-K. Plattner, M. Tignor, S.K. Allen, J., Boschung, A. Nauels, Y. Xia, V. Bex and P.M. Midgley (eds.)]* Cambridge University Press, Cambridge, United Kingdom and New York, NY, USA. doi: [10.1017/CB09781107415324.004](https://doi.org/10.1017/CB09781107415324.004).
- Jacquín, Alexandra P. and Asaad Y. Shamseldin (2007). "Development of a possibilistic method for the evaluation of predictive uncertainty in rainfall-runoff modeling." *Water Resources Research* 43.4, Pages 1–18. doi: [10.1029/2006WR005072](https://doi.org/10.1029/2006WR005072).

- Jia, Haifeng et al. (2015). "LID-BMPs planning for urban runoff control and the case study in China." *Journal of Environmental Management* 149, Pages 65–76. DOI: [10.1016/j.jenvman.2014.10.003](https://doi.org/10.1016/j.jenvman.2014.10.003).
- Jia, Xiaoxu et al. (2017). "Soil moisture decline due to afforestation across the Loess Plateau, China." *Journal of Hydrology* 546, Pages 113–122. DOI: [10.1016/j.jhydrol.2017.01.011](https://doi.org/10.1016/j.jhydrol.2017.01.011).
- Jiang, Aijun et al. (2005). "Climatic Trends of Heavy Precipitation Spatial and Temporal Concentration in China." *Acta Geographica Sinica* 60.6, Pages 1007–104.
- Jiang, Chong and Fei Wang (2016). "Temporal changes of streamflow and its causes in the Liao River Basin over the period of 1953–2011, northeastern China." *Catena* 145, Pages 227–238. DOI: [10.1016/j.catena.2016.06.015](https://doi.org/10.1016/j.catena.2016.06.015).
- Jiang, Cong et al. (2015). "Separating the impacts of climate change and human activities on runoff using the Budyko-type equations with time-varying parameters." *Journal of Hydrology* 522, Pages 326–338. DOI: [10.1016/j.jhydrol.2014.12.060](https://doi.org/10.1016/j.jhydrol.2014.12.060).
- Jiang, Shanhu et al. (2011). "Quantifying the effects of climate variability and human activities on runoff from the Laohahe basin in northern China using three different methods." *Hydrological Processes* 25.16, Pages 2492–2505. DOI: [10.1002/hyp.8002](https://doi.org/10.1002/hyp.8002).
- Jiang, Zhongcheng, Yanqing Lian, and Xiaoqun Qin (2014). "Rocky desertification in Southwest China: Impacts, causes, and restoration." *Earth-Science Reviews* 132, Pages 1–12. DOI: [10.1016/j.earscirev.2014.01.005](https://doi.org/10.1016/j.earscirev.2014.01.005).
- Kavetski, Dmitri, George Kuczera, and Stewart W. Franks (2006). "Bayesian analysis of input uncertainty in hydrological modeling: 2. Application." *Water Resour. Res.* 42.3, Pages 1–10. DOI: [10.1029/2005WR004376](https://doi.org/10.1029/2005WR004376).
- Kay, J. E. et al. (2015). "The community earth system model (CESM) large ensemble project : A community resource for studying climate change in the presence of internal climate variability." *Bulletin of the American Meteorological Society* 96.8, Pages 1333–1349. DOI: [10.1175/BAMS-D-13-00255.1](https://doi.org/10.1175/BAMS-D-13-00255.1).
- Kibler, Kelly M. and Desiree D. Tullos (2013). "Cumulative biophysical impact of small and large hydropower development in Nu River, China." *Water Resources Research* 49.6, Pages 3104–3118. DOI: [10.1002/wrcr.20243](https://doi.org/10.1002/wrcr.20243).
- Knutti, Reto et al. (2010). "Challenges in combining projections from multiple climate models." *Journal of Climate* 23.10, Pages 2739–2758. DOI: [10.1175/2009JCLI3361.1](https://doi.org/10.1175/2009JCLI3361.1).
- Koch, J et al. (2016). "Spatial validation of large-scale land surface models against monthly land surface temperature patterns using innovative performance metrics." *Journal of Geophysical Research: Atmospheres* 121, Pages 5430–5452. DOI: [10.1002/2013JD021190](https://doi.org/10.1002/2013JD021190). Received.
- Kong, Dongxian et al. (2016). "Impact assessment of climate change and human activities on net runoff in the Yellow River Basin from 1951 to 2012." *Ecological Engineering* 91, Pages 566–573. DOI: [10.1016/j.ecoleng.2016.02.023](https://doi.org/10.1016/j.ecoleng.2016.02.023).
- Kong, Xiaole et al. (2018). "Impact of water transfer on interaction between surface water and groundwater in the lowland area of North China Plain." *Hydrological Processes* 32.13, Pages 2044–2057. DOI: [10.1002/hyp.13136](https://doi.org/10.1002/hyp.13136).
- Kong, Yanlong and Zhonghe Pang (2012). "Evaluating the sensitivity of glacier rivers to climate change based on hydrograph separation of discharge." *Journal of Hydrology* 434–435, Pages 121–129. DOI: [10.1016/j.jhydrol.2012.02.029](https://doi.org/10.1016/j.jhydrol.2012.02.029).
- Kottek, Markus et al. (2006). "World map of the Köppen-Geiger climate classification updated." *Meteorologische Zeitschrift* 15.3, Pages 259–263. DOI: [10.1127/0941-2948/2006/0130](https://doi.org/10.1127/0941-2948/2006/0130).
- Kryanova, Valentina et al. (2015). "Analysis of current trends in climate parameters, river discharge and glaciers in the Aksu River basin (Central Asia)." *Hydrological Sciences Journal* 60.4, Pages 566–590. DOI: [10.1080/02626667.2014.925559](https://doi.org/10.1080/02626667.2014.925559).
- Krzysztofowicz, Roman (2001). "The case for probabilistic forecasting in hydrology." *Journal of Hydrology* 249.1–4, Pages 2–9. DOI: [10.1016/S0022-1694\(01\)00420-6](https://doi.org/10.1016/S0022-1694(01)00420-6).
- (2002). "Bayesian system for probabilistic river stage forecasting." *Journal of Hydrology* 268.1–4, Pages 16–40. DOI: [10.1016/S0022-1694\(02\)00106-3](https://doi.org/10.1016/S0022-1694(02)00106-3).

- Kuczera, George and Eric Parent (1998). "Monte Carlo assessment of parameter uncertainty in conceptual catchment models: The Metropolis algorithm." *Journal of Hydrology* 211.1-4, Pages 69–85. DOI: [10.1016/S0022-1694\(98\)00198-X](https://doi.org/10.1016/S0022-1694(98)00198-X).
- Kundzewicz, Z. W. et al. (2014). "Analysis of changes in climate and river discharge with focus on seasonal runoff predictability in the Aksu River Basin." *Environmental Earth Sciences* 73.2, Pages 501–516. DOI: [10.1007/s12665-014-3137-5](https://doi.org/10.1007/s12665-014-3137-5).
- Lai, Xijun et al. (2014a). "Impoundment Effects of the Three-Gorges-Dam on Flow Regimes in Two China's Largest Freshwater Lakes." *Water Resources Management* 28.14, Pages 5111–5124. DOI: [10.1007/s11269-014-0797-6](https://doi.org/10.1007/s11269-014-0797-6).
- Lai, Xijun et al. (2014b). "Should the Three Gorges Dam be blamed for the extremely low water levels in the middle-lower Yangtze River?" *Hydrological Processes* 28.1, Pages 150–160. DOI: [10.1002/hyp.10077](https://doi.org/10.1002/hyp.10077).
- Langley, R. S. (2000). "Unified approach to probabilistic and possibilistic analysis of uncertain systems." *Journal of Engineering Mechanics-Asce* 126.11, Pages 1163–1172. DOI: [10.1061/\(ASCE\)0733-9399\(2000\)126:11\(1163\)](https://doi.org/10.1061/(ASCE)0733-9399(2000)126:11(1163)).
- Lehner, Bernhard et al. (2011). "Global Reservoir and Dam (GRanD) database." *European Environment* March, Page 12.
- Lenderink, Geert and Erik Van Meijgaard (2008). "Increase in hourly precipitation extremes beyond expectations from temperature changes." *Nature Geoscience* 1.8, Pages 511–514. DOI: [10.1038/ngeo262](https://doi.org/10.1038/ngeo262).
- Li, Chao et al. (2016a). "Damming effect on the Changjiang (Yangtze River) river water cycle based on stable hydrogen and oxygen isotopic records." *Journal of Geochemical Exploration* 165. June 2003, Pages 125–133. DOI: [10.1016/j.gexplo.2016.03.006](https://doi.org/10.1016/j.gexplo.2016.03.006).
- Li, Hongmei, Lei Feng, and Tianjun Zhou (2011a). "Multi-model Projection of July – August Climate Extreme Changes over China under CO<sub>2</sub> Doubling. Part I: Precipitation." *Advances in Atmospheric Sciences* 28.2, Pages 433–447. DOI: [10.1007/s00376-010-0013-4](https://doi.org/10.1007/s00376-010-0013-4).
- Li, Jianfeng et al. (2016b). "Future Changes in Floods and Water Availability across China: Linkage with Changing Climate and Uncertainties." *Journal of Hydrometeorology* 17.4, Pages 1295–1314. DOI: [10.1175/JHM-D-15-0074.1](https://doi.org/10.1175/JHM-D-15-0074.1).
- Li, K. Y. et al. (2007). "Modeling the hydrological impact of land-use change in West Africa." *Journal of Hydrology* 337.3-4, Pages 258–268. DOI: [10.1016/j.jhydrol.2007.01.038](https://doi.org/10.1016/j.jhydrol.2007.01.038).
- Li, Li et al. (2008). "Impact of Future Climate Change on Runoff in the Head Region of the Yellow River." *Journal of Hydrologic Engineering* 13.5, Pages 347–354. DOI: [10.1061/\(ASCE\)1084-0699\(2008\)13:5\(347\)](https://doi.org/10.1061/(ASCE)1084-0699(2008)13:5(347)).
- Li, Xuemei et al. (2011b). "Spatial and temporal variability of precipitation concentration index, concentration degree and concentration period Xinjiang, China." *International Journal of Climatology* 31.11, Pages 1679–1693. DOI: [10.1002/joc.2181](https://doi.org/10.1002/joc.2181).
- Li, Yue et al. (2018). "Divergent hydrological response to large-scale afforestation and vegetation greening in China." *Science Advances* 4.5. DOI: [10.1126/sciadv.aar4182](https://doi.org/10.1126/sciadv.aar4182).
- Li, Zhenwei et al. (2016c). "Quantifying the impacts of climate and human activities on water and sediment discharge in a karst region of southwest China." *Journal of Hydrology* 542, Pages 836–849. DOI: [10.1016/j.jhydrol.2016.09.049](https://doi.org/10.1016/j.jhydrol.2016.09.049).
- Liu, Dedi et al. (2010a). "Impacts of climate change and human activities on surface runoff in the Dongjiang River basin of China." *Hydrological Processes* 24.11, Pages 1487–1495. DOI: [10.1002/hyp.7609](https://doi.org/10.1002/hyp.7609).
- Liu, Feng et al. (2014a). "Hydrological responses to the combined influence of diverse human activities in the Pearl River delta, China." *Catena* 113, Pages 41–55. DOI: [10.1016/j.catena.2013.09.003](https://doi.org/10.1016/j.catena.2013.09.003).
- Liu, Jiyuan et al. (2003). "Study on spatial pattern of land-use change in China during 1995 -2000." *Science In China (Series D)* 46.4, Pages 373–384.
- Liu, Jiyuan et al. (2014b). "Spatiotemporal characteristics, patterns and causes of land use changes in China since the late 1980s." *Dili Xuebao/Acta Geographica Sinica* 69.1, Pages 3–14. DOI: [10.11821/dlxb201401001](https://doi.org/10.11821/dlxb201401001).

- Liu, Mingliang and Hanqin Tian (2010). "China's land cover and land use change from 1700 to 2005: Estimations from high-resolution satellite data and historical archives." *Global Biogeochemical Cycles* 24.3. DOI: [10.1029/2009GB003687](https://doi.org/10.1029/2009GB003687).
- Liu, Mingliang et al. (2008). "Effects of land-use and land-cover change on evapotranspiration and water yield in China during 1900-2000." *Journal of the American Water Resources Association* 44.5, Pages 1193–1207. DOI: [10.1111/j.1752-1688.2008.00243.x](https://doi.org/10.1111/j.1752-1688.2008.00243.x).
- Liu, Shiyin et al. (2006). "Glacier retreat as a result of climate warming and increased precipitation in the Tarim river basin, northwest China." *Annals of Glaciology* 43, Pages 91–96. DOI: [10.3189/172756406781812168](https://doi.org/10.3189/172756406781812168).
- Liu, Yangyang et al. (2013a). "Impacts of Land-Use and Climate Changes on Hydrologic Processes in the Qingyi River Watershed, China." *Journal of Hydrologic Engineering* 18.11, Pages 1495–1512. DOI: [10.1061/\(ASCE\)HE.1943-5584.0000485](https://doi.org/10.1061/(ASCE)HE.1943-5584.0000485).
- Liu, Yanli et al. (2012). "Quantifying uncertainty in catchment-scale runoff modeling under climate change (case of the Huaihe River, China)." *Quaternary International* 282, Pages 130–136. DOI: [10.1016/j.quaint.2012.04.029](https://doi.org/10.1016/j.quaint.2012.04.029).
- Liu, Z. et al. (2014c). "Land use and climate changes and their impacts on runoff in the Yarlung Zangbo river basin, China." *Land Degradation and Development* 25.3, Pages 203–215. DOI: [10.1002/ldr.1159](https://doi.org/10.1002/ldr.1159).
- Liu, Zhaofei et al. (2010b). "Impacts of climate change on hydrological processes in the headwater catchment of the Tarim River basin, China." *Hydrological Processes* 24.2, Pages 196–208. DOI: [10.1002/hyp.7493](https://doi.org/10.1002/hyp.7493).
- Liu, Zhaofei et al. (2013b). "Assessing the hydrological impacts of climate change in the headwater catchment of the Tarim River basin, China." *Hydrology Research* 44.5, Page 834. DOI: [10.2166/nh.2012.237](https://doi.org/10.2166/nh.2012.237).
- Lohmann, Dag, Ralph Nolte-Holube, and Ehrhard Raschke (1996). *A large-scale horizontal routing model to be coupled to land surface parametrization schemes*. DOI: [10.1034/j.1600-0870.1996.t01-3-00009.x](https://doi.org/10.1034/j.1600-0870.1996.t01-3-00009.x).
- Lu, Shanlong et al. (2015). "Quantifying impacts of climate variability and human activities on the hydrological system of the Haihe River Basin, China." *Environmental Earth Sciences* 73.4, Pages 1491–1503. DOI: [10.1007/s12665-014-3499-8](https://doi.org/10.1007/s12665-014-3499-8).
- Mamitim, Yusuyunjiang et al. (2014). "Irrigation in the Tarim Basin, China: farmers' response to changes in water pricing practices." *Environmental Earth Sciences* 73.2, Pages 559–569. DOI: [10.1007/s12665-014-3245-2](https://doi.org/10.1007/s12665-014-3245-2).
- Mao, Dazhi and Keith A. Cherkauer (2009). "Impacts of land-use change on hydrologic responses in the Great Lakes region." *Journal of Hydrology* 374.1-2, Pages 71–82. DOI: [10.1016/j.jhydrol.2009.06.016](https://doi.org/10.1016/j.jhydrol.2009.06.016).
- McMahon, T. A. et al. (2013). "Estimating actual, potential, reference crop and pan evaporation using standard meteorological data: A pragmatic synthesis." *Hydrology and Earth System Sciences* 17.4, Pages 1331–1363. DOI: [10.5194/hess-17-1331-2013](https://doi.org/10.5194/hess-17-1331-2013).
- McMillan, Hilary, Tobias Krueger, and Jim Freer (2012). "Benchmarking observational uncertainties for hydrology: Rainfall, river discharge and water quality." *Hydrological Processes* 26.26, Pages 4078–4111. DOI: [10.1002/hyp.9384](https://doi.org/10.1002/hyp.9384).
- McSweeney, Carol F. and Richard G. Jones (2013). "No consensus on consensus: The challenge of finding a universal approach to measuring and mapping ensemble consistency in GCM projections." *Climatic Change* 119.3-4, Pages 617–629. DOI: [10.1007/s10584-013-0781-9](https://doi.org/10.1007/s10584-013-0781-9).
- McVicar, Tim R. et al. (2007). "Developing a decision support tool for China's re-vegetation program: Simulating regional impacts of afforestation on average annual streamflow in the Loess Plateau." *Forest Ecology and Management* 251.1-2, Pages 65–81. DOI: [10.1016/j.foreco.2007.06.025](https://doi.org/10.1016/j.foreco.2007.06.025).
- Meehl, Gerald A. et al. (2007). "The WCRP CMIP3 multimodel dataset: A new era in climatic change research." *Bulletin of the American Meteorological Society* 88.9, Pages 1383–1394. DOI: [10.1175/BAMS-88-9-1383](https://doi.org/10.1175/BAMS-88-9-1383).

- Meigh, J. R., A. A. McKenzie, and K. J. Sene (1999). "A grid-based approach to water scarcity estimates for eastern and southern Africa." *Water Resources Management* 13.2, Pages 85–115. doi: [10.1023/A:1008025703712](https://doi.org/10.1023/A:1008025703712).
- Miao, Chiyuan et al. (2011). "A preliminary estimate of human and natural contributions to the changes in water discharge and sediment load in the Yellow River." *Global and Planetary Change* 76.3-4, Pages 196–205. doi: [10.1016/j.gloplacha.2011.01.008](https://doi.org/10.1016/j.gloplacha.2011.01.008).
- Milly, P C D, K a Dunne, and a V Vecchia (2005). "Global pattern of trends in streamflow and water availability in a changing climate." *Nature* 438.7066, Pages 347–350. doi: [10.1038/nature04312](https://doi.org/10.1038/nature04312).
- Ministry of Water Resources, P.R.China (2016). *Bulletin of National Water Resources*. Technical report.
- Montanari, Alberto (2005). "Large sample behaviors of the generalized likelihood uncertainty estimation (GLUE) in assessing the uncertainty of rainfall-runoff simulations." *Water Resources Research* 41.8, Pages 1–13. doi: [10.1029/2004WR003826](https://doi.org/10.1029/2004WR003826).
- (2007). "What do we mean by 'uncertainty'? The need for a consistent wording about uncertainty assessment in hydrology." *Hydrological Processes* 21.6, Pages 841–845. doi: [10.1002/hyp.6623](https://doi.org/10.1002/hyp.6623).
- Montanari, Alberto and Armando Brath (2004). "A stochastic approach for assessing the uncertainty of rainfall-runoff simulations." *Water Resources Research* 40.1, Pages 1–11. doi: [10.1029/2003WR002540](https://doi.org/10.1029/2003WR002540).
- Montanari, Alberto, Christine A Shoemaker, and Nick Van De Giesen (2009). "Introduction to special section on uncertainty assessment in surface and subsurface hydrology: An overview of issues and challenges." *Water Resources Research* 45.12, Pages 2005–2008. doi: [10.1029/2009WR008471](https://doi.org/10.1029/2009WR008471).
- Moradkhani, Hamid et al. (2005). "Uncertainty assessment of hydrologic model states and parameters: Sequential data assimilation using the particle filter." *Water Resources Research* 41.5, Pages 1–17. doi: [10.1029/2004WR003604](https://doi.org/10.1029/2004WR003604).
- Mueller, Charles C. and Ernest H. Kidder (1972). "Rain gage catch variation due to airflow disturbances around a standard rain gage." *Water Resources Research* 8.4, Pages 1077–1082. doi: [10.1029/WR008i004p01077](https://doi.org/10.1029/WR008i004p01077).
- Myhre, Gunnar and Arne Myhre (2003). "Uncertainties in radiative forcing due to surface Albedo changes caused by land-use changes." *Journal of Climate* 16.10, Pages 1511–1524. doi: [10.1175/1520-0442-16.10.1511](https://doi.org/10.1175/1520-0442-16.10.1511).
- Nazemi, A. and H. S. Wheater (2015a). "On inclusion of water resource management in Earth system models -Part 1: Problem definition and representation of water demand." *Hydrology and Earth System Sciences* 19.1, Pages 33–61. doi: [10.5194/hess-19-33-2015](https://doi.org/10.5194/hess-19-33-2015).
- (2015b). "On inclusion of water resource management in Earth system models Part 2: Representation of water supply and allocation and opportunities for improved modeling." *Hydrology and Earth System Sciences* 19.1, Pages 63–90. doi: [10.5194/hess-19-63-2015](https://doi.org/10.5194/hess-19-63-2015).
- Neff, E.L. (1977). "How much does a rain gauge gauge?" *Journal of Hydrology* 35, Pages 213–220.
- Neverre, Noémie, Patrice Dumas, and Hypatia Nassopoulos (2016). "Large-scale water scarcity assessment under global changes: insights from a hydroeconomic framework." *Hydrology and Earth System Sciences Discussions* February, Pages 1–26. doi: [10.5194/hess-2015-502](https://doi.org/10.5194/hess-2015-502).
- Ngo-Duc, T. (2005). "Effects of land water storage on global mean sea level over the past half century." *Geophysical Research Letters* 32.9, Page L09704. doi: [10.1029/2005GL022719](https://doi.org/10.1029/2005GL022719).
- Nguyen-Quang, Trung et al. (2018). "ORCHIDEE-ROUTING: A new river routing scheme using a high resolution hydrological database." *Geoscientific Model Development Discussions* 2010, Pages 1–34. doi: [10.5194/gmd-2018-57](https://doi.org/10.5194/gmd-2018-57).
- Niu, Jun and Bellie Sivakumar (2014). "Study of runoff response to land use change in the East River basin in South China." *Stochastic Environmental Research and Risk Assessment* 28.4, Pages 857–865. doi: [10.1007/s00477-013-0690-5](https://doi.org/10.1007/s00477-013-0690-5).
- Normile, Dennis (2007). "Getting at the roots of killer dust storms." *Science* 317.5836, Pages 314–316. doi: [10.1126/science.317.5836.314](https://doi.org/10.1126/science.317.5836.314).
- Oki, Taikan and Y. C. Sud (1998). "Design of Total Runoff Integrating Pathways (TRIP)-A Global River Channel Network." *Earth Interactions* 2.1, Pages 1–1. doi: [10.1175/1087-3562\(1998\)002<0001:DoTRIP>2.0.CO;2](https://doi.org/10.1175/1087-3562(1998)002<0001:DoTRIP>2.0.CO;2).

- OL'DEKOP, E. M. (1991). *On evaporation from the surface of river basins*, *Trans. Meteorol. Obs. Univ. Tartu*. Technical report. Lur-evskogo (in Russian): Univ. of Tartu, Tartu, Estonia, Page 200.
- Orlowsky, Boris and Sonia I. Seneviratne (2014). "On the spatial representativeness of temporal dynamics at European weather stations." *International Journal of Climatology* 34.10, Pages 3154–3160. DOI: [10.1002/joc.3903](https://doi.org/10.1002/joc.3903).
- Ouyang, Wei et al. (2011). "Cascade Dam-Induced Hydrological Disturbance and Environmental Impact in the Upper Stream of the Yellow River." *Water Resources Management* 25.3, Pages 913–927. DOI: [10.1007/s11269-010-9733-6](https://doi.org/10.1007/s11269-010-9733-6).
- Pechlivanidis, I G et al. (2011). "Catchment Scale Hydrological Modelling: A Review Of Model Types, Calibration Approaches And Uncertainty Analysis Methods In The Context Of Recent Developments In Technology And Applications." *Global NEST Journal* 13.3, Pages 193–214. DOI: [10.1002/hyp](https://doi.org/10.1002/hyp).
- Piao, S et al. (2010). "The impacts of climate change on water resources and agriculture in China." *Nature* 467.7311, Pages 43–51. DOI: [10.1038/nature09364](https://doi.org/10.1038/nature09364).
- Pike, J. G. (1964). "The estimation of annual run-off from meteorological data in a tropical climate." *Journal of Hydrology* 2.2, Pages 116–123. DOI: [10.1016/0022-1694\(64\)90022-8](https://doi.org/10.1016/0022-1694(64)90022-8).
- Pitman, A. J. (2003). "The evolution of, and revolution in, land surface schemes designed for climate models." *International Journal of Climatology* 23.5, Pages 479–510. DOI: [10.1002/joc.893](https://doi.org/10.1002/joc.893).
- Pitman, A. J. et al. (1999). "Uncertainty in the simulation of runoff due to the parameterization of frozen soil moisture using the Global Soil Wetness Project methodology." *Journal of Geophysical Research* 104.D14, Pages 16879–16888. DOI: [10.1029/1999JD900261](https://doi.org/10.1029/1999JD900261).
- Ponce, V., R. Pandey, and S. Ercan (2000). "Characterization of drought across climatic spectrum." *Journal of Hydrologic Engineering* 5.2, Pages 222–224. DOI: [Doi10.1061/\(ASCE\)1084-0699\(2000\)5:2\(222\)](https://doi.org/10.1061/(ASCE)1084-0699(2000)5:2(222)).
- Potter, N. J. et al. (2005). "Effects of rainfall seasonality and soil moisture capacity on mean annual water balance for Australian catchments." *Water Resources Research* 41.6, Pages 1–11. DOI: [10.1029/2004WR003697](https://doi.org/10.1029/2004WR003697).
- Pritchard, Hamish D. (2017). "Asia's glaciers are a regionally important buffer against drought." *Nature* 545.7653, Pages 169–174. DOI: [10.1038/nature22062](https://doi.org/10.1038/nature22062).
- Qi, Wei et al. (2016). "Quantifying Uncertainties in Extreme Flood Predictions under Climate Change for a Medium-Sized Basin in Northeastern China." *Journal of Hydrometeorology* 17.12, Pages 3099–3112. DOI: [10.1175/JHM-D-15-0212.1](https://doi.org/10.1175/JHM-D-15-0212.1).
- Qin, Youwei, Dmitri Kavetski, and George Kuczera (2018a). "A Robust Gauss-Newton algorithm for the optimization of hydrological models: Benchmarking against industry-standard algorithms." *Water Resources Research*. DOI: [10.1029/2017WR022489](https://doi.org/10.1029/2017WR022489).
- (2018b). "A Robust Gauss-Newton algorithm for the optimization of hydrological models: From Standard Gauss-Newton to Robust Gauss-Newton." *Water Resources Research*. DOI: [10.1029/2017WR022488](https://doi.org/10.1029/2017WR022488).
- Refsgaard, Jens Christian (1997). "Parameterisation, calibration and validation of distributed hydrological models." *Journal of Hydrology* 198.1-4, Pages 69–97. DOI: [10.1016/S0022-1694\(96\)03329-X](https://doi.org/10.1016/S0022-1694(96)03329-X).
- Refsgaard, Jens Christian et al. (2006). "A framework for dealing with uncertainty due to model structure error." *Advances in Water Resources* 29.11, Pages 1586–1597. DOI: [10.1016/j.advwatres.2005.11.013](https://doi.org/10.1016/j.advwatres.2005.11.013).
- Ren, Weiwei et al. (2018). "A probabilistic method for streamflow projection and associated uncertainty analysis in a data sparse alpine region." *Global and Planetary Change* 165, Pages 100–113. DOI: [10.1016/j.gloplacha.2018.03.011](https://doi.org/10.1016/j.gloplacha.2018.03.011).
- Renard, Benjamin et al. (2010). "Understanding predictive uncertainty in hydrologic modeling: The challenge of identifying input and structural errors." *Water Resources Research* 46.5, Pages 1–22. DOI: [10.1029/2009WR008328](https://doi.org/10.1029/2009WR008328).
- Rocheta, Eytan et al. (2014). "How well do general circulation models represent low-frequency rainfall variability?" *Water Resources Research* 50.3, Pages 2108–2123. DOI: [10.1002/2012WR013085](https://doi.org/10.1002/2012WR013085).

- Rodell, BY M et al. (2004). "THE GLOBAL LAND DATA ASSIMILATION SYSTEM This powerful new land surface modeling system integrates data from advanced observing systems to support improved forecast model initialization and hydrometeorological investigations." *Bull. Amer. Meteor. Soc.* 85.3, Pages 381–394. DOI: [10.1175/BAMS-85-3-381](https://doi.org/10.1175/BAMS-85-3-381).
- Roe, Gerard H (2005). "Orographic Precipitation." *Annu. Rev. Earth Planet. Sci* 33.1, Pages 645–71. DOI: [10.1146/annurev.earth.33.092203.122541](https://doi.org/10.1146/annurev.earth.33.092203.122541).
- Rosnay, P. de and J. Polcher (1998). "Modelling root water uptake in a complex land surface scheme coupled to a GCM." *Hydrology and Earth System Sciences* 2.2/3, Pages 239–255. DOI: [10.5194/hess-2-239-1998](https://doi.org/10.5194/hess-2-239-1998).
- Rosnay, P. de et al. (2002). "Impact of a physically based soil water flow and soil-plant interaction representation for modeling large-scale land surface processes." *Journal of Geophysical Research: Atmospheres* 107.D11, ACL 3–1–ACL 3–19. DOI: [10.1029/2001JD000634](https://doi.org/10.1029/2001JD000634).
- Rosnay, P. de et al. (2003). "Integrated parameterization of irrigation in the land surface model ORCHIDEE. Validation over Indian Peninsula." *Geophysical Research Letters* 30.19, Pages 1–4. DOI: [10.1029/2003GL018024](https://doi.org/10.1029/2003GL018024).
- Rost, Stefanie et al. (2008). "Agricultural green and blue water consumption and its influence on the global water system." *Water Resources Research* 44.9. DOI: [10.1029/2007WR006331](https://doi.org/10.1029/2007WR006331).
- Scheff, Jacob and Dargan M.W. Frierson (2015). "Terrestrial aridity and its response to greenhouse warming across CMIP5 climate models." *Journal of Climate* 28.14, Pages 5583–5600. DOI: [10.1175/JCLI-D-14-00480.1](https://doi.org/10.1175/JCLI-D-14-00480.1).
- Scheffe, Henry (1999). *The analysis of variance*. Volume 72. John Wiley & Sons.
- Schewe, Jacob et al. (2014). "Multimodel assessment of water scarcity under climate change." *Proceedings of the National Academy of Sciences* 111.9, Pages 3245–3250. DOI: [10.1073/pnas.1222460110](https://doi.org/10.1073/pnas.1222460110).
- Schneider, A. et al. (2017). "Global scale river network extraction based on high-resolution topography and constrained by lithology, climate, slope, and observed drainage density." *Geophysical Research Letters*, Pages 2773–2781. DOI: [10.1002/2016GL071844](https://doi.org/10.1002/2016GL071844).
- Schreiber, P. (1904). "Über die Beziehungen zwischen dem Niederschlag und der Wasserführung der Flüsse in Mitteleuropa." *Z. Meteorol* 21.10, Pages 441–452.
- Seneviratne, Sonia I. et al. (2016). "Allowable CO<sub>2</sub> emissions based on regional and impact-related climate targets." *Nature* 529.7587, Pages 477–483. DOI: [10.1038/nature16542](https://doi.org/10.1038/nature16542).
- Sevruk, B. (1982). "Methods of correction for systematic error in point precipitation measurement for operational use." *World Meteorological Organisation* 589, Page 91.
- Shangguan, Donghui et al. (2009). "Glacier changes during the last forty years in the Tarim Interior River basin, northwest China." *Progress in Natural Science* 19.6, Pages 727–732. DOI: [10.1016/j.pnsc.2008.11.002](https://doi.org/10.1016/j.pnsc.2008.11.002).
- Shen, Mingxi et al. (2018). "Estimating uncertainty and its temporal variation related to global climate models in quantifying climate change impacts on hydrology." *Journal of Hydrology* 556, Pages 10–24. DOI: [10.1016/j.jhydrol.2017.11.004](https://doi.org/10.1016/j.jhydrol.2017.11.004).
- Shen, Y. et al. (2010). "Interpolation methods of China daily precipitation data." *Journal of Applied Meteorology Science* 21.3, Pages 279–286.
- Shen, Yan et al. (2014). "A high spatiotemporal gauge-satellite merged precipitation analysis over China." *Journal of Geophysical Research* 119.6, Pages 3063–3075. DOI: [10.1002/2013JD020686](https://doi.org/10.1002/2013JD020686).
- Shi, Pei Jun et al. (2007). "The effect of land use/cover change on surface runoff in Shenzhen region, China." *Catena* 69.1, Pages 31–35. DOI: [10.1016/j.catena.2006.04.015](https://doi.org/10.1016/j.catena.2006.04.015).
- Shi, Pengfei et al. (2016). "Large-scale climate patterns and precipitation in an arid endorheic region: linkage and underlying mechanism." *Environ. Res. Lett.* 11.4, Page 044006. DOI: [10.1088/1748-9326/11/4/044006](https://doi.org/10.1088/1748-9326/11/4/044006).
- Siebert, S. et al. (2013). *Global Map of Irrigation Areas version 5*. March 2013, Pages 1–2. DOI: [10.13140/2.1.2660.6728](https://doi.org/10.13140/2.1.2660.6728).

- Sirajul Haque, S. M., Sanatan Das Gupta, and Sohag Miah (2014). "Deforestation effects on biological and other important soil properties in an upland watershed of Bangladesh." *Journal of Forestry Research* 25.4, Pages 877–885. DOI: [10.1007/s11676-014-0534-2](https://doi.org/10.1007/s11676-014-0534-2).
- Sitch, Stephen et al. (2005). "Impacts of future land cover changes on atmospheric CO<sub>2</sub> and climate." *Global Biogeochemical Cycles* 19.2, Pages 1–15. DOI: [10.1029/2004GB002311](https://doi.org/10.1029/2004GB002311).
- Song, Xinzhang et al. (2014). "Chinese Grain for Green Program led to highly increased soil organic carbon levels: A meta-analysis." *Scientific Reports* 4. DOI: [10.1038/srep04460](https://doi.org/10.1038/srep04460).
- Stocker, T F et al. (2013). "Climate change 2013: The physical science basis. Intergovernmental panel on climate change, working group I contribution to the IPCC fifth assessment report (AR5)."
- Sun, Fubao et al. (2010). "Partitioning the variance between space and time." *Geophysical Research Letters* 37.12, Pages 1–6. DOI: [10.1029/2010GL043323](https://doi.org/10.1029/2010GL043323).
- Sun, Fubao, Michael L. Roderick, and Graham D. Farquhar (2012). "Changes in the variability of global land precipitation." *Geophysical Research Letters* 39.18, Pages 1–6. DOI: [10.1029/2012GL053369](https://doi.org/10.1029/2012GL053369).
- Sun, Ge et al. (2006). "Potential water yield reduction due to forestation across China." *Journal of Hydrology* 328.3-4, Pages 548–558. DOI: [10.1016/j.jhydrol.2005.12.013](https://doi.org/10.1016/j.jhydrol.2005.12.013).
- Sun, Qiaohong et al. (2018). "A Review of Global Precipitation Data Sets: Data Sources, Estimation, and Intercomparisons." *Reviews of Geophysics* 56.1, Pages 79–107. DOI: [10.1002/2017RG000574](https://doi.org/10.1002/2017RG000574).
- Sutanudjaja, Edwin H. et al. (2017). "PCR-GLOBWB 2: a 5 arc-minute global hydrological and water resources model." *Geoscientific Model Development Discussions* December, Pages 1–41. DOI: [10.5194/gmd-2017-288](https://doi.org/10.5194/gmd-2017-288).
- Tallaksen, Lena M. and Kerstin Stahl (2014). "Spatial and temporal patterns of large-scale droughts in Europe: Model dispersion and performance." *Geophysical Research Letters* 41.2, Pages 429–434. DOI: [10.1002/2013GL058573](https://doi.org/10.1002/2013GL058573).
- Tang, Y. et al. (2007). "Comparing sensitivity analysis methods to advance lumped watershed model identification and evaluation." *Hydrol. Earth Syst. Sci.* 11, Pages 793–817. DOI: [10.5194/hess-11-793-2007](https://doi.org/10.5194/hess-11-793-2007).
- Tang, Y. et al. (2013). "Responses of natural runoff to recent climatic variations in the Yellow River basin, China." *Hydrology and Earth System Sciences* 17.11, Pages 4471–4480. DOI: [10.5194/hess-17-4471-2013](https://doi.org/10.5194/hess-17-4471-2013).
- Tao, Hui et al. (2011). "Trends of streamflow in the Tarim River Basin during the past 50years: Human impact or climate change?" *Journal of Hydrology* 400.1-2, Pages 1–9. DOI: [10.1016/j.jhydrol.2011.01.016](https://doi.org/10.1016/j.jhydrol.2011.01.016).
- Tapiador, Francisco J. et al. (2012). "Global precipitation measurement: Methods, datasets and applications." *Atmospheric Research* 104-105, Pages 70–97. DOI: [10.1016/j.atmosres.2011.10.021](https://doi.org/10.1016/j.atmosres.2011.10.021).
- Tebaldi, Claudia and Reto Knutti (2007). "The use of the multi-model ensemble in probabilistic climate projections." *Philos. Trans. A. Math. Phys. Eng. Sci.* 365.1857, Pages 2053–75. DOI: [10.1098/rsta.2007.2076](https://doi.org/10.1098/rsta.2007.2076).
- Tebaldi, Claudia, Julie M. Arblaster, and Reto Knutti (2011). "Mapping model agreement on future climate projections." *Geophysical Research Letters* 38.23, Pages 1–5. DOI: [10.1029/2011GL049863](https://doi.org/10.1029/2011GL049863).
- Thyer, Mark et al. (2009). "Critical evaluation of parameter consistency and predictive uncertainty in hydrological modeling: A case study using Bayesian total error analysis." *Water Resources Research* 45.12. DOI: [10.1029/2008WR006825](https://doi.org/10.1029/2008WR006825).
- Tian, Ye et al. (2015). "Impact assessment of multiple uncertainty sources on high flows under climate change." *Hydrology Research*, nh2015008. DOI: [10.2166/nh.2015.008](https://doi.org/10.2166/nh.2015.008).
- Trenberth, Kevin E. et al. (2007). "Estimates of the Global Water Budget and Its Annual Cycle Using Observational and Model Data." *Journal of Hydrometeorology* 8.4, Pages 758–769. DOI: [10.1175/JHM600.1](https://doi.org/10.1175/JHM600.1).
- Twine, Tracy E., Christopher J. Kucharik, and Jonathan A. Foley (2004). "Effects of Land Cover Change on the Energy and Water Balance of the Mississippi River Basin." *Journal of Hydrometeorology* 5.4, Pages 640–655. DOI: [10.1175/1525-7541\(2004\)005<0640:EOLCCO>2.0.CO;2](https://doi.org/10.1175/1525-7541(2004)005<0640:EOLCCO>2.0.CO;2).

- UNESCO (2005). "Model Sensitivity and Uncertainty Analysis." In: *Water Resources Systems Planning and Management*, Pages 254–291.
- Vörösmarty, Charles J. et al. (1997). "The storage and aging of continental runoff in large reservoir systems of the world." *Ambio* 26.4, Pages 210–219.
- Wada, Yoshihide et al. (2017). "Human–water interface in hydrological modelling: current status and future directions." *Hydrology and Earth System Sciences* 21.8, Pages 4169–4193. DOI: [10.5194/hess-21-4169-2017](https://doi.org/10.5194/hess-21-4169-2017).
- Wang, Guoqing et al. (2017a). "Runoff sensitivity to climate change for hydro-climatically different catchments in China." *Stochastic Environmental Research and Risk Assessment* 31.4, Pages 1011–1021. DOI: [10.1007/s00477-016-1218-6](https://doi.org/10.1007/s00477-016-1218-6).
- Wang, Huaqi et al. (2012a). "Hydro-climatic trends in the last 50 years in the lower reach of the Shiyang River Basin, NW China." *Catena* 95, Pages 33–41. DOI: [10.1016/j.catena.2012.03.003](https://doi.org/10.1016/j.catena.2012.03.003).
- Wang, J., H. Li, and X. Hao (2010a). "Responses of snowmelt runoff to climatic change in an inland river basin, Northwestern China, over the past 50 years." *Hydrology and Earth System Sciences* 14.10, Pages 1979–1987. DOI: [10.5194/hess-14-1979-2010](https://doi.org/10.5194/hess-14-1979-2010).
- Wang, Jiahu et al. (2010b). "Quantitative assessment of climate change and human impacts on long-term hydrologic response: A case study in a sub-basin of the Yellow River, China." *International Journal of Climatology* 30.14, Pages 2130–2137. DOI: [10.1002/joc.2023](https://doi.org/10.1002/joc.2023).
- Wang, Kai et al. (2015). "Effects of land-use/cover change on hydrological processes using a GIS/RS-based integrated hydrological model: case study of the East River, China." *Hydrological Sciences Journal* 60.10, Pages 1724–1738. DOI: [10.1080/02626667.2014.949723](https://doi.org/10.1080/02626667.2014.949723).
- Wang, Lin and Wen Chen (2014). "A CMIP5 multimodel projection of future temperature, precipitation, and climatological drought in China." *International Journal of Climatology* 34.6, Pages 2059–2078. DOI: [10.1002/joc.3822](https://doi.org/10.1002/joc.3822).
- Wang, Shuai et al. (2011a). "A comparative analysis of forest cover and catchment water yield relationships in northern China." *Forest Ecology and Management* 262.7, Pages 1189–1198. DOI: [10.1016/j.foreco.2011.06.013](https://doi.org/10.1016/j.foreco.2011.06.013).
- Wang, Tao et al. (2013a). "Evaluation of an improved intermediate complexity snow scheme in the ORCHIDEE land surface model." *Journal of Geophysical Research Atmospheres* 118.12, Pages 6064–6079. DOI: [10.1002/jgrd.50395](https://doi.org/10.1002/jgrd.50395).
- Wang, Tongli et al. (2012b). "ClimateWNA-high-resolution spatial climate data for western North America." *J. Appl. Meteorol. Climatol.* 51.1, Pages 16–29. DOI: [10.1175/JAMC-D-11-043.1](https://doi.org/10.1175/JAMC-D-11-043.1).
- Wang, Xiaoyan et al. (2017b). "Analysis of multi-dimensional hydrological alterations under climate change for four major river basins in different climate zones." *Climatic Change* 141.3, Pages 483–498. DOI: [10.1007/s10584-016-1843-6](https://doi.org/10.1007/s10584-016-1843-6).
- Wang, Xiaoyan et al. (2018). "Impacts of climate change on flow regime and sequential threats to riverine ecosystem in the source region of the Yellow River." *Environmental Earth Sciences* 77.12. DOI: [10.1007/s12665-018-7628-7](https://doi.org/10.1007/s12665-018-7628-7).
- Wang, Yan et al. (2013b). "Contributions of climate and human activities to changes in runoff of the Yellow and Yangtze rivers from 1950 to 2008." *Science China Earth Sciences* 56.8, Pages 1398–1412. DOI: [10.1007/s11430-012-4505-1](https://doi.org/10.1007/s11430-012-4505-1).
- Wang, Yonggui et al. (2016). "Modelling water quality and quantity with the influence of inter-basin water diversion projects and cascade reservoirs in the Middle-lower Hanjiang River." *Journal of Hydrology* 541, Pages 1348–1362. DOI: [10.1016/j.jhydrol.2016.08.039](https://doi.org/10.1016/j.jhydrol.2016.08.039).
- Wang, Yunqiang et al. (2011b). "Impacts of land use and plant characteristics on dried soil layers in different climatic regions on the Loess Plateau of China." *Agricultural and Forest Meteorology* 151.4, Pages 437–448. DOI: [10.1016/j.agrformet.2010.11.016](https://doi.org/10.1016/j.agrformet.2010.11.016).
- Webster, Peter J. (1976). *Climate and life. M. I. Budyko (David H. Miller, Translator). Academic Press, New York, \$35.00. Volume 6. 03. Academic Press, New York, Pages 461–463.* DOI: [10.1016/0033-5894\(67\)90014-2](https://doi.org/10.1016/0033-5894(67)90014-2).

- Weedon, Graham P. et al. (2014). "The WFDEI meteorological forcing data set: WATCH Forcing data methodology applied to ERA-Interim reanalysis data." *Water Resources Research* 50.9, Pages 7505–7514. DOI: [10.1002/2014WR015638](https://doi.org/10.1002/2014WR015638).
- Wei, Yanhong et al. (2016). "Spatial-temporal variation and periodic change in streamflow and suspended sediment discharge along the mainstream of the Yellow River during 1950-2013." *Catena* 140, Pages 105–115. DOI: [10.1016/j.catena.2016.01.016](https://doi.org/10.1016/j.catena.2016.01.016).
- Wei, M and L Menzel (2008). "A global comparison of four potential evapotranspiration equations and their relevance to stream flow modelling in semi-arid environments." *Adv. Geosci* 18, Pages 15–23. DOI: [10.5194/adgeo-18-15-2008](https://doi.org/10.5194/adgeo-18-15-2008).
- Weng, QIHAO (2001). "Modeling urban growth effects on surface runoff with the integration of remote sensing and GIS." *Environmental Management* 28.6, Pages 737–748. DOI: [10.1007/s002670010258](https://doi.org/10.1007/s002670010258).
- Westerberg, I. K. et al. (2011). "Calibration of hydrological models using flow-duration curves." *Hydrology and Earth System Sciences* 15.7, Pages 2205–2227. DOI: [10.5194/hess-15-2205-2011](https://doi.org/10.5194/hess-15-2205-2011).
- Wilby, R. L. et al. (2014). "The Statistical DownScaling Model -Decision Centric (SDSM-DC): Conceptual basis and applications." *Climate Research* 61.3, Pages 251–268. DOI: [10.3354/cr01254](https://doi.org/10.3354/cr01254).
- Willmott, C. J. and K. Matsuura (2012). "Terrestrial Air Temperature and Precipitation: Monthly and Annual Time Series (1900 - 2010)."
- Wisser, D et al. (2010). "Reconstructing 20th century global hydrography: a contribution to the Global Terrestrial Network-Hydrology (GTN-H)." *Hydrol. Earth Syst. Sci* 14.2, Pages 1–24. DOI: [10.5194/hess-14-1-2010](https://doi.org/10.5194/hess-14-1-2010).
- Woo, Ming Ko and Philip Marsh (2005). "Snow, frozen soils and permafrost hydrology in Canada, 1999-2002." *Hydrol. Process.* 19.1, Pages 215–229. DOI: [10.1002/hyp.5772](https://doi.org/10.1002/hyp.5772).
- Wu, C. S., S. L. Yang, and Ya ping Lei (2012a). "Quantifying the anthropogenic and climatic impacts on water discharge and sediment load in the Pearl River (Zhujiang), China (1954-2009)." *Journal of Hydrology* 452-453, Pages 190–204. DOI: [10.1016/j.jhydrol.2012.05.064](https://doi.org/10.1016/j.jhydrol.2012.05.064).
- Wu, L. et al. (2018). "Impacts of land use change on river systems for a river network plain." *Water (Switzerland)* 10.5. DOI: [10.3390/w10050609](https://doi.org/10.3390/w10050609).
- Wu, Yong ping, Yong ping Shen, and B. Larry Li (2012b). "Possible physical mechanism of water vapor transport over Tarim River Basin." *Ecological Complexity* 9, Pages 63–70. DOI: [10.1016/j.ecocom.2011.12.002](https://doi.org/10.1016/j.ecocom.2011.12.002).
- Xie, Pingping et al. (2003). "GPCP pentad precipitation analyses: An experimental dataset based on gauge observations and satellite estimates." *Journal of Climate* 16.13, Pages 2197–2214. DOI: [10.1175/2769.1](https://doi.org/10.1175/2769.1).
- Xie, Pingping et al. (2007). "A Gauge-Based Analysis of Daily Precipitation over East Asia." *Journal of Hydrometeorology* 8.3, Pages 607–626. DOI: [10.1175/JHM583.1](https://doi.org/10.1175/JHM583.1).
- Xiong, Lihua et al. (2013). "Annual runoff change in the headstream of Yangtze River and its relation to precipitation and air temperature." *Hydrology Research* 44.5, Page 850. DOI: [10.2166/nh.2012.120](https://doi.org/10.2166/nh.2012.120).
- Xu, Guanglai et al. (2014). "Temporal and spatial variation of water level in urbanizing plain river network region." *Water Science & Technology* 69.11, Page 2191. DOI: [10.2166/wst.2014.133](https://doi.org/10.2166/wst.2014.133).
- Xu, H. and Y. Luo (2015). "Climate change and its impacts on river discharge in two climate regions in China." *Hydrology and Earth System Sciences* 19.11, Pages 4609–4618. DOI: [10.5194/hess-19-4609-2015](https://doi.org/10.5194/hess-19-4609-2015).
- Xu, Jiongxin (2004). "A study of anthropogenic seasonal rivers in China." *Catena* 55.1, Pages 17–32. DOI: [10.1016/S0341-8162\(03\)00089-4](https://doi.org/10.1016/S0341-8162(03)00089-4).
- Xu, Z X, Y N Chen, and J Y Li (2004). "Impact of Climate Change on Water Resources in the Tarim River Basin." *Water Resources Management* 18.5, Pages 439–458. DOI: [10.1023/B:WARM.0000049142.95583.98](https://doi.org/10.1023/B:WARM.0000049142.95583.98).

- Xu, Zongxue and Gang Zhao (2016). "Impact of urbanization on rainfall-runoff processes: Case study in the liangshui river basin in Beijing, China." *IAHS-AISH Proceedings and Reports* 373, Pages 7–12. doi: [10.5194/piahs-373-7-2016](https://doi.org/10.5194/piahs-373-7-2016).
- Yan, D. H. et al. (2012). "Quantitative analysis on the environmental impact of large-scale water transfer project on water resource area in a changing environment." *Hydrology and Earth System Sciences* 16.8, Pages 2685–2702. doi: [10.5194/hess-16-2685-2012](https://doi.org/10.5194/hess-16-2685-2012).
- Yang, Dawen et al. (2007). "Analyzing spatial and temporal variability of annual water-energy balance in nonhumid regions of China using the Budyko hypothesis." *Water Resources Research* 43.4, Pages 1–12. doi: [10.1029/2006WR005224](https://doi.org/10.1029/2006WR005224).
- Yang, Hanbo et al. (2008a). "New analytical derivation of the mean annual water-energy balance equation." *Water Resources Research* 44.3, Pages 1–9. doi: [10.1029/2007WR006135](https://doi.org/10.1029/2007WR006135).
- Yang, S. L. et al. (2005). "Trends in annual discharge from the Yangtze River to the sea (1865-2004)." *Hydrological Sciences Journal* 50.5, Pages 825–836. doi: [10.1623/hysj.2005.50.5.825](https://doi.org/10.1623/hysj.2005.50.5.825).
- Yang, S. L. et al. (2015a). "Decline of Yangtze River water and sediment discharge: Impact from natural and anthropogenic changes." *Scientific Reports* 5. doi: [10.1038/srep12581](https://doi.org/10.1038/srep12581).
- Yang, Tao et al. (2008b). "A spatial assessment of hydrologic alteration caused by dam construction in the middle and lower Yellow River, China." *Hydrological Processes* 22.18, Pages 3829–3843. doi: [10.1002/hyp.6993](https://doi.org/10.1002/hyp.6993).
- Yang, Tao et al. (2010). "Temporal and spatial patterns of low-flow changes in the Yellow River in the last half century." *Stochastic Environmental Research and Risk Assessment* 24.2, Pages 297–309. doi: [10.1007/s00477-009-0318-y](https://doi.org/10.1007/s00477-009-0318-y).
- Yang, Tao et al. (2011). "Changes of climate extremes in a typical arid zone: Observations and multimodel ensemble projections." *J. Geophys. Res. Atmos.* 116.19, Pages 1–18. doi: [10.1029/2010JD015192](https://doi.org/10.1029/2010JD015192).
- Yang, Tao et al. (2012a). "Multi-model ensemble projections in temperature and precipitation extremes of the Tibetan Plateau in the 21st century." *Global and Planetary Change* 80-81, Pages 1–13. doi: [10.1016/j.gloplacha.2011.08.006](https://doi.org/10.1016/j.gloplacha.2011.08.006).
- Yang, Tao et al. (2012b). "Statistical downscaling of extreme daily precipitation, evaporation, and temperature and construction of future scenarios." *Hydrological Processes* 26.23, Pages 3510–3523. doi: [10.1002/hyp.8427](https://doi.org/10.1002/hyp.8427).
- Yang, Tao et al. (2015b). "Drought projection based on a hybrid drought index using Artificial Neural Networks." *Hydrol. Process.* 29.11, Pages 2635–2648. doi: [10.1002/hyp.10394](https://doi.org/10.1002/hyp.10394).
- Yang, Tao et al. (2017). "Development of a new IHA method for impact assessment of climate change on flow regime." *Global and Planetary Change* 156, Pages 68–79. doi: [10.1016/j.gloplacha.2017.07.006](https://doi.org/10.1016/j.gloplacha.2017.07.006).
- Yang, Xiankun and Xixi Lu (2014). "Drastic change in China's lakes and reservoirs over the past decades." *Scientific Reports* 4, Pages 1–10. doi: [10.1038/srep06041](https://doi.org/10.1038/srep06041).
- Yang, Zhenni (1991). *Glacier Water Resources in China (in Chinese)*. Lanzhou: Gansu Science and Technology Press.
- Ye, Xuchun et al. (2013). "Distinguishing the relative impacts of climate change and human activities on variation of streamflow in the poyang lake catchment, china." *Journal of Hydrology* 494, Pages 83–95. doi: [10.1016/j.jhydrol.2013.04.036](https://doi.org/10.1016/j.jhydrol.2013.04.036).
- Yu, Meixiu et al. (2011). "Impacts of the gezhouba and three gorges reservoirs on the sediment regime in the yangtze river, china." *Journal of Hydrology* 403.3-4, Pages 224–233. doi: [10.1016/j.jhydrol.2011.03.043](https://doi.org/10.1016/j.jhydrol.2011.03.043).
- Yu, Z. (2000). "Assessing the response of subgrid hydrologic processes to atmospheric forcing with a hydrologic model system." *Global and Planetary Change* 25.1-2, Pages 1–17. doi: [10.1016/S0921-8181\(00\)00018-7](https://doi.org/10.1016/S0921-8181(00)00018-7).
- Yu, Z. et al. (1999). "Simulating the river-basin response to atmospheric forcing by linking a mesoscale meteorological model and hydrologic model system." *Journal of Hydrology* 218.1-2, Pages 72–91. doi: [10.1016/S0022-1694\(99\)00022-0](https://doi.org/10.1016/S0022-1694(99)00022-0).

- Yu, Zhongbo, David Pollard, and Li Cheng (2006). "On continental-scale hydrologic simulations with a coupled hydrologic model." *Journal of Hydrology* 331.1-2, Pages 110–124. DOI: [10.1016/j.jhydrol.2006.05.021](https://doi.org/10.1016/j.jhydrol.2006.05.021).
- Yu, Zhongbo et al. (2014). "Spatial and Temporal Scale Effect in Simulating Hydrologic Processes in a Watershed." *Journal of Hydrologic Engineering* 19.1, Pages 99–107. DOI: [10.1061/\(ASCE\)HE.1943-5584.0000762](https://doi.org/10.1061/(ASCE)HE.1943-5584.0000762).
- Yuan, Fei et al. (2017). "Evaluation on uncertainty sources in projecting hydrological changes over the Xijiang River basin in South China." *Journal of Hydrology* 554, Pages 434–450. DOI: [10.1016/j.jhydrol.2017.08.034](https://doi.org/10.1016/j.jhydrol.2017.08.034).
- Yuan, Yujie et al. (2016). "Quantitative assessment of the contribution of climate variability and human activity to streamflow alteration in Dongting Lake, China." *Hydrological Processes* 30.12, Pages 1929–1939. DOI: [10.1002/hyp.10768](https://doi.org/10.1002/hyp.10768).
- Zadeh, Lotfi A. (2005). "Toward a generalized theory of uncertainty (GTU)—an outline." *Information Sciences* 172.1-2, Pages 1–40. DOI: [10.1016/j.ins.2005.01.017](https://doi.org/10.1016/j.ins.2005.01.017).
- Zhang, Biao et al. (2015). "Effect of urban green space changes on the role of rainwater runoff reduction in Beijing, China." *Landscape and Urban Planning* 140, Pages 8–16. DOI: [10.1016/j.landurbplan.2015.03.014](https://doi.org/10.1016/j.landurbplan.2015.03.014).
- Zhang, Jianyun et al. (2007). "Study of runoff trends of the six larger basins in China over the past 50 years (in Chinese)." *Advances in Water Science* 18.2, Pages 230–234. DOI: [10.14042/j.cnki.32.1309.2012.04.007](https://doi.org/10.14042/j.cnki.32.1309.2012.04.007).
- Zhang, L, W R Dawes, and G R Walker (2001). "Response of mean annual evapotranspiration to vegetation changes at catchment scale." *Water Resources Research* 37.3, Pages 701–708. DOI: [10.1029/2000WR900325](https://doi.org/10.1029/2000WR900325).
- Zhang, L. et al. (2004). "A rational function approach for estimating mean annual evapotranspiration." *Water Resources Research* 40.2, W025021–W02502114. DOI: [10.1029/2003WR002710](https://doi.org/10.1029/2003WR002710).
- Zhang, Mingfang et al. (2017). "Review papers A global review on hydrological responses to forest change across multiple spatial scales : Importance of scale , climate , forest type and hydrological regime." *Journal of Hydrology* 546, Pages 44–59. DOI: [10.1016/j.jhydrol.2016.12.040](https://doi.org/10.1016/j.jhydrol.2016.12.040).
- Zhang, Qiang, Chong-Yu Xu, and Tao Yang (2009). "Variability of Water Resource in the Yellow River Basin of Past 50 Years, China." *Water Resources Management* 23.6, Pages 1157–1170. DOI: [10.1007/s11269-008-9320-2](https://doi.org/10.1007/s11269-008-9320-2).
- Zhang, Qiang et al. (2013). "Abrupt behaviours of streamflow and sediment load variations of the Yangtze River basin, China." *Hydrological Processes* 27.3, Pages 444–452. DOI: [10.1002/hyp.9278](https://doi.org/10.1002/hyp.9278).
- Zhang, Quanfa (2009). "The South-to-North Water Transfer Project of China: Environmental implications and monitoring strategy." *Journal of the American Water Resources Association* 45.5, Pages 1238–1247. DOI: [10.1111/j.1752-1688.2009.00357.x](https://doi.org/10.1111/j.1752-1688.2009.00357.x).
- Zhang, Shulei et al. (2018). "Excessive Afforestation and Soil Drying on China's Loess Plateau." *Journal of Geophysical Research: Biogeosciences* 123.3, Pages 923–935. DOI: [10.1002/2017JG004038](https://doi.org/10.1002/2017JG004038).
- Zhang, Shulei et al. (2016). "Quantifying the effect of vegetation change on the regional water balance within the Budyko framework." *Geophysical Research Letters* 43.3, Pages 1140–1148. DOI: [10.1002/2015GL066952](https://doi.org/10.1002/2015GL066952).
- Zhang, T. et al. (2003). "Distribution of seasonally and perennially frozen ground in the Northern Hemisphere." *Permafrost*, Pages 1289–1294.
- Zhang, Xiaoping et al. (2008). "Responses of streamflow to changes in climate and land use/cover in the Loess Plateau, China." *Water Resources Research* 44.7, Pages 1–12. DOI: [10.1029/2007WR006711](https://doi.org/10.1029/2007WR006711).
- Zhang, Yongfang et al. (2014). "Impacts of climate change and land use change on runoff of forest catchment in northeast China." *Hydrological Processes* 28.2, Pages 186–196. DOI: [10.1002/hyp.9564](https://doi.org/10.1002/hyp.9564).
- Zhang, Yongyong et al. (2010). "Impact of water projects on river flow regimes and water quality in Huai River Basin." *Water Resources Management* 24.5, Pages 889–908. DOI: [10.1007/s11269-009-9477-3](https://doi.org/10.1007/s11269-009-9477-3).

- Zhao, Guangju et al. (2013). "Climate changes and their impacts on water resources in semiarid regions: A case study of the wei river basin, China." *Hydrological Processes* 27.26, Pages 3852–3863. doi: [10.1002/hyp.9504](https://doi.org/10.1002/hyp.9504).
- Zhao, Guangju et al. (2014). "Quantifying the impact of climate variability and human activities on streamflow in the middle reaches of the Yellow River basin, China." *Journal of Hydrology* 519.PA, Pages 387–398. doi: [10.1016/j.jhydrol.2014.07.014](https://doi.org/10.1016/j.jhydrol.2014.07.014).
- Zhao, Tianbao and Congbin Fu (2006). "Comparison of products from ERA-40, NCEP-2, and CRU with station data for summer precipitation over China." *Advances in Atmospheric Sciences* 23.4, Pages 593–604. doi: [10.1007/s00376-006-0593-1](https://doi.org/10.1007/s00376-006-0593-1).
- Zhou, Feng et al. (2013). "Hydrological response to urbanization at different spatio-temporal scales simulated by coupling of CLUE-S and the SWAT model in the Yangtze River Delta region." *Journal of Hydrology* 485, Pages 113–125. doi: [10.1016/j.jhydrol.2012.12.040](https://doi.org/10.1016/j.jhydrol.2012.12.040).
- Zhou, Haiying et al. (2011). "Influences of climate change and human activities on Tarim River runoff's in China over the past half century." *Environmental Earth Sciences* 67.1, Pages 231–241. doi: [10.1007/s12665-011-1502-1](https://doi.org/10.1007/s12665-011-1502-1).
- Zhou, Hongwei et al. (2000). "Irrigated agriculture and sustainable water management strategies in the Tarim Basin." In: *Proceedings of the workshop "New Approaches to water management in Central Asia, Aleppo, Syria, 6–11 Nov*, Pages 9675–9695. doi: [10.1002/2013WR014696](https://doi.org/10.1002/2013WR014696).Received.
- Zhou, Xudong et al. (2018). "Understanding the water cycle over the upper Tarim Basin: retrospectively the estimated discharge bias to atmospheric variables and model structure." *Hydrology and Earth System Sciences* 22, Pages 6087–6108. doi: [10.5194/hess-22-6087-2018](https://doi.org/10.5194/hess-22-6087-2018).
- Zomer, Robert J et al. (2007). *Trees and Water: Smallholder Agroforestry on Irrigated Lands in Northern India*. Colombo, Sri Lanka: International Water Management Institute, Page 45.
- Zomer, Robert J et al. (2008). "Climate change mitigation : A spatial analysis of global land suitability for clean development mechanism afforestation and reforestation." *Agric. Ecosyst. Envir* 126, Pages 67–80. doi: [10.1016/j.agee.2008.01.014](https://doi.org/10.1016/j.agee.2008.01.014).
- Zong, Yongqiang and Xiqing Chen (2000). "The 1998 flood on the Yangtze, China." *Natural Hazards* 22.2, Pages 165–184. doi: [10.1023/A:1008119805106](https://doi.org/10.1023/A:1008119805106).



**Titre :** Impact du changement climatique et de la gestion humaine sur le cycle de l'eau en Chine: faire face aux incertitudes

**Mots clés :** Les incertitudes, Impact humain, Changement climatique, Cycle de l'eau, Chine

**Résumé :** En se concentrant sur différentes sources d'incertitude pouvant affecter la précision des modèles de modélisation hydrologique et d'analyse d'impact, cette thèse passe en revue les études antérieures et propose de nouvelles approches pour estimer et comparer les incertitudes avec leurs applications concentrées sur la Chine. Cette thèse propose d'abord une approche tridimensionnelle de la partition de la variance qui estime l'incertitude des multiples produits de précipitation de types différents. La nouvelle estimation utilise des informations complètes dans les dimensions temporelle et spatiale et constitue donc un indicateur plus complet pour l'évaluation de l'incertitude, en particulier pour plusieurs jeux de données. Cette thèse propose ensuite un cadre ORCHIDEE-Budyko permettant d'attribuer le biais de décharge entre la simulation du modèle (fournie par le modèle de surface ORCHIDEE) et les observations aux sources d'incertitude des variables atmosphériques et de la structure du modèle. Le cadre qualifie la possibilité d'incertitudes différentes avec l'hypothèse de Budyko basée sur des facteurs physiques et le soutien de

littératures existante. Cette thèse passe enfin en revue les activités humaines et leur impact sur le débit des rivières en Chine, ainsi que les approches associées utilisées pour la quantification. L'impact humain qui a été quantifié par la différence entre le débit fluvial observé et celui qui a été naturalisé est ensuite comparé à des simulations multi-modèles conduites par différents forçages. Les résultats montrent que l'incertitude dans les variables atmosphériques (par exemple, les précipitations) est grande, en particulier pour les modèles de circulation générale (GCMs). L'incertitude des précipitations est très probablement supérieure à celle de l'incertitude du modèle. L'incertitude associée au débit modélisé avec différents forçages est supérieure à l'ampleur de l'impact humain pour la plupart des régions, en particulier dans le sud de la Chine, ce qui rend la la quantification de l'impact humain pour ces régions difficile. Cette compréhension des incertitudes dans le cycle naturel de l'eau et de la gestion que lui imposent les hommes est une condition préalable à toute tentative de modélisation des pressions anthropiques.

**Title :** The Impact of Climate Change and Human Management on the Water Cycle of China: Dealing with Uncertainties

**Keywords :** Uncertainties, Human impact, Climate change, Water cycle, China

**Abstract :** Focusing on different uncertainty sources that can affect the model accuracy of hydrological modeling and impact analysis, this thesis reviews the past studies and provides new approaches for estimating and comparing the uncertainties with their applications concentrated over China. This thesis first proposes a three-dimensional variance partitioning approach that estimates the uncertainty among multiple precipitation products with different types. The new estimation uses full information in temporal and spatial dimensions and thus is a more comprehensive metric for uncertainty assessment especially for multiple datasets. This thesis then proposes a ORCHIDEE-Budyko framework that helps attribute the discharge bias between model simulation (provided by land surface model ORCHIDEE) and observations to uncertainty sources of atmospheric variables and model structure. The framework qualifies the possibility of different uncertainties with physical-based Budyko hypothesis and support of related lite-

ratures. This thesis finally reviews the human activities and their impact on river discharge over China regions as well as the related approaches that used for the quantification. The human impact that quantified as the difference between observed river discharge and the naturalized ones is then compared with multi-model simulations driven by different forcing inputs. Results show that the uncertainty in atmospheric variables (e.g., precipitation) is large especially for General Circulation Models (GCMs). Precipitation uncertainty is very likely larger than that of the model uncertainty. The uncertainty in the modeled discharge with different forcing is larger than the magnitude of human impact for most of the regions especially in south China, which impedes the credibility of human impact quantification for those regions. This understanding of uncertainties in the natural water cycle and the management humans impose on it is a prerequisite before attempting to model the anthropogenic pressures.

